NASA/CR–2016-219201

Application of Deterministic and Probabilistic System Design Methods and Enhancements of Conceptual Design Tools for ERA Project Final Report

Dimitri N. Mavris and Jeff S. Schutte
Georgia Institute of Technology, Atlanta, Georgia

NASA STI Program . . . in Profile

Since its founding, NASA has been dedicated to the advancement of aeronautics and space science. The NASA scientific and technical information (STI) program plays a key part in helping NASA maintain this important role.

The NASA STI program operates under the auspices of the Agency Chief Information Officer. It collects, organizes, provides for archiving, and disseminates NASA's STI. The NASA STI program provides access to the NTRS Registered and its public interface, the NASA Technical Reports Server, thus providing one of the largest collections of aeronautical and space science STI in the world. Results are published in both non-NASA channels and by NASA in the NASA STI Report Series, which includes the following report types:

- TECHNICAL PUBLICATION. Reports of completed research or a major significant phase of research that present the results of NASA Programs and include extensive data or theoretical analysis. Includes compilations of significant scientific and technical data and information deemed to be of continuing reference value. NASA counter-part of peer-reviewed formal professional papers but has less stringent limitations on manuscript length and extent of graphic presentations.

- TECHNICAL MEMORANDUM. Scientific and technical findings that are preliminary or of specialized interest, e.g., quick release reports, working papers, and bibliographies that contain minimal annotation. Does not contain extensive analysis.

- CONTRACTOR REPORT. Scientific and technical findings by NASA-sponsored contractors and grantees.

- CONFERENCE PUBLICATION. Collected papers from scientific and technical conferences, symposia, seminars, or other meetings sponsored or co-sponsored by NASA.

- SPECIAL PUBLICATION. Scientific, technical, or historical information from NASA programs, projects, and missions, often concerned with subjects having substantial public interest.

- TECHNICAL TRANSLATION. English-language translations of foreign scientific and technical material pertinent to NASA's mission.

Specialized services also include organizing and publishing research results, distributing specialized research announcements and feeds, providing information desk and personal search support, and enabling data exchange services.

For more information about the NASA STI program, see the following:

- Access the NASA STI program home page at http://www.sti.nasa.gov

- E-mail your question to help@sti.nasa.gov

- Phone the NASA STI Information Desk at 757-864-9658

- Write to:
  NASA STI Information Desk
  Mail Stop 148
  NASA Langley Research Center
  Hampton, VA 23681-2199

NASA/CR–2016-219201

Application of Deterministic and Probabilistic System Design Methods and Enhancements of Conceptual Design Tools for ERA Project Final Report

Dimitri N. Mavris and Jeff S. Schutte
Georgia Institute of Technology, Atlanta, Georgia

National Aeronautics and
Space Administration

Langley Research Center
Hampton, Virginia 23681-2199

Prepared for Langley Research Center
under Contract NNL12AA12C

MAY 2016

Acknowledgment

This report documents a three year study conducted for the National Aeronautics and Space Administration, Aeronautics Research Mission Directorate, Integrated System Research Program, Environmentally Responsible Aviation (ERA) Project. This report was prepared under NASA Contract NNL12AA12C "Application of Deterministic and Probabilistic System Design Methods and Enhancements of Conceptual Design Tools for ERA Project" from March 2012 through March 2015. This study was conducted by the Aerospace Systems Design Lab, School of Aerospace Engineering, Georgia Institute of Technology in Atlanta, GA. Georgia Tech is thankful for the opportunity to conduct system level assessments in order to help NASA meet the goal of simultaneously meeting ERA's N+2 targets for fuel burn, noise and emissions reductions. Georgia Tech the leadership provided by the project manager Dr. Fayette Collier, the NRA COTR Dr. Frank Gern and other members of the NASA system assessment team Craig Nickol, Andy Hahn and Doug Wells.

The Principal Investigator for Georgia Tech was Prof. Dimitri Mavris. The Co-PI was Dr. Jeff Schutte. The following individuals were technical contributors to this report: Dr. Jimmy Tai, Mr. Russell Denney, Dr, Hernando Jimenez, Dr. Brian Kestner, Mr. Chris Perullo, Mr. Carl Johnson, Dr. Hongjun Ran, Dr. Elena Garcia, Dr. Jon Sands, Mr. Turab Zaidi, Mr. Kyung Hak Choo, Mr. Adam Siegel, Mr. Gregory Busch, Mr. Michael Bozeman, Mr. Eric Fuerst, Mrs. Caroline Ingram, Ms. Mathilde Deveraux, and Mr. Michael Anderson.

Available from:

NASA STI Program / Mail Stop 148
NASA Langley Research Center
Hampton, VA 23681-2199
Fax: 757-864-6500

Table of Contents

List of Figures

List of Tables

Nomenclature

ACD	Acoustic Data Module
ADD	Advanced Direct Drive
ADP	Aerodynamic Design Point
AEDT	Aviation Environmental Design Tool
ANN	Artificial Neural Network
ANOPP	Aircraft Noise Prediction Program
AP	Approach
ASDL	Aerospace Systems Design Lab
ATF	Advanced Turbofan
BPR	Bypass Ratio
BRAINN	Basic Regression Analysis for Integrated Neural Networks
BXW	Box Wing
BWB	Blended-Wing-Body
CAEP	Committee on Aviation Environmental Protection
CDF	Cumulative Distribution Function
CMC	Ceramic Matrix Composite
CRN	Chemical Reactor Network
CRPFAN	Counter Rotation Prop Fan Noise, NASA
CO	Cut Out throttle setting
DDTF	Direct Drive Turbofan
DOE	Design of Experiments
EDS	Environmental Design Space
EINOX	Emissions Indices NOx
EPNdB	Effective Perceived Noise in Decibels
ERA	Environmentally Responsible Aviation
FAR	Fuel to Air Ratio
FEM	Finite Element Method
FCDO	Lift-Independent Drag
FCDI	Lift-dependent Drag
FLOPS	Flight Optimization System, NASA
FPI	Fast Probability Integration
FPR	Fan Pressure Ratio
GF	Geared Fan
GW	Gross Weight
HPC	High Pressure Compressor
HPC	High Pressure Turbine
HWB	Hybrid Wing body
ID	Idle throttle setting
ITD	Integrated Technology Demonstrator
JMP	jmp statistical software program
LDI	Lean Direct Injection
LPC	Low Pressure Compressor
LPT	Low Pressure Turbine
LSA	Large Single Aisle
LTA	Large Twin Aisle

LTO	Landing/Takeoff
MFN	Mid-Fuselage Nacelle
MLP	Multi-Layer Perceptron
MMC	Metal Matrix Composite
MPP	Most Probable Point
MOGA	Multi-Objective Genetic Algorithm
NASA	National Aeronautics and Space Administration
NSGA	Non-dominated Sorting Genetic Algorithm
NPSS	Numerical Propulsion System Simulation
NOx	Nitrous Oxides
OLH	Optimal Latin Hypercube
OPR	Overall Pressure Ratio
OR	Open Rotor
OWN	Over Wing Nacelle
PFR	Plug-Flow Reactors
PM	Powder Metal
PMC	Polymer Matrix Composites
PSR	Perfectly-Stirred Reactors
RJ	Regional Jet
RPM	Rotations per Minute
RQL	Rich Quench Lean
RTC	Reference Technology Collector
SME	Subject Matter Expert
SLS	Sea Level Static
SSA	Small Single Aisle
STA	Small Twin Aisle
T3	Stage 3 Temperature (Burner Inlet)
T4	Stage 4 Temperature (Turbine Inlet)
TBC	Thermal Barrier Coating
TC	Technology Collector
TCM	Technology Compatibility Matrix
TIM	Technology Impact Matrix
TO	Take Off
TOC	Top of Climb
TOGW	Take Off Gross Weight
TRL	Technology Readiness Level
TSFC	Thrust Specific Fuel Consumption
T&W	Tube and Wing
TWR, T/W	Thrust to Weight Ratio
UDF	UnDucted Fan (Open Rotor)
Vapp	Approach Velocity
VLA	Very Large Aircraft
WATE++	Weight Analysis of Turbine Engines, NASA
WSR, W/S	Wing loading

1.0 Introduction

This report documents work done by the Aerospace Systems Design Lab (ASDL) at the Georgia Institute of Technology, Daniel Guggenheim School of Aerospace Engineering for the National Aeronautics and Space Administration, Aeronautics Research Mission Directorate, Integrated System Research Program, Environmentally Responsible Aviation (ERA) Project. This report was prepared under contract NNL12AA12C, "Application of Deterministic and Probabilistic System Design Methods and Enhancement of Conceptual Design Tools for ERA Project".

There are three additional reports that cover work performed under this contract as well. The first two reports titled "Environmentally Responsible Aviation Systems Analysis Report: Technology Portfolio and Advanced Configurations" and "Environmentally Responsible Aviation Systems Analysis Report: Technology Portfolio and Advanced Configurations Executive Summary" provide details of each of the technologies modeled in this report including a general description, TRL values, mapping of the impacts to various codes, values of the impacts and the compatibility with other technologies. The third report titled "Application of Strategic Planning Process with Fleet Level Analysis Methods and Enhancement of Technology Portfolio Assessment Methods for the ERA" uses the vehicles and technologies modeled in this report applied to various fleet scenarios and uses the surrogates and probabilistic information from this report for the creation of the ERA dashboard, a strategic planning and prioritization tool.

1.1 Background

The research within this report addressed the Environmentally Responsible Aviation (ERA) project goal stated in the NRA solicitation "to advance vehicle concepts and technologies that can simultaneously reduce fuel burn, noise, and emissions." To identify technology and vehicle solutions that simultaneously meet these three metrics requires the use of system-level analysis with the appropriate level of fidelity to quantify feasibility, benefits and degradations, and associated risk. In order to perform the system level analysis, the Environmental Design Space (EDS) [Kirby 2008, Schutte 2012a] environment developed by ASDL was used to model both conventional and unconventional configurations as well as to assess technologies from the ERA and N+2 timeframe portfolios. A well-established system design approach was used to perform aircraft conceptual design studies, including technology trade studies to identify technology portfolios capable of accomplishing the ERA project goal and to obtain accurate tradeoffs between performance, noise, and emissions. The ERA goal, shown in Figure 1, is to simultaneously achieve the N+2 benefits of a cumulative noise margin of 42 EPNdB relative to stage 4, a 75% reduction in LTO NOx emissions relative to CAEP 6 and a 50% reduction in fuel burn relative to the 2005 best in class aircraft.

There were 5 research task associated with this research: 1) identify technology collectors, 2) model technology collectors in EDS, 3) model and assess ERA technologies, 4) LTO and cruise emission prediction, and 5) probabilistic analysis of technology collectors and portfolios. The following section provides the specifics for each of the tasks and associated subtasks.

TECHNOLOGY BENEFITS*	TECHNOLOGY GENERATIONS (Technology Readiness Level = 4-6)		
	N+1 (2015)	N+2 (2020**)	N+3 (2025)
Noise (cum margin rel. to Stage 4)	-32 dB	-42 dB	-52 dB
LTO NOx Emissions (rel. to CAEP 6)	-60%	-75%	-80%
Cruise NOx Emissions (rel. to 2005 best in class)	-55%	-70%	-80%
Aircraft Fuel/Energy Consumption‡ (rel. to 2005 best in class)	-33%	-50%	-60%

* Projected benefits once technologies are matured and implemented by industry. Benefits vary by vehicle size and mission. N+1 and N+3 values are referenced to a 737-800 with CFM56-7B engines, N+2 values are referenced to a 777-200 with GE90 engines
** ERA's time-phased approach includes advancing "long-pole" technologies to TRL 6 by 2015
‡ CO2 emission benefits dependent on life-cycle CO2e per MJ for fuel and/or energy source used

Figure 1. NASA Subsonic Transport System Level Metrics

1.2 Program Description

1.2.1 Task 1: Identify Technology Collectors

In consultation with NASA, ASDL identified conventional and unconventional aircraft configurations as technology collectors (TCs) for use in the systems level analysis. There were 5 aircraft configurations modeled as technology collectors. These aircraft configurations included conventional tube and wing (T&W), Hybrid Wing Body (HWB), Over Wing Nacelle (OWN), Mid-fuselage Nacelle (MFN) and Box Wing (BXW). Descriptions of the modeling of each of these aircraft can be found in section 3.4. There were also 3 engine configurations identified as technology collectors, a direct drive turbofan engine, a geared fan engine, and an open rotor or unducted fan. Descriptions of the modeling of each of these engines can be found in section 3.3.

1.2.2 Task 2: Model Technology Collectors in EDS

In order to perform a systems level assessment of the vehicle configurations identified in Task 1, each TC was parametrically modeled in EDS to allow for the evaluation of different technology portfolios and optimization of design parameters. The following subtasks were performed to generate the EDS models:

- Develop VSP Models for New Unconventional Configurations (section 3.4.1)
- Integrate VSP into EDS Framework (section 3.4.3.3)
- Identify and Integrate Aerodynamic Prediction Codes into EDS (section 3.4.3.3)
- Identify and Integrate Aircraft Component Weight Sizing Algorithm into EDS (section 3.4.6.4 and section 3.4.3.4 for HWB centerbody)
- Develop Engine Models (section 3.3)
- Develop Vehicle Sizing and Performance Models (section 3.4)
- Develop Noise Models (section 0 and 3.4)
- Develop Fleet Coefficient Generator Algorithm (section 3.5)

1.2.3 Task 3: Model and Assess ERA Technologies

To model and assess ERA technologies, the following subtasks were performed:

- Identify and Review ERA Technologies (section 2.0)
- Collect and Compile Technology Data (section 2.1)
- Select Engine Cycles for Technology Portfolios (section 3.3)
- Technology Portfolio Assessment and Surrogate Model Generation (section 4.0)

1.2.4 Task 4: LTO and Cruise Emission Predictions

To assess the capabilities of advanced combustion technologies to meet the ERA landing and take-off (LTO) and cruise emissions metrics, ASDL has developed a semi-analytical model to predict emissions during a three-year research effort sponsored by NASA Glenn Research Center. This task was to mature the emissions prediction model for advanced combustors to a level appropriate for systems-level technology assessments for EDS. The following subtasks were performed for the emissions modeling and can be found in section 4.4:

- Reformulate Chemical Reactor Network Models
- Reformulate 1-D Flow Models
- Verify Predictive Capability of Reformulated Models for LTO NOx
- Extend Emissions Model for Cruise NOx Predictions
- Improve Emissions Model Integration for Design Space Exploration

1.2.5 Task 5: Probabilistic Analysis of Technology Collectors and Portfolios

A probabilistic technology assessment was conducted that includes a rigorous, traceable, and quantitative assessment of technology benefits which explicitly incorporates uncertainty and risk. The following subtasks were performed for the probabilistic assessment and can be found in section 6.0:

- Conduct Literature Review of Uncertainty Quantification
- Solicit NASA Technology SMEs for Input to Construct Uncertainty Distributions
- Perform Probabilistic Analysis and Visualize Results

2.0 Technology Portfolios

The ERA mission is to conduct system research to bridge the gap between fundamental research (TRL 1-4) and product prototyping (TRL 7) thus expanding the viable and well-informed trade space for vehicle design decisions enabling simultaneous realization of national noise, emissions, and performance goals. ERA is focused on N+2 timeframe technologies, those that can achieve a TRL of 4-6 by 2020 as shown in Figure 1. The initial list of technologies compiled for this report was selected based on the current estimate of TRL and the anticipated time to TRL 6 based on work by [Peisen 1999] and modified by direct input from NASA technologists, engineers and management.

Three different portfolios of technologies have been created for this report, the Reference Technology Collector (RTC) technology portfolio, the ERA technology portfolio and the N+2 technology portfolio. Each portfolio builds on the subsequent portfolio, as shown in the Venn

diagram in Figure 2 unless there is an incompatibility in which case a new technology replaces one from the previous portfolio. An example would be PRSEUS composite system replacing sandwich composites. Since the ERA goals are referenced to 2005 best in class vehicles, some additional technologies that are potentially on current aircraft but are not included on the reference system have been grouped as the Reference Technology Collector (RTC) baseline technologies. These technologies are included to determine the absolute improvements in aircraft performance with respect to ERA goals but are not included in the ERA portfolio as they are already in the fleet. There should not be an expectation for ERA technology development in these areas unless to further improve the SOA.

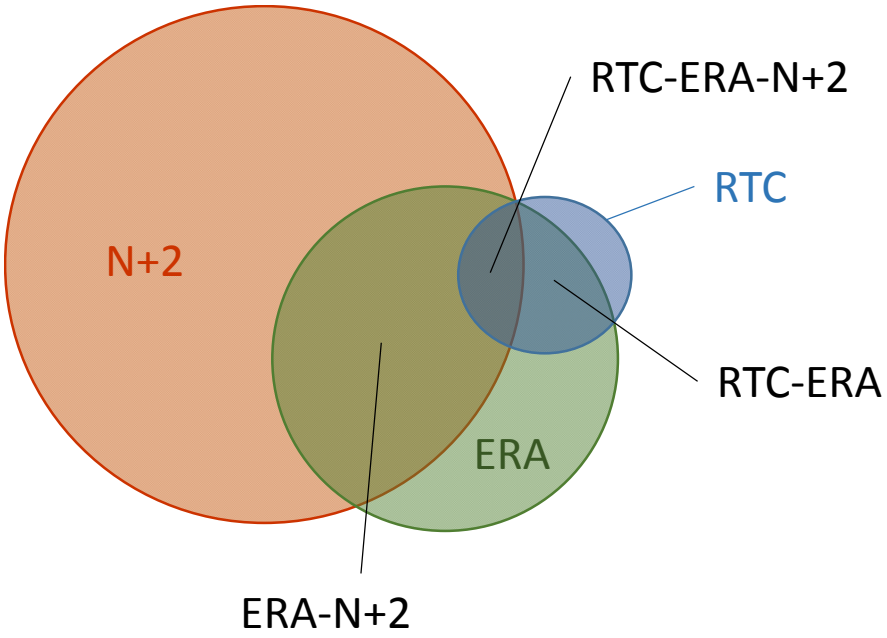

Figure 2. Technology Portfolio Venn Diagram

The ERA technology portfolio includes technologies developed in both phase 1 and phase 2 of the ERA project. The phase 2 technologies are referred to as the Integrated Technology Demonstrators (ITD). The third group of technologies are the N+2 technologies. These were technologies that NASA ERA was not maturing but which were found to be potentially available in the N+2 timeframe. As such they represent technologies being matured by other government agencies and by industry. While the actual technologies being developed outside the ERA project might differ materially from those selected for the N+2 portfolio, their impact on the different metrics is most likely captured. For example, there may be several potential technologies that reduce flap edge noise. The selection of one over the other would be left to the detailed design. For the system assessment study, they can be treated equally since they would be modeled to have the same impact on the flap edge noise source. Thus, it is more important for the system assessment to capture the impact than the specific technology. An example of the expected progression in performance as one advances from RTC to ERA to N+2 technology portfolios is shown in Figure 3.

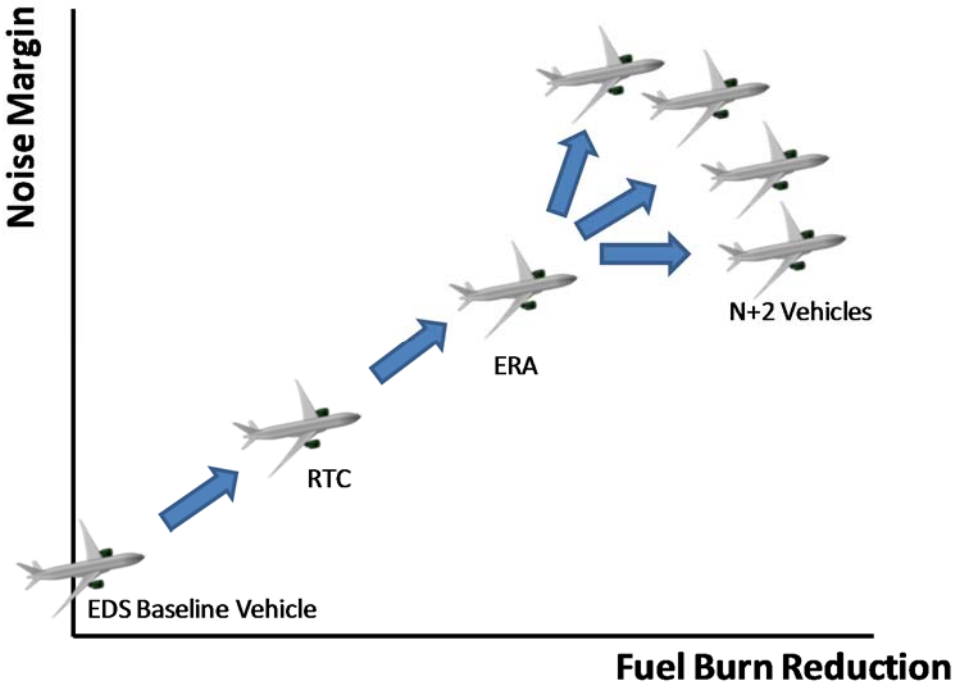

Figure 3. Technology Portfolios Impact on Metrics

A total of 68 technologies were evaluated across the three technology portfolios. They can be grouped by their primary impact into one of the seven following categories: Airframe lightweight structure and subsystem technologies, Airframe aerodynamic technologies, Airframe noise technologies, Engine fuel burn technologies, Engine noise technologies, Engine emission technologies and RTC Baseline Technologies. The number of categories is shown in Table 1. A listing of the technologies in each category is shown in Table 2 through Table 8.

Table 1. Technology Categories

Number of Technologies	Category
11	Airframe lightweight structure and subsystem technologies
6	Airframe aerodynamic technologies
6	Airframe noise technologies
16	Engine fuel burn technologies
11	Engine noise technologies
5	Engine emission technologies
13	RTC Baseline Technologies

Table 2. Airframe Lightweight Structural and Sub-System Technologies

Technology ID	Name
T3	Damage Arresting Stitched Composites
T6	Electro Mechanical Actuator System
T7	Solid Oxide Fuel Cell APU
T78	Primary Structure Joining Methodologies
T79	Damage Tolerant Laminates
T80	Advanced Sandwich Composites
T81	Post Buckled Structures
T82	Out-of-Autoclave Composite Fabrication
T83	Unitized Metallic Structures
T84	Tow Steered Composite Structures
T94	Adaptive Compliant Trailing Edge

Table 3. Airframe Aerodynamic Technologies

Technology ID	Name
T10	Hybrid Laminar Flow Control - Suction
T11	Natural Laminar Flow Control
T12	Riblets
T66	Active Flow Control for Tail
T68	Advanced Aero Wing
T69	HLFC Discrete Roughness Elements

Table 4. Airframe Noise Technologies

Technology ID	Name
T14	Continuous Moldline Link for Flaps
T15	Flap Fences / Flaplets
T16	Landing Gear Integration
T17	Flap Edge Treatment
T18	Slat Inner Surface Acoustic Liner
T19	Slat-Cover Filler

Table 5. Engine Fuel Burn Technologies

Technology ID	Name
T20	Active Compressor Clearance Control
T21	Active Compressor Flow Control
T22.1	Compressor Intercooler
T22.2	Cooled Cooling
T23	Active Turbine Clearance Control
T24	Active Turbine Flow Control
T25	Active Film Cooling
T26	Advanced Powder Metallurgy (PM) Disk Bonded to a Single Crystal (SX) Rim
T28	Advanced Turbine Superalloys
T29	Ceramic Matrix Composites (CMC's)
T32	Highly Loaded Compressor
T33	Highly Loaded Turbine
T67	Advanced Engine Components
T72	Low Interference Nacelle
T74	Thrust Reversers - Nacelle
T75	PAI Thrust Reverser

Table 6. Engine Emission Technologies

Technology ID	Name
T61	Active Combustion Control
T62	Lean Direct Injection (LDI)
T63	Lightweight CMC Liners
T64	LPP Combustor
T65	RQL Combustor

Table 7. Engine Noise Technologies

Technology ID	Name
T40	Acoustic Splitter
T41	Advanced Blade Tone Control
T42	Noise Cancelling Stator
T47	Fluidic Injection
T52 - GF	Lip Liner (for GF)
T53	Over-the-Rotor Treatment
T54	Compound Rotor Sweep for Low Tip Speed Fan
T56	Soft Vane
T57	Stator Sweep & Lean
T59	Variable Geometry Chevrons
T76	Active Pylon Shaping/Blowing

Table 8. RTC Baseline Technologies

Technology ID	Name
T1	Composite Technologies
T4	Gust Load Alleviation
T9	Excrescence Reduction
T27	Advanced TBC Coatings
T36 + T37	Polymer Matrix Composites (PMC)
T43	Aft Cowl Liners
T45	Combustor Noise Plug Liner
T46	Fixed Geometry Core Chevrons
T52 - ADD	Lip Liner (for ADD)
T60	Zero Splice Inlet
T77	Variable Area Nozzle (for GF)
T92	Blisk Compressors
T93	Ti-Al Low Pressure Turbine Components

2.1 Technology Report

Two additional reports titled “Environmentally Responsible Aviation Systems Analysis Report: Technology Portfolio and Advanced Configurations” and “Environmentally Responsible Aviation Systems Analysis Report: Technology Portfolio and Advanced Configurations Executive Summary” provide details of each of the technologies modeled in this report including a general description, TRL values, mapping of the impacts to various codes, values of the impacts and the compatibility with other technologies. The technologies that make up each of the portfolios is listed in the following sections.

2.2 Reference Technology Collector

The RTC portfolio is shown in Table 9 with impact and values for each technology.

Table 9. RTC Technologies and Impacts

Name	Impact	Value
RTC Composite Technologies	Fuselage Weight	-5%
	Bending Material Weight	-15%
	Control Surfaces/Spars/Ribs Weight	-5%
	Horizontal Tail Weight	-15%
	Vertical Tail Weight	-15%
Gust Load Alleviation	Gust Load	-15%
Excrescence Reduction	Lift independent drag	-0.5%
Advanced TBC Coating	HPT Blade/Vane Temperature	+150
	LPT Blade/Vane Temperature	+150
Polymer Matrix Composites	Inlet Nacelle Density	-46.9%
	Fan Case Density	-48%
	Fan Stator Density	-48%
	Bypass Duct Density	-48%
	Fan Blade	-34.8%
Aft Cowl Liners	Bypass Duct Pressure Drop	+1.8%
	Fan Discharge Noise Suppression TO	-3 dB
	Fan Discharge Noise Suppression AP	-3 dB
Combustor Noise Plug Liner	Core Noise Reduction at TO	-3 dB
	Core Noise Reduction at AP	-3 dB
Fixed Geometry Core Chevrons	Core Nozzle Velocity Coefficient	-0.5%
	Core Nozzle Perimeter Ratio	1.3
Lip Liner for ADD	Fan Inlet Noise Reduction at TO	-1 dB
	Fan Inlet Noise Reduction at AP	-3 dB
Zero Splice Inlet	Fan Inlet Noise Reduction at TO	-2 dB
Variable Area Nozzle for GF	Nozzle Exit Area	Variable
Blisk Compressors	Compressor Disk Material Density	-10%
Ti-Al Low Pressure Turbine Components	LPT Stator Material Density	-50%
	LPT Forward Blade Material Density	-50%
	LPT Aft Blade Material Density	-50%

2.3 ERA Technology Portfolio

Table 10. ERA Technologies

ERA Technologies
Damage arresting stitched composites (fuselage and wing)
Natural laminar flow wing (RJ, SSA, LSA only)
Active flow control tail
Advanced aero wing
Flap edge noise
Landing gear integration (main and nose)
Highly loaded compressors
Lightweight ceramic matrix composite liners (combustor)
Advanced combustor
Adaptive compliant trailing edge
Discrete Roughness Elements
UHB Engine (Geared fan) Advanced engine components (efficiency improvements) SMA variable area nozzle Soft vanes Over the rotor acoustic treatment Laminar flow nacelle Low interference nacelle Advanced PM disk Advanced turbine super alloys CMC exhaust core nozzle Lightweight CMC liners Advanced TBC coatings CMC turbine vanes
Open rotor engine

2.4 N+2 Technology Portfolio

Table 11. N+2 Technologies

N+2 Technologies		
Active Compressor Clearance Control	Active Pylon Shaping/Blowing	Acoustic Splitter
Active Compressor Flow Control	Active Turbine Clearance Control	Active Film Cooling
Out-of-Autoclave Composite Fabrication	Advanced Sandwich Composites	Metallic Structures
Highly Loaded Turbine Unitized	Advanced Turbine Superalloys	Lip Liner - GTF
Compound Rotor Sweep for Low Tip Speed Fan	Post Buckled Structures	Fluidic Injection
Electro Mechanical Actuator System	Damage Tolerant Laminates	PAI Thrust Reverser
Hybrid Laminar Flow Control - Suction	Discrete Roughness Elements	Riblets
Ceramic Matrix Composites (CMC's)	Variable Geometry Chevrons	Slat-Cover Filler
Porous / Absorbent Flap Edge Treatment	Advanced Blade Tone Control	Solid Oxide Fuel Cell APU
Primary Structure Joining Methodologies	Compressor Intercooler	Stator Sweep & Lean
Slat Inner Surface Acoustic Liner	Active Turbine Flow Control	Thrust Reversers - Nacelle
Tow Steered Composite Structures	Noise Cancelling Stator	Flap Fences / Flaplets

3.0 Aircraft Modeling

3.1 EDS Background

The foundation for this systems analysis capability is advanced methods developed at ASDL coupled with the integrated aircraft modeling and simulation environment known as EDS. EDS is capable of predicting the fuel burn, NO_x emissions, and noise metrics in a single environment with an automated link to provide necessary data for a fleet level assessment (see Figure 4). The majority of EDS analysis components are NASA developed programs which have been integrated using the object oriented software, Numerical Propulsion Simulation System (NPSS [Lytle, 1999 and Lytle, 2000]). The resulting engine and aircraft models from EDS are directly transferrable back to NASA since they are natively NASA software models. EDS is capable of modeling the thermodynamic performance (NPSS) of any engine cycle coupled with a parametric component map generation tool (CMPGEN [Converse, 1984 and Glassman, 1995]) and with a 1-D aeromechanical design/analysis for flowpath and weight estimation purposes (WATE++ [Onat, 1979 and Tong, 2002]). This propulsion system simulation is well suited to assess the ERA engine technology portfolio and is unique in its ability to match the engine to a sized airframe using a simultaneous, multi-design point sizing algorithm develop by ASDL [Schutte, 2009]. The propulsion simulation module is coupled with the mission analysis module (FLOPS [McCullers, 2009]) in an iterative fashion to ensure that all coupling variables are internally consistent and have converged. EDS ensures this convergence and consistency in order to provide more accurate mission fuel burn results and more accurate data to the noise prediction module (ANOPP [Zorumski, 1982]) to assess acoustic impacts, including the generation of engine state tables from NPSS and the resulting aircraft noise flight trajectories for the sized vehicle. This data is used within ANOPP to generate the three certification noise values for sideline, cutback and approach as well as characteristic NPD curves.

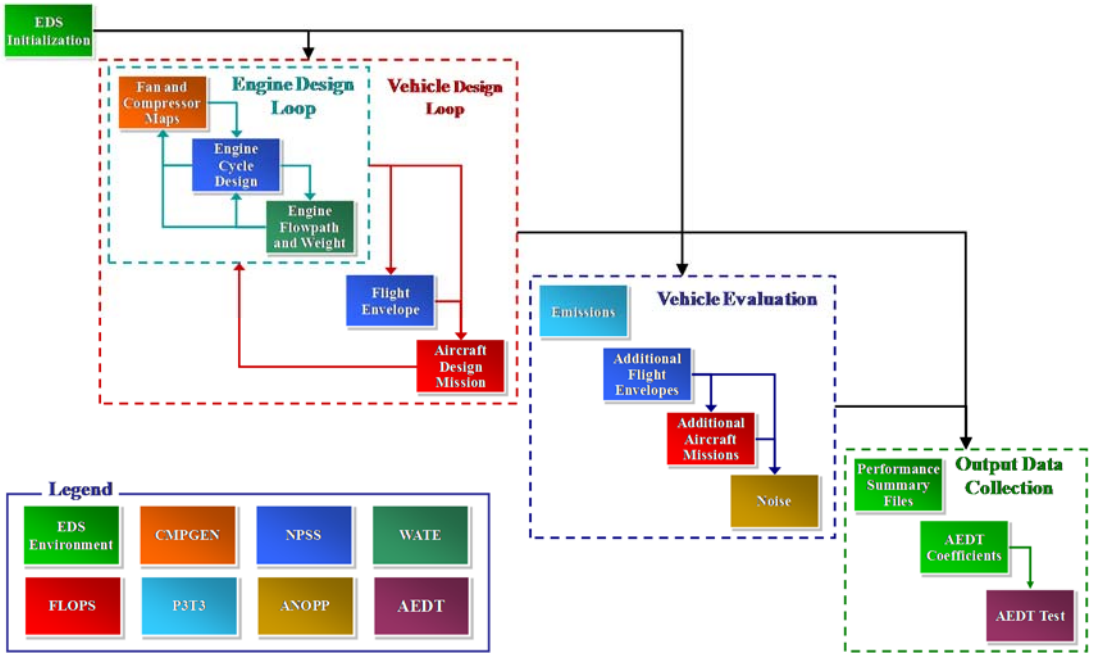

Figure 4. Environmental Design Space (EDS)

Another important EDS module is the NO_x prediction algorithm which comprises a low fidelity flow model, implemented in NPSS and integrated with the engine cycle model, and a separate Chemical Reactor Network (CRN) implemented in Chemkin. The low fidelity flow model provides engine cycle and combustor geometry information to the CRN, and the CRN performs the non-equilibrium chemical kinetics calculations to predict the emissions. The current emissions prediction model was developed during a three-year research effort sponsored by NASA Glenn Research Center (NRA NNX07AO08A). The model has been validated against data from the ICAO engine emissions databank [ICAO, 2010], as well as some advanced low-emissions designs such as the Lean-Direct-Inject (LDI) combustor. Finally, EDS is capable of direct linkage to a fleet level analysis since it generates the vehicle/engine/noise information necessary to provide replacement aircraft [de Luis, 2008]. EDS coupled with ASDL's well-structured technology assessment approach utilizing deterministic and probabilistic methods allow NASA to obtain accurate tradeoffs between performance, noise, and emissions.

3.2 Aircraft Classes

The baseline, tube and wing, vehicle classes used as the starting points for this project are summarize in Table 12. These tube and wing baseline aircraft systems serve as the calibration points for vehicles in each passenger class. The calibration process followed for each passenger class is depicted in Figure 5.

Table 12: EDS Baseline Vehicles

Passenger Class	Airframe	Engine
Regional Jet (RJ)	CRJ900	CF34-8C5
Small Single Aisle (SSA)	737-200	CFM56-7B27
Large Single Aisle (LSA)	737-800	CFM56-7B27
Small Twin Aisle (STA)	767-300ER	CF6-80C2
Large Twin Aisle (LTA)	777-200ER	GE90-94B
Very Large Aircraft (VLA)	747-400	PW4056

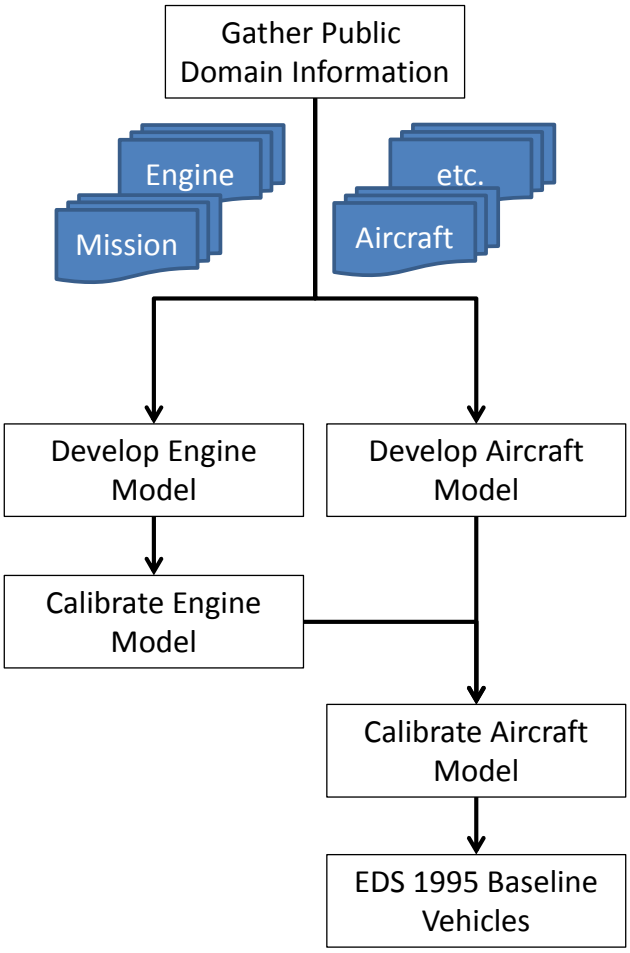

Figure 5. EDS 1995 Baseline Calibration Process

The vehicle calibration process begins with collecting data from public domain on the propulsion system, aircraft, mission, etc. The sources data include FAA's type certification datasheets, airport planning documents, engine cross section data, three-view drawings, etc. Next, the engine model is developed using NPSS and calibrated for both on-design and off-design (SLS) conditions. The calibrate engine results are tabular engine performance data table, propulsion system weight, maximum diameter and length. In parallel of the engine model development and calibration exercise, the aircraft model, including mission analysis, is developed. The aircraft calibration is performed with calibrated engine performance data. The procedure of calibrating the engine first and then calibrating the aircraft model is crucial to establish a well-grounded model.

The mission segments assumed for the design mission profile are taxi-out, take-off, climb, cruise, descent, land, and taxi-in with a reserve mission, as depicted in Figure 6. The 10,000 foot cruise segment is needed in order to extract performance data needed to calculate vehicle performance coefficients for fleet assessments. Step cruise is also performed during the cruise segment. The common elements of the mission profile for all vehicles classes are summarized in Table 13, and the mission profile elements that are specific to each vehicle class are summarized in Table 14.

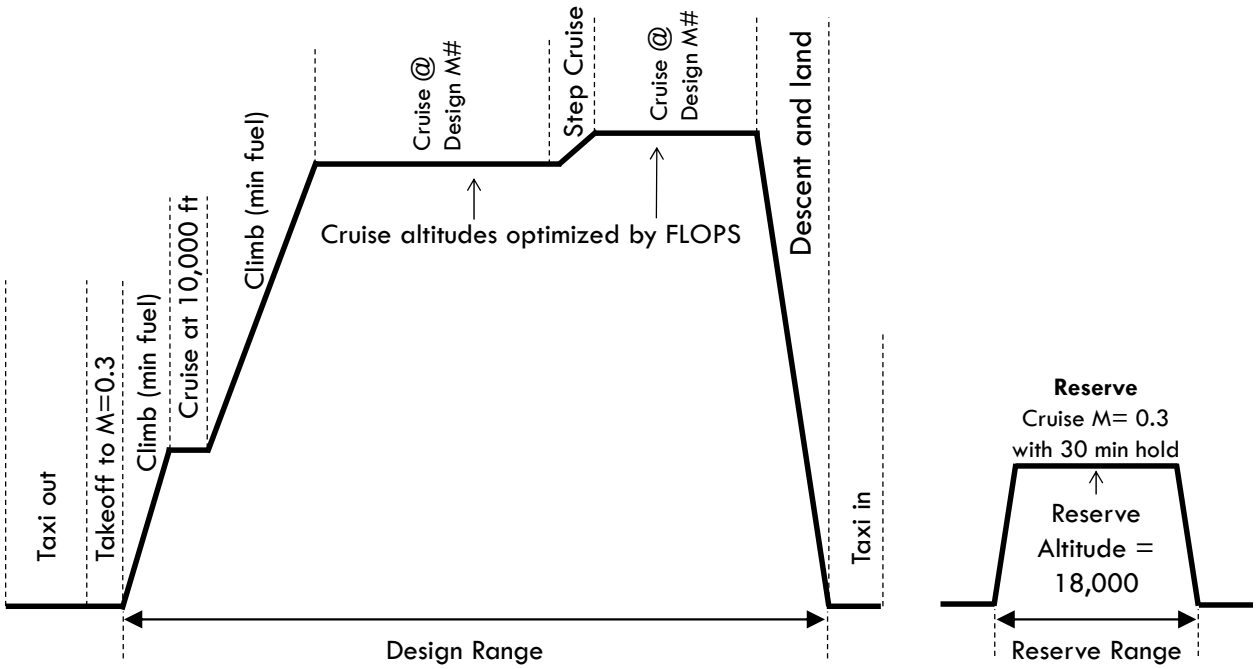

Figure 6. Design Mission Profile

Table 13. Common Mission Profile Assumptions Across Seat Classes

Parameter	Value
Baggage Weight per Passenger (lbs)	30
Weight per Passenger (lbs)	180
Reserve Cruise Altitude (ft)	18,000
Reserve Cruise Mach	0.3
Reserve Cruise Mach	0.3
Reserve Hold Time (min)	30

Table 14. Mission Assumptions

Mission Profile Elements	RJ	SSA	LSA	STA	LTA	LQ
Design Range (nmi)	1,980	3,330	2,960	5,920	7,530	7,060
Design Cruise Mach	0.80	0.78	0.78	0.80	0.84	0.85
Design Payload (lbs)	18,060	26,880	37,170	54,810	64,050	87,570
No. of First Class Passengers	0	8	12	24	24	32
No. of Business Class Passengers	0	0	0	0	54	76
No. of Tourist Class Passengers	86	120	165	237	227	309
Reserve Range (nmi)	100	200	200	200	200	200

In addition to the tube and wing (T&W) configuration, unconventional configurations were also modeled. The unconventional airframes include hybrid wing body (HWB), over-wing-nacelle (OWN), and mid-fuselage-nacelle (MFN), and boxed wing (BXW) configurations. Another combinatorial factor is the engine architectures modeled which are the advanced direct drive (ADD), geared fan (GF), and open rotor (OR) architectures. Table 15 shows the airframe-propulsion combinations modeled for each vehicle seat class.

Table 15. Vehicle Matrix

RJ	SSA	LSA	STA	LTA	VLA
T&W – ADD	T&W – ADD	T&W – ADD	T&W – ADD	T&W – ADD	T&W – ADD
T&W – GF	T&W – GF	T&W – GF	T&W – GF	T&W – GF	T&W – GF
		T&W – OR			
			HWB – ADD	HWB – ADD	HWB – ADD
			HWB – GF	HWB – GF	HWB – GF
				HWB – OR	
		OWN – ADD		MFN – ADD	
		OWN – GF		MFN – GF	
				BXW – GF	

Only a subset of the vehicle listed in Table 15 were included for surrogate generation (see section 5.0). These include the T&W – GF, T&W – OR and OWN – GF in the LSA class and the T&W – GF, HWB – GF, HWB – OR, MFN – GF and BXW – GF in the LTA class.

3.3 Engine Modeling

The values of specific assumptions for the RTC and ITD engines can be found in the Propulsion System Characteristics tables located in section 7.1.

3.3.1 Direct Drive

The Advanced Direct Drive (ADD) engine represents an improved version of conventional turbofans in terms of both bypass ratio and overall pressure ratio. It maintains the traditional architecture with the low pressure turbine directly driving the fan. The engine technology level modeled for the ADD engine within EDS is anchored to the CFM LEAP-X for the single aisle thrust class (LSA) and the GE GEnX for the twin aisle thrust class (LTA). The higher bypass ratio will allow for savings in specific fuel consumptions and the higher overall pressure ratio represents gains in efficiency. An increase in allowed turbine inlet temperature or overall pressure ratio will result in larger allowable bypass ratios. The advanced direct drive baseline, which represents approximately 2010 level technology and from which the N+2 technologies will be integrated into, operates at a fan pressure ratio of about 1.5, an SLS uninstalled overall pressure ratio around 45, and bypass ratios of about 10-12. The ADD engines are predicted to have up to 12% improvement in fuel efficiency, 50% reduction in emissions, and 15 EPNdB margin on FAA Stage IV noise regulations [McKay 2009]. GE proposes an advanced

configuration operating at a bypass ratio of around 9, which could yield around 13 EPNdB margin on FAA Stage IV noise regulations and around 16% improvement in fuel burn [Hughes 2008]. A recent study from NASA suggests the Large Single Aisle (LSA) configuration would have a 15% improvement in TSFC over the 1995 baseline engine [Guynn 2011], which agrees with the EDS baseline model prediction of 14.5%. Some key engine specification parameters and assumptions for each engine class (LSA and LTA) are summarized in Table 16, and the turbomachinery component design assumptions are summarized in Table 17.

Table 16. Engine Specifications for Advanced Direct Drive Architecture

Engine Specifications	LSA Engine	LTA Engine
Thrust Class (SLS, lbs)	25,180	83,260
Bypass Ratio (ADP)	10.1	12.4
Overall Pressure Ratio (ADP)	46.7	42.6
Fan Diameter (in)	69.4	123.5
Compressor Stages (Fan/LPC/HPC)	1/4/10	1/3/10
Turbine Stages (HP/LP)	2/7	2/7
Number of Fan Blades	18	18

Table 17. Turbomachinery Component Design Points for Advanced Direct Drive Architecture

Component Design Point (ADP)	LSA Engine	LTA Engine
Fan Polytropic Efficiency	0.919	0.925
Fan Pressure Ratio	1.55	1.50
LPC Polytropic Efficiency	0.933	0.904
LPC Pressure Ratio	1.39	1.26
HPC Polytropic Efficiency	0.905	0.926
HPC Pressure Ratio	22.0	23.0
HPT Adiabatic Efficiency	0.899	0.925
HPT Pressure Ratio	4.47	4.26
LPT Adiabatic Efficiency	0.900	0.933
LPT Pressure Ratio	6.81	7.80

3.3.2 Geared Fan

3.3.2.1 Cycle Selection Studies

Cycle optimization is an important consideration for technology assessment. As shown in [Hall 2007], the optimization of the cycle for a given technology package may result in about a 4% reduction in engine TSFC. However, depending on the technology package being analyzed, the optimal cycle may drastically change. For example the optimal OPR on an engine using current technology is much lower than on an engine that has advanced cooling technologies. Further technologies such as an intercooler may push the optimal OPR even higher. In 1999, Kurzke proposed using different numerical optimizers wrapped around an engine cycle code to find the optimal cycle of a derivative engine [Kurzke 1999]. More recent studies have used methods such as genetic algorithms integrated with an engine cycle code to optimize the cycle and vehicle design simultaneously [Rallabhandi 2008, Ghenaiet 2010]. Other studies by NASA

have explored how optimal cycles differ based on the weightings of the multi- objective function used to perform the optimization [Berton 2010].

As the number of technologies and the resulting potential technology packages becomes large, the selection of the optimal cycle for multiple potential technology packages becomes challenging. For the NASA ERA project, there are 68 potential technologies being considered. The number of permutations of technology combinations becomes too large to manage effectively if each combination were to be investigated on its own. Performing a direct engine cycle optimization on each potential package is virtually impossible. Even if a smaller subset of technology packages is chosen, the computational burden of performing the optimization using the cycle analysis code directly remains large. This is especially true when the analysis code (EDS) is really several codes integrated in a multi-disciplinary optimization (MDO) framework. Such environments can assess multiple vehicle characteristics such as fuel burn, emissions, and noise. Furthermore, as assumptions about the impacts of the technologies change, the corresponding optimal cycle may also change. Therefore two cycle selection studies were performed for the geared fan. Although the metrics of interest for the NASA ERA project are fuel burn, noise, and NOx, both studies focused only on cycle optimization relative to fuel burn and noise. The first study [Kestner 2011, Kestner 2012] looked at all available technologies applied to a LTA T&W vehicle. To enable faster cycle optimization and analysis of the technologies, surrogate models trained on the higher fidelity analysis codes were used. The second study examined cycle selection for the ERA ITD technology package applied to a HWB vehicle with variation in some parameters to understand certain sensitivities. It was thought that applying the geared fan to the HWB with its better aerodynamics and noise shielding might result in a different cycle preference.

3.3.2.1.1 All Technology Portfolio on LTA T&W

Due to the large number of design (technology and cycle) variables it is nearly impossible to query the entire design space. In the present analysis 68 technologies being investigated in addition to the cycle parameters that are being varied. The end result is a design space that consists of more than 100 independent input variables. Even if one were to simply evaluate only the minimum and maximum values for a given variable there are more than $1.26 * 10^{30}$ permutations. As a result this work employs surrogate modeling techniques to sample the design space in a flexible and relatively rapid manner. Section 5.0 details the methodology used to create surrogate models.

The baseline model for a large twin aisle configuration aircraft in EDS is based on a Boeing 777-200 with General Electric GE90-94B engines. The relevant cycle parameters in addition to vehicle fuel burn and noise margin for the baseline vehicle are shown in Table 18. Similar to the ERA project, the fuel burn reduction in the subsequent runs will be compared to this baseline value. On the other hand, all noise results will be compared against stage 4 noise stringency levels per the ERA goals.

Table 18. Baseline Vehicle Values for All Technology Cycle Selection Study

	Parameter	Value
Inputs	FPR	1.58
	LPCPR	1.26
	HPCPR	20
	T4max, R	3450
	Gear Ratio	1
	Extraction Ratio	1.09
Outputs	Fuel Burn, lbs	246519
	Noise Margin, dB	11.3
	SLS BPR	8.3
	SLS OPR	40.5

3.3.2.1.1.1 Technology Design Space

The technology design space is defined data formally recorded into the Technology Interaction Matrix and Technology Compatibility Matrix respectively (see sections 4.2 and 4.3). These matrices provide both traceability and transparency to the technology modeling and auditing process. Using these matrices, a technology design space can be defined. It is important to note that while there are more than 100 inputs into EDS for this study, each input can be labeled as either a "technology" or "cycle" variable. The majority of inputs fall into the "technology" category. These variables are set as a function of the technology package that has been selected. Furthermore, the "technology" inputs are for the most part invariant with respect to the chosen engine cycle. In order to apply a technology package the correct input vector must be selected using the TIM and TCM tables.

3.3.2.1.1.2 Cycle Design Space

The cycle design space is defined through the inputs that fall into the "cycle" category. These are design variables such as engine FPR and OPR. Ranges are established for these variables by understanding historical trends, other published studies, and assessment of current industry capabilities. The significant cycle parameters were determined to be bypass ratio (BPR), overall pressure ratio (OPR), maximum turbine inlet temperature, gear ratio, and extraction ratio. Due to the nature of gas turbine thermodynamics there exists an optimum fan pressure ratio for a given jet velocity ratio. The jet velocity ratio is defined as the ratio of the core nozzle jet velocity divided by the bypass nozzle jet velocity [Guha 2001]. Effectively the engine cycle designer may chose two of the three design variables of FPR, BPR, or jet velocity ratio. The third will be a resulting fallout of the cycle. For simplicity of calculation the EDS environment has been set up to take in FPR and extraction ratio with BPR as a resulting calculated parameter. Extraction ratio, defined as the ratio of the total pressure of the bypass stream relative to the core stream, is representative of the total potential energy in the two streams. Since jet velocity ratio is also indicative of the energy in the two streams, the two parameters may be used interchangeably in engine design. The benefit allowing the BPR to be calculated is that the resulting engine will be near-optimal with additional fine tuning allowed by the use of extraction ratio. If the designer were to input FPR and BPR it would be far easier to select designs that are far from the optimum FPR-BPR relationship and as a result many analysis runs would be wasted.

Over the last few decades there has been an increase in the OPR of in-production engines [Young 2002]. This upward trend has been driven primarily by improvements in material

temperature limits in the compressor and turbine, improvements in compressor performance, as well as improvements in turbine blade cooling technology. With a higher OPR, there is an increase in thermal efficiency and corresponding reduction in TSFC and fuel burn, which is a driving motivation for this study. The current 2010 maximum OPR is around 45; this is the value used for the RTC geared turbofan cycles. As a guideline, the anticipated OPR for the 2025 N+2 simulations could range from conservative estimates of approximately 45 to more aggressive values closer to 60 [Hall 2007]. However, the choice of the optimal OPR depends on the technologies integrated into the engine. Cost and risk may also enter into the choice of OPR; however, neither metric is considered in this report.

OPR is a function of the fan, LPC, and HPC pressure ratios. To increase propulsive efficiency, the BPR on next generation engines needs to increase. As a result, the FPR must be continuously lowered to maintain optimum propulsive efficiency, with some estimates of pressure ratio as low as 1.25 [Guha 2001]. Given the potentially lower FPR, higher values of OPR will be realized through higher pressure ratio LPC and/or HPC.

Similar to OPR, T4 has increased over past few decades from values of 2950R in the 1970s to around 3450R on a GE90 [Young 2002]. The primary enablers for this have been the development of high temperature materials and improved cooling techniques which allow higher T4 without incurring a large penalty in system TSFC because of an increase in required turbine cooling flows. As the design T4 becomes higher, assuming required cooling flows remain constant, the TSFC can be reduced. However as either OPR or T4 increase, assuming constant metal temperature, the required turbine cooling flow to maintain the metal temperature has to also increase which has a negative impact on TSFC. Further improvements in turbine materials such as CMC or cooling technology may enable T4 up to potentially 3950R [Young 2002] without incurring significant cooling flow penalties. However, because of the likelihood of a high OPR design, the maximum T4 considered in the N+2 timeframe may be more conservative.

Since the gear is a fairly new technology for turbofan applications, there is not a large historical database to understand trends in gear ratio. Using current industry trends as well as similar studies [Kurzke 2009] the gear ratio design space was chosen to range from 2.25 to 3.0. Similarly, the design space for extraction ratio was quantified using similar studies. Previous studies by NASA assumed a value of 1.25 [Guyann 2009], although this number may result in too large of an engine for the LTA class. However to capture potential interactions with other cycle parameters, the design space of extraction ratio was chosen to vary around this point. The cycle design space explored for this study is defined by the variables in Table 19.

Table 19. Engine Cycle Design Space for All Technology Cycle Selection Study

Variable	Min	Max
FPR	1.25	1.55
LPCPR	1.35	1.6875
HPCPR	23	30
GearRatio	2.25	3.00
Max T4, R	3300	3600
Extraction Ratio	1.1	1.3

3.3.2.1.1.3 Anticipated Trends

One of the benefits of using surrogate models is the ability to generate partial derivative information of each response relative to the design inputs. The resulting partial derivative space

for the cycle optimization DOE is shown in Figure 7. Running across the bottom of Figure 7 are the engine cycle design parameter from Table 19, and running up the y-axis are the response variables of interest: fuel burn, noise margin, maximum T3, and fan diameter. Recall that T3 and fan diameter are constraints on the design space. At the intersection of each response and independent variable lies a box which contains the partial derivative of a given response relative to a given input design variable. For example, noise margin decreases linearly with FPR increases.

Immediately apparent by examining Figure 7 is that FPR is the largest driver on both the objective metrics and the constraints. Decreasing FPR increases fuel burn and reduces noise (via increased noise margin). This effect is due to the correlation between FPR and BPR. Increasing BPR reduces the jet velocity and reduces noise. Increasing BPR also increases propulsive efficiency which reduces TSFC; however, as BPR increases the nacelle size and engine weight also grow, which creates a second order effect as seen in the FPR vs. fuel burn relationship in Figure 7. The increased weight and drag outweigh TSFC gains. One can see increasing OPR helps to offset the fuel burn increases from decreasing FPR too far. As LPCPR or HPCPR increase the engine OPR will also increase. Increases in OPR will increase engine TSFC due to increased thermal efficiency. An extremely important secondary effect is the increase in core specific power that is enabled by higher OPR engines. By making the core more thermally efficient, it can provide similar power output with less flow. Flow is a primary driver on both size and weight in the core. Smaller cores will reduce the overall engine size for a given fan diameter. The end effect will be the shift in the FPR vs. fuel burn 'bucket' to the area of lower FPR; thereby enabling further noise and fuel burn reductions

Relative to pressure ratios, T4, gear ratio, and extraction ratio have smaller derivatives relative to the responses. In general to obtain lower fuel burn, T4, gear ratio, and extraction ratio would tend to the upper end of the design space. T4 does not have any noticeable effect on noise margin. In fact T4 is a secondary driver on thermal efficiency.

Although cycles with high OPR and BPR are generally desired, not all of the cycles in the design space are feasible because of violation of certain constraints. Cycles which have a T3 that exceeds the maximum temperature capability of the materials in the HPC would result in a drastic reduction in the useful life of the engine. Increasing the pressure ratio of the engine via an increase in FPR, LPCPR, or HPCPR will result in an increase in the maximum cycle T3. Additionally, for tube and wing aircraft engines having diameters much larger than the wing clearance would result in significant potential system redesign at significant cost and risk. Thus cycles that violate either of these constraints would be considered infeasible. These are only two of many potential design constraints and are used to illustrate how constraints effect the resultant optimal cycle

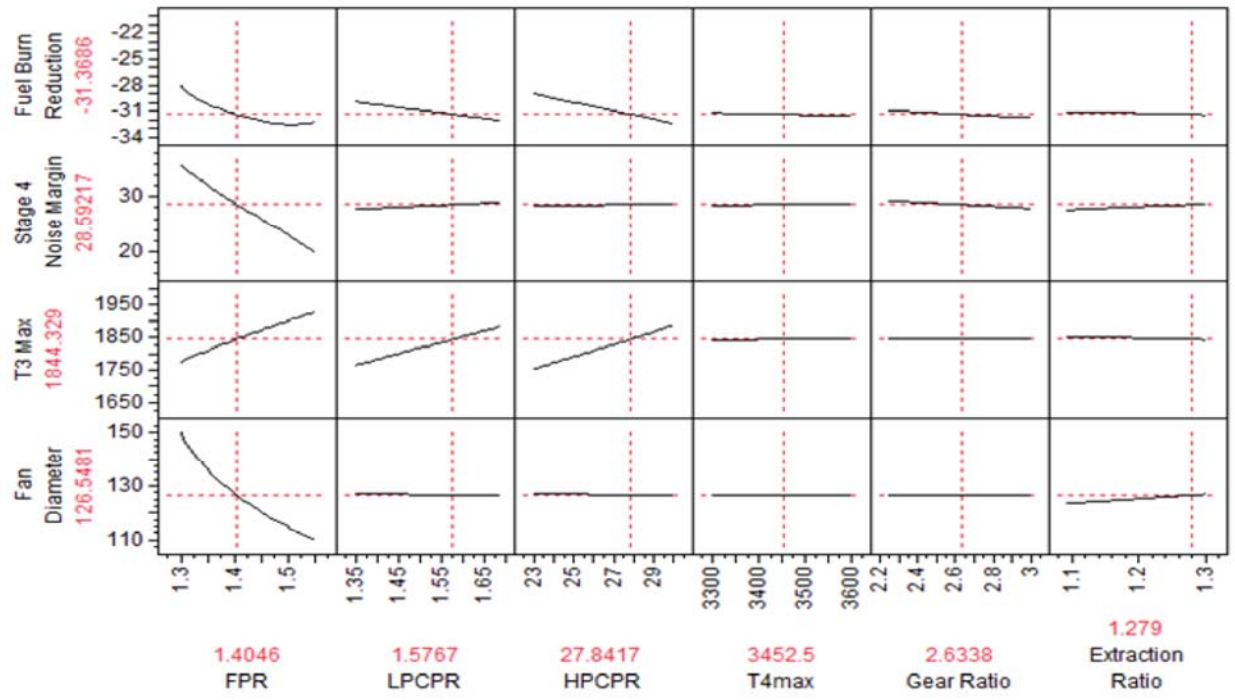

Figure 7. Cycle Optimization Trends

3.3.2.1.1.4 Cycle Optimization using EDS

EDS was used to directly simulate 300 sample engine cycles. While this is a somewhat time intensive process relative to using surrogate models, the purpose is to provide a secondary validation of the surrogate model results. The results of the cycle simulations in Figure 8 will be subsequently compared to the results of the exact same study using surrogate models in place of EDS, shown in Figure 9. The EDS results of the 300 case DOE are shown in Figure 8 with fuel burn plotted against noise margin for each case. Each point in Figure 8 represents a set of engine cycle settings. All of the points in Figure 8 have the same technology package applied. In other words, only the engine cycle variables in Table 19 differ between the points. The points highlighted in blue violate the somewhat arbitrary fan diameter constraint of 130 in. which is similar to the diameter of a GE90. The points highlighted in red violate the maximum T3 limit of 1850R, which is the limit of advanced PM disk materials. Given these constraints, the cycle which best optimizes both fuel burn and noise margin has been highlighted as the "Best Constrained" point on Figure 8. Certain aircraft configurations such as an over the wing nacelle may not have as strict a fan diameter constraint as a traditional wing mounted nacelle. The resultant engine cycle used on these aircraft could potentially be different and is highlighted as the "Best T3 Constrained" on Figure 8. Relative to the "Best Constrained" cycle, this cycle has a significant increase in the noise margin with minimal fuel burn penalty. For reference, a "Best Unconstrained" point is highlighted also. That point is selected by picking the point that has the largest noise margin value and whose fuel burn is within about 1% of the minimum fuel burn case.

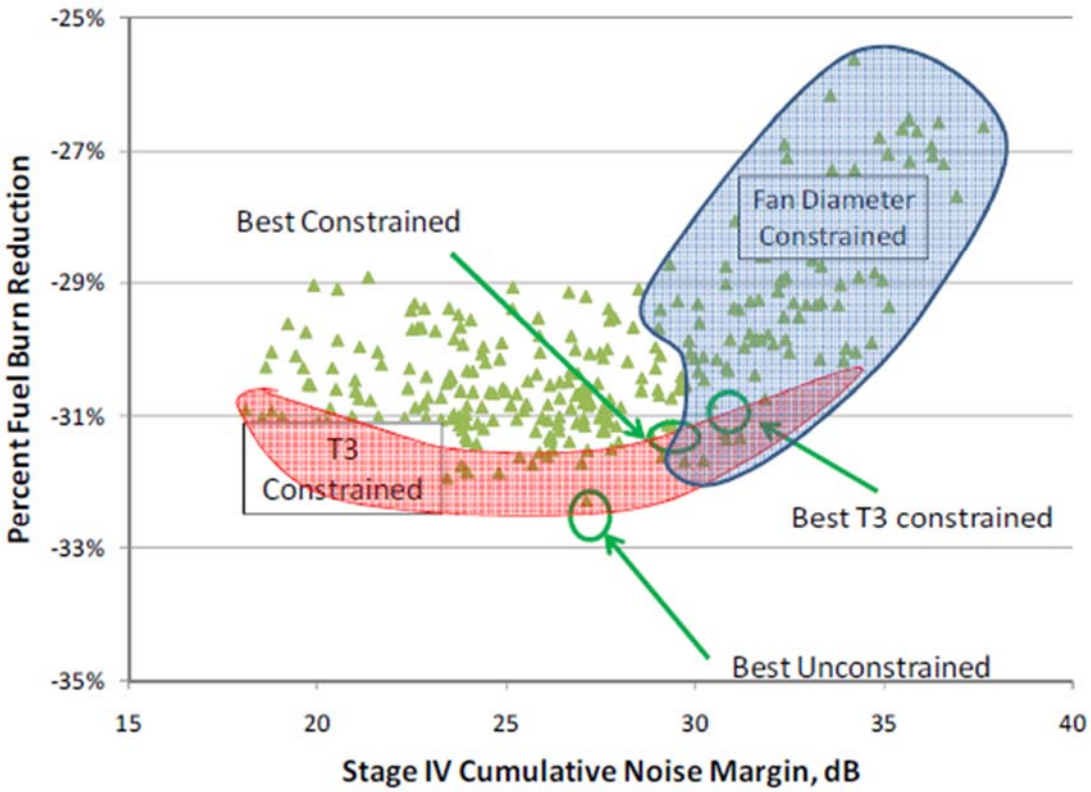

Figure 8. Constrained Cycle Design Space Using EDS

3.3.2.1.1.5 Cycle Optimization using Surrogate Models

Figure 9 below shows the constrained design space for running the 300 case DOE using the surrogate models to analyze the design space. The feasible design space for the surrogate runs has a similar shape as that of the EDS runs. Similar to the EDS DOE runs, the "Best Constrained", "Best T3 Constrained", and "Best Unconstrained" cases were selected as highlighted on Figure 9.

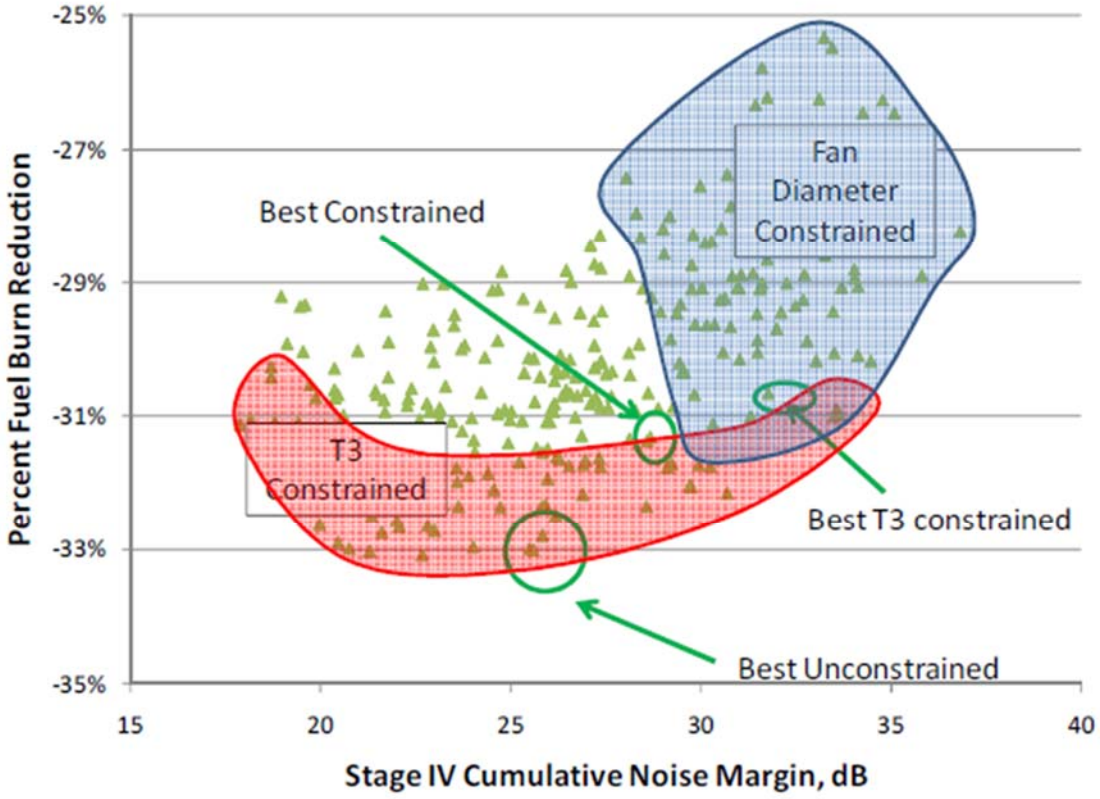

Figure 9. Constrained Cycle Design Space Using Surrogate Models

3.3.2.1.1.6 Cycle Optimization Comparison

Table 20 compares the chosen cycles using each method and calculates the difference between the cycle inputs and estimated outputs. The selected "Best Compromise" and "Best T3 Constrained" cycle is the same DOE case using both models. The "Best Constrained Case" picked a different optimal cycle. For the two constrained cases the difference in the resultant fuel burn, OPR, and BPR estimates between the EDS and surrogate model are within 1%. The noise margin estimates were within 0.6 dB. The resultant optimal cycle chosen in an unconstrained design space, however, differs. All metrics are within 10% of each other, but relative to the EDS results, the differences are large. This is because the optimal solution is at the edge of the design space explored with the surrogate models. These results validate that a surrogate model can be used to make fairly accurate estimates of the optimal engine cycle for a constrained design space. However, the surrogate model approach can only be used to make order of magnitude estimates if the resulting cycle is at the edge of the design space.

Table 20. EDS and Surrogate Model Cycle Optimization Comparison

		Best Constrained			Best T3 Constrained			Best Unconstrained		
		EDS	Surr	Diff	EDS	Surr	Diff	EDS	Surr	Diff
Input	FPR	1.4	1.4	0.0%	1.36	1.36	0.0%	1.43	1.45	1.4%
	LPCPR	1.58	1.58	0.0%	1.52	1.52	0.0%	1.52	1.67	9.9%
	HPCPR	27.8	27.8	0.0%	29.6	29.6	0.0%	30	28.5	-5.0%
	T4max, R	3552	3552	0.0%	3543	3543	0.0%	3450	3533	2.4%
	Gear Ratio	2.63	2.63	0.0%	2.78	2.78	0.0%	2.63	2.95	12.2%
	Extraction Ratio	1.28	1.28	0.0%	1.25	1.25	0.0%	1.2	1.19	-0.8%
Output	Fuel Burn Reduction	31.1%	31.4%	-0.2%	30.7%	31.0%	0.3%	32.3%	33.0%	0.7%
	Noise Margin, dB	29.2	28.6	0.6 dB	31.8	31.3	0.5 dB	27.1	25.5	1.6 dB
	SLS BPR	16.3	16.4	0.6%	19.7	19.9	1.0%	14.7	14.2	-3.4%
	SLS OPR	55.1	55.2	0.2%	52.7	52.5	-0.4%	59.5	63.9	7.4%

3.3.2.1.1.7 Technology Package Evaluation

Using the same surrogate models, the optimal cycles for different technology packages can be quickly selected. Using only 300 cases, the resultant fuel burn and noise margin design space shown in Figure 8 and Figure 9 are sparsely populated. The surrogate models allow for a larger DOE, which will better populate the design space, with minimal additional CPU burden. To demonstrate this capability, the surrogate models were used to optimize the cycle for three different technology packages. The first technology package is the RTC. The second technology package is a subset of the N+2 technology package used in the validation cases. The third package augments the N+2 technology package with an intercooler between the LPC and HPC. In addition to increasing the specific power of the engine core, an intercooler has the potential of allowing significantly higher OPR engine cycles without having to drastically increase the temperature capability of the materials.

3.3.2.1.1.8 RTC Evaluation

The results for the RTC package are shown in Figure 10. The feasible design space for the RTC is drastically smaller than that of the N+2 technology package, discussed subsequently and shown in Figure 11. This is due to the maximum allowable T3 of only 1750R, thereby significantly increasing the T3 constrained area. Similar to the validation cases, a “Best Constrained”, “Best T3 Constrained”, and “Best Unconstrained” case are selected.

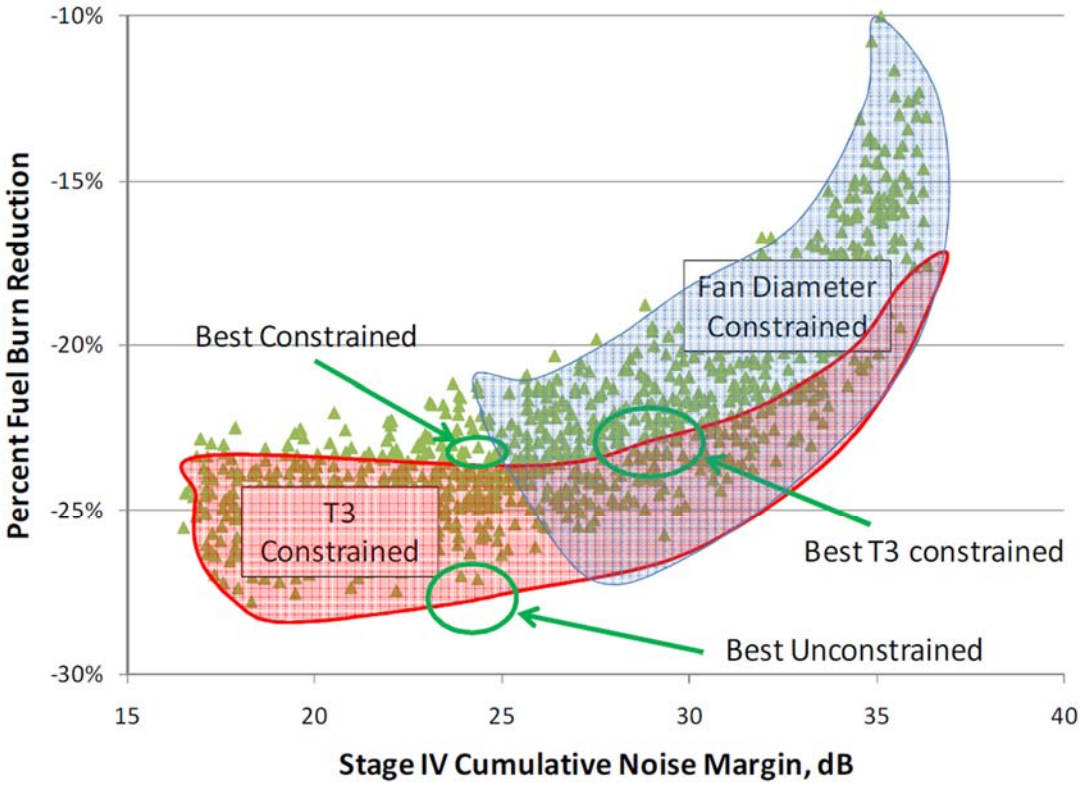

Figure 10. Constrained Cycle Design Space for RTC

The three highlighted cycles have been summarized in Table 21. Both the T3 constrained cycles have SLS OPR values of 45 whereas the unconstrained cycle has a SLS OPR of 65 and a 6% lower fuel burn relative to the constrained cycles. This highlights the need for technologies that enable higher OPRs. The "Best T3 Constrained" cycle has a lower FPR and higher BPR than the "Best Constrained" cycle with an almost a 5 dB increase in noise margin. This highlights that going to different aircraft configurations or investing in technologies that shift the fan constraint may enable significantly lower FPR cycles with drastic increase in noise margin.

Table 21. Cycle Selection for RTC

		Best Constrained	Best T3 Constrained	Best Unconstrained
Inputs	FPR	1.42	1.33	1.43
	LPCPR	1.401	1.36	1.67
	HPCPR	25.03	29.3	29.8
	T4max, R	3438	3529	3454
	Gear Ratio	2.75	2.78	2.89
	Extraction Ratio	1.23	1.29	1.23
Outputs	Fuel Burn Reduction	-22.50%	-22.70%	-27.10%
	Noise Margin, dB	24.2	29.7	24.3
	SLS BPR	15.6	21.5	13.9
	SLS OPR	45.5	45	64.9

3.3.2.1.1.9 N+2 Technology Package

Using the same surrogate model as was used in the last section, an N+2 level technology package can be evaluated. Figure 11 below shows the constrained design space for both the RTC (green triangles) and N+2 (blue diamonds) technology packages. For the same cycle design space, the N+2 design space is shifted down and to the right. The downward shift is largely due to the drag and weight reduction technologies. The rightward shift is a result of the inclusion of the noise technologies. The design points constrained by the fan diameter and T3 constraints are highlighted in blue and red, respectively. The feasible design space for the N+2 technology package is significantly larger than the RTC package. The T3 constraint shifted downwards because of the increase temperature materials in the HPC. The fan diameter constraint shifted to the right because of incorporation of weight and drag reduction technologies which reduce the thrust requirement for the engine. The reduced thrust engine enables a lower FPR engine to meet the engine diameter requirement.

As done in the previous sections, “Best Constrained”, “Best T3 Constrained” and “Best Unconstrained” cycles have been identified and are shown in Table 22. To capture the benefits of cycle optimization, the cycles chosen in Table 21 were run for the N+2 technology package. The results of these cycle runs are labeled as RTC Cycle in the table. Assuming the cycle remains constant when moving from a RTC to N+2 technology package, the N+2 “Best Constrained” technology package results in approximately a 7% reduction in fuel burn and a 2.5 dB increase in noise margin relative to the RTC “Best Constrained” technology package. Further optimization of the cycle enables an additional 2.8% reduction in fuel burn and a 3 dB increase in noise margin. The fuel burn reduction is primarily a result of the increase in OPR while the noise margin increase is a result of a lower FPR. Similar trends can be seen for the “Best T3 Constrained” case. One observation noted is that the “Best T3 Constrained” cycle for the N+2 technology package has an OPR of only 53. Because of how the DOE was setup combinations of high OPR and low FPR would require extrapolation of the surrogate model and were not explored.

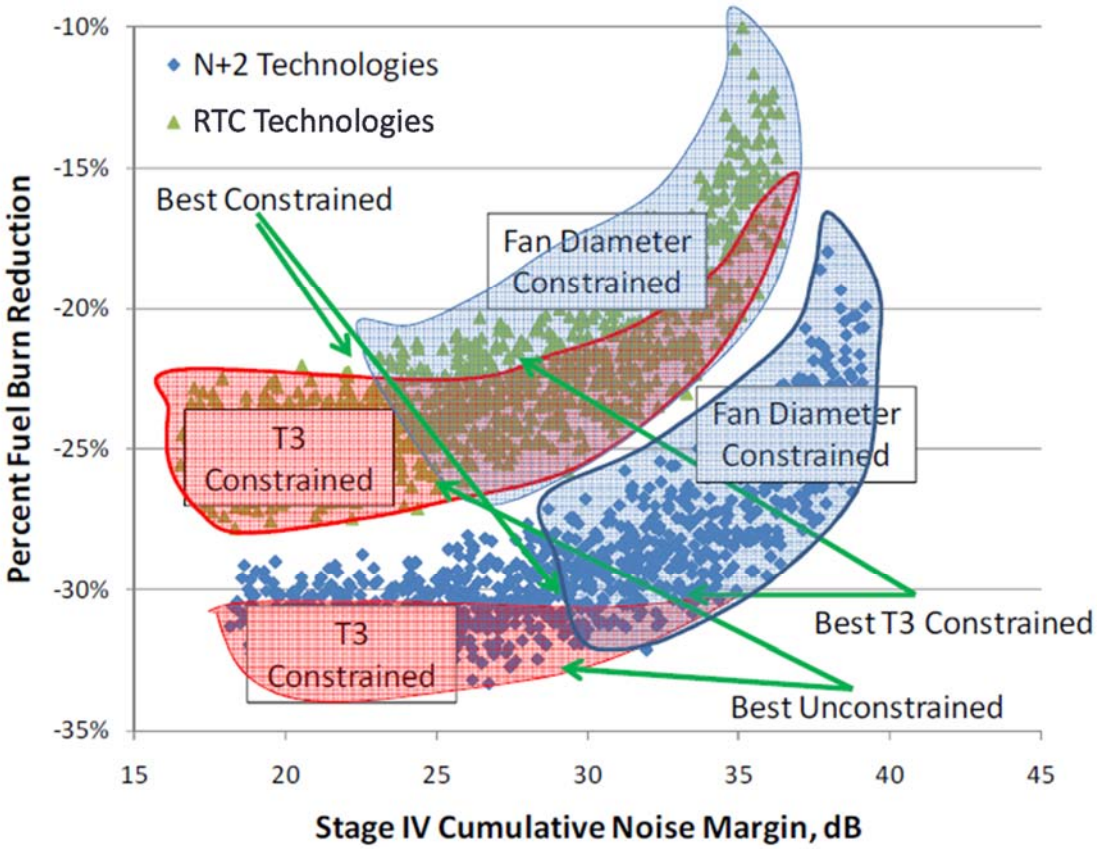

Figure 11. Constrained Cycle Design Space for N+2 Technology Package

Table 22. Cycle Selection for N+2 Technology Package

		Best Constrained		Best T3 Constrained		Best Unconstrained	
		RTC Cycle	N+2 Cycle	RTC Cycle	N+2 Cycle	RTC Cycle	N+2 Cycle
Inputs	FPR	1.42	1.38	1.33	1.33	1.43	1.43
	LPCPR	1.401	1.68	1.36	1.57	1.67	1.67
	HPCPR	25.03	26.6	29.3	29.8	29.8	29.8
	T4max, R	3438	3415	3529	3487	3454	3454
	Gear Ratio	2.75	2.86	2.78	2.75	2.89	2.89
	Extraction Ratio	1.23	1.28	1.29	1.18	1.23	1.23
Outputs	Fuel Burn Reduction	-29.2%	-31.2%	-29.3%	-30.5%	-33.3%	-33.3%
	Noise Margin, dB	26.6	29.7	32.2	28.3	26.7	26.7
	SLS BPR	15.9	17.1	21.8	16.5	14.24	14.24
	SLS OPR	45.7	54.4	45.2	53.3	65.2	65.2

3.3.2.1.1.10 N+2 Technolgy Package with Intercooler

As shown in the previous sections, as OPR increases, fuel burn decreases. Unfortunately, the maximum potential increase in OPR is constrained by the temperature limits of the materials in the HPC. An intercooler, which is a heat exchanger using fan bypass air to cool the core airflow between the LPC and HPC, is a technology which enables a further increase in OPR without requiring a further increase in material temperature capability. There are, however, significant performance issues related to the intercooler such as potentials for large pressure drops in both the core and bypass streams as well as the heat exchanger weight which is estimated to be on the order of the LPC [Gronstedt 2009].

Using similar assumptions of fan bypass bleed flow, pressure drops, heat exchanger effectiveness, and weights as [Gronstedt 2009], the surrogate model was used to estimate the cycle design space for an N+2 technology package with an intercooler. Figure 12 shows the constrained design space for both the RTC and an N+2 technology package with an intercooler. The T3 constrained space is pushed further down such that except for a few points the T3 constrained space has virtually disappeared. This is a result of the choice of cycle design space and will be discussed later. Relative to the other N+2 technology package, the fan diameter constrained space remains unchanged. Since the explored design space is no longer T3 constrained, there are no "Best Constrained" and "Best T3 Constrained". The "Best Unconstrained" cycle can be chosen using the "Best Compromise" process from earlier sections. Unlike previous sections, the "Best Unconstrained" cycle is now feasible.

Results of this cycle are shown in Table 23 under the "Best Compromise" column. Three other cycles have been selected for comparison: the RTC cycle, the N+2 cycle, and a N+2 intercooled cycle that minimizes fuel burn. The RTC and N+2 cycles are the "Best Compromise" cycles chosen from the analysis in the previous sections. Using the N+2 "Best Compromise" cycle settings, the intercooler offers the potential for only minimal fuel burn benefits. With the RTC "Best Compromise" cycle the integration of an intercooler actually increases the fuel burn. Using the N+2 intercooled "Best Compromise" cycle, there is a potential for a 2.3% fuel burn reduction. This fuel burn gain is offset by a 2.3 dB reduction in noise margin. The "Best Fuel Burn" cycle offers a further 1% fuel burn reduction with an additional 3 dB reduction in noise margin.

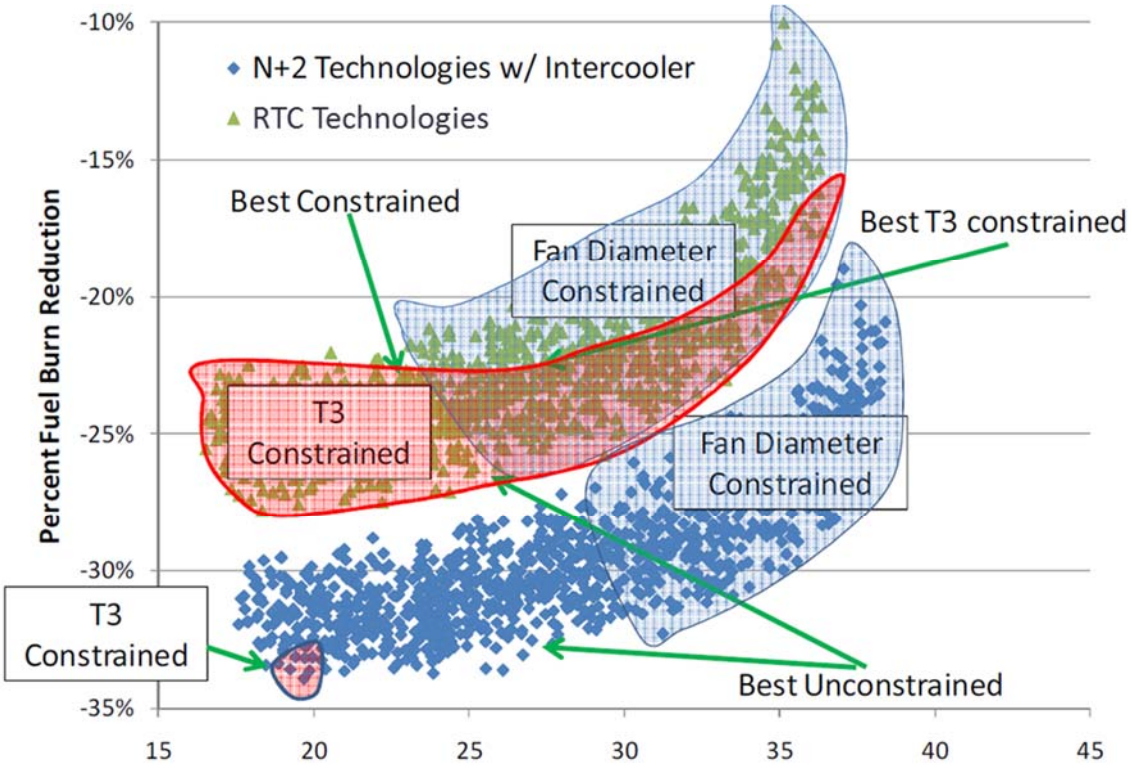

Figure 12. Constrained Design Space for N+2 Technology Package with Intercooler

As noted throughout the paper, the highest OPR cycles resulted in the best fuel burn. The "Best Compromise" intercooled cycle only had an OPR of only 60 because the chosen design space used to train the surrogate models did not include cycles with OPR much greater than 60 for which values of FPR was less than 1.5. The T3 for this case was only 1700F which indicates there is significant margin available to increase OPR before the maximum T3 constraint is hit. The surrogate model can be used to estimate potential performance of the cycle in these high OPR and low FPR regions; however, since the model was not trained on data in that region, caution must be taken with the extrapolated results, especially if the trends are significantly different than expected. Two points were estimated to see if there is potential to obtain significant fuel burn reduction from the higher OPR without the large noise penalty incurred from selecting a higher FPR cycle. Using cycle chosen for the N+2 "Best Fuel Burn", the FPR was lowered to 1.38 and the LPCPR was increased to maintain OPR. When this case was run using the surrogate model, the fuel burn estimates were on the same order as the N+2 intercooled "Best Compromise" case with the noise margin estimates similar to the case with FPR equal to 1.38. The next cycle estimated assumed a FPR equal to 1.38, but raised the LPCPR to obtain an OPR on the order of 75. In this case, the surrogate estimated that there was potential for a further 3% fuel burn reduction from operating at OPR around 75. To validate, these claims, the "Low FPR Extrapolated" and "Low FPR/High OPR Extrapolated" case were run through EDS. For these two cases, the difference in fuel burn estimates between EDS and the surrogates were within 0.5%. EDS also estimated that the fuel burn difference between these two cycles was about 2.5%, thus validating that the surrogate models can be used to make cycle estimates outside of the region for which they were trained. An interesting observation is that the T3 for both these cases remained around 1700 F. This is because as the

LPCPR is increased, the temperature difference in the intercooler becomes larger, increasing heat transfer, and resulting in the core temperature exiting the intercooler to remain approximately constant. If HPCPR is constant, the higher OPR from an increase in LPCPR will not increase the cycle T3 significantly whereas T3 increases proportionally to increases in HPCPR assuming everything else is fixed. Thus for intercooled cycles with the same FPR, a cycle with a larger LPCPR will enable a cycle with a larger OPR and in turn more potential fuel burn benefit than a cycle with a larger HPCPR. This indicates that for an intercooled cycle, larger values LPCPR instead of HPCPR are desired. As the cycle moves to higher values of OPR by increasing LPCPR, minimum HPC size, not maximum T3, may be the OPR limiting constraint. For smaller thrust class engines, the minimum HPC size constraint may limit the maximum OPR of intercooled cycles to be much lower than values shown in this study thus limiting the intercooler potential.

Table 23. Cycle Selection for N+2 Technology Package with Intercooler

		RTC Cycle	N+2 Cycle	Best Compromise	Best Fuel Burn	Low FPR Extrapolated	Low FPR and High OPR Extrapolated
Inputs	FPR	1.42	1.38	1.42	1.47	1.38	1.38
	LPCPR	1.40	1.68	1.67	1.68	1.79	2.13
	HPCPR	25.03	26.6	28.8	29.5	29.5	29.5
	T4max, R	3438	3415	3362	3582	3582	3582
	Gear Ratio	2.75	2.86	2.95	2.62	2.62	2.62
	Extraction Ratio	1.23	1.28	1.27	1.19	1.19	1.19
Outputs	Fuel Burn Reduction	-29.3%	-31.4%	-33.1%	-33.7%	-33.1%	-35.3%
	Noise Margin, dB	25.9	29.0	26.7	23.9	30.1	31.3
	SLS BPR	17.2	19.8	16.76	15.3	21.3	22
	SLS OPR	44.3	52.7	60.0	67.1	62.4	74.0

3.3.2.1.2 ITD Technology Portfolio on LTA HWB

This second cycle selection study was performed to understand the impact of FPR on fuel burn and noise for the geared fan installed on a LTA HWB. The technology portfolio used for the study was the ITD portion of the ERA portfolio. The following parameters were varied for this study to capture uncertainties around the geared fan; FPR, extraction ratio to vary the BPR, FCDO to capture uncertainty from nacelle and installation drag and inlet/nacelle material density to capture uncertainty in nacelle weight. The maximum and minimum value of each of the parameters is listed in Table 24. Several graphs were constructed to display the sensitivity of fuel burn and noise as each of the variables was parametrically varied.

Table 24. Sensitivity Variables for Geared Fan Pressure Ratio Study

Variable	Min	Max
FPR	1.3	1.5
Extraction Ratio	1.05	1.45
FCDO	0.99	1.03
Inlet/Nacelle Density	0.1	0.5

Figure 13 shows fuel burn vs noise with the different FPR values highlighted (only values of 1.3, 1.35, 1.4, 1.45 and 1.5 were used). This graph shows that the minimum fuel burn occurs at a FPR of 1.45 for the study. A reduction in noise of 7dB could be achieved by lowering the FPR to 1.3, but this would be at the expense of a fuel burn increase of 2.75%.

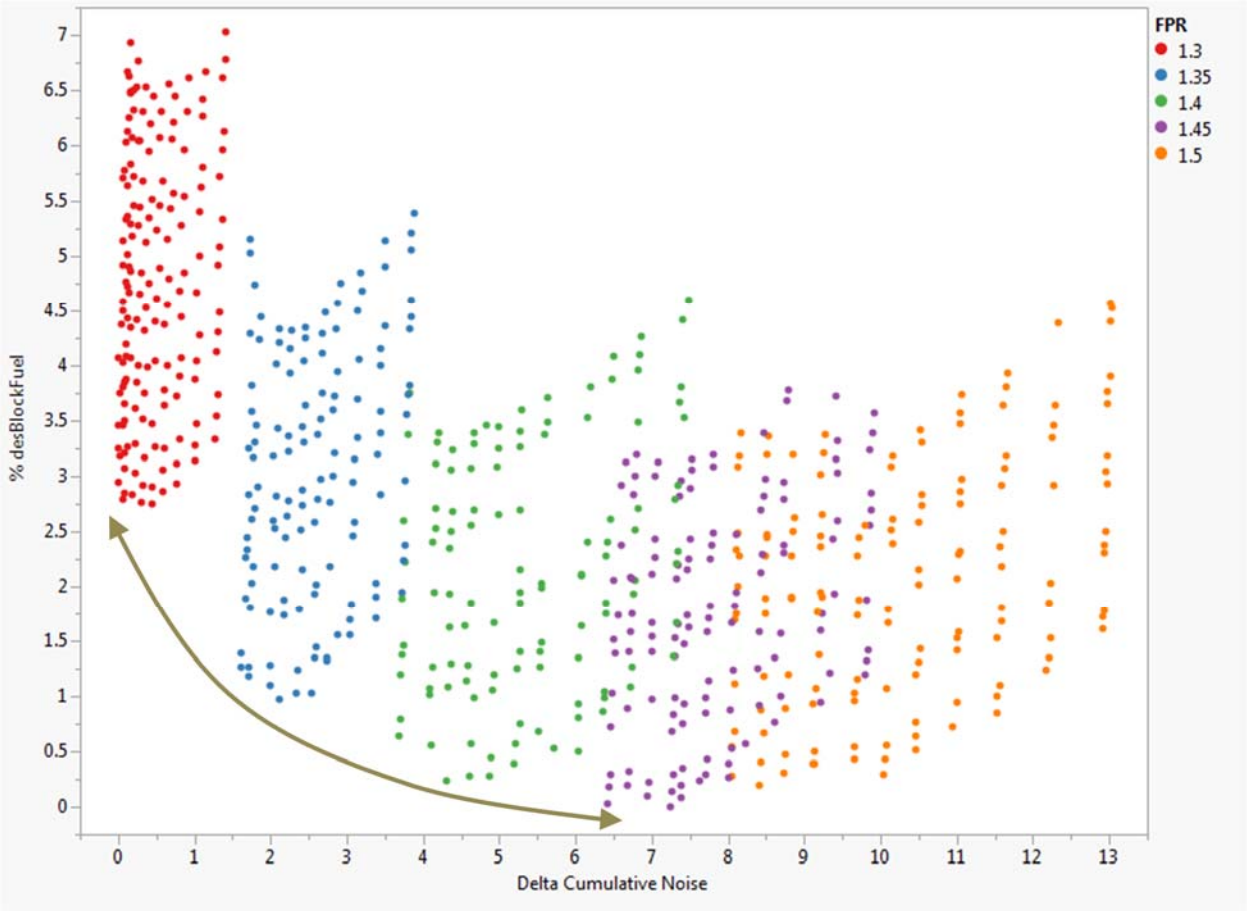

Figure 13. Fuel Burn vs. Noise Highlighting FPR Variation

Figure 14 is the same chart of fuel burn vs noise but now with changes to lift-independent drag (FCDO) highlighted. It shows that there is very little impact on noise from changes in drag. There is the expected change in fuel burn of 3-4% from a change in drag from 99% to 103%. The fuel burn is also more sensitive to changes in FCDO as FPR is decreased due to the larger engine and nacelle wetted area that results.

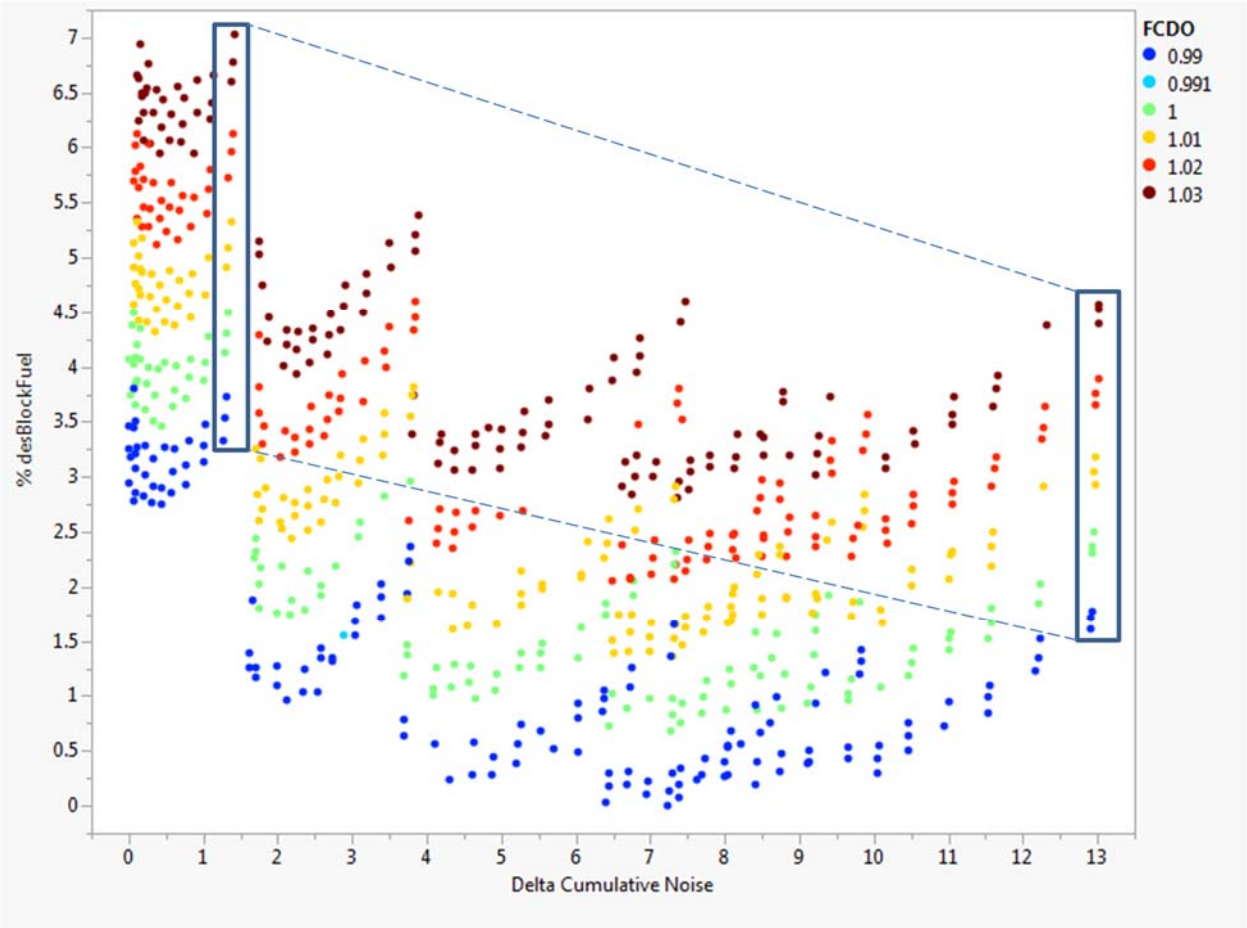

Figure 14. Fuel Burn vs. Noise Highlighting FCDO Variation

Figure 15 is again the same graph of fuel burn vs noise but now with changes in the extraction ratio (ratio of core nozzle to bypass nozzle inlet pressure). From this graph it can be seen that there is an extraction ratio for each FPR that minimizes fuel burn. The impact of extraction ratio on noise is much greater for higher FPR than lower fan pressure ratios from a range of 1.5 dB for a FRP of 1.3 to a range of 5 dB for a FPR of 1.5.

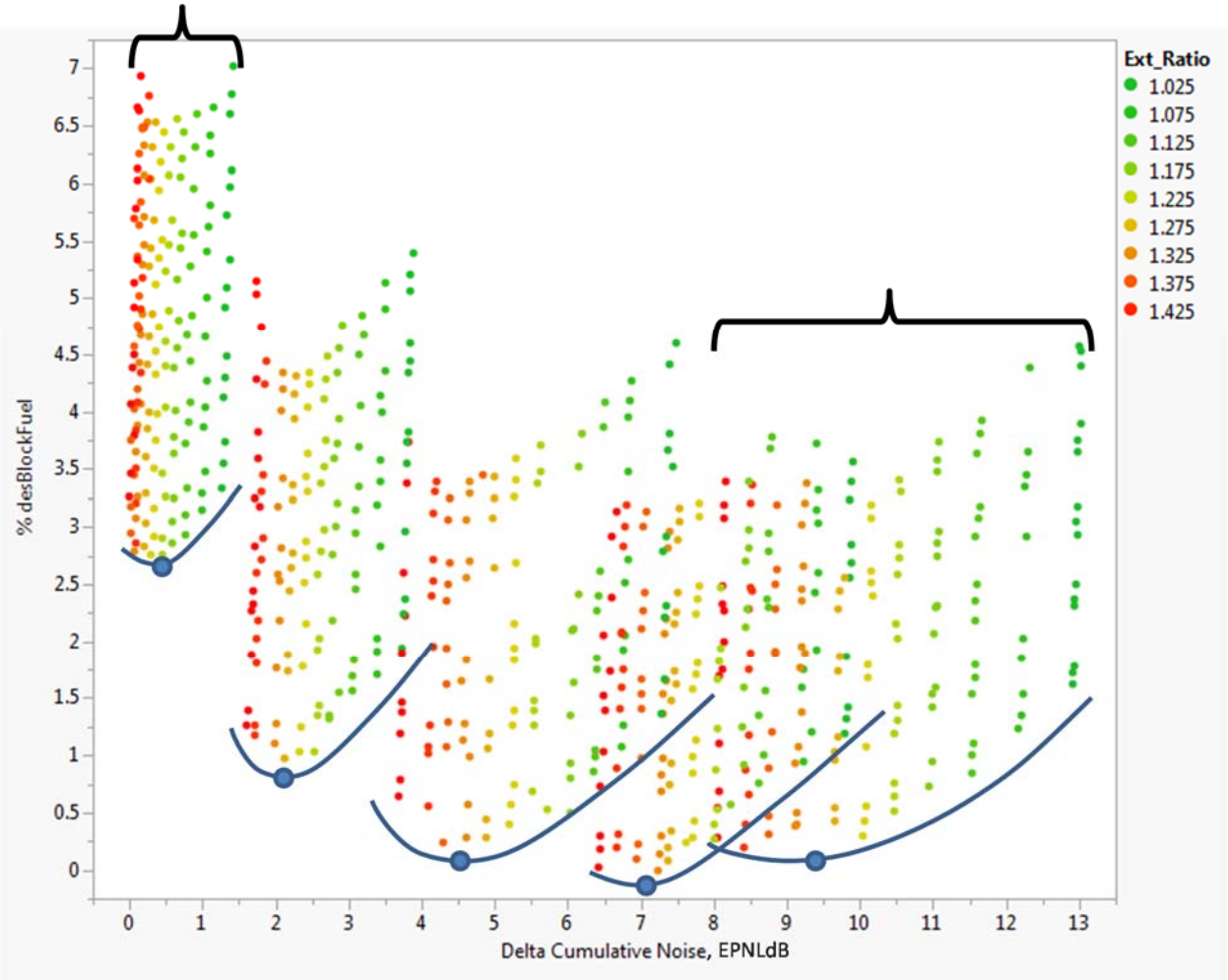

Figure 15. Fuel Burn vs. Noise Highlighting Extraction Ratio Variation

An additional 2000 data points were added with randomly selected FPRs between 1.3 and 1.5 to generate Figure 16. This graph was generated to define the Pareto frontier for fuel burn and noise. It shows that the best FPR is between 1.42 and 1.5 which will achieve a fuel burn with 0.25% of lowest value while minimizing noise.

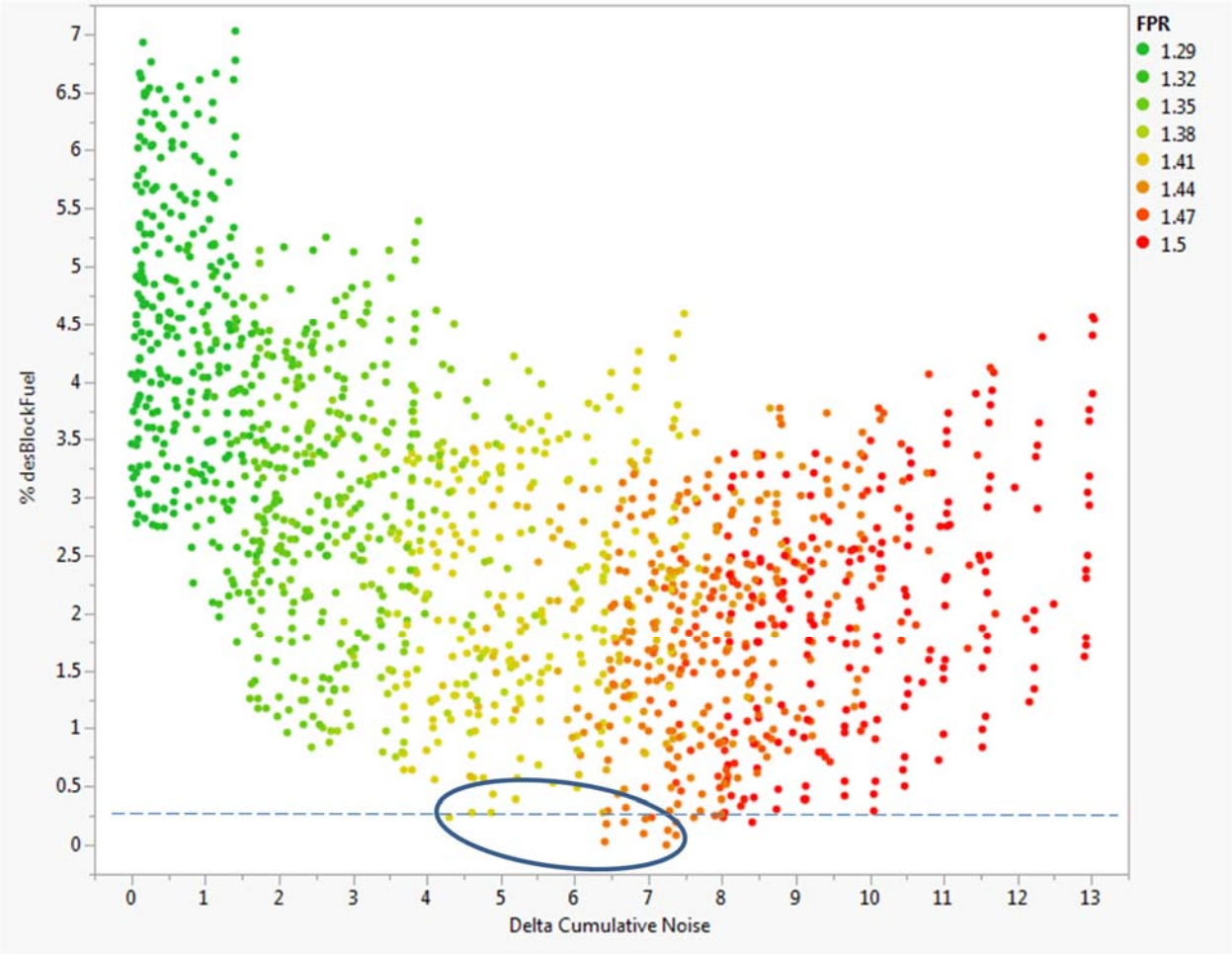

Figure 16. Fuel Burn vs. Noise Pareto Frontier

Figure 17 shows SLS uninstalled thrust vs fan diameter for the same data points in Figure 16. It show that for the geared fan, a fan diameter of around 130 inches will be required for engines generating 60,000 lbf of thrust. This is about half the thrust that would be generated by a similarly sized direct drive engine with today's fan pressure ratios. This points to the possibility that there may be a thrust capability limit where the geared fan is no longer practical. Either the engine would be too large and the drag and weight penalties would overwhelm and TSFC benefits from a lower FPR or the FPR would be raised to the point that the advantages of a geared fan over a direct drive architecture would no longer be applicable.

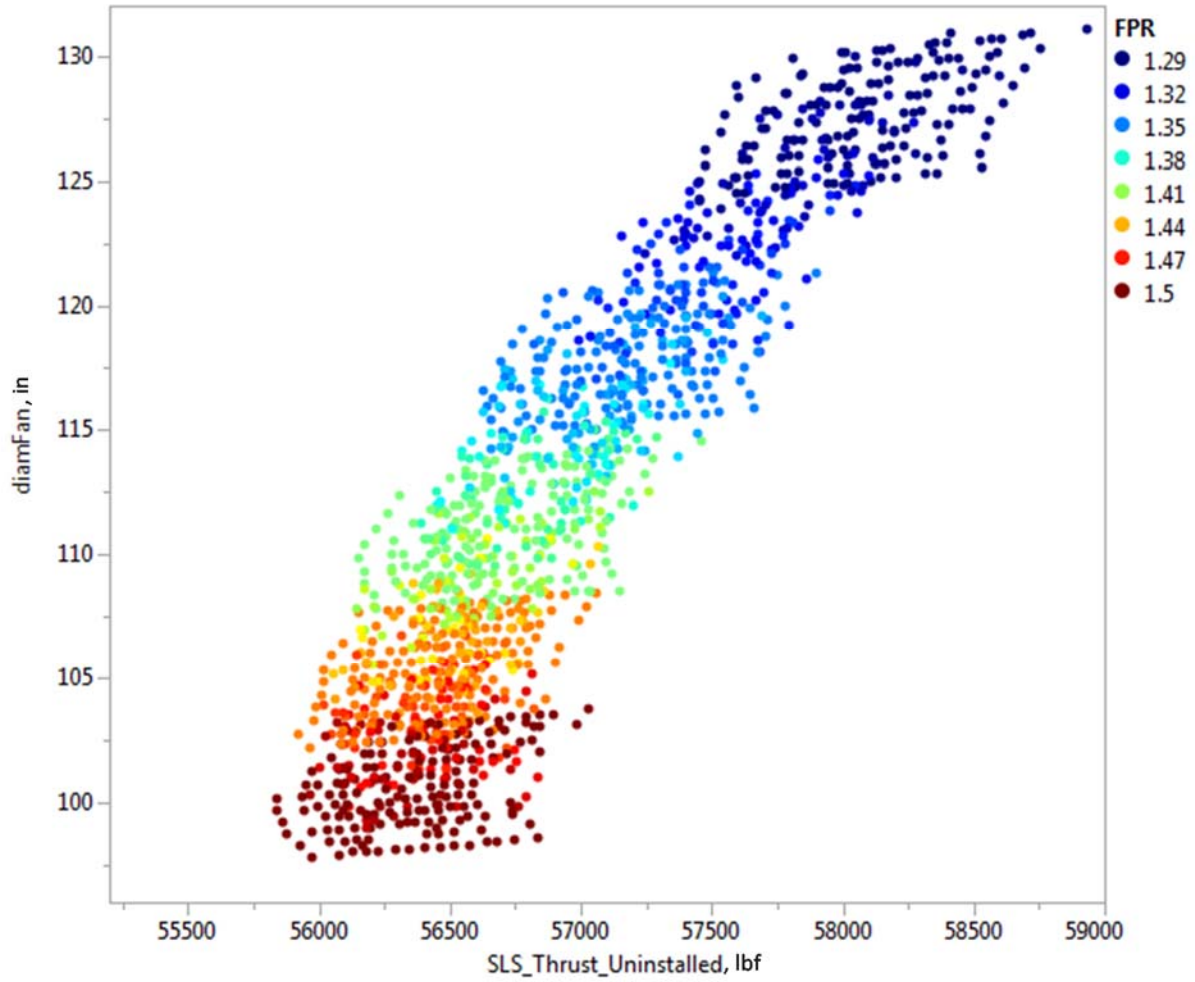

Figure 17. SLS Thrust vs Fan Diameter

The final graph of the study, Figure 18, uses the same data points as the previous two graphs but displays minimum cruise TSFC vs FPR while highlighting fuel burn. It again shows that minimum fuel burn occurs in the FPR range of 1.42-1.45. The lowest TSFC occurs at the lowest FPR, but has a high fuel burn due to increases in engine weight and drag. This demonstrates that ERA's ITD goal of 15% TSFC reduction may be at odds with its overall goal of 50% fuel burn reduction. The TSFC goal may need to be sacrificed in order to achieve the fuel burn goal.

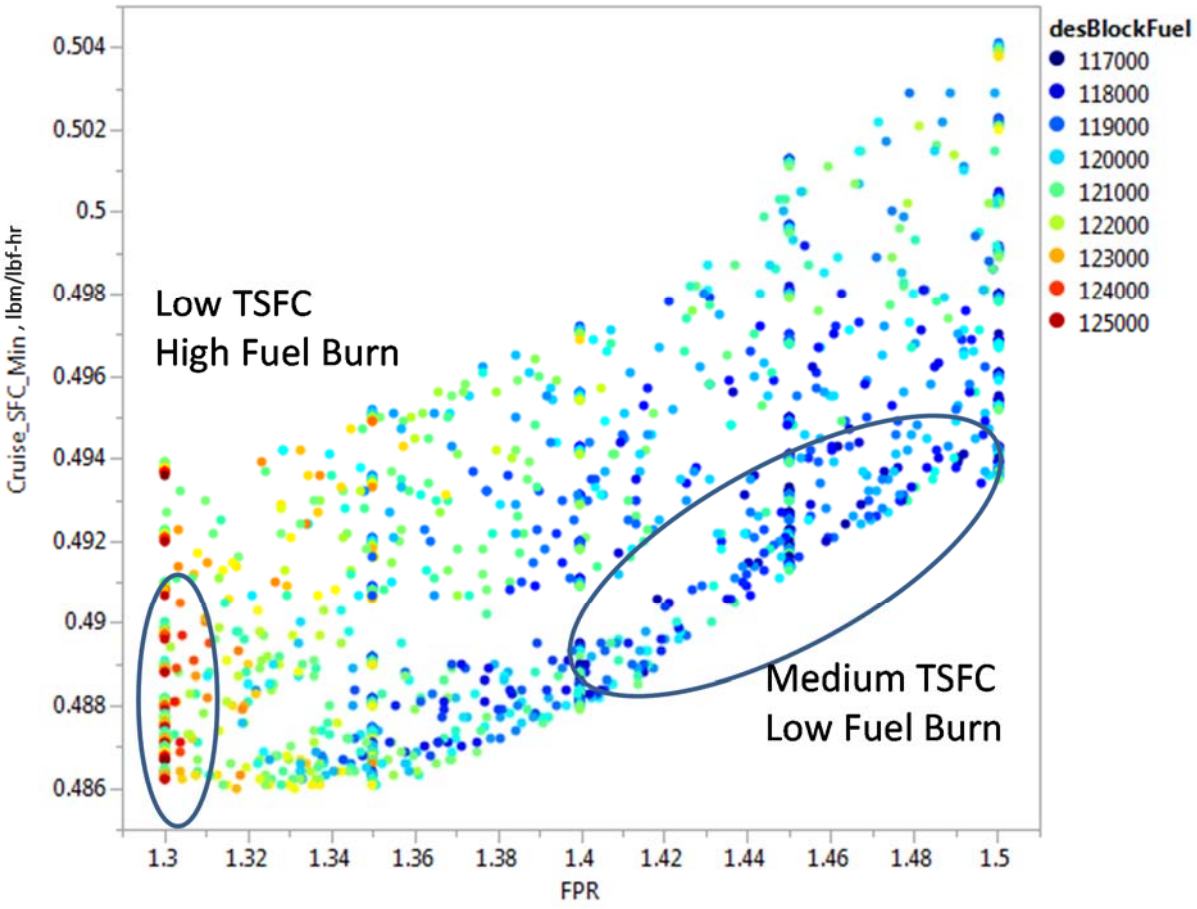

Figure 18. Cruise TSFC vs FPR Highlighting Fuel Burn Variation

3.3.3 Open Rotor

3.3.3.1 Performance Modeling Approach

Modeling the open rotor requires synthesis of public domain data and analysis codes with available modeling data and result to establish a firm baseline configuration. Once a baseline is verified and established, technologies can be applied in the same manner as other engine architectures. The next few sections describe the establishment of a baseline along with major modeling assumptions.

3.3.3.1.1 Overview

The open rotor (GE36) was flight tested in the late 1980's and early 1990's by GE and a wealth of information exists in the detailed design reports that accompanied the demonstration [Hoff 1990, GE Aircraft 1987]. These reports contain detailed information about the open rotor configuration, general performance, and noise characteristics and serve as an important departure point for establishing a baseline for any current study, including the work presented herein. More recent work has sought to fuse a combination of test data and analytically generated engine and airframe performance in order to assess the combined benefits of the integrated engine and airframe system [Guynn 2011, Berton 2011]. These studies offer important insight into the installed benefits of an open rotor architecture, but are tied a specific engine cycle and aircraft configuration. In essence, they are predictive estimates of fixed designs.

Modeling work under this work has focused on modeling the open rotor engine components in significant detail for use in a multidisciplinary environment [Bellocq 2010].The referenced work focuses heavily on the engine and lacks a specific methodology to assess the installed vehicle performance or noise. Nonetheless, Georgia Tech has incorporated many of the engine modeling features and recommendations directly into this assessment. Recent NASA work has also focused on creating parametric models of the open rotor engine architecture [Hendricks 2011], specifically the focus is on multi-design point engine sizing. This work, more than any other, has served as the basis for the open rotor model being developed in EDS.

In order to include the open rotor in EDS' assessment capabilities a development road map was created to identify required modifications to the EDS framework. An overview of the long-term development roadmap for open rotor to be included into EDS is shown in Figure 19 and is discussed below.

The development roadmap to fully address configurations employing open rotor propulsion system starts with the designer defining the initial counter rotating propeller and blade geometry, such as chord and twist distribution along the blade and the number of blades. In this work available performance maps from the F31/A31 test dataset were scaled to modern performance levels. Propeller source noise estimates are generated using NASA's CRPFAN [Whitfield 1990]. The predicted propeller noise sources are then passed to an aircraft noise prediction and propagation program, such as NASA's Aircraft Noise Prediction Program (ANOPP) [Zorumski 1982]. The aircraft noise prediction program will need to combine the propeller, engine, and aircraft noise sources and propagate them to compute noise levels at the three certification points.

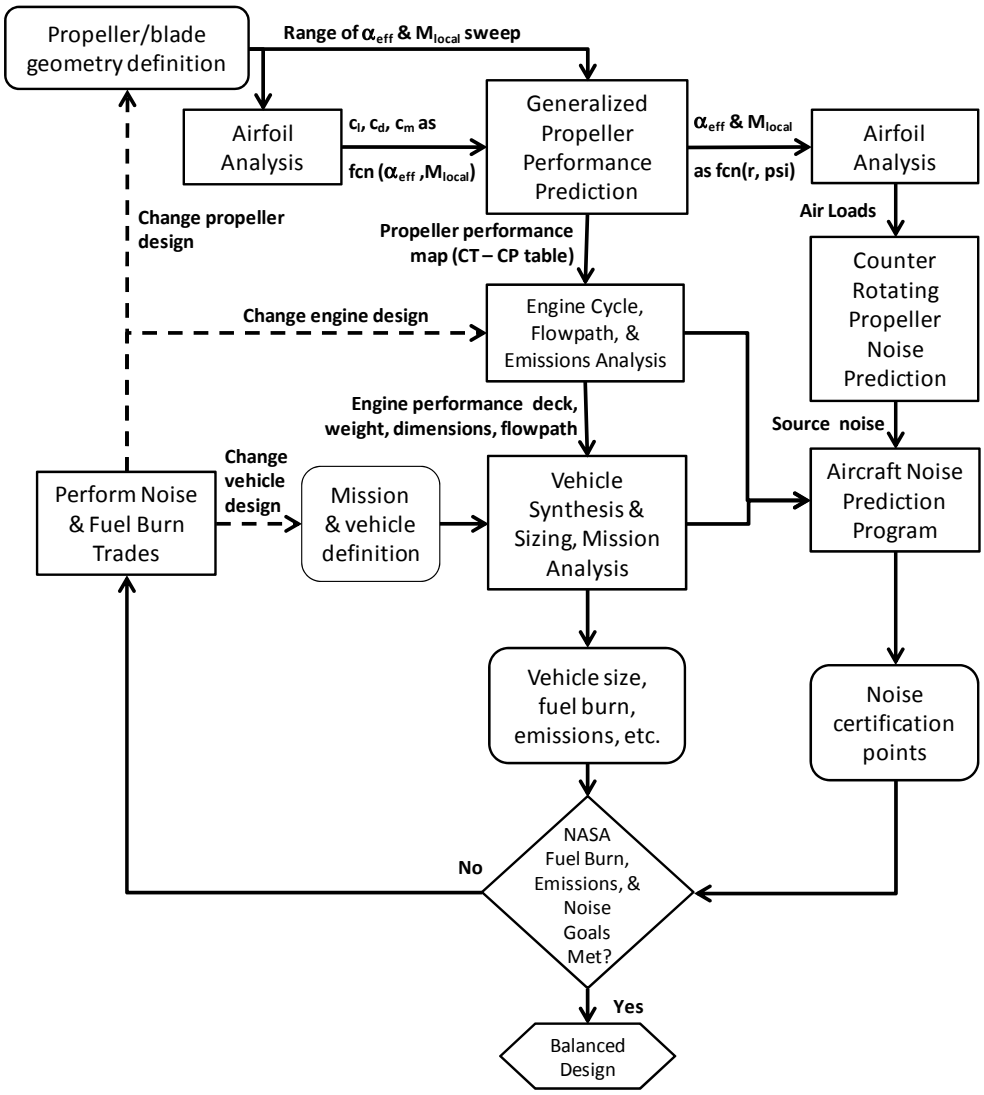

Figure 19. Open Rotor Modeling Methodology

One of the challenges in capturing the fuel burn metrics for vehicles using counter rotating propellers is the power management of the engine, which is highly coupled to the propeller performance. The counter rotating propeller performance is usually characterized by a set of performance maps. These maps are needed to provide the loads to the counter rotating turbines that drives the propellers. The loading conditions and the variable pitch angles of the propellers along with propeller efficiency for all the flight conditions are needed to develop a reasonable operating schedule, e.g. power management, for the engine. How the engine is power managed through the flight envelope obviously impacts the fuel burn of the vehicle. Details of developing a set of power management rules for a counter rotating propeller propulsion system will be addressed in section 3.3.3.1.4

The modeling of a gas turbine powering a counter rotating turbine propulsor is accomplished using a 0-D thermodynamic cycle analysis program, NPSS [NASA 2006]. Along with the thermodynamic performance, a flow path analysis for counter rotating propeller propulsion system is also needed to estimate the propulsion system weight. A potential candidate for this flow path analysis is be NASA's Weight Approximation for Turbine Engines (WATE++)

[Tong 2009] with augmentations to estimate propeller weight. This gas turbine model is also providing input into the emissions correlations that are modeled according to section 4.4.1.

The engine modeling step is necessary in order to generate a suitable engine performance deck and propulsion system weight to perform vehicle sizing/synthesis and mission analysis to capture the fuel burn metric (for a given mission), which can be done using NASA's FLight Optimization System (FLOPS) [McCullers 2009]. The results of the mission analysis (i.e. vehicle size, geometric information, take-off and landing trajectories, etc.) are then fed into ANOPP. ANOPP also needs the engine state tables and engine mechanical design details from the combined NPSS/WATE++ engine model to predict the engine related noise sources. In total, ANOPP requires outputs from the propeller noise prediction code, engine state tables, engine flow path analysis, and vehicle synthesis/sizing and mission analysis to estimate the effective perceived noise level (EPNL) at the three certification locations, measured in EPNdB.

Using this open rotor EDS analysis roadmap described above, the system analyst can now perform tradeoffs between the three critical system metrics (fuel burn, emissions, and noise) by perturbing either the counter rotating propeller/blade design variables, the engine design variables, or the vehicle design parameters.

Major technical accomplishments include:

- Updating the open rotor propeller map performance assumptions developed by Reference [Hendricks 2011]
- Extending the engine multi-design point sizing algorithms to the five conditions used in EDS (sea level static, sea level hot day, rolling takeoff, cruise, and top of climb)
- Developing power management logic in a manner that allows for future flexibility and optimization when integrated with noise assessment
- Adding a predictive weight capability to assess open rotor weight
- Accounting for aircraft design changes necessary to incorporate large diameter open rotor engines

In each of the following sections, the EDS modifications are described and assumptions are noted.

3.3.3.1.2 Propeller Modeling

The work presented in [Hendricks 2011] used historical performance data from the GE un-ducted fan (UDF) [Hoff 1990] in order to estimate the counter-rotating propeller performance.

One of the issues with using the GE historical data is its lack of completeness and continuity across the flight envelope. It is provided for cruise conditions and a rolling takeoff condition, but no other operating points. This makes it useful for obtaining back of the envelope calculations in order to estimate cruise efficiency or takeoff thrust; however, in a multidisciplinary, numerical M&S environment, such as EDS, it is necessary to obtain complete engine performance data for the entire vehicle flight envelope. The vehicle synthesis and sizing program (FLOPS [McCullers 2009]) in EDS requires a complete engine performance deck in order to evaluate climb and descent performance. Detailed engine data is also needed to evaluate vehicle noise trajectories and engine operating information for ANOPP [Zorumski 1982]. [Hendricks 2011] tried to overcome these data limitations by using surrogate modeling techniques to effectively interpolate the data between cruise and takeoff. The authors tried this approach but found it can lead to discontinuous and discrete engine thrust and fuel flow trends.

The surrogate modeling approach also led to an inability to tradeoff performance using different pitch settings. Variable pitch settings are necessary for the power management scheme.

Since EDS requires smooth, continuous maps, an alternate approach was undertaken to predict the propeller performance. The Georgia Tech research team conducted a more thorough literature search and discovered that NACA performed several full scale tests of counter-rotating propellers in the 1940's [Biermann 1942]. While these performance tests were of straight-bladed, low speed propellers, they had the advantage that they contained complete performance data for a wide range of advance ratios and blade pitch settings. The old NACA maps were scaled until their trends matched the published performance of the historical F31/A31 set [Hoff 1990]. By scaling the diameter, the efficiency, and the thrust coefficient by fixed adders and scalars, the resulting performance maps were created and are shown in Figure 20. Figure 21 shows comparison to available F31/A31 data via the solid black and dashed lines. Good agreement is shown at the two test conditions for which data is available.

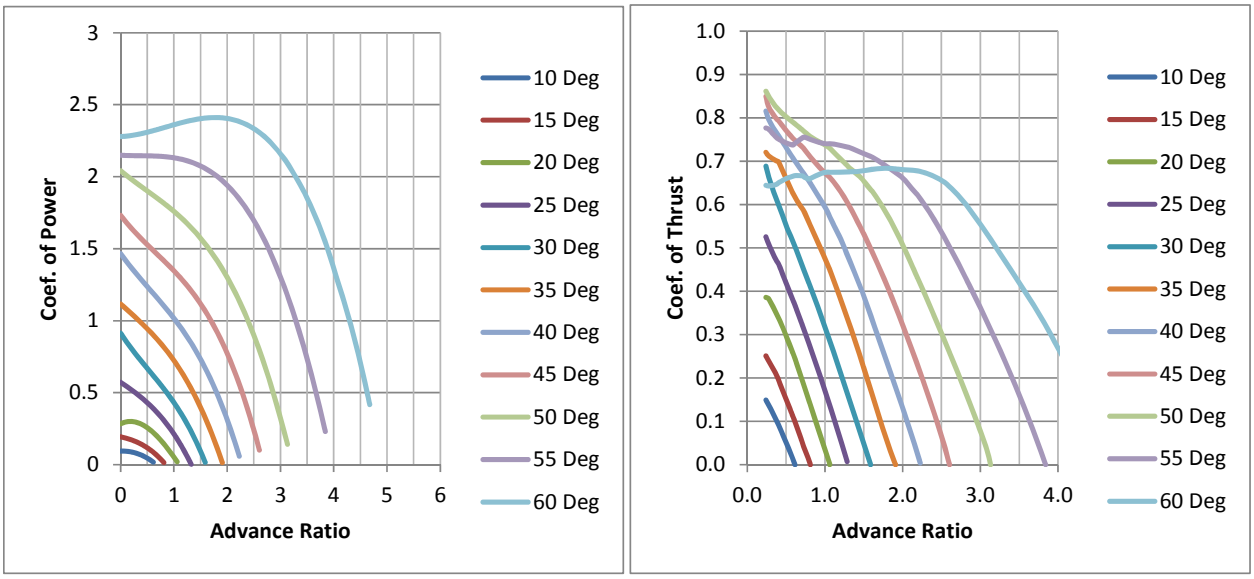

Figure 20. EDS Counter Rotating Propeller Map

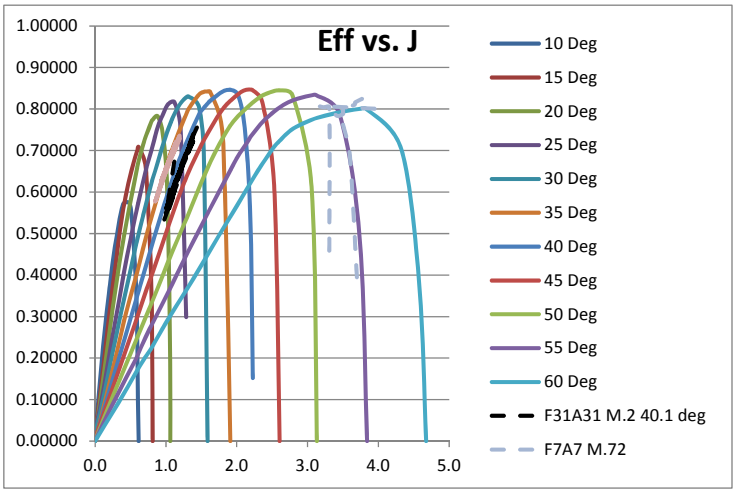

Figure 21. EDS Counter-rotating propeller map comparison to F31/A31 data

3.3.3.1.3 Multi-design Point Approach

The EDS environment uses a multi-design point (MDP) approach to size the engine. For a conventional turbofan the MDP process is thoroughly described in [Schutte 2012b], but it is summarized here for completeness. The engine's aerodynamic design point is specified at cruise conditions. This is where the engine pressure ratios and efficiencies are set. There are also several off-design conditions where the engine sized at ADP is "flown" in order to satisfy other requirements. These include a top of climb condition which sets the fan over speed and thrust, the rolling takeoff condition which sets the maximum combustor temperature and sizes the cooling flows, the sea level static uninstalled condition which sets the rated thrust, and the seal level static hot day condition which ensures hot day performance can be met. The work in Reference [Hendricks 2011] served as a starting point because it contained the aerodynamic design point and rolling takeoff conditions. The three other points were added such that the final aerothermodynamic sizing logic is as shown in Table 25.

Table 25. EDS Open Rotor MDP Setup

Independent Variable	Dependent Condition
ADP Mass Flow	Takeoff Thrust
ADP Fuel-Air Ratio	Top of Climb Thrust
Top of Climb Fuel-Air Ratio	TOC Core Mass Flow Ratio
TOC/TO/SLS Blade Angle	Max Corrected Prop Speed
Propeller Power	TOC Core Nozzle PR
Prop Design RPM	Design Advance Ratio
Hot Day Fuel-Air Ratio	Hot Day Thrust
SLS Uninstalled FAR	SLS Uninstalled Thrust
Takeoff Fuel-Air Ratio	Takeoff Max T4

When NPSS, the core engine design and analysis component of EDS, sizes the engine, it uses physical sizing parameters such as mass flow, combustor fuel-to-air ratio, design propeller power, and component physical areas. In contrast the designer usually sizes the engine according to a set of mission requirements such as thrust and maximum combustor temperatures. In order to relate the physical sizing variables with the design requirements, the NPSS Newton-Raphson solver is used to vary all of the independent variables in Table 25 until the dependent conditions are met. While each independent often affects multiple dependent conditions, they are presented as pairs in order to discuss the philosophy behind the sizing process. The aerodynamic design point (ADP) mass flow sets the engine takeoff thrust and effectively sets the engine size. The ADP FAR and TOC FAR both set the TOC thrust and the ADP thrust. The ADP thrust it not directly specified; rather it is implicitly calculated through the TOC Core Mass Flow Ratio which is the ratio of mass flow through the engine core at TOC relative to the ADP sizing point. This value has an effect on the location of the minimum TSFC "bucket" or "bottom-of-loop" which affects the engine vehicle matching. The TOC thrust is set by the vehicle TOC rate of climb requirements and also sizes the propellers. For the off-design conditions, the blade angles, or blade pitch settings on the prop, are varied such that the propeller runs at a constant corrected tip speed. This assumption was made after reviewing data from [General Electric Company 1987] and keeping the assumption that maximum power in a conventional turbofan is often defined by 100% corrected fan speed, relative to the aerodynamic design point. Propeller power obviously

sets engine and propeller thrust, but the dependent condition is the TOC core nozzle pressure ratio. In conventional separate flow turbofans, the bypass ratio is often set by the extraction ratio (ratio of nozzle total pressures), or the velocity ratio (ratio of core to bypass jet velocities). Regardless of the exact method used to set the effective BPR, the idea is to maintain the appropriate energy balance between the core and bypass ratio to optimize propulsive efficiency. Since EDS is using a propeller map to calculate propeller thrust, there is no available information on the ambient pressure or velocity rise across the propeller. The propeller performance map implicitly sets these values; therefore, the core nozzle pressure ratio is the appropriate variable to control the thrust split between the core and propeller. The propeller design RPM is set to match a user specified advance ratio, and finally the combustor fuel-to-air ratios at the other off-design points to match specified thrust conditions.

3.3.3.1.4 Power Management Logic

The five sizing points for the engine are all at maximum power. Once the engine is sized, it is necessary to generate engine performance information at a wide variety of ambient flight conditions and power settings. While NPSS automatically performs the continuity and energy balances necessary to assess off-design performance, the modeler must specify how to control the free variables, which are essentially the parameters the operator would have either explicit or implicit control over during the course of flight. The burner fuel-to-air ratio (set by the throttle) controls engine core speed and power. The propeller blade pitch setting angle controls the power and torque extracted by the propeller. There are obviously many different ways to set these parameters, but the following control scheme has been implemented in EDS.

The maximum core power setting at any flight condition is defined by 100% corrected low pressure compressor (LPC) speed and 100% corrected propeller speed. The combustor fuel-to-air ratio and blade pitch settings are varied until these two speed requirements are satisfied. The propeller and LPC speeds are constrained by:

- Maximum physical shaft speeds (mechanical constraint)
- Minimum nozzle pressure ratio (assumed 1.05, necessary for core operability)
- Maximum burner temperature (T4 – design choice)
- Maximum and minimum blade pitch settings (15 to 60 degrees for the maps shown in Figure 20)

For any given flight altitude and Mach number the above methodology is used to find the maximum engine power. A throttle hook of part-power thrust settings is then generated by varying the burner FAR until the specified part power thrust as a percentage of the maximum power thrust is achieved. During part power operation blade pitch setting is varied to maintain 100% corrected propeller speed. The maximum power operating constraints also apply to part power conditions in addition to intrinsic limits on combustor operability and compressor surge margin constraints.

It is worth noting that the assumption of a constant speed propeller was decided upon after trying several different control strategies. Obviously the blade pitch setting can be set to maximize thrust, propulsive efficiency, or minimize TSFC. These control schemes were evaluated, but some require optimization techniques to be embedded in the power management or pre-defined pitch setting schedules to be input. The constant speed assumption requires the least amount of additional run time or pre-defined data and also provides performance results that are in-line with the expected performance of more conventional systems, as shown in Figure 24 and Figure 25.

3.3.3.1.5 Weight Modeling

EDS already uses the WATE++ [Tong 2009] code to predict the weight of conventional turbofan engine architectures. For the open rotor model, WATE++ is still used to predict the weight of the core engine components and the size of the core nacelle packaging; however, it must be augmented to predict the weight of the propeller system including the supporting subsystems and the pitch change mechanism. This was modeled using data available in [General Electric Company 1977] and recreated in Figure 22. The propeller weight is a function of the propeller disk loading, assumed to be 55 SHP/D^2 for this analysis, and the propeller diameter. The propeller diameter is sized by the assumed disk loading and the power requirements that result from the MDP sizing discussed previously. These weights are added to the uninstalled engine total. The gearbox and power turbine weights are estimated through standard WATE++ analysis elements.

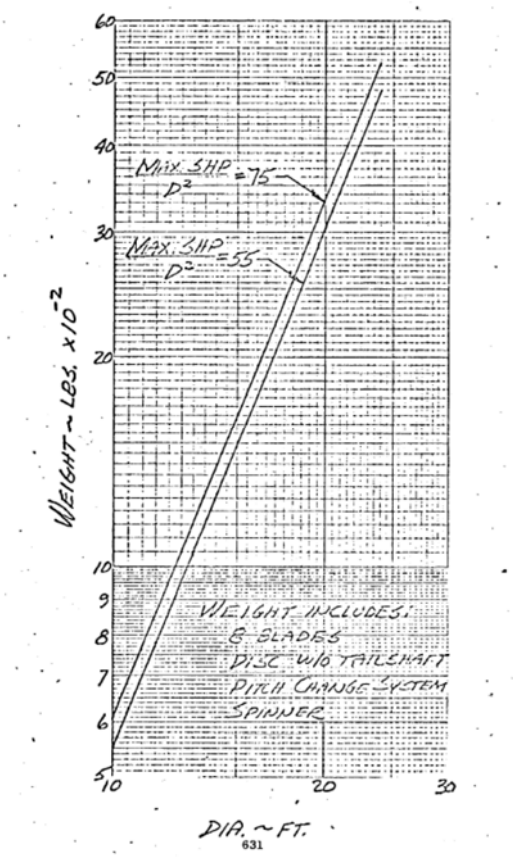

Figure 22. Propfan Weight Estimation [General Electric Company 1977]

3.3.3.1.6 Aircraft Installation Effects

Since the vehicle configuration being considered is a tube and wing design, the most logical place for the engine location is an aft-mounted fuselage installation. By examining data from [General Electric Company 1977, Fischer 1989], an installation factor of 1.6 on top of the bare engine weight including the prop fan was assumed within EDS. The Douglas Aircraft Company was able to design a pylon installation that resulted in little-to-no interference drag, so no additional drag other than pylon wetted area is assumed in EDS [Henne 1989]. In addition to

the added engine weight, an additional fuselage structural weight penalty must also be accounted. Currently, FLOPS internal modeling is used to account for the effect of aft fuselage mounted engines. The present study also does not account for potential additional weight resulting from extra fuselage noise insulation material, which may represent on the order of one to two thousand pounds of weight on a single aisle aircraft.

3.3.3.1.7 Verification of Expected Trends

While it is difficult to fully validate the model due to the limitations and lack of available and complete public domain data, an attempt was undertaken to ensure that the model predicts benefits that are in line with what other research projects. In order to accomplish this goal, an open rotor engine of "modern design" was evaluated on a 737-800 type aircraft with all of the design modifications and features mentioned above. The results are compared against information GE has presented in the public domain in terms of engine efficiency gains and vehicle fuel burn benefits [Niskode 2010]. GE's quoted benefits at the engine level are in terms of propulsive efficiency benefits relative to the current day CFM56. In order to have a fair comparison, the EDS model has assumed an overall pressure ratio (OPR) of 30, which is similar to the CFM56, with correspondingly similar turbomachinery component efficiencies and temperatures. The propeller design parameters are compared to the historical GE F7/A7 blade set at the ADP design condition as shown in Table 26.

Table 26. EDS Prop Design Comparison

Design Parameter	F7/A7	EDS
Front Rotor Diameter(ft)	11.67	11.33
Advance Ratio	2.8	2.8
CPQA	4.1	4.112
CTQA	1.256	1.248
Net Prop Efficiency	0.858	0.85
Front Rotor Power (hp)	3767	3562
Rear Rotor Power (hp)	3787	3562
OPR	N/A	29.7

Figure 23 shows propulsive efficiency improvements of the open rotor relative to a CFM56-7B architecture. Since the EDS open rotor baseline has a similar OPR to the CFM56 and TSFC improvement is proportional to the product of the propulsive and thermal efficiencies of the engine, the EDS model should predict TSFC gains in line with the trends shown in Figure 23. The EDS open rotor model was used to generate thrust and TSFC information at Mach 0.8 at cruise altitude and Mach 0.25 at sea level. The results were then compared to the EDS model of a CFM56-7B and are shown in Figure 24 and Figure 25.

In Figure 24 and Figure 25 the blue line represents the EDS representation of the CFM56, which has been previously calibrated. The red line represents the EDS performance of the open rotor using the propeller design parameters in Table 26 with a CFM56-like core. EDS predicts a

23.8% reduction in TSFC at high speed cruise and predicts a 53% TSFC improvement at the takeoff condition. These results are encouraging since GE shows a 23% gain at cruise relative to the CFM56 and a 70% benefit at takeoff. The EDS model may be under predicting the takeoff benefit some, however, the EDS predicted TSFC is in line with the values calculated when GE designed the GE36 demonstrator [Hoff 1990]. While the EDS results do not fully validate the model, they do serve to show the benefits are in line with industry expectations. It should also be noted that no additional tuning of the model was performed in order to produce the results shown in In Figure 24 and Figure 25

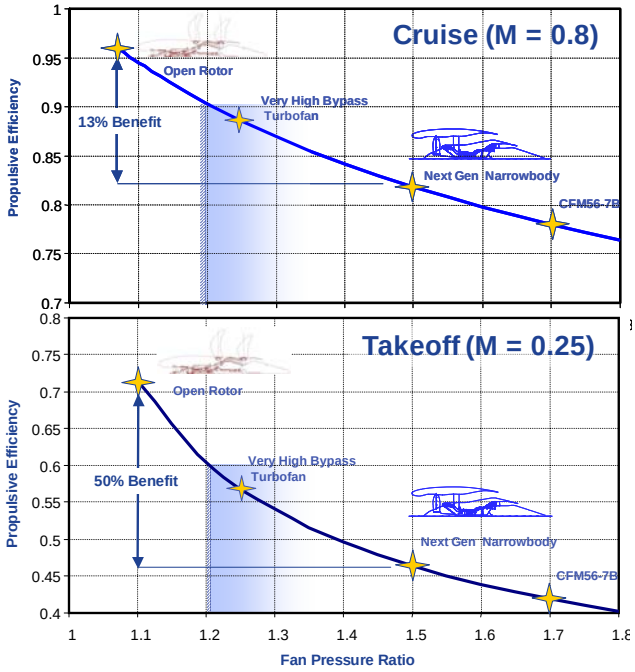

Figure 23. GE Representative Open Rotor Improvements [Niskode 2010]

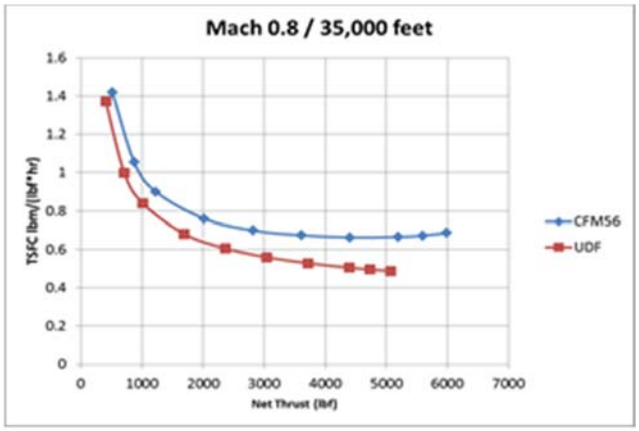

Figure 24. EDS Open Rotor High Speed Cruise Performance

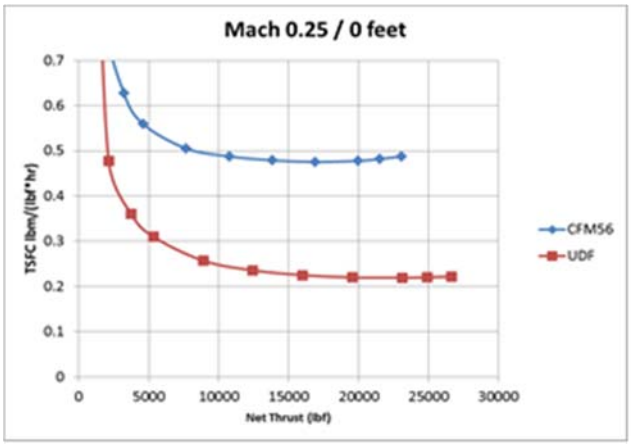

Figure 25. EDS Open Rotor Takeoff Performance

In order to baseline the vehicle performance benefits, the EDS 737-800 model was retrofitted with a tail mounted open rotor configuration and the resulting fuel burn benefit at the vehicle design range was assessed. The vehicle fuel burn relative to the baseline was 29.6%. This exceeds the benefits shown by GE, in Figure 26, but is acceptable for the purpose of establishing a baseline for technology assessments.

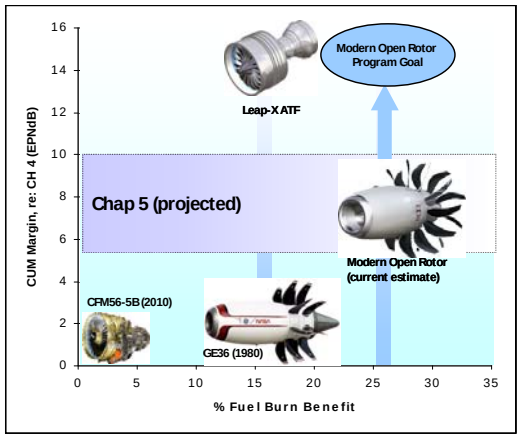

Figure 26. Projected Open Rotor Fuel Burn Benefit [Niskode 2010]

There may be additional installation impacts such as cabin noise insulation and it is also unknown what the baseline aircraft and mission rules are for the benefits shown in Figure 26. As another comparison, a recent NASA study estimated a 40% fuel burn benefit on an MD-90 type aircraft; albeit the reduction is relative to an early 1990's MD-90 [Guynn 2011]. This shows that the benefit is highly dependent on the set of baseline technology assumptions.

3.3.3.2 Noise Modeling Approach

3.3.3.2.1 CRPFAN

In order to model the fuel burn aspects of the open rotor, EDS required several involved, but not overly complex changes to its layout and computational modules. The biggest changes included the ability to power manage the propeller, integrate the counter-rotating propeller performance, and include the vehicle installation effects from a weight perspective. Noise prediction required more extensive EDS modifications. The GE developed and NASA funded Counter-Rotation PropFan Noise (CRPFAN) program was incorporated into the modeling loop for estimation of rotor noise [Whitfiled 1990]. The output of CRPFAN was incorporated into the ANOPP input file through the use of ANOPP's Acoustic Data Module (ACD) which allows for the input of externally calculated source noise. This module introduces its own limitations and drawbacks that will be discussed in this section.

Modeling of the open rotor engine noise comprises two major elements: source noise modeling with CRPFAN and incorporation of the engine noise into the ANOPP run using the ACD module. The use of CRPFAN requires a lengthy list of inputs including geometry, engine operating state, and performance values. Performance, state, and dimensional geometry values are gathered from several EDS modules while the blade sectional information is taken from the full scale F7/A7 blade set tested in the 1980s by NASA and GE. CRPFAN program outputs one-third octave band spectra of the steady loading and interaction tones produced by the two blade rows at the desired polar directivity angles.

This propeller source noise estimation method has two substantial limitations. First, the semi-empirical model is validated for the F7/A7 blade set from the 1980s and may not provide a good estimation of noise produced by more modern blade designs that incorporate advanced features such as proplets. Indeed, current studies use the F31/A31 blade set as the historical baseline. The F31/A31 blade set is referred to as the historical baseline because it represents the best aerodynamic design from the 1980's era with noise levels lower than that of the F7/A7 [Van Zante 2013]. In order to implement CRPFAN with noise levels similar to the F31/A31 blade set, a parametric sensitivity study was performed in order to calibrate the CRPFAN inputs to replicate the source noise levels given by F31/A31 experimental data, provided by NASA. This process will be detailed in the following sections. Second, the model makes no estimation of the broadband noise component produced by the rotors. In order to overcome this, a broadband component is generated to mimic that observed in the F7/A7 tests performed by Hoff [Hoff 1990]. The broadband component is assumed constant about the polar arc, and is added to the tonal noise calculated by CRPFAN.

In order to incorporate the engine noise calculated by CRPFAN into the ANOPP run, the CRPFAN calculated open rotor source noise was input using the ANOPP ACD module. The ACD module requires input of noise data tables of one third octave band spectra for with variation in polar and azimuthal directivity angles. A table is required for a set of Mach numbers and power settings in a matrix form (for each power setting, a table is required for each Mach number). ANOPP then selects the appropriate table with the Mach number and power setting corresponding to that of each time step in the input flight path. Ideally, the tables would be constructed such that a unique Mach number and power setting would be present for each time step in the flight path to avoid interpolation error. However, as the takeoff trajectory tables are quite detailed, doing so routinely leads to an exceeded ACD input data limit. To avoid this, the time steps in the flight path are grouped intelligently and given a determined set of Mach

numbers and power settings to reduce the number of data sets while minimizing the error in noise calculations. This logic has been automated and integrated within EDS so that it can be done in-line with the analysis process.

3.3.3.2.2 Parametric Modeling Approach

CRPFAN requires a set of input parameters in order to produce the source noise of a blade set. The original program is set to produce the source noise of the heritage F7/A7 blade set. In order to produce source noise of the more modern and quieter F31/A31 blade set a parametric study was performed. This involved altering the inputs to CRPFAN, which consist of geometric, aerodynamic, and performance parameters, to mimic experimental data given by NASA. It should be noted that the inputs to CRPFAN are quite involved and many are hard-coded into the input files for the F7/A7 blade set. Most are unknown for the F31/A31 blade set without performing experimental tests and having the physical blades. In order to model the open rotor parametrically, it becomes necessary to discover the physics and trends for both the CRPFAN program and the experimental data provided by NASA.

The experimental data used for this study came from tests carried out in NASA Glenn's 9 by 15 ft. Low Speed Wind Tunnel in 2010. The test rig used was configured with a 1/5th scale F31/A31 blade set consisting of 12 forward and 10 aft blades. The test rig was placed in proximity to a sideline microphone array to take noise measurements at various geometric angles and distances from the blades. The microphone array consisted of 18 microphones and was located 60 inches from the centerline of the engine [Van Zante 2011]. The microphone array was set up to take noise measurements at geometric angles ranging from 18 to 140 degrees relative to the engine where zero degrees is referenced toward the oncoming flow. The test consisted of taking noise measurements for various Mach numbers and angles of attack for power settings ranging from 12 to 100% power [Van Zante 2011]. The noise measurement data was then converted to full-scale and to both flight and static conditions. This was performed by application of an atmospheric attenuation model, removal of the background noise, scaling of the data, and correction of the spectral densities to account for spherical spreading. Also, the data was converted to 1/3rd octave band center frequencies to smooth out the peakedness of the data [Berton 2011]. An example of the noise spectrum for the F31/A31 blade set for 12%, 60%, and 100% power at an observer angle of 90 degrees can be seen in Figure 27.

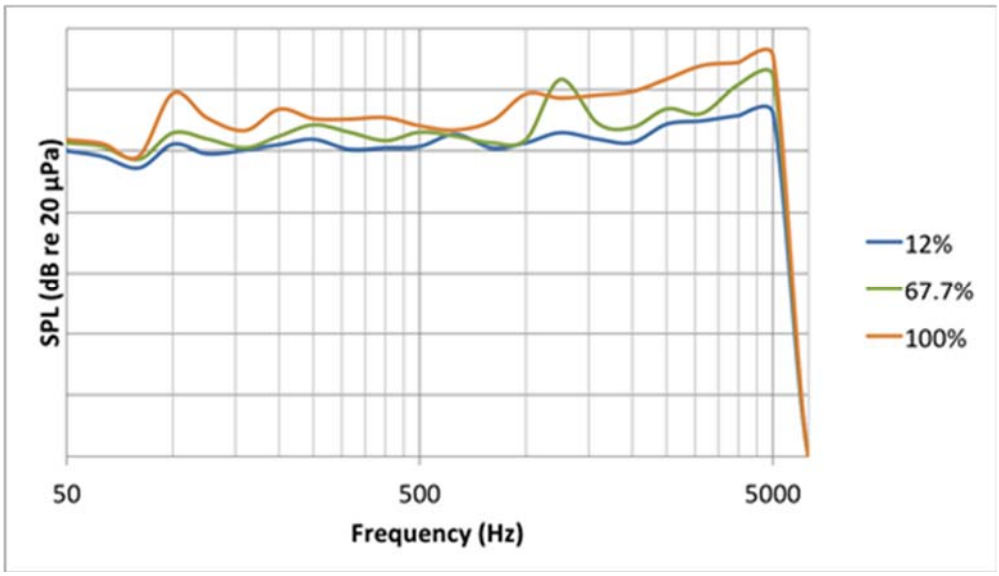

Figure 27. Measured SPL versus Frequency for Mach Number of 0.2 at 12, 67.7, 100% Power and Geometric Angle of 90°.

In order to better understand the inputs to CRPFAN and their relative influence on the predicted noise, a parametric trade study was performed. There were two main goals of this parametric study. The first goal was to determine the rotor geometry inputs that are the most influential in noise source generation and how these inputs affect the noise. This information will give insight to the influence of the geometry parameters on the noise source generation, which will be helpful in modeling the F31/A31 blade set. The second goal was to determine the most influential of the unknown inputs and what their relative effect is on the noise. This information will help to decide which of the unknown parameters is most important for defining the F31/A31 blade set and will define the relationship between these parameters and the predicted noise, which will be useful when calibrating the inputs to match the predicted noise to the experimentally measured noise discussed previously.

In an effort to accomplish the first goal, a screening study was performed to determine which of the known (geometry) parameters affected the source noise levels the most. This turned out to be the tip diameter of the fore rotor, the rotor spacing, the number of blades of the fore rotor, and the chord lengths of the rotors. To determine the sensitivity of these parameters, all other parameters were held constant and the parameter in question was varied over a pre-determined range that encompassed values realistic to both the f7/A7 blade set as well as the F31/A31 blade set. An example of the number of blades for the fore rotor is given in Figure 28. This was done at fixed power setting, RPM, and observer angle. This provided insight into how to alter the most important geometric parameters, in tandem with performance parameters such as power setting and RPM, to achieve source noise results similar to the NASA data for the F31/A31 blade set.

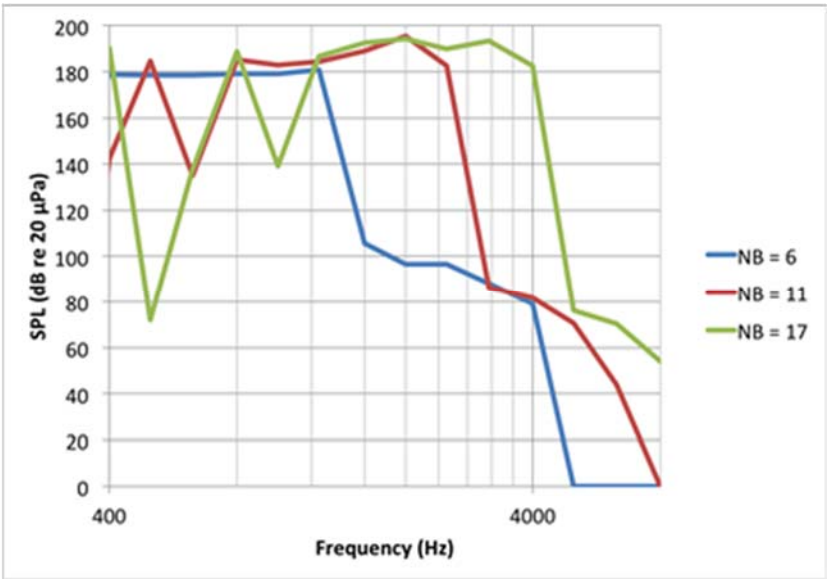

Figure 28. SPL versus Frequency for an Observer Angle of 90 Degrees and Variations in Number of Blades for the Fore Rotor

A similar study was done for the unknown, or mostly aerodynamic, input parameters. This study was more crucial to determining the correct source noise for the F31/A31 blades, as the geometry and performance were more readily available than the aerodynamic characteristics. It was found, through an additional sensitivity study, that the circulation index, the tip vortex trajectory index, the lift coefficients of the aft rotor, and drag coefficients of the fore rotor were the significant unknown input parameters. To determine the sensitivity of the source noise levels to these parameters, a parametric study was done keeping all other parameters constant including power setting, RPM, and observer angle. An example of the unknown parameters is given for circulation index and can be seen in Figure 29. This provided insight into how to alter the most important aerodynamic parameters, in tandem with performance parameters such as power setting and RPM, to achieve source noise results similar to the NASA data for the F31/A31 blade set.

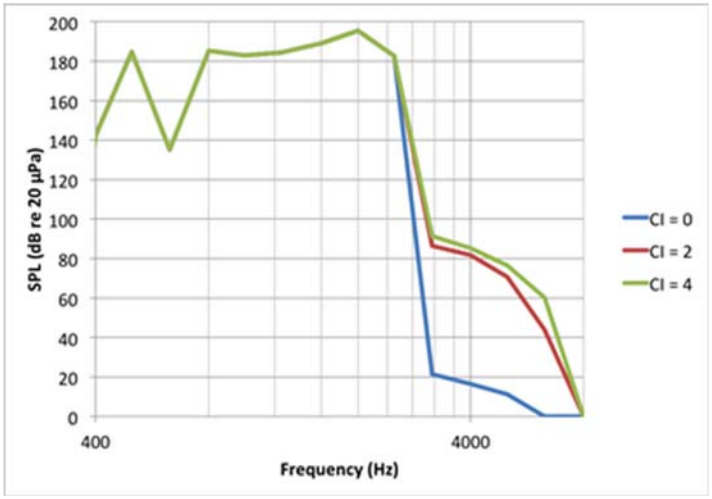

Figure 29. SPL versus Frequency for an Observer Angle of 90 Degrees and Variations in Circulation Index

After the parametric studies of both known and unknown parameters was completed, the input variables were varied over a range of values realistic to both the F7/A7 and F31/A31 blade sets through the use of a design of experiments. The results were analyzed and compared to the experimental F31/A31 data provided by NASA. Input parameters were then chosen and calibrated to best match the CRPFAN output source noise levels to the F31/A31 source noise levels.

3.3.3.2.3 Verification of Expected Trends

Once acceptable input parameters to CRPFAN were chosen, and the results mimicked the trends of the F31/A31 blade set, the results were verified against the NASA experimental data at wide range of power settings, Mach numbers, and RPM settings. This provided assurance that the trade study produced appropriate trends for the source noise not only at the design points, but at all points within the range of the data and possible configurations to be used within EDS. This verification was performed by holding constant the CRPFAN input parameters determined optimal through the parametric trade study and varying the power setting, Mach number, and RPM, diameter, and rotor blade angle inputs over the range required for EDS and the ACD table module. This was dictated by the geometry produced by other modules within EDS and the flightpath of the aircraft during departure and approach. An example of the CRPFAN SPL spectrum compared to the NASA experimental data prior to the parametric study is shown in Figure 30. The same comparison after the parametric study is shown in Figure 31. It should be noted that these comparisons were for the same power setting, Mach number, rotor diameter, observer angle, and RPM. The only difference is the calibration of the CRPFAN input parameters.

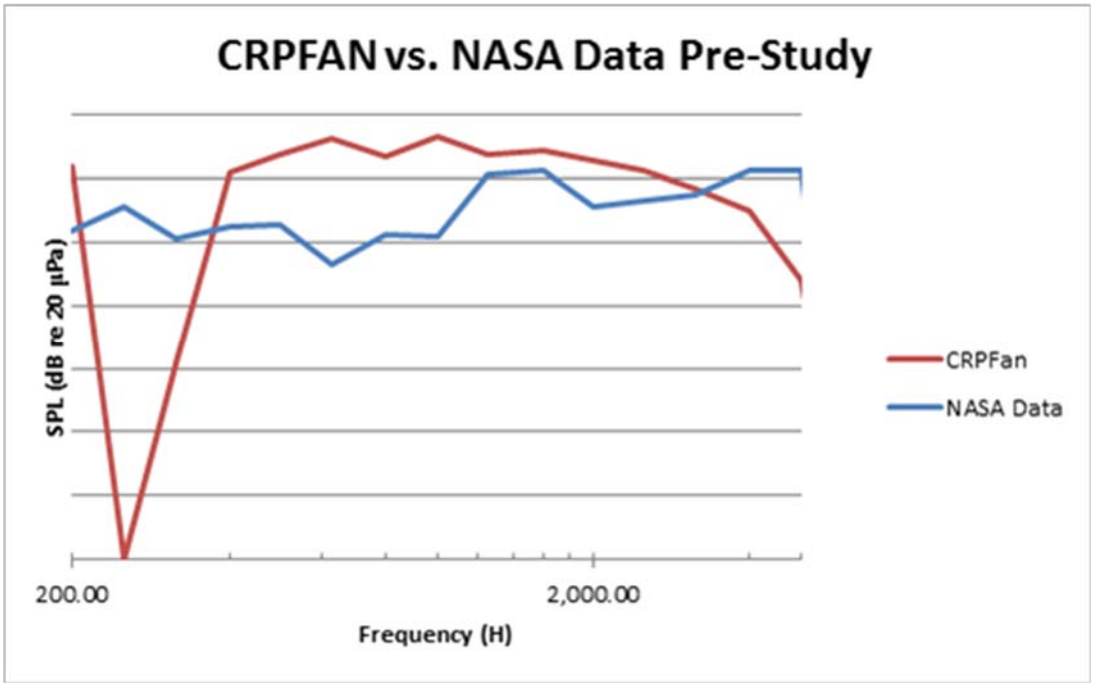

Figure 30. Comparison of CRPFAN and NASA Experimental Data Source Noise for Observer Angle of 90° Pre-Parametric Study

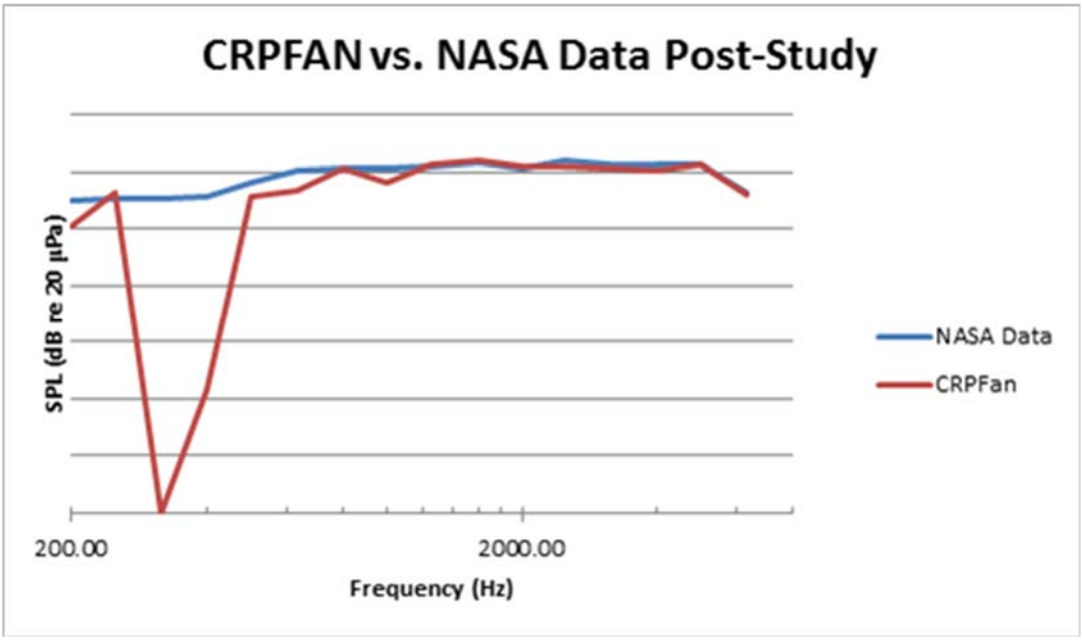

Figure 31. Comparison of CRPFAN and NASA Experimental Data Source Noise for Observer Angle of 90° Post-Parametric Study

As can be observed in the figures, the SPL levels for the open rotor source noise prior to the parametric study differ greatly between the CRPFAN output, representative of F7/A7 blade set, and the experimental data, representative of the F31/A31 blade set. Indeed, the SPL levels are much higher for the CRPFAN output which is logical because the F7/A7 blade set represents an older and louder technology. The comparison from the post-parametric study is a great improvement in the difference in noise levels. The CRPFAN output is much closer to the SPL levels of the NASA experimental data, allowing it to be used as a representative of the F31/A31 blade set. It should be noted that in both comparisons there are "gaps" in the noise spectrum at lower frequencies. This is a function of the limitations of CRPFAN. In order to overcome this limitation, the missing frequency levels were interpolated from the available data inside of EDS to produce complete ACD tables for ANOPP. This verification process allowed for confidence in the source noise levels modeled by CRPFAN to be closely representative of the F31/A31 blade set and suitable to integrate in EDS for complete noise analysis.

3.3.3.2.4 CRPFAN-EDS Integration

It is difficult to conduct a direct validation between EDS and publically available data; however, much can be done to baseline the model and check that the results being generated are within the realm of reasonableness. Making a direct comparison between EDS and real data is challenging in this specific application for several reasons. In terms of fuel burn, the EDS environment seeks to assess the performance benefits of a modern open rotor. In the past, GE performed a flight test of the open rotor using an F404 engine as the gas generator. The actual propulsor was essentially "bolted on" to the back of the fighter engine. While this type of test is important in assessing the feasibility of an open rotor, it does not provide the actual fuel burn benefit that could be gained using the system on a modern, high efficiency commercial engine

core. Using an environment such as EDS allows the engineer to bring the F31/A31 blade set into the modern age by driving it with a LEAP-X type of engine core that will be seen on the next generation of commercial aircraft. Furthermore, since the propulsive efficiency of modern open rotor blade designs has only improved a point or two, the results will still be representative of the system benefit.

Noise represents a bigger challenge due to the massive engineering leaps that have occurred since the 1980s in terms of noise analysis and engineering for noise. While previous generation open rotors were estimated to fall short of Stage IV noise regulations by as much as 7 EPNdB, current designs are projected to exceed Stage IV margin by as much as 13-17 EPNdB [Croft 2012] [Van Zante 2014]. As a result it is difficult to use historical, empirical data while providing a modern representation of the noise capabilities of a next generation system. To overcome this, the EDS model benchmarking will be done in two parts. The EDS predicted fuel burn benefits will be performed using a modern engine core and will be compared to publically stated benefits on a next generation system. The EDS predicted noise benefits will be performed using the F31/A31 blade set and results will be compared to the NASA experimental data for F31/A31 as described previously. It is worth restating that this first iteration serves to check that all of the EDS linkages and prediction schemes are working as expected; following iterations will include more modern data input for noise prediction.

The performance prediction methodology has been well outlined in previous work by the authors and will not be repeated here for the sake of brevity. However, several updates to the previous work have been made including the addition of approximately 1,200 lbm of noise insulation to the rear cabin of the aircraft using data from [Goldsmith 1981]. Also, the parametric propfan prediction model has been updated to include data from [Weisbrich 1982]. The authors believe the updated data is more representative of a modern configuration and the end result has been a small but significant increase in vehicle weight relative to the previous work.

To baseline the fuel burn performance the following engine cycle, shown in Table 27, is used. Comparisons between the prop design on the EDS model and the F7/A7 engine data are also shown. Additionally, modifications to the aircraft include mounting the engines on the tail, redesigning the landing gear, shifting the wing, and resizing the horizontal and vertical tails. The OPR is not shown for the original F7/A7 design report because it is irrelevant for the purposes of comparison due to the fact that it was used on a military and not a commercial platform. The OPR selected for the EDS cycle is representative of the core engine pressure ratio, including the booster, of a LEAP-X or PW1000G technology level engine.

Table 27. EDS Open Rotor Engine Cycle

Cycle Parameter	F7/A7	EDS
Front Rotor Diameter(ft)	11.67	11.33
Advance Ratio	2.8	2.8
CPQA	4.1	4.112
CTQA	1.256	1.248
Net Prop Efficiency	0.858	0.85
Front Rotor Power (hp)	3767	3562
Rear Rotor Power (hp)	3787	3562
OPR	N/A	29.7

Using the cycle assumptions in Table 27, the EDS model predicts a 23.8% reduction in vehicle fuel burn on a 737-800 aircraft. The reference point for comparison is a 737-800 with CFM56-7B27 engines. Publically available information presented by GE has shown an estimated 26% reduction in fuel burn relative to the same platform [Niskode 2010]. The end result is a platform capable of predicting fuel burn to within a reasonable degree of accuracy. Assessing the baseline EDS model noise also shows a good match to public domain data. Comparisons are made between EDS, GE estimated noise levels from the original testing of the F7/A7, and NASA 1998 generated noise results using the F31/A31 blade set. Results are shown in Table 28 [Croft 2012, Van Zante 2014]. This noise analysis is for a narrow body aircraft.

Table 28. EDS Open Rotor Noise Comparisons

	EDS (F31/A31)	GE-Hoff (F7/A7)	NASA (F31/A31)
Sideline (EPNdB)	90.17	96.8	92.8
Cutback (EPNdB)	84.24	88.2	87.6
Approach (EPNdB)	92.34	97.9	91.7
Cumulative (EPNdB)	266.7	282.9	272.1
Margin to Stg. IV	10.9	-7.1	5.7

EDS predictions see a vast improvement over the heritage F7/A7 blade set and a slight improvement over the NASA 1998 F31/A31 improvement. While it is hard to draw direct comparison due to many changes in the underlying assumptions such as engine OPR and vehicle trajectories assumed, EDS does appear to perform well and follow the trends of the older F31/A31 blade set predictions. It should also be noted, that because of the rotor placement on the current EDS vehicle, noise shielding is also be implemented within EDS allowing for quieter certification noise levels. Current studies using more advanced blade sets predict the noise margin to Stage IV to be in the range of 15EPNdB – 17EPNdB [Van Zante 2014]. The EDS open rotor noise model is well on its way to being able to model the acoustics of the open rotor, but must rely on the F31/A31 data for calibration due to proprietary concerns of advanced blade designs.

3.4 Aircraft Configurations

3.4.1 Vehicle Sketch Pad

Vehicle Sketch Pad (VSP) is a parametric airplane geometry modeling tool originally developed by NASA, but now open source. It enables airplanes to be modeled rapidly and efficiently for conceptual and preliminary design levels of analysis, without requiring a fully featured CAD program and a large time investment. All of the EDS models developed for ERA had a VSP model created for that geometry. Example wireframe and fully shaded VSP models are shown in Figure 32.

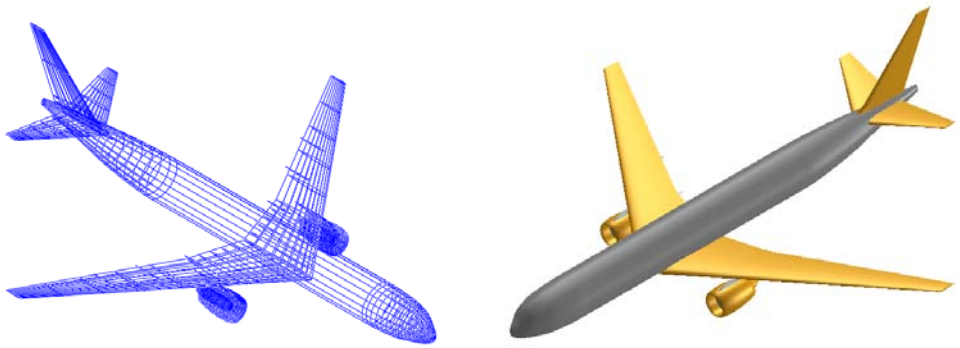

Figure 32. Example VSP Wireframe and Shaded Model

The geometry required to create a VSP model and the geometry required for an EDS model have a significant amount of overlap, but are not identical. The EDS model has simplified geometry for the fuselage and engine, only utilizing the length and diameter. The lifting surfaces are modeled with a reasonable amount of detail in EDS, but airfoils are still missing.

The VSP models had to have the information missing from the EDS models approximated for all the configurations. Every configuration, except the HWB, had a baseline aircraft from which the fuselage and engine geometry could be approximated. The HWB geometry was a smoothed version of the EDS wing geometry, with additional sections added to the relatively coarse definition from FLOPS. The airfoils for all these models were simple NACA 4-series that matched the thickness to chord ratios of the EDS models, since they were intended primarily for visualization purposes and not used in any detailed analysis.

3.4.2 Tube and Wing

The standard configuration for transport aircraft since the B-47's development in the late 1940s has been the Tube and Wing (T&W). This configuration has a roughly cylindrical fuselage containing the passengers and/or cargo, an aft swept wing with pod mounted engines, and a horizontal and vertical tail attached to the end of the fuselage. The configuration has the advantage of being separable into its disparate parts for design and manufacturing, as well as making it easy to develop stretched or shrunk versions to accommodate more or fewer passengers, respectively.

The Tube and Wing configuration was used as the baseline aircraft for all vehicle classes. Each vehicle class was modeled in EDS with the geometry displayed in Vehicle SketchPad (VSP) models. An example T&W vehicle is shown for the RTC of the LSA in Figure 33. Table 29 through Table 34 contains data for the 1995 baseline vehicles modeled in EDS.

Figure 33. Tube and Wing Configuration

Table 29. Regional Jet 1995 Baseline

Description	RJ 1995 Baseline
TOGW, lbs	85000
Operating Empty Weight, lbs	47250
Fuel Weight, lbs	19690
Design Payload, lbs	18060
Block Fuel, lbs	15579
Passengers	86
Design Range, nmi	1980.0
Wing Area, sq ft	752.5
Aspect Ratio	8.289
Fuselage Length, ft	109.9
Fuselage Diameter, ft	8.83
T/W	0.34
W/S, psf	113

Table 30. Small Single Aisle 1995 Baseline

Description	SSA 1995 Baseline
TOGW, lbs	155000
Operating Empty Weight, lbs	83000
Fuel Weight, lbs	45120
Design Payload, lbs	26880
Block Fuel, lbs	37415
Passengers	128
Design Range, nmi	3330
Wing Area, sq ft	1409
Aspect Ratio	9.74
Fuselage Length, ft	105.6
Fuselage Diameter, ft	13.2
T/W	0.335
W/S, psf	110

Table 31. Large Single Aisle 1995 Baseline

Description	LSA 1995 Baseline
TOGW, lbs	174857
Operating Empty Weight, lbs	91289
Fuel Weight, lbs	46398
Design Payload, lbs	37170
Block Fuel, lbs	38161
Passengers	179
Design Range, nmi	2960
Wing Area, sq ft	1409
Aspect Ratio	9.74
Fuselage Length, ft	125
Fuselage Diameter, ft	13.2
T/W	0.31
W/S, psf	124

Table 32. Small Twin Aisle 1995 Baseline

Description	STA 1995 Baseline
TOGW, lbs	413000
Operating Empty Weight, lbs	198440
Fuel Weight, lbs	159750
Design Payload, lbs	54810
Block Fuel, lbs	141988
Passengers	261
Design Range, nmi	5920
Wing Area, sq ft	3200
Aspect Ratio	8.09
Fuselage Length, ft	176
Fuselage Diameter, ft	17.7
T/W	0.29
W/S, psf	129

Table 33. Large Twin Aisle 1995 Baseline

Description	LTA 1995 Baseline
TOGW, lbs	657000
Operating Empty Weight, lbs	317000
Fuel Weight, lbs	275950
Design Payload, lbs	64050
Block Fuel, lbs	249180
Passengers	305
Design Range, nmi	7530
Wing Area, sq ft	4927
Aspect Ratio	8.81
Fuselage Length, ft	206.5
Fuselage Diameter, ft	20.2
T/W	0.296
W/S, psf	133

Table 34. Very Large Aircraft 1995 Baseline

Description	VLA 1995 Baseline
TOGW, lbs	876999
Operating Empty Weight, lbs	403399
Fuel Weight, lbs	386029
Design Payload, lbs	87570
Block Fuel, lbs	347168
Passengers	417
Design Range, nmi	7060
Wing Area, sq ft	6203
Aspect Ratio	7.61
Fuselage Length, ft	225
Fuselage Diameter, ft	26.6
T/W	0.26
W/S, psf	141

Figure 34 through Figure 39 show the VSP models for the RTC tube and wings for the various class sizes.

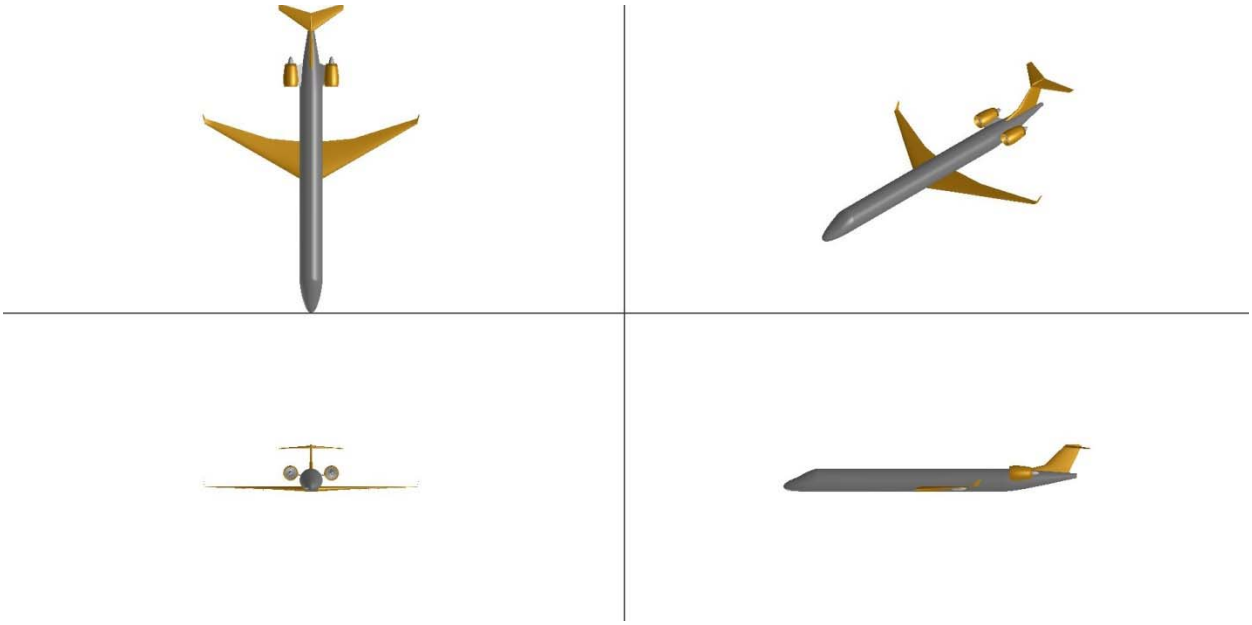

Figure 34. RJ RTC VSP Model

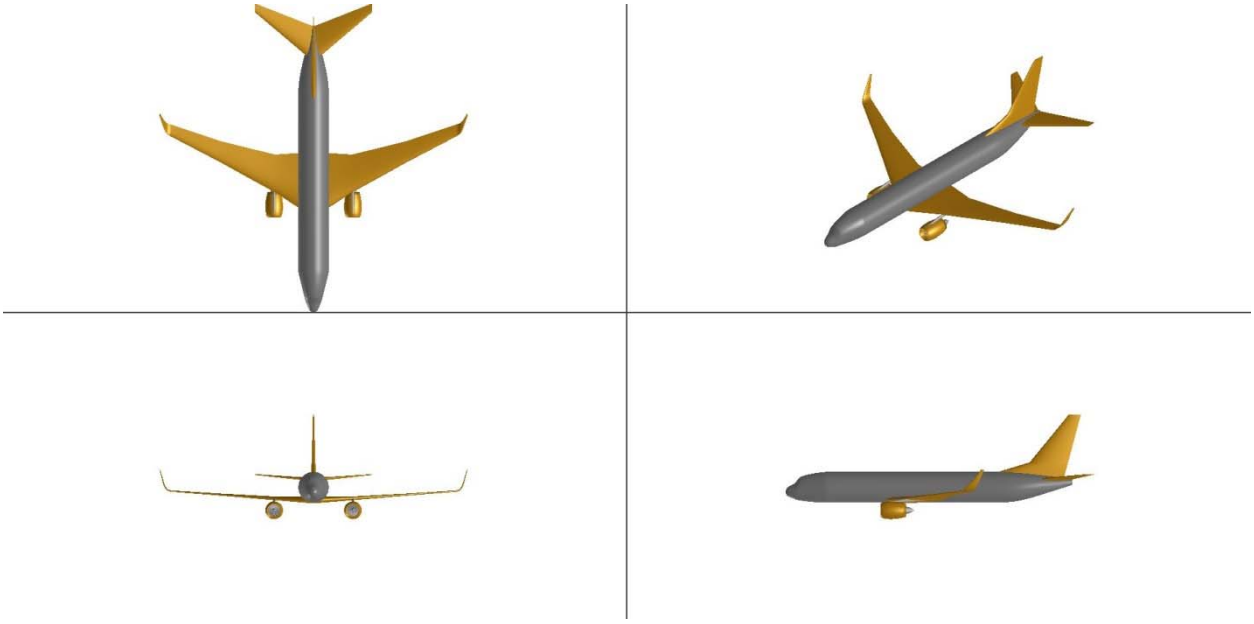

Figure 35. SSA RTC VSP Model

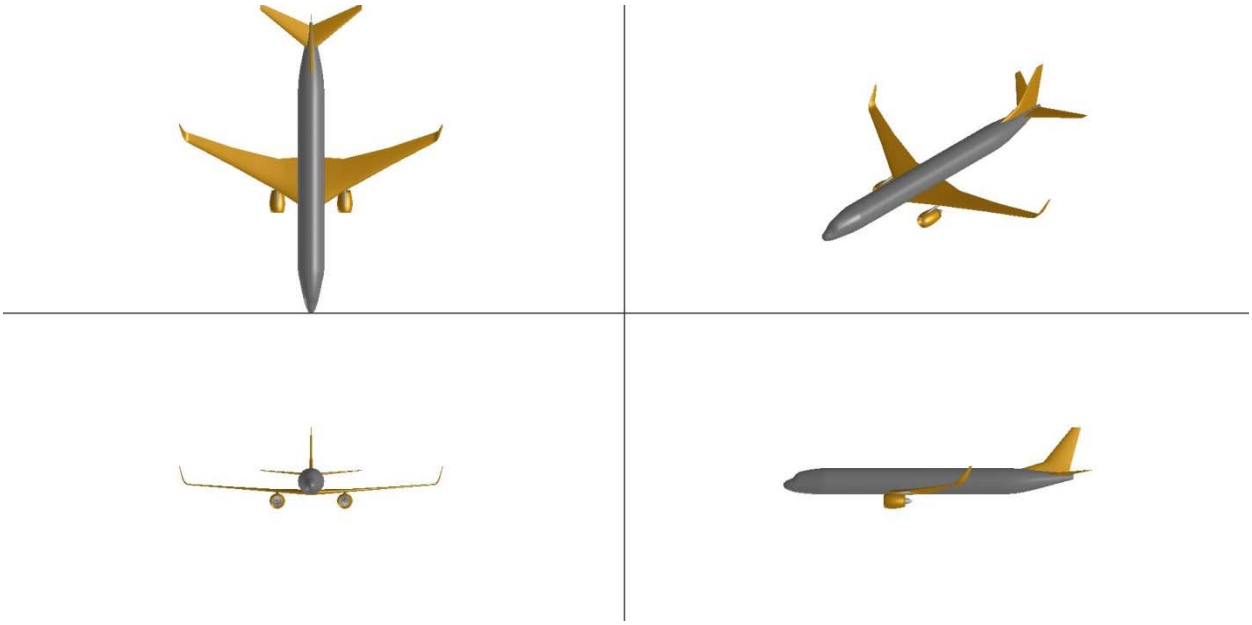

Figure 36. LSA RTC VSP Model

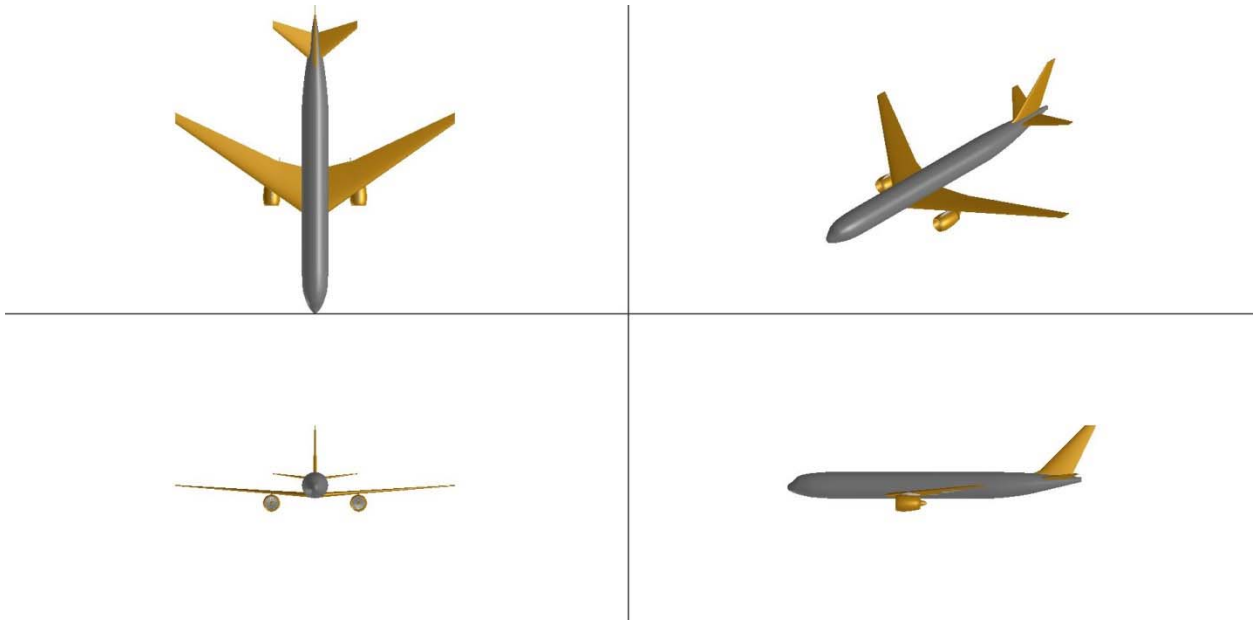

Figure 37. STA RTC VSP Model

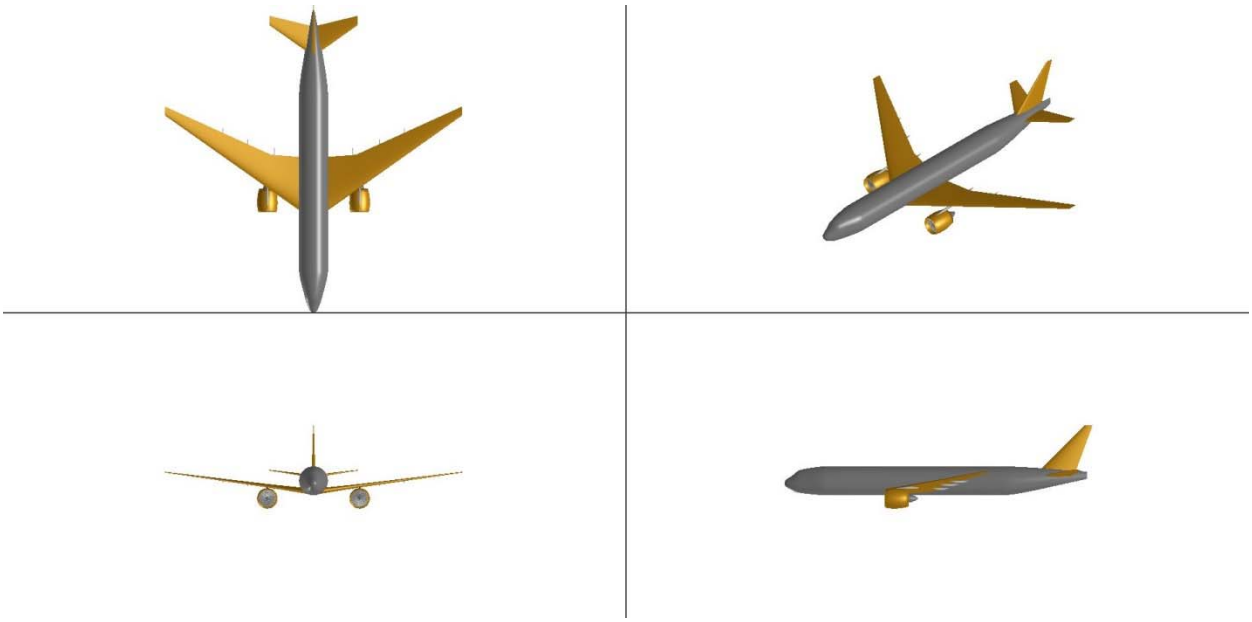

Figure 38. LTA RTC VSP Model

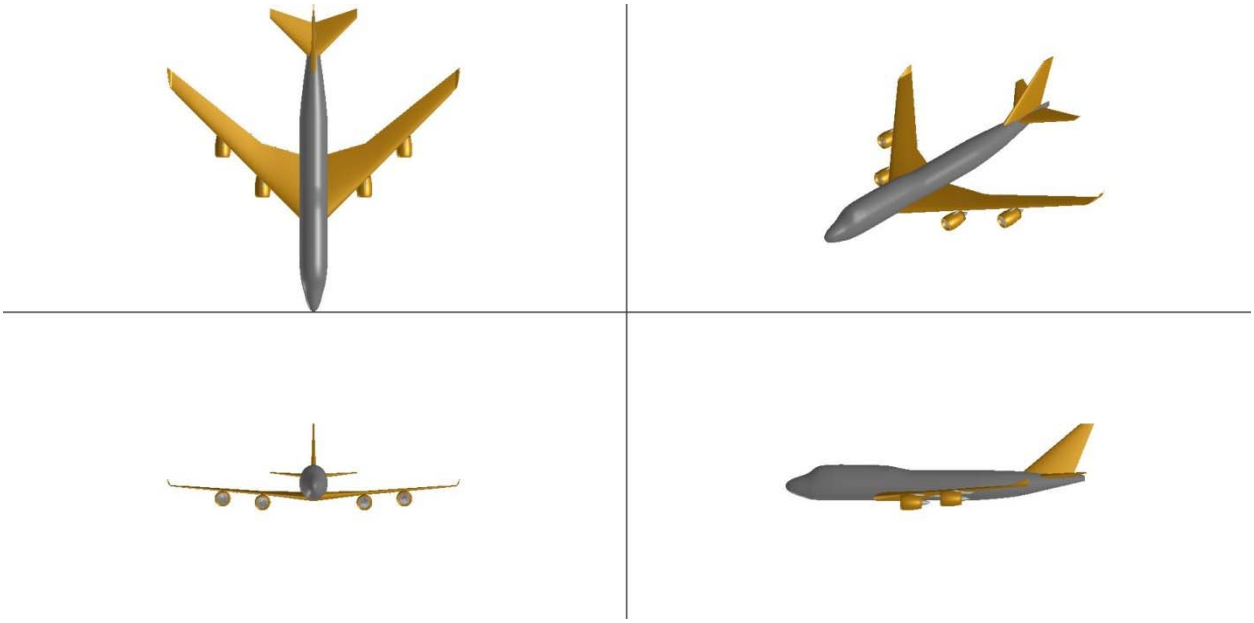

Figure 39. VLA RTC VSP Model

3.4.3 Hybrid Wing Body

The Hybrid Wing Body (HWB) is a configuration where the fuselage is smoothly integrated into the wing to provide additional lift, and the tail is eliminated. The aerodynamic performance of this configuration is superior to the T&W because of the increased lift, from the centerbody, and decreased drag, due to the lack of interference between the wing-fuselage and

the lack of a tail. Another critical advantage of the HWB is the noise shielding provided by placing the engines on the aft end of the centerbody.

There are some disadvantages to the HWB configuration as well. The integration of the payload into the blended centerbody requires the pressure vessel to be non-cylindrical, which is a significant structural challenge. The placement of the engines above the airplane makes maintenance more difficult. It is also challenging to design stretched or shortened variants of a given design relative to a tube and wing. Finally, the stability and control of an HWB is more challenging. The range of acceptable center of gravity locations tends to be narrower, because longitudinal control power is limited by the smaller moment arm of the elevons.

The HWB configuration was applied to the STA, LTA and VLA vehicle classes. The LTA had both turbofan and open rotor engine variants developed in EDS. An example of the turbofan powered LTA vehicle is shown as a VSP model in Figure 40.

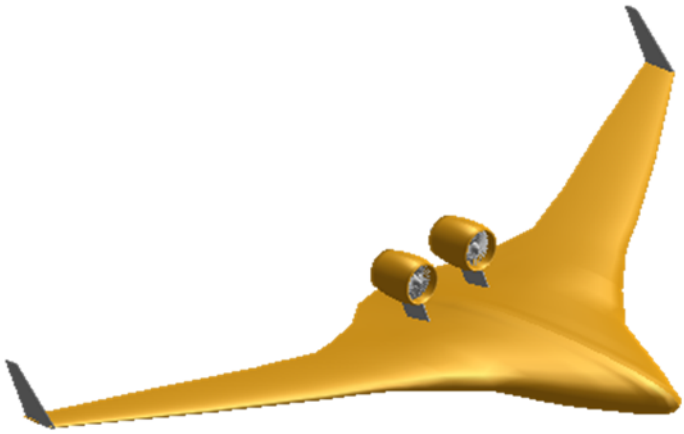

Figure 40. Hybrid Wing Body Configuration

3.4.3.1 Modeling References and EDS Baseline

There is no in service HWB for passenger transport that can be used to calibrate the models and create the Reference Technology Collector EDS model for each vehicle class. It was therefore necessary to start by calibrating to notional vehicles from published data. Two configurations were modeled; one from the Boeing ERA report labeled the 0009A in [Bonet 2011], and the second from the NASA OREIO study in [Pitera 2011].

The Boeing ERA report vehicle is a 2025 technology level vehicle capable of carrying 224 passengers for 8000 nm. The technology added to the vehicle includes hybrid laminar flow control, riblets, composite structure, a geared turbofan, and an advanced APU. The configuration includes two podded engines, winglets, and canted vertical tails as seen in Figure 41.

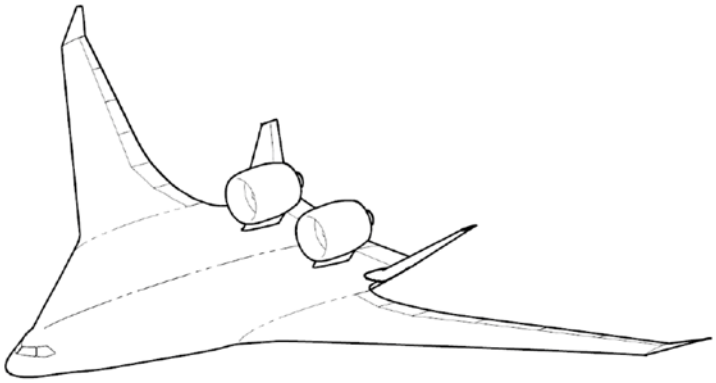

Figure 41. Boeing 0009A HWB Configuration [Bonet 2011]

The mission, geometry, and technology assumptions were translated from [Bonet 2011] into an EDS model, with some of the fixed equipment weights hardcoded to reduce error. The technology assumptions were then adjusted to more closely match the final results. The final EDS model results are shown in Table 35. The overall weight distribution was closely matched with the largest variance in the approach speed, possibly resulting from a difference in the estimated maximum lift coefficient.

Table 35. EDS Validation to Boeing ERA Report

Description	Boeing Report	EDS Model
TOGW, lbs	412,199	412,171
Operating Empty Weight, lbs	229,935	229,306
Fuel Weight, lbs	132,264	132,865
Design Payload, lbs	50,000	50,000
Block Fuel, lbs	121,288	120,878
Design Range, nmi	8,000	8,000
Wing Area, sq ft	8,048	8,048
Aspect Ratio	5.62	5.62
Cruise L/D	22.64	23.1
Approach Speed, kts	131.38	127.5
T/W	0.23	0.22
W/S, psf	51.0	51.2

The OREIO report vehicle is a 2025 technology level vehicle capable of carrying 100,000 lbs of cargo for 6500 nm. The technology added to the vehicle includes hybrid laminar flow control, riblets, composite structure, an open rotor, and an advanced APU. The configuration includes three podded engines and canted vertical tails as seen in Figure 42.

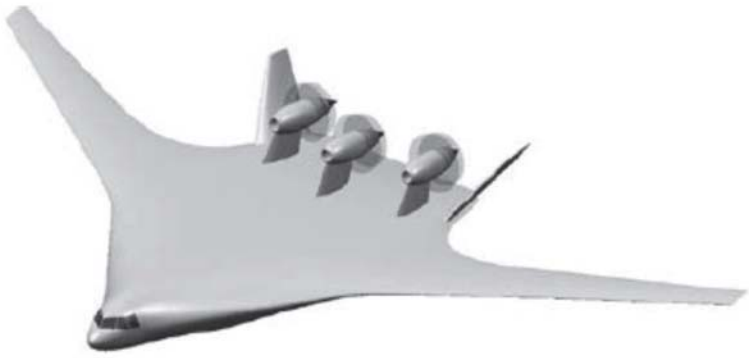

Figure 42. OREIO HWB Configuration [Pitera 2011]

The mission, geometry, and technology assumptions were translated from [Pitera 2011] into an EDS model, with the open rotor engine deck generated as described in Section 3.3.3. The technology assumptions were then adjusted to more closely match the final results. The final EDS model results are shown in Table 36. The overall weight distribution was closely matched with the largest variance again in the approach speed.

Table 36. EDS Validation to OREIO Study

Description	OREIO Report	EDS Model
TOGW, lbs	475,800	475,576
Operating Empty Weight, lbs	229,935	229,306
Fuel Weight, lbs	127,010	126,878
Design Payload, lbs	100,000	100,000
Design Range, nmi	6,500	6,500
Wing Area, sq ft	8,010	8,010
Aspect Ratio	5.646	5.646
Cruise L/D	23.274	23.242
Approach Speed, kts	131.38	127.5
T/W	0.262	0.262
W/S, psf	59.4	59.37

The EDS model for both vehicles was able to adequately capture the most important characteristics. These were used as references and points of comparison for the final EDS HWB vehicles in the absence of better information. Neither vehicle is directly usable as an RTC reference. Therefore adjustments were made for each of the four EDS vehicles in three different size classes.

3.4.3.2 HWB EDS Modeling

Modifications to the EDS environment were necessary to model the HWB vehicles. The modifications were in the aerodynamic modeling (described in Section 3.4.3.3), and in the way the vehicles were automatically resized to maintain a fixed wing loading.

A traditional T&W configuration in EDS has a fixed fuselage geometry based on the number of passengers, with the wing geometry dynamically scaling internal to FLOPS to

maintain a fixed wing loading. It is possible to run FLOPS with fixed wing geometry and a floating wing loading, but this could easily result in an infeasible configuration, incapable of meeting performance requirements such as takeoff or climb. An HWB configuration, however, cannot be dynamically scaled inside of FLOPS because a large part of the reference wing area is contained in the centerbody, which must be sized for the payload and cannot be resized.

The solution was to add an EDS solver loop to iterate externally to FLOPS to maintain a fixed wing loading. This necessitated the definition of a resizing strategy, which was to scale everything outboard of the centerbody while maintaining a constant aspect ratio for the entire vehicle. It would be possible to only scale the local chords of the outboard sections, but this would quickly result in the outboard sections having an unrealistically small chord from a structural standpoint.

The resizing strategy also required surrogate models to be created for each vehicle class for each local chord of the outboard section and the total outboard semi-span as a function of total wing area. These simple surrogate models were created in Excel based on resizing studies using FLOPS to maintain constant vehicle aspect ratio.

3.4.3.3 Aerodynamic Modeling

The use of FLOPS as the sizing and synthesis tool in EDS limits the ability to accurately capture the unique aerodynamic characteristics of the HWB configuration, because the semi-empirical aerodynamic model inside FLOPS is based on data from conventional tube and wing aircraft. The team therefore identified AVID APEX as an improved an analytical tool to integrate into the EDS environment.

APEX was developed as part of a NASA contract specifically to model HWB configurations [AVID 2014] and has been validated against wind tunnel results in [Re 2005]. It integrates the vortex lattice aerodynamic analysis of VORLAX with a transonic airfoil code called TSFOIL and includes numerous other extensions and corrections.

Even though APEX has been validated the team chose to build an APEX model of 0009A and compare the output to the limited aerodynamic results reported in [Bonet 2011]. The planform geometry for the 0009A was easily scaled from the report, but it was also necessary to include airfoil and twist distributions that were not available. The airfoil and twist distributions were therefore taken from [Re 2005], which should be representative of the Boeing vehicle. The geometry input to APEX is in the form of a VSP model. A simplified VSP model of the 0009A was created excluding the engine nacelles, pylons, and vertical tails. The geometry comparison between the modeled and Boeing vehicle is shown in Figure 43.

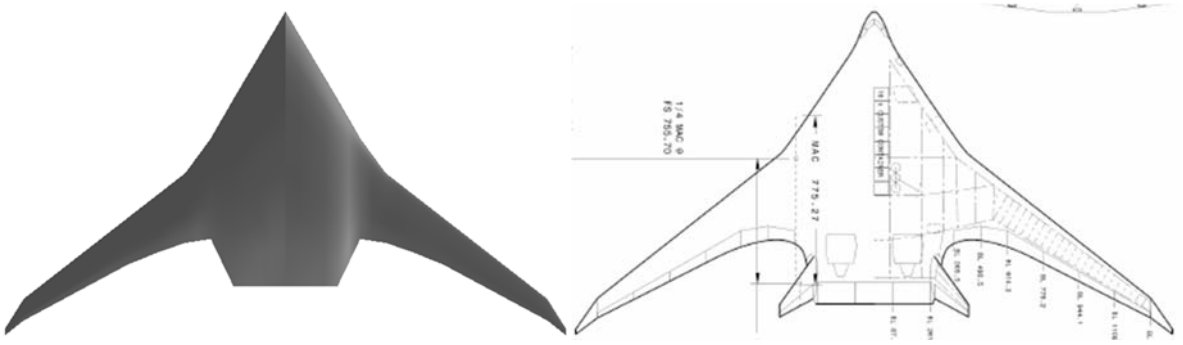

Figure 43. Comparison of Actual to Modeled 0009A Geometry, right image from [Bonet 2011]

There were only three points available in [Bonet 2011] to directly compare the APEX output. The model was able to closely capture the Boeing reported values. The direct comparison can be seen numerically in Table 37, and graphically in Figure 44. The settings used for this analysis were then used for the full aerodynamic analysis integrated into FLOPS.

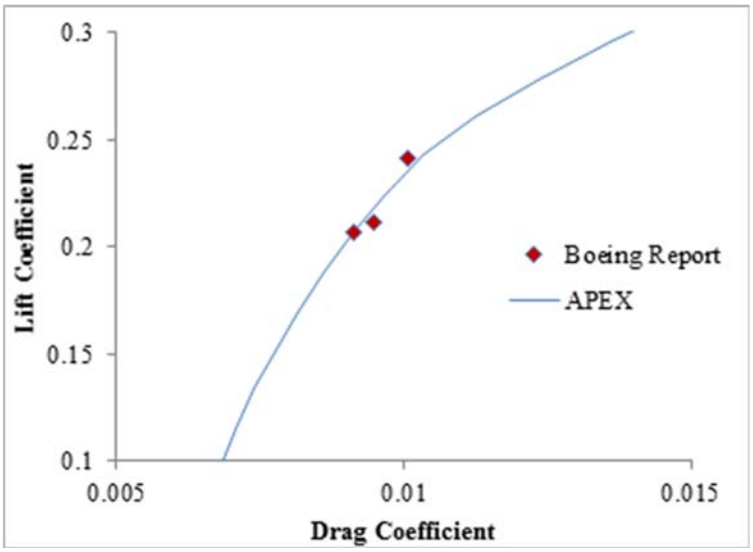

Figure 44. Comparison of APEX Aero to 0009A values from [Bonet 2011]

Table 37. Comparison of APEX Aero to 0009A values from [Bonet 2011]

Description	Boeing Report	APEX Model
L/D at M=0.85, h=39k ft, C_l=0.2067	22.64	22.69
L/D at M=0.85, h=43k ft, C_l=0.2119	22.38	22.87
L/D at M=0.85, h=35k ft, C_l=0.2412	23.92	23.42

Direct integration of APEX into EDS was considered to be too expensive in computational time, and therefore a different strategy was used. A surrogate model of the lift and drag was generated for each vehicle class as a function of the geometry and technology factors that would vary. This surrogate was integrated into EDS and used to build a FLOPS external aero deck. A depiction of this integration process is shown in Figure 45.

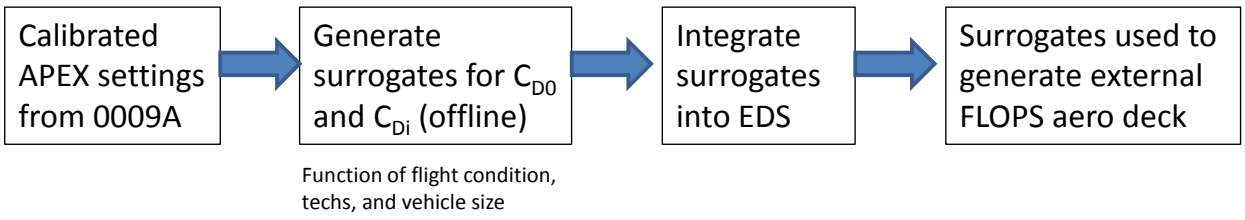

Figure 45. APEX Integration into EDS

3.4.3.4 HWB Centerbody/Aft Body Weight

3.4.3.4.1 Formulation and Motivation of HWB Centerbody

The complex geometry and lack of data for innovative designs such as the HWB aircraft makes the optimization and design of such aircraft difficult. For this reason, finite element model (FEM) based analyses are used to provide enhanced capabilities for HWB sizing and weight estimation.

This work focused on the centerbody and aft-body weight estimations. The centerbody of the HWB is shaped like a "home plate" in baseball as shown in Figure 46 [Nickol 2009]. The size of the centerbody is determined by similar requirements to a conventional aircraft including number of passengers, utility areas, aisles, and etc [Nickol 2009]. The aft body is defined as the area directly aft of the cabin as shown in Figure 47 [Nickol 2009].

The specified geometry of the HWB is then used to create a Vehicle Sketch Pad (VSP) surface model of the aircraft. Utilizing the structural model and specifying various inputs within MATLAB script, "HCD_Struct.m", NASTRAN compatible bulk data files were generated. Some of the inputs included: primary structure definition, material properties of primary structural components, and parameter weights (landing gear, engine, systems, and etc.). The structural analysis, optimization, and weight calculation of the primary HWB structural components were then based on the Nastran finite element models for the centerbody, aft body, mid-section, and outboard wings.

Data obtained from finite element analysis for five distinct, representative centerbody structural layouts was used to find the coefficients of a weight estimate equation in the form,

$$W_{cabin} = K_s * 0.316422(TOGW)^{0.166552}(S_{cabin})^{1.061158}$$

FLOPS was then modified to include a new fuselage design subroutine for the HWB centerbody [Bradley 2004]. A fourth term for wing weight was also added to FLOPS to account for the aft-body weight. The standard wing weight estimation for the outboard wing section included three terms including W1, W2, and W3, relating to wing bending loads, control surfaces and shear material, and wing area, respectively. W3 also accounts for a variety of miscellaneous terms.

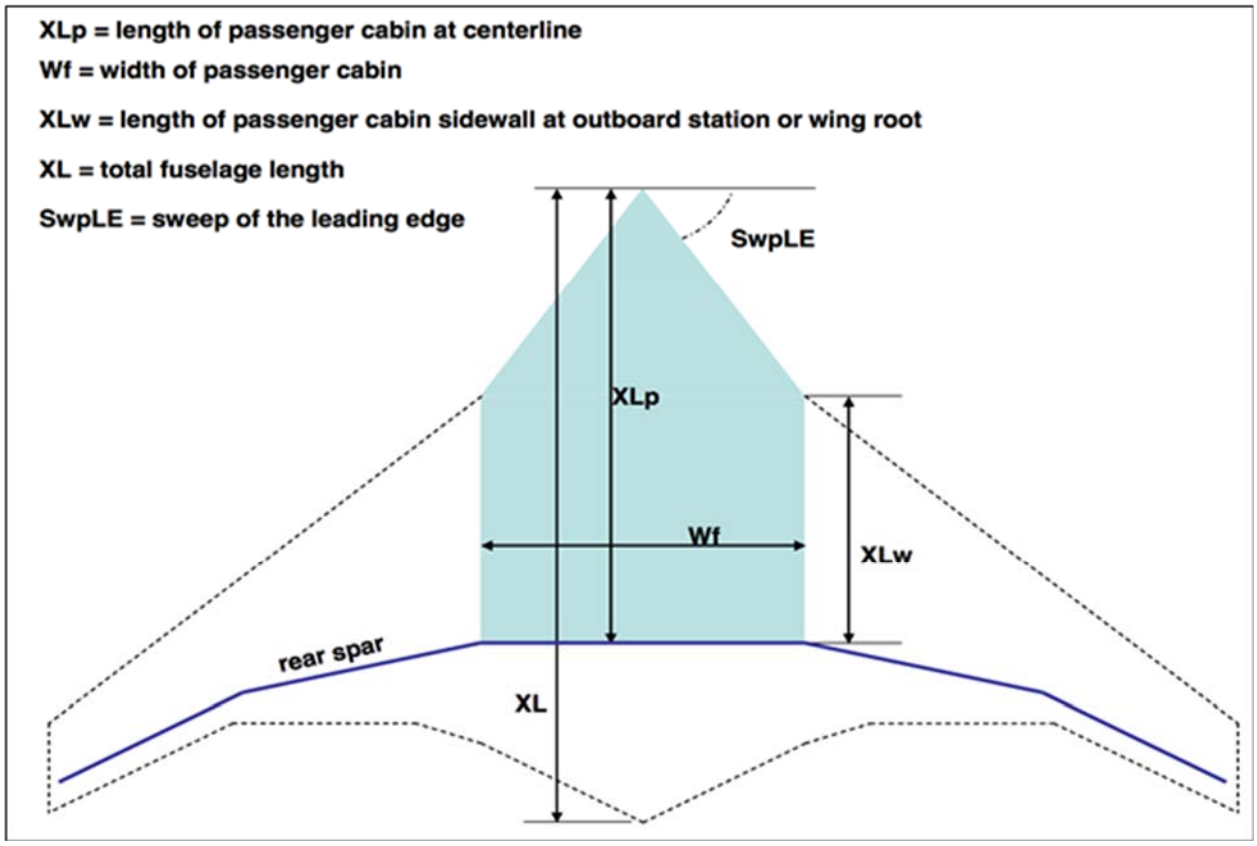

Figure 46. HWB FLOPS Implementation Geometric Layout [Nickol 2009]

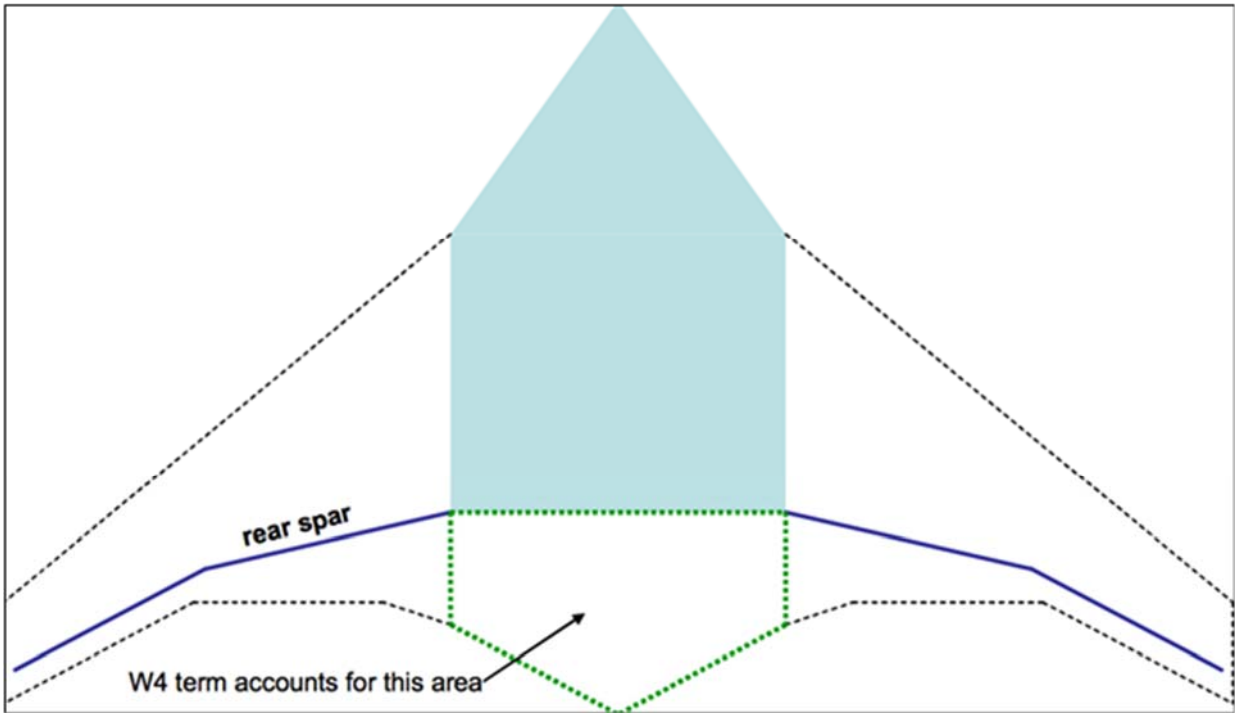

Figure 47. Aft Body Weight Accounted for by Wing Weight W4 Term [Nickol 2009]

While the weight regression shown in equation 1 was based off of a few centerbody structural layouts, further goals are to examine whether this weight calculation will be representative of the centerbody structural layouts of the current HWB model. Also there is interest in how the weight estimation of the aft body compares to the FLOPS calculation.

3.4.3.4.2 Inputs to Model

To perform the finite element modeling in NASTRAN, compatible bulk data files need to be created. To do this, MATLAB script, "HCD_struct" was utilized, requiring five input files along with a VSP file. The VSP file specifically needed to be exported as a, ".dat" file to be read correctly in MATLAB. The VSP model used for this study's specific geometry is shown again in Figure 48 and was based off of the geometry specified in FLOPS case 4. The five input files (Bwb_param_mat_PR_DISP, Bwb_param_lift, Bwb_param_aero, BWB_Struct_inputs, and BWB_ Param_Weights) did not differ much from the files provided. The datafiles provided were those used in the Boeing OREIO analysis, as will be discussed further in the validation section [Gern 2013].

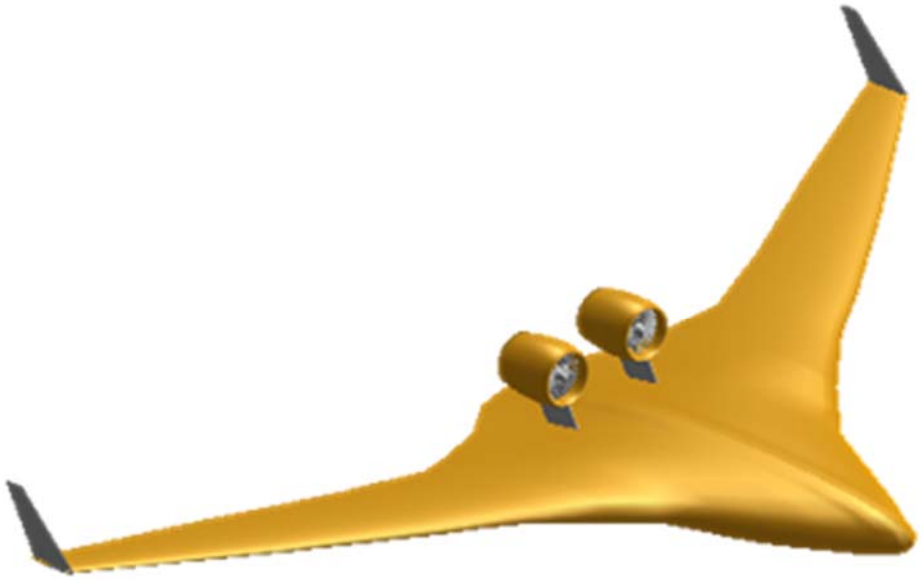

Figure 48. HWB VSP Model

The structural input file was modified to coordinate with the VSP structure and vehicle from FLOPS corresponding to the HWB with ITD technology package. A comparison of the data for the structural input file is shown in Table 38. It's important to note that the same chordwise location assumptions of the front and rear spars for both mid-section and outboard were used in this study to correspond to previous studies similar to the OREIO. These specific chordwise spar locations were 12.5% and 62.5% for the front and rear, respectively. Along with this assumption, the front bulk head of the centerbody was again defined by the same standard cockpit size assumptions as previous studies.

Table 38. Structural Input File Comparison

Original Inputs	GT Inputs	Units	Variable Name	Comment
Centerbody				
1051.7	1104	In	XLp	Length of passenger cabin at centerline
450.0	528	In	Wf	Width of passenger cabin
656.4	528	In	XLw	Length of passenger cabin sidewall at outboard station or wing root
96.0	96	In	CPl	Cockpit length, position of front bulkhead (fixed)
30.0	30	In	FSsb	Front spar set back from leading edge
3	3	-	-	Numofbays, number of centerbody bays
3	3	-	-	Numofbaysaft, number of aftbody bays (must be identical to numofbays for now)
Mid section *is defined by centerbody and outboard wing parameters*				
Outboard wing				
12.5	12.5	%	Fspercent	Front spar chord percentage
62.5	62.5	%	Fspercent	Rear spar chord percentage
480.0	552	In	Wgbrky	Spanwise location of wing break (connection between mid section and outboard)
Aft body				
178.4	132	In	Aftblen	Length of aft body (from centerbody rear spar to center flap hingeline)
450.0	528	In	aftbwid	Width of aft body at center flap hingeline

Table 39. Parameter Weights Input File

Original Inputs	GT Inputs	Units	Variable Name	Comment
Weights				
100000.0	64050.0	lbs	Payload	payload weight
128045.0	120104	lbs	Fuel	fuel weight (Flops)
23108.0	52370.0	lbs	systems	systems weight (Flops)
Landing Gear Parameters				
19404	20180	lbs	gear	landing gear weight (Flops)
100	136.9	in	maingl	main landing gear strut length
75	87.3	in	nosegl	nose landing gear strut length
0.2	0.2	-	gearrat	ratio of nose gear weight vs total gear weight
0.6	0.6	-	gearloc	chordwise location of main gear on centerbody SOB
Engine Parameters				
54222	22531	Lbs	Engweight	engine weight (Flops propulsion total)
3	2	-	Engnum	number of engines
126.6	126.6	In	Rotordia	rotor diameter for CONM2 (75% of 168.8in)
48	48	In	Rotclear	rotor clearance from HWB upper skin
77.7	134.1	In	Nacdia	nacelle diameter
45	45	In	Inplane	distance from inlet plane to engine CG
73.8	73.8	In	Rplane	distance from CG to mean rotor plane
0.6	0.6	-	engloc	chordwise location of outboard engine on aftbody SOB
Vertical Tail Parameters				
2381	2381	Lbs	tailweight	vertical tail weight (Flops)
80	80	In	VT_off_y	spanwise offset of VT from aftbody rear spar
-80	-80	In	VT_off_x	chordwise offset of VT from aftbody rear spar
35	35	Deg	VT_q_swp	VT quarter chord sweep
222	222	In	VT_span	VT span (18.5ft OREIO report)
190.7	190.7	In	VT_rt_c	VT root chord (1.13 * rotor diameter)
81	81	In	VT_tp_c	VT tip chord (0.48 * rotor diameter)
45	45	Deg	VT_cant	VT cant angle (zero means VT is vertical) was 32.4
-16.9	-16.9	Deg	VT_toe	VT toe angle (zero is in direction of aircraft x-axis) was -16.9

3.4.3.4.3 Incorporation into EDS

All of the MATLAB plots created by HCD_struct are included in Figure 51. To focus on the resulting HWB structural representation, Figure 49 shows the resulting structural components for FEM modeling. This can be then compared to the original files in Figure 50 to further illustrate the differences between the structure of the OREIO [Gern 2013] and the model used.

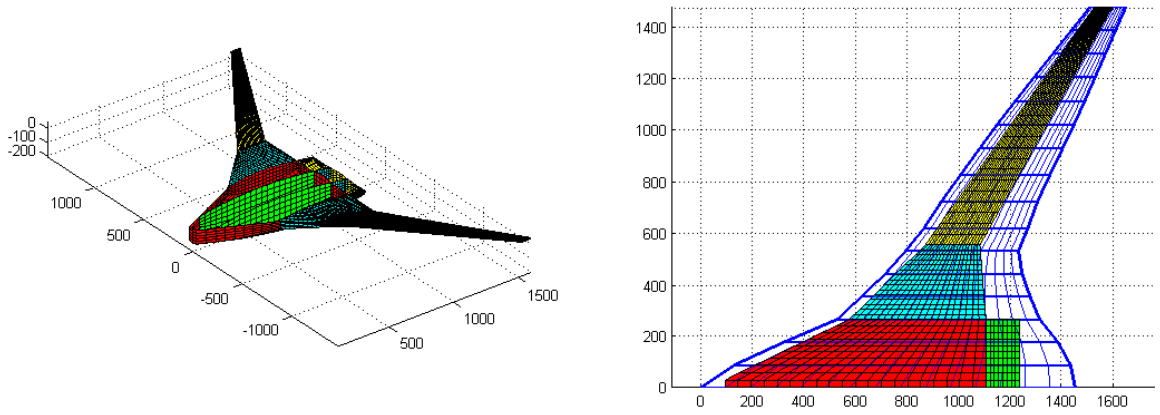

Figure 49. (Left) Primary Structure for FEM Modeling and (Right) Primary Structure with Overlay of Nastran Doublet Lattice Aerodynamic Paneling for Specified Geometry

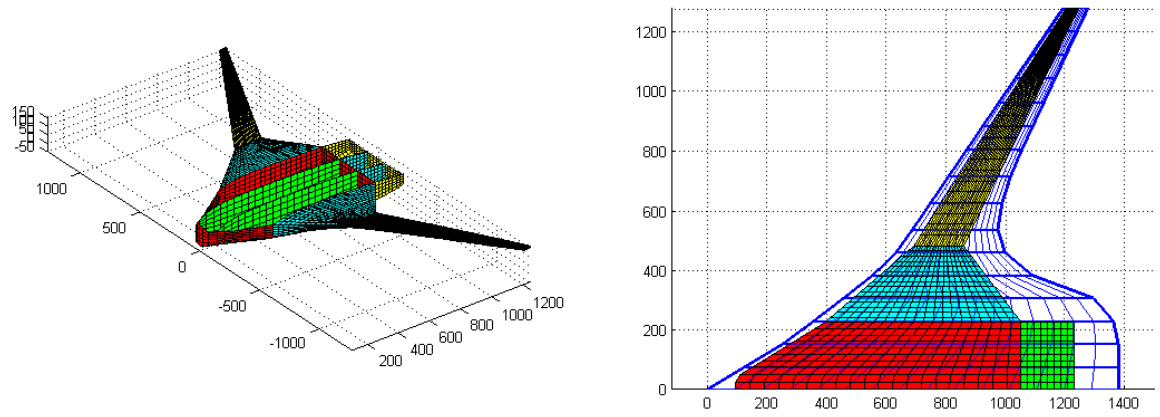

Figure 50. (Left) Primary Structure for FEM Modeling and (Right) Primary Structure with Overlay of Nastran Doublet Lattice Aerodynamic Paneling for Original Inputs

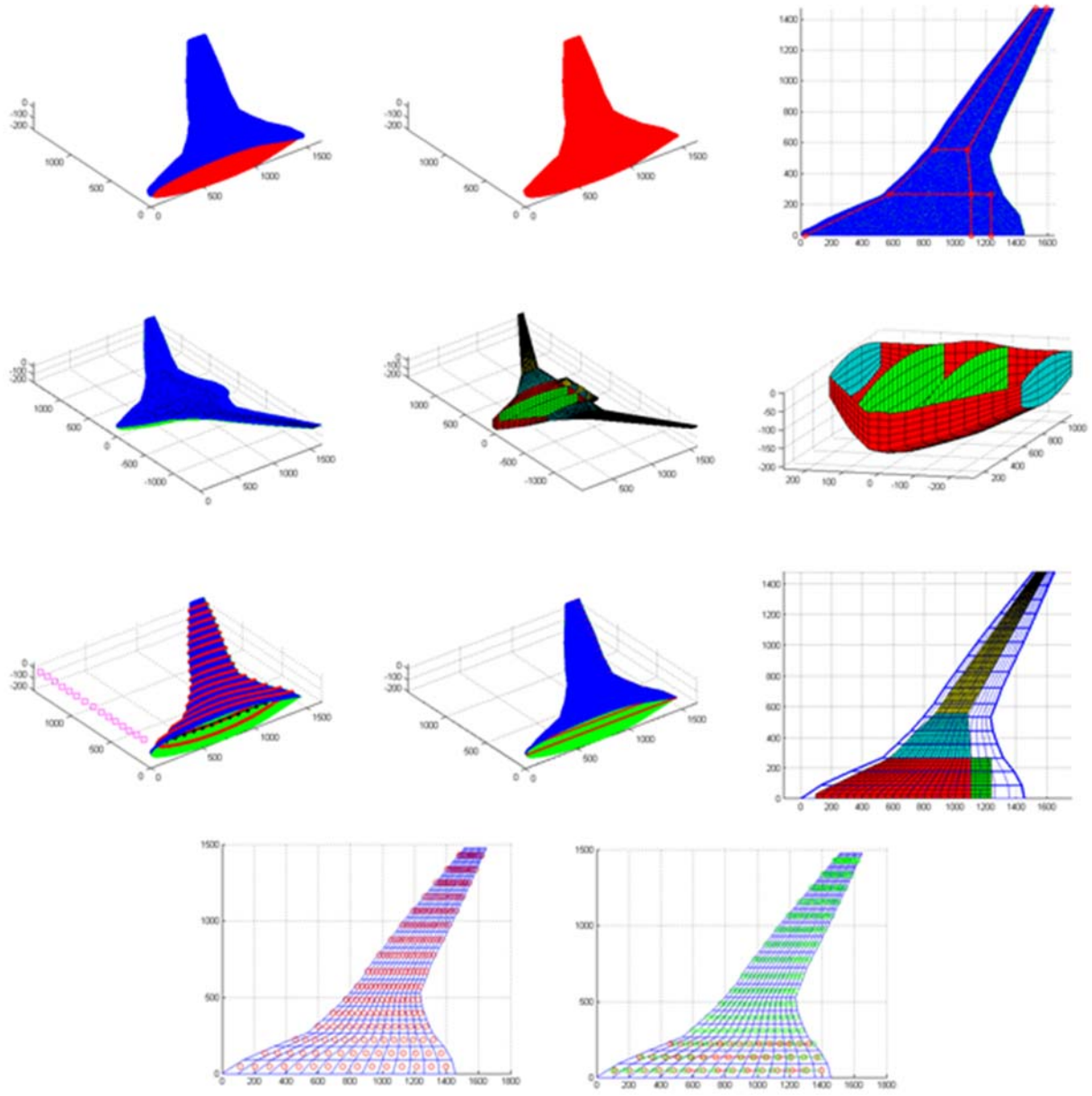

Figure 51. MATLAB Figures Generated for the Specified Geometry

3.4.3.4.4 Validation of Model

Upon receiving the HWB centerbody tool, the data files were run without any modification. The structure, as well as, the input files resembled the OREIO study [Gern 2013]. The landing gear weight, systems weight, fuel weight, and propulsion total weight, detailed in the parameter weight input file shown in the Table 39, matched those detailed in the OREIO weight table shown in Table 40. The output weights for the given vehicle also resembled the same weights as shown in Figure 52 from the same study [Gern 2013]. The centerbody weight estimate, through FEM based analysis, was 50,708 lbs; the aft body weight being 11,892 lbs and the total primary structural weight being 121,590lbs. The MATLAB plots that were generated

are shown below in Figure 53. For these reasons, it is believed that the same study was passed to us and that the method used was the same as previous studies and we were able to then apply the similar method to our own study.

Table 40. Boeing OREIO Weights Statement [Pitera 2005, Gern 2013]

FUNCTIONAL GROUP	WEIGHT (lbs)
WING (incl. outboard wing, mid and aft section)	63,791
VERTICAL TAIL	2,381
FUSELAGE (centerbody)	77,412
LANDING GEAR	19,404
PAINT	1,614
STRUCTURE TOTAL	**164,602**
ENGINES	50,254
FUEL SYSTEM-TANKS AND PLUMBING	3,968
PROPULSION TOTAL	**54,222**
SURFACE CONTROLS	9,821
AUXILIARY POWER	661
INSTRUMENTS	976
HYDRAULICS	3,894
ELECTRICAL	2,523
AVIONICS	2,237
FURNISHINGS AND EQUIPMENT	254
AIR CONDITIONING	2,361
ANTI-ICING	381
SYSTEMS AND EQUIPMENT TOTAL	**23,108**
WEIGHT EMPTY	**241,931**
CREW AND BAGGAGE-FLIGHT, 2	450
UNUSABLE FUEL	1,335
ENGINE OIL	231
OPERATING WEIGHT	**243,948**
CARGO	100,000
ZERO FUEL WEIGHT	**343,948**
MISSION FUEL	128,045
RAMP (GROSS) WEIGHT	**471,993**

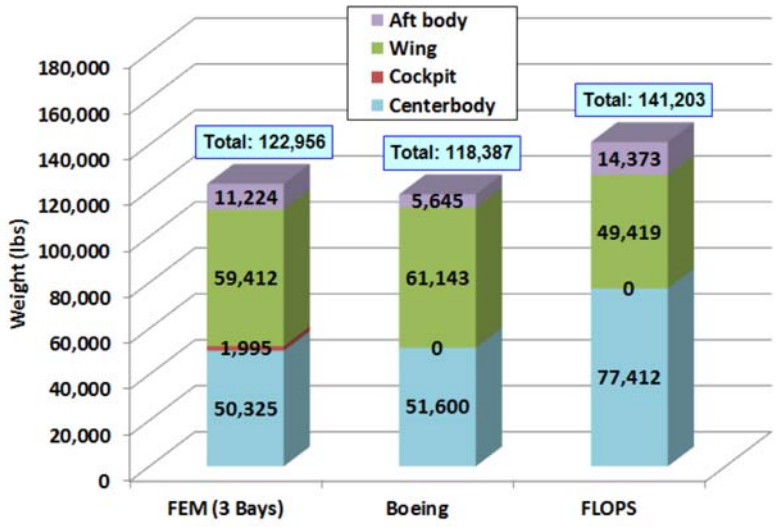

Figure 52. OREIO Weights Comparison for Different Analyses. [Gern 2013]

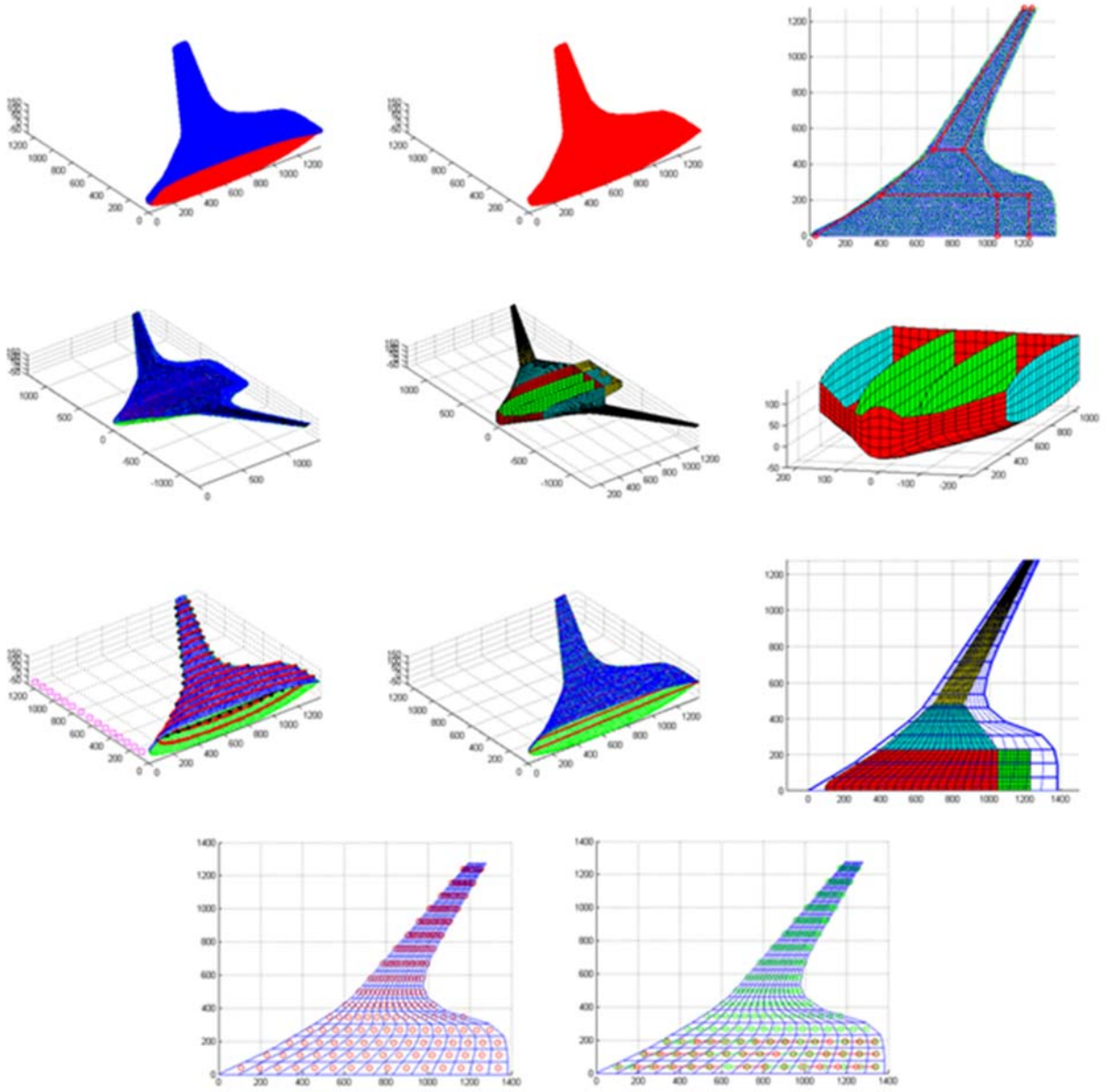

Figure 53. MATLAB Figures Generated for the Original Files

3.4.3.4.5 Comparison of Weights

Centerbody Weight: The centerbody weight from the FEM-based analysis (65,493 lbs) is about 2.8% lighter than the FLOPs prediction value (67,382 lbs).

Aft Body Weight: For HWB analyses in FLOPS, Term 4 of the wing weight breakdown corresponds to the weight of the aft body. The FEM based aft body weight prediction of 11,961 lbs is about 5.3% lighter than the FLOPS aft body weight (12,635 lbs).

The centerbody weight calculated from the FEM-based analysis, when compared to the FLOPs predicted value, is similar to the 2% difference shown in the ORIEO study [Gern 2013].

The 5.3% difference for the aft body of this study is a considerable improvement to that compared to the difference of roughly 24% in the ORIEO study; this is perhaps due to the inertia and thrust loads of the engines. The propulsion total weight in Table 40 shows a large difference between the OREIO study and our models. In general though, it's observed that the aft-body structure has the higher degree of uncertainty for structural weight prediction when compared to the centerbody weight estimation.

3.4.3.5 Development of HWB RTC

One of the key requirements for the RTC development was maintaining the maximum amount of commonality in the assumptions and technology levels as possible between the HWB and the T&W baseline vehicles. The engine technology level and modeling parameters for the HWB vehicles were taken directly from the T&W engines. The mission and payload requirements were also directly translated from the T&W vehicles. The commonality was deemed necessary to make the comparisons between the configurations and the technology assessments as even as possible.

The RTC EDS HWB vehicle geometry was developed based on the Boeing and OREIO vehicles with the centerbody geometry sized in FLOPS for the passenger load for the three vehicle classes. The reference vehicles were used in the selection of wing outboard geometry and

The initial values of wing loading and thrust-to-weight ratio were taken from the Boeing 0009A, but had to be modified. The wing loading was slightly increased to 52 psf to maintain commonality on the approach speed. The thrust-to-weight was increased from 0.22 to 0.27 for the STA and LTA, and up to 0.31 for the VLA. These increases were necessary to enable the vehicle to climb to a sufficiently high altitude. It is probable that the thrust lapse predicted for the EDS engine models is significantly worse than that predicted by Boeing.

The final HWB RTC vehicle characteristics are shown in Table 41 for the STA, Table 42 for the LTA, and Table 43 for the VLA.

Table 41. Vehicle Characteristics of HWB STA RTC with a Geared Fan

Description	STA HWB GF RTC
TOGW, lbs	367366
Operating Empty Weight, lbs	192139
Fuel Weight, lbs	120417
Design Payload, lbs	54810
Block Fuel, lbs	107953
Passengers	261
Design Range, nmi	5920
Wing Area, sq ft	7070
Aspect Ratio	7.95
T/W	0.27
W/S, psf	52

Table 42. Vehicle Characteristics of HWB LTA RTC with a Geared Fan

Description	LTA HWB GF RTC
TOGW, lbs	537229
Operating Empty Weight, lbs	273149
Fuel Weight, lbs	200030
Design Payload, lbs	64050
Block Fuel, lbs	181210
Passengers	305
Design Range, nmi	7530
Wing Area, sq ft	10339
Aspect Ratio	6.04
T/W	0.27
W/S, psf	52

Table 43. Vehicle Characteristics of HWB VLA RTC with a Geared Fan

Description	VLA HWB GF RTC
TOGW, lbs	805565
Operating Empty Weight, lbs	435615
Fuel Weight, lbs	282379
Design Payload, lbs	87570
Block Fuel, lbs	253681
Passengers	417
Design Range, nmi	7060
Wing Area, sq ft	15489
Aspect Ratio	7.08
T/W	0.31
W/S, psf	52

3.4.4 Over Wing Nacelle

The Over Wing Nacelle (OWN) configuration is a modification of the conventional tube and wing with the turbofans integrated into the wing structure. This engine integration provides some noise shielding of the jet exhaust. An additional modification from the T&W is that the tail is a T-tail configuration; the tail change is driven by the need to keep the horizontal tail out of the jet wash of the engine.

The OWN model is based on the T&W SSA, which is the only vehicle class modeled as an OWN. The wing geometry is modified for the engine installation based on [Hahn 2010]. The VSP model for the SSA RTC of the OWN is shown in Figure 54, with the reference geometry from [Hahn 2010] shown in Figure 55.

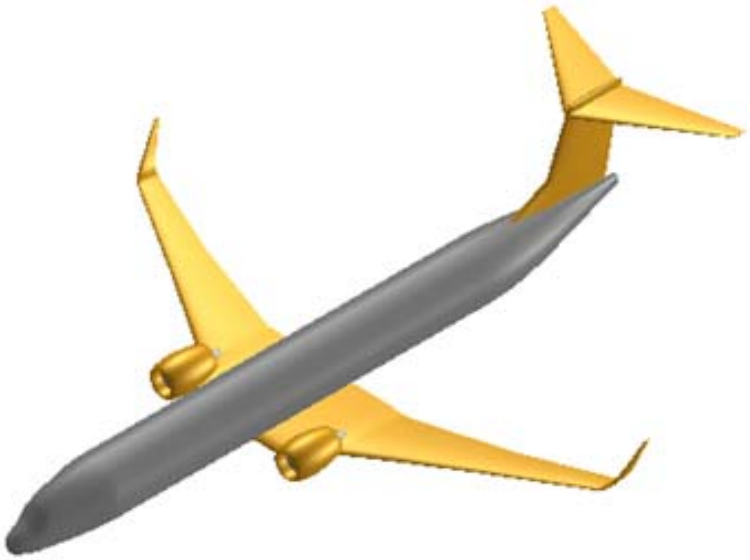

Figure 54. Over Wing Nacelle Configuration

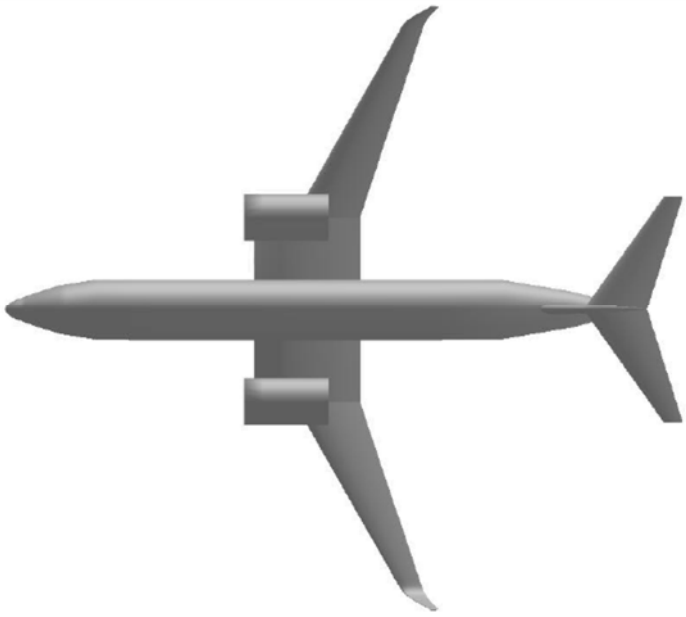

Figure 55. Over Wing Nacelle Reference Geometry from [Hahn 2010]

3.4.5 Mid Fuselage Nacelle

The Mid Fuselage Nacelle (MFN) aircraft refer to an unconventional aircraft configuration for which the engines are installed on the fuselage. This configuration also includes two decks in the fuselage. The engines are not necessarily installed at the rear fuselage as the conventional fuselage-mounted-engine aircraft, instead, they are installed close to the trailing edge of the wing or mid fuselage to provide noise shielding of the engine from the wing. Figure 56 shows an illustration of this concept.

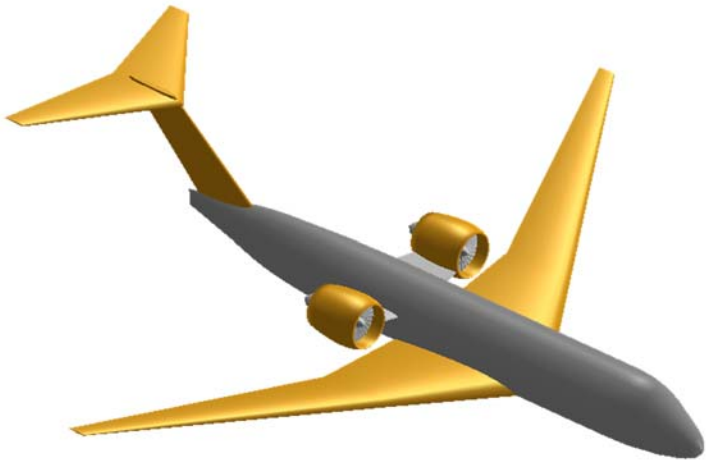

Figure 56. Concept of MFN Aircraft

3.4.5.1 Baseline aircraft creation, design mission and configuration

The EDS model of the baseline MFN aircraft is created based on the similar concept (2025-0027A) designed by Boeing in [Bonet 2011], which is referred to as the reference aircraft. An EDS aircraft model was created and calibrated/validated against this reference aircraft, which is referred as reference (EDS) model. This reference model is then modified to match the design mission, configuration/geometry, technology portfolio and performance of this research, resulting in the (EDS) baseline aircraft model.

The design mission, configuration/geometry and performance data of this reference aircraft are from [Bonet 2011], and its Advanced Turbofan (ATF) engine configuration/geometry, cycle and performance data are from [Manglesdorf 2012]. The reason that the engine data of [Manglesdorf 2012] are used instead of those in [Bonet 2011] is because the ATF engines used in the two reports are similar but the former report has significant more details of the engine.

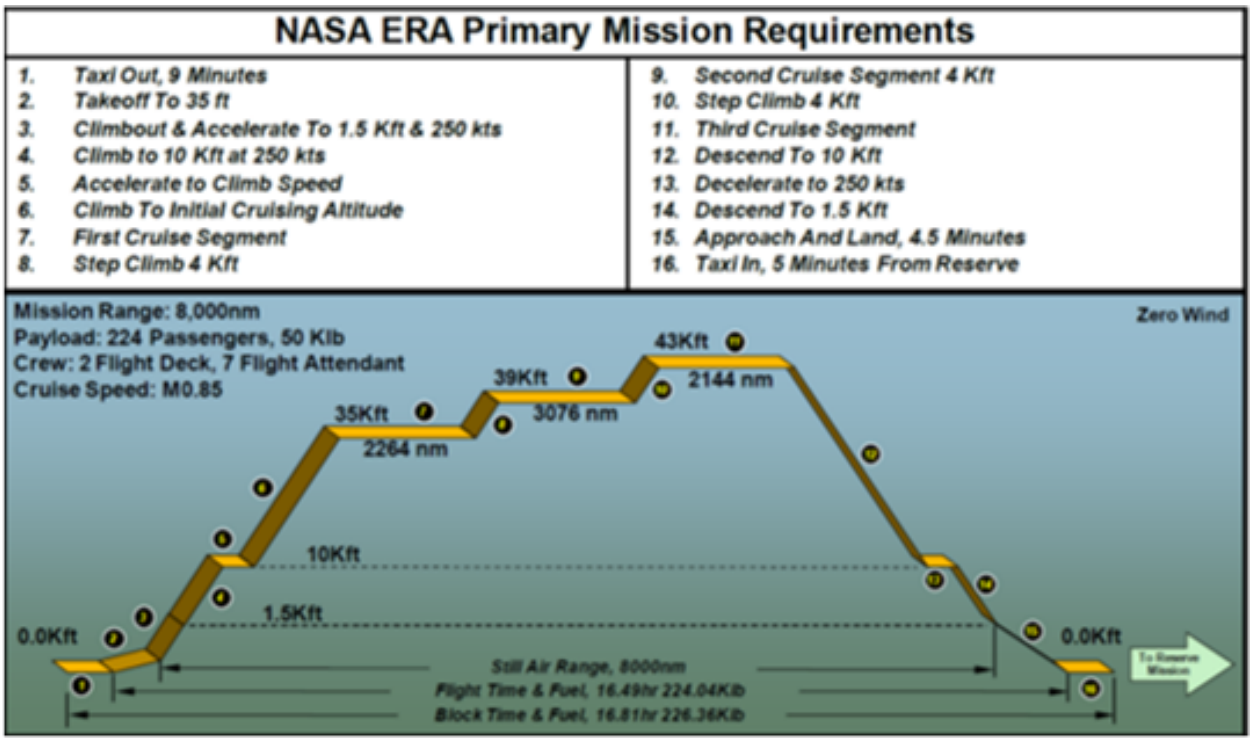

Figure 57. NASA ERA Primary Mission Requirements (from [Manglesdorf 2012])

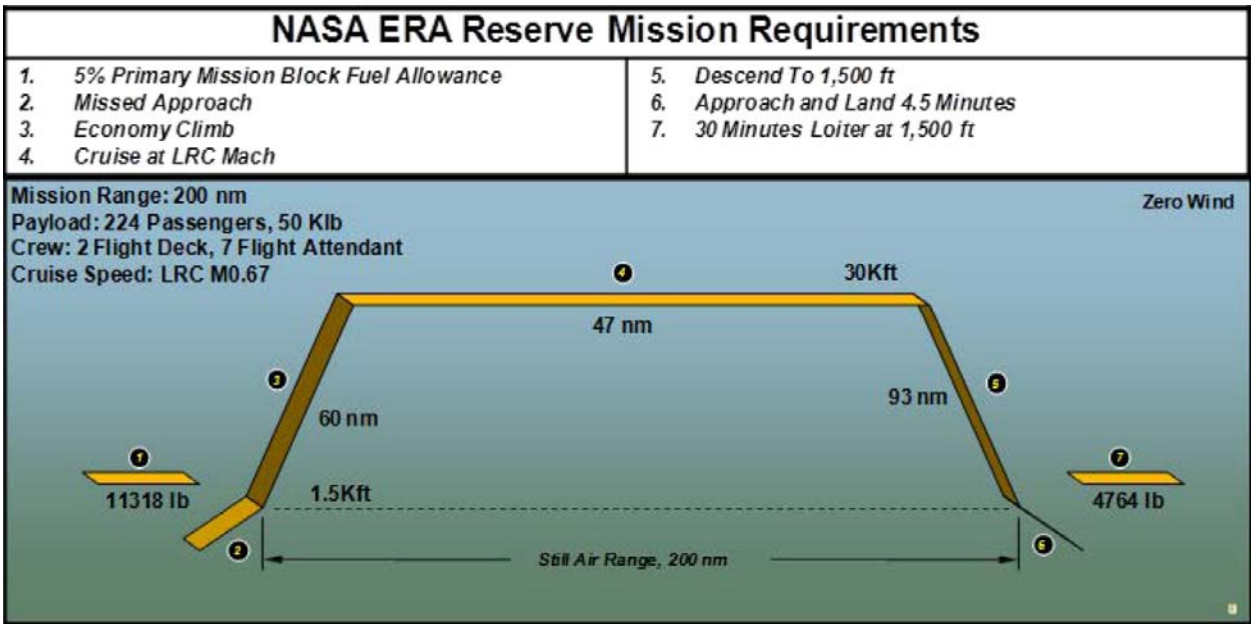

Figure 58. NASA ERA Reserve Mission Requirements (from [Manglesdorf 2012])

Table 44. MFN Vehicle and Mission Assumptions

Variable Description	NASA ERA	MFN (LTA)
Design Range, n.mi.	8000	7440
Cruise Mach Number	0.85	0.84
Number of Passengers	224	300

3.4.5.2 Modeling and Design Considerations

The configuration of the MFN aircraft is similar to that of conventional tube-wing aircraft with engines installed on the fuselage, except for two major differences. The first difference is that there are two decks in the passenger cabin/fuselage. This double deck fuselage configuration results in a shorter fuselage, which may in turn results in lighter weight and less aerodynamic drag. The second difference is that the engine inlet lip/face is very close to the trailing edge of the wing; actually it is above and a little bit upstream of the wing trailing edge. This engine-wing configuration is proposed with the expectation to have good shielding of the engine inlet noise.

With those two main differences in mind, the design process for MFN is generally the same as for the conventional tube-wing configuration. During the design process, special models were made for weight and aerodynamic estimation of the double-deck fuselage; for aerodynamic estimation of the wing affected by close coupled engine; and for the noise shielding effect because of the engine-wing configuration.

3.4.5.3 Modeling wing and double deck fuselage in FLOPS

In FLOPS, for the conventional tube-wing configuration, the aerodynamics of the fuselage is captured by three main OML sizes, i.e. fuselage length, maximum fuselage width and maximum fuselage depth, while its weight needs an additional size, i.e. length of passenger compartment. Note here the fuselage weight estimation is for a fuselage with single deck passenger compartment.

The double deck fuselage of MFN is equivalent to a longer single deck one of conventional tube-wing aircraft. It is found that FLOPS can also estimate both the aerodynamics and weight of a MFN fuselage by extrapolation usage of its fuselage weight estimation. That is, the nominal fuselage OML sizes will be given for aerodynamic estimation while a longer length of passenger compartment will be given for weight estimation. Since the number of passengers of MFN aircraft is 300 and that of the reference aircraft is 224, the fuselage and passenger compartment were scaled up for MFN aircraft from the reference aircraft. The double deck fuselage modeling results are shown in Table 45. As one can see, the length of passenger compartment is even greater than the fuselage length because of the extrapolation.

Table 45. Double Deck Fuselage Modeling

Variable Description	[Bonet 2011]	MFN (LTA)
Fuselage Length, ft	154.8	171.5
Maximum fuselage width, ft	17.5	21.1
Maximum fuselage depth, ft	19.92	21.7
Length of passenger compartment, ft	168.7	182.6

Because of close coupling between the wing and engine, the lift and drag of the wing are expected to be affected. In FLOPS, those effects can be captured by three factors, i.e. airfoil technology parameter, factor to increase or decrease lift-independent drag coefficient, and factor to increase or decrease lift-dependent drag coefficient. Those factors are determined during the calibration process.

3.4.5.4 Noise modeling

The noise modeling for the MFN is very similar to that of a traditional configuration for a T&W aircraft. The airframe noise sources, such are leading edge noise, flap noise, horizontal tail noise, etc. The primary difference in in the modeling of the engine mounts, as it is in a different location than most large twin aisle aircraft. The more challenging part of the noise modeling for the MFN occurs with the engine noise sources. Since the engine is mounted above and in close proximity to the main wing, the engine noise will benefit from shielding effects from the shielding surface, the main wing. This was done through the use of the WING module in ANOPP. The WING module allows the user to input either a shielding or reflecting surface and alters the source noise propagation to ground the observers appropriately. The shielding surface was selected to be the main wing and defined for various engine sources. The shielding plane was defined differently for different engine source because the engine is large enough that the distance between the origins of the engine noise sources is not insignificant when accounting for shielding benefits. The engine noise sources that originate in the physical engine, such as fan inlet noise and combustor noise, were given a different shielding plane definition than the single stream jet noise sources, and the mixing jet noise source as well as the total jet noise source were given yet an altogether separate definition. This allowed for confidence that each noise source was receiving the appropriate amount of shielding benefit and an over/under compensation for shield would not occur.

3.4.5.5 Engine and aircraft calibration

As mentioned previously, the EDS model of the baseline MFN aircraft is modified from the reference aircraft model, which is calibrated/validated against the reference aircraft. The good quality of the calibration results can provide the confidence on the MFN aircraft model, and thus the calibration results of the reference model are provided.

The ATF engine used on the reference aircraft is first calibrated/validated. As mentioned previously, the engine configuration, cycle and performance data are from [Manglesdorf 2012]. In Figure 59, the Lockheed Report ATF represents the ATF engine described in [Manglesdorf 2012], and EDS ATF represents the ATF engine model created in EDS for the reference aircraft.

As one can see, the engine calibration/validation results are very satisfactory in terms of cruise performance.

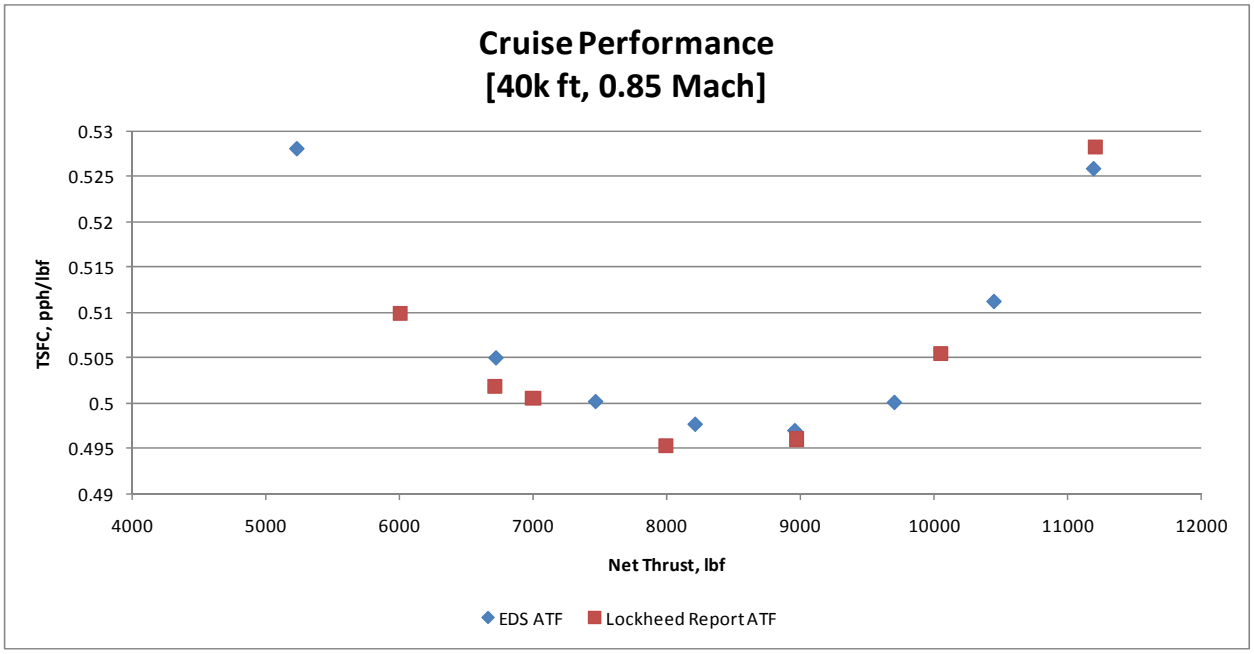

Figure 59. Calibration of ATF Engine for MFN Reference Aircraft

The reference aircraft model is then calibrated/validated against the reference aircraft described in [Bonet 2011]. During the calibration process, subsystem weights are matched; structural weights are matched by varying structural factors in FLOPS; and fuel burn is matched by varying drag factors in FLOPS with the AFT engines calibrated above. As one can see in Table 46, the aircraft calibration/validation results are very satisfactory for most of the differences being less than ±1%.

Table 46. MFN Reference Aircraft Model Calibration/Validation Results

Variable Description	[Bonet 2011]	EDS Output	% Difference
MTOGW (lb)	453,159	452,241	-0.20%
OEW (lb)	242,354	242,271	-0.03%
Wing Weight (lb)	63,665	63,278	-0.61%
Propulsion System Weight (lb)	27,356	27,326	-0.11%
Fuel Capacity at MTOGW (lb)	160,805	159,971	-0.52%
Net Thrust (SLS, lb)	62,800	63,333	0.85%
Fan Diameter (in)	109*	109.2	0.18%
Bypass Ratio (Cruise)	13.7*	14.1	2.92%
Fan Pressure Ratio (TOC)	1.58*	1.58	0.00%
Overall Pressure Ratio (TOC)	65*	64.96	-0.06%
Cruise TSFC	0.495**	0.495**	-0.0%
*2025 ATF data from Lockheed Report ([Manglesdorf 2012]) **Defined at calibrated throttle hook flight conditions			

3.4.6 Box Wing

The box wing (BXW) aircraft refer to such an unconventional aircraft configuration that has two tandem wings connected at the wing tips with offsets or winglets, forming a box shape in the front or rear view. The forward wing is swept back and the aft wing forward, forming a diamond shape in a plan view; and the engines are installed under the aft wing; see Figure 60 for the illustration of this concept.

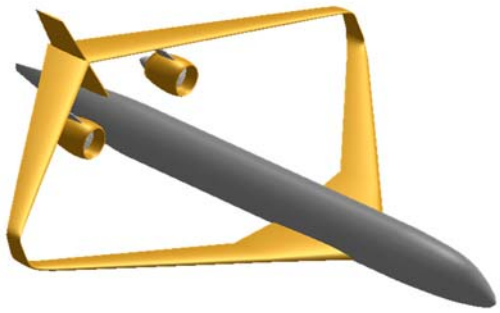

Figure 60. Concept of Box Wing Aircraft

3.4.6.1 Baseline aircraft creation, design mission and configuration

The EDS model of the baseline BXW aircraft is created based on the similar concept designed by Lockheed Martin in [Manglesdorf 2012], which is referred as reference aircraft. An EDS aircraft model is created and validated against this reference aircraft, which is referred as intermediate/validation aircraft. This intermediate/validation aircraft is then modified to match the design mission, configuration/geometry, technology portfolio and performance of this research, resulting in the baseline aircraft.

The design mission, configuration/geometry and performance data of this intermediate aircraft are from [Manglesdorf 2012], and its Ultra Fan 2025 engine configuration/geometry, cycle and performance data are also from [Manglesdorf 2012].

The mission requirements of BXW are developed based on those of the Boeing 777-200 and the NASA ERA mission requirements. The resulting mission requirements of BXW are similar to the NASA ERA mission requirements, the primary and reserve missions of which are shown in Figure 57 and Figure 58, respectively, except for the major difference shown in Table 47.

Table 47. BXW Vehicle and Mission Assumptions

Variable Description	NASA ERA	BXW (LTA)
Design Range, n.mi.	8000	7440
Cruise Mach Number	0.85	0.84
Number of Passengers	224	300

3.4.6.2 Modeling and Design Considerations

This reference aircraft was the best result in terms of three measures of merit: fuel consumption, noise and emission, and those measures are used to evaluate and select configuration and technologies, as described in the Lockheed Martin report [Manglesdorf 2012]. For emission, the Lockheed Martin research team looked into more details including LTO NOx, particulate matter, hydrocarbon emissions, smoke, and anticipated fuel sulphur content. In this research, the emission measure of merit is focused on LTO NOx, cruise NOx and hydrocarbon emissions (represented by fuel consumption).

The configuration of the BXW aircraft is quite different from that of conventional tube-wing aircraft with engines installed under the wing. It is a special kind of biplane or joined wings, both the front and aft wings producing positive lift, while the horizontal tail of the conventional tube-wing usually produces negative lift. Because the two wings are joined/supported at the tips by a vertical offset or wing let, it has the promise to significantly reduce the induced drag and moderately reduce the total structural weight of the two wings.

Because of those aerodynamic and structural differences, special models/methods will be made for aerodynamic and weight estimation of the wings; and the design process of the conventional tube-wing configuration will be modified to accommodate those special models/methods.

3.4.6.3 Box wing aircraft aerodynamic modeling

Box wing is a special kind of biplane or joined wings with two wing tips being joined by a vertical winglet and both wings producing positive lift. In this closed wing system, the vertical winglets significantly reduce or even inhibit the formation of wingtip vortices, which are the major cause of the induced drag; in addition, there is no significant adverse wing interference because of no overlapping in the plan view and the offset between wings ([Wolkovitch 1986]). These features result in substantial reduction of induced drag with comparison to that of an equivalent monoplane wing of the same total lift and span ([Wolkovitch 1986] and [Prandtl 1924]).

For high speed (transonic) transport aircraft, since the induced drag is a large portion of the total drag, this configuration has the promise to substantially reduce the total drag at cruise, comparing to that of a conventional tube-wing configuration with the same total wing area and span ([Lange 1974] and [Salam 2012]).

As a fast modeling method in FLOPS, a box wing airplane is represented by two FLOPS models (because lift of canard is ignored in FLOPS):

- Front model: front wing + fuselage + winglets + engines;
- Aft model: aft wing as a fly wing + engines.

The (back-swept) front wing and the (forward-swept) aft wing have the same span, and the fly wing is modeled as a Blended-Wing-Body (BWB) airplane in FLOPS. The internal drag polars of the two models outputted by FLOPS are combined with correction to the induced drag as a function of sweep angles and offset. The resulting drag polar is used as the drag polar of the box wing aircraft. The following describes the process to combine the drag polars. The drag outputted by FLOPS includes the following components:

$$C_D = (C_D)_{lift\_dependent} + (C_D)_{lift\_independent}$$

$$(C_D)_{lift\_dependent} = C_{Dp} + C_{Di}$$

$$(C_D)_{lift\_independent} = C_{D\Delta} + C_{Dc}$$

where C_{Dp} is the pressure drag, C_{Di} is the induced drag, and $C_{D\Delta}$ is the drag component as a function of altitude and Mach number, and C_{Dc} the compressive drag or wave drag. The total wing area of the box wing aircraft is the sum of the areas of the front and aft wings:

$$S_T = S_F + S_A$$

where S_T is the total wing reference area, S_F is the front wing reference area, and S_A the aft wing reference area.

The lift and drag coefficients (drag polar) of the box wing aircraft can be calculated from those of the two aircraft models with correction for reference area, respectively. And after the correction for reference area, the resulting drag polar is deemed as that of an equivalent monoplane wing with the same span and total wing area.

$$C_{L,monoplane} = (C_{L,F})_{FLOPS} \frac{S_F}{S_T} + (C_{L,A})_{FLOPS} \frac{S_A}{S_T}$$

$$C_{Dx,monoplane} = (C_{Dx,F})_{FLOPS} \frac{S_F}{S_T} + (C_{Dx,A})_{FLOPS} \frac{S_A}{S_T}$$

where the subscript $_F$ means the front wing, $_A$ the aft wing; and C_{Dx} can be any of C_{Dp}, C_{Di}, $C_{D\Delta}$, or C_{Dc}. Since there is no significant adverse wing interference because of no overlapping in the plan view and the offset between wings, we assume that the lift coefficient of the box wing equals to that of the equivalent monoplane wing, i.e.

$$C_{L,BW} = C_{L,monoplane}$$

For the drag components of the box wing and the equivalent monoplane wing, we assume that only the component of induced drag is different and needs to be adjusted/modified to get $C_{Di,BW}$ From [Buttazzo 2009], the relationship of minimum or theoretical induced drag between the box wing and equivalent monoplane wing is

$$\frac{(C_{Di})_{BW,\,theoretical}}{(C_{Di})_{monoplane,theoretical}} = \frac{1+0.45h/b}{1.04+2.81h/b}$$

where h is the offset or the vertical distance at the tip of the two wings and b is the wing span. FLOPS actually outputs the minimum induced drag for a wing planform, therefore,

$$C_{Di,monoplane} = (C_{Di})_{monoplane,theoretical}$$

From [Wolkovitch 1986], the main difference between an actual box wing and its theoretical one, which has the minimum induced drag, is their span efficiency factor, and the relationship based on data fitting is,

$$\frac{e_{actual}}{e_{theoretical}} = 1 + \frac{0.04(\tan\Lambda_F + \tan\Lambda_A)}{(\tan 29^\circ + \tan 20^\circ)}$$

where e is span efficiency factor and Λ is the sweep angle.

Since $C_{Di} = \frac{C_L^2}{\pi A e}$ and the lift coefficients of the actual and theoretical box wings are the same, we have,

$$\frac{C_{Di,BW}}{(C_{Di})_{BW,theoretical}} = \frac{e_{theoretical}}{e_{actual}}$$

Combining the previous equations, the induced drag of a box wing can be estimated as

$$C_{Di,BW} = \frac{K_1}{K_2} \times C_{Di,monoplane}$$

where $K_1 = \frac{1+0.45h/b}{1.04+2.81h/b}$, $K_2 = 1 + \frac{0.04(\tan\Lambda_F + \tan\Lambda_A)}{(\tan 29^\circ + \tan 20^\circ)}$

3.4.6.4 Estimation of the box wing weight

FLOPS currently does not have the option to estimate the weight of a box wing, therefore it has to be done externally. [Howe 1996] suggests a general form of semi-empirical box wing weight estimation,

$$M_W = C_1 \left[\frac{bS}{\cos \Lambda_{1/4}} \left(\frac{1+2\lambda}{3+3\lambda} \right) \left(\frac{M_{TOM} N}{S} \right)^{0.3} \left(\frac{V_D}{\tau} \right)^{0.5} \right]^{0.9}$$

where C_1 is a coefficient to be determined by data fitting, and the other symbols and units are listed in Table 48.

Table 48. Symbols and Units of the Box Wing Weight Estimation Equation

Symbol	Note	Unit
M_w	(Metal) wing mass/weight	Kg
b	Span	Meter
S	Wing Area	Square meter
$\Lambda_{1/4}$	Quarter-chord sweep angle	Degree
λ	Taper ratio	
M_{TOM}	Maximum takeoff mass	Kg
N	Normal acceleration factor (2.5)	
V_D	Design diving speed	Meter/second
τ	Average thickness to chord ratio (simple average of ratios at different spanwise locations)	

[Jemitola 2013] gives C_1=0.028 for each *metal* half (front or aft) wing of *medium* range box wing aircraft based on fitting the results of FEM structural analyses. For the box wing aircraft of this research, we assume it still can use the above general form of wing weight estimation equation; since its range is long range and thus its aspect ratio is different, C_1 needs to be re-estimated.

The data of passenger and cargo box wing aircraft from the Lockheed Martin report [Manglesdorf 2012] are used to estimate the coefficient C_1 for long range box wing aircraft. For each of passenger and cargo box wing aircraft, a coefficient is estimated; the average of two values is used for *metal* wing of *long* range box wing aircraft; and finally,

$$C_1 = 0.021$$

There are three notes. One note is that if composite material is used in the box wings, C_1 needs to be further adjusted. The fact is considered during the coefficient estimation that the Lockheed Martin report uses composite material in the wings, resulting in 35% weight reduction from an otherwise metal wing. The last note is, for the design diving speed, we assume:

$$V_D = 1.02V_C$$

where V_C is the design cruise speed.

3.4.6.5 Scaling of the box wing planform

The scaling of the box wing planform is different from those of other aircraft types in this research. For box wing, the wing area and span are inputs and the aspect ratio is calculated; while for other aircraft types the area and aspect ratio are inputs and the span is calculated. Assuming the sweep angles of the box wing planform in the Lockheed Martin report [Manglesdorf 2012] have been optimized, we want to keep those values when the two wings are scaled according to the change of total wing area. This can be done by the following scaling procedure.

A. Get the new total wing area, span and front wing area ratio (the ratio of the front wing area and total wing area, based on that of the Lockheed Martin report);

B. Get the data of wing station location and chord length for the baseline wings;

C. Calculate the new area of each wing according to the front wing area ratio;

D. For each wing, calculate a temporary wing area based on the wing station locations and chord lengths of the baseline wing and the new span (match the span);

E. For each wing, calculate the new chord lengths by scaling the baseline chord lengths with the ratio of the new wing area and the temporary wing area (match the area);

F. For each wing, use the baseline wing station locations, new chord lengths and new span.

3.4.6.6 Flowchart of box wing aerodynamic and weight estimation in EDS

During the sizing/design process of the box wings, the convergence of the aerodynamic estimation and the convergence of weight estimation are coupled, since both the wing aerodynamics and wing weight estimations interact with aircraft total weight estimation. Therefore, the convergences of those two estimations need to be achieved at the same iteration step. The following flowchart in Figure 61 shows how this is achieved.

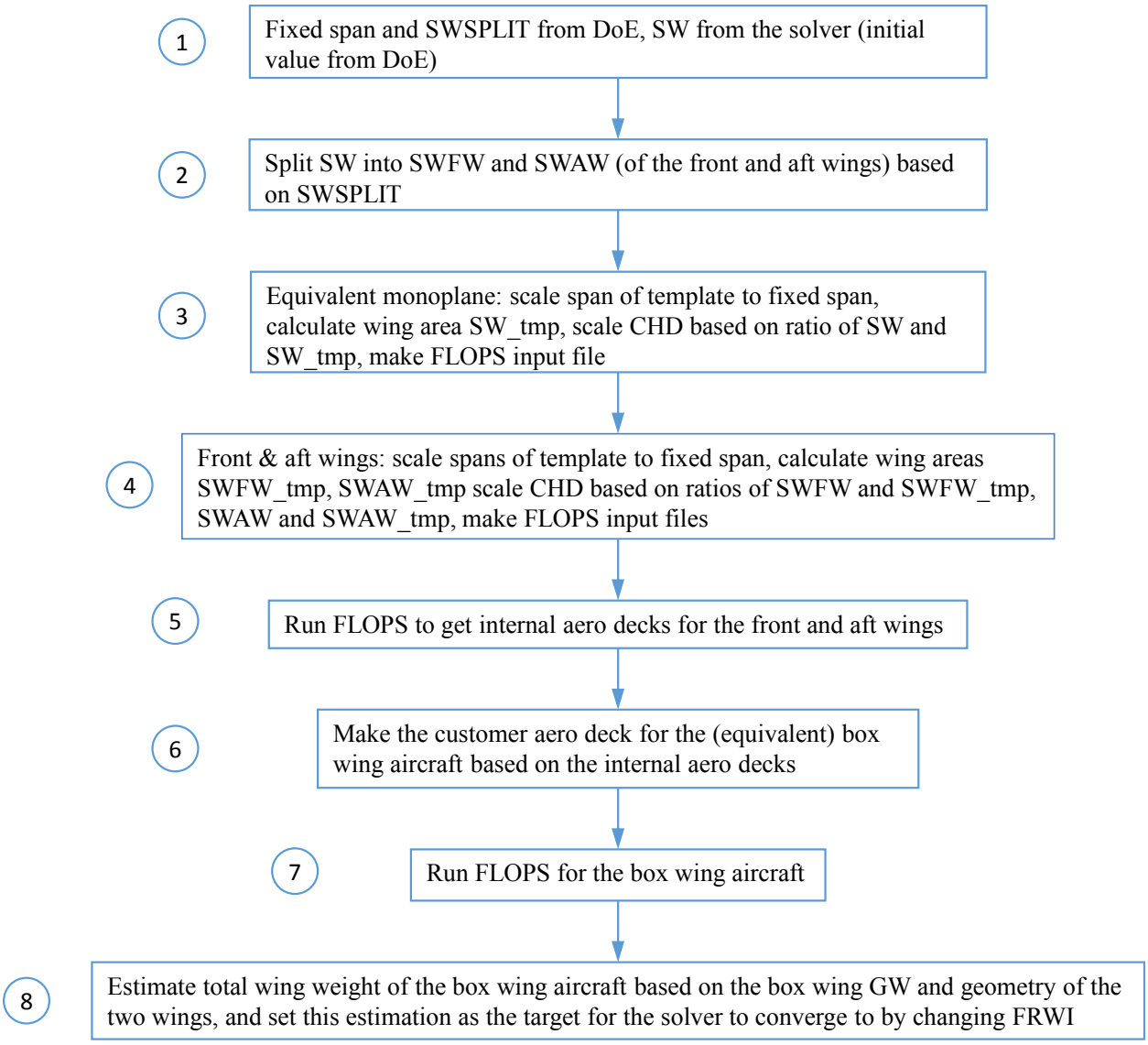

Figure 61. Box Wing Aero and Weight Estimation FlowChart

For Step 6 to make the customer aero deck for the box wing aircraft, the details are described in Section 3.4.6.3; and for Step 8 to estimate total wing weight, the details are described in Section 3.4.6.4.

3.4.6.7 Box wing aerodynamic modeling in APEX

One suggestion was to use APEX ([AVID 2014]) to model the aerodynamics of the box wing aircraft. APEX is a fast, medium-fidelity aerodynamic analysis tool based on a robust vortex-lattice theory, capable of analyses of transonic speed range and full aircraft configuration including wing, and fuselage. The main advantages of APEX include it can be fast, accurate and handle the full aircraft (although vertical tail, engine and its pylon are not modeled). If it could be shown to be appropriate for the box wing aircraft as well, it could provide a fast and accurate solution.

Limited by the vortex-lattice theory that APEX based on, in addition to no vertical tail, engine or pylon, the closed wing system of the box wing aircraft has to be modeled as two separate parts in APEX, as shown in Figure 62

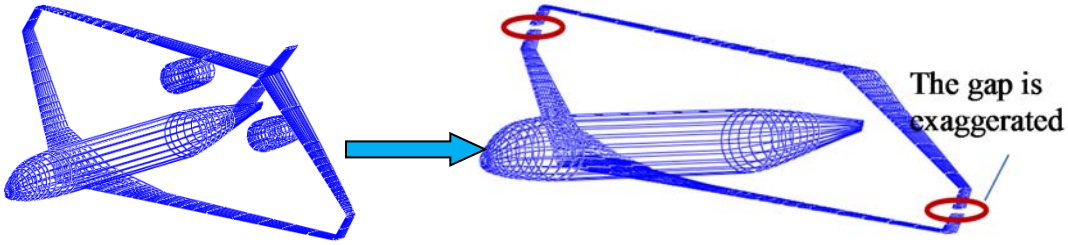

Figure 62. Open Wing System for Modeling Box Wing in APEX

A validation case has been executed for modeling box wing aircraft with APEX. The box wing aircraft described in the Lockheed Martin report [Manglesdorf 2012] was modeled in APEX Versions 1.1.3 and 1.5.0, at Mach 0.85, 0.75, 0.65, and altitude between 20,000 feet to 50,000 feet. The aerodynamic results of APEX were compared to those in the Lockheed Martin report, and the following were observed:

- APEX gives much greater induced drag and parasite drag Cdo, even though there are no vertical tail, engine and pylon;
- APEX did not capture the effect of altitudes on drag polars, i.e. the drag polars almost do not change with altitude.

Because of those discrepancies above, which are thought due to the limitation of its theory, APEX was not used for modeling the aerodynamics of box wing aircraft, instead, an approximation method using FLOPS was developed, as described in Section 3.4.6.3.

3.4.6.8 Noise modeling

The noise modeling for the box wing aircraft is separated into two parts, airframe noise source analysis and engine source noise analysis. The engine source noise analysis is done exactly as the T&W aircraft engine noise analysis (utilizing ANOPP) with the engine placement being designated to the aft of the aircraft. The airframe noise source analysis is done slightly different due the addition of the aft wing. Due to the fact that ANOPP cannot model a box wing configuration naturally, some creative manipulation was done to provide the most accurate and realistic airframe noise analysis as possible. The airframe sources that reside on the wing, such as leading edge noise, flap noise and slat noise, were modeled separately for the fore wing and source noise was evaluated at the fore wing location. The same was done for the aft wing noise sources with the source noise evaluation done at the aft wing location. These two separate noise groupings, fore wing sources and aft wing sources, were then propagated down to the observer location and summed together to provide a total airframe source noise analysis (with the addition of the vertical stabilizer noise). However, because of the limitations of ANOPP, there is a possibility of missing possible new noise sources produced by a boxed wing configuration.

3.4.6.9 Engine and aircraft calibration

As mentioned previously, the EDS model of the baseline BXW aircraft is modified from the reference aircraft model, which is calibrated/validated against the reference aircraft. The

good quality of the calibration results can provide the confidence on the BXW aircraft model, and thus the calibration results of the reference model are provided.

The Ultra Fan engine used on the reference aircraft is first calibrated/validated. As mentioned previously, the engine configuration, cycle and performance data are from [Manglesdorf 2012]. In Figure 63, the Rolls Royce – Ultra Fan represents the Ultra Fan engine described in [Manglesdorf 2012], and EDS – Ultra Fan represents the Ultra Fan engine model created in EDS for the reference aircraft. As one can see, the engine calibration/validation results are very satisfactory in terms of cruise performance.

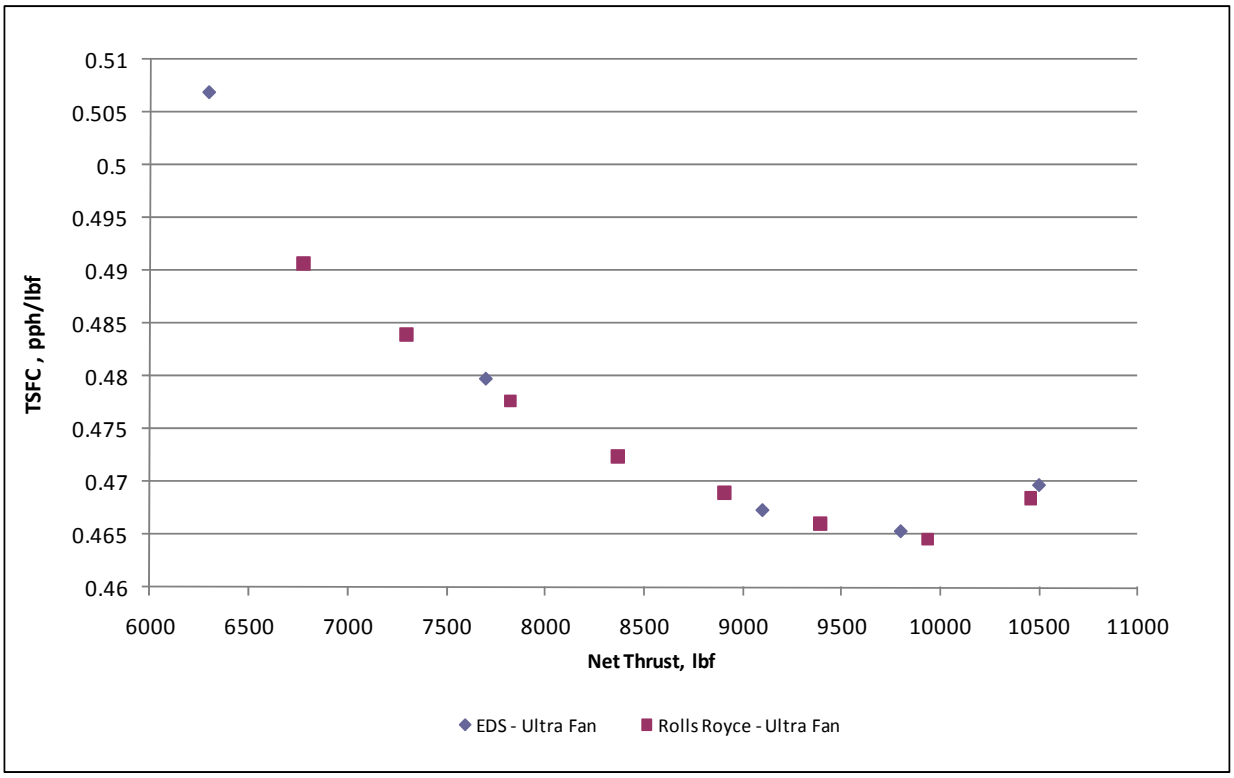

Figure 63. Calibration of Ultra Fan Engine for BXW Reference Aircraft

The reference aircraft model is then calibrated/validated against the reference aircraft described in [Manglesdorf 2012]. During the calibration process, subsystem weights are matched; structural weights are matched by varying structural factors in FLOPS; and fuel burn is matched by varying drag factors in FLOPS with the Ultra Fan engines calibrated above. As one can see in Table 49, the aircraft calibration/validation results are very satisfactory for most of the differences being less than ±1%.

Table 49. BXW Reference Aircraft Model Calibration/Validation Results

Variable Description	[Manglesdorf 2012]	EDS Output	% Difference
MTOGW (lb)	365,914	364,680	-0.34%
OEW (lb)	191,381	191,737	0.19%
Wing Weight (lb)	36,070	36,070	0.00%
Propulsion System Weight (lb)	31,612	31,613	0.00%
Mission Fuel Burn (lb)	122,460	122,768	0.25%
Net Thrust (SLS, lb)	63,600	63,600	0.00%
Nacelle Diameter (in)	184.0	184.0	0.00%
Cruise L/D	21.5	21.7	0.93%
Cruise TSFC	0.465	0.475	2.15%

3.5 Vehicle Coefficients for Fleet Assessment

Vehicle technology impacts were to be rolled up to the fleet level as part of this work by executing a fleet level environmental impact tool called AEDT. AEDT calculations are based on BADA vehicle definitions for high altitude and SAE Air1845 for calculations below 10,000ft. The generation of the necessary input xml files had been automated as part of the creation of EDS, but the sheer number of vehicles being considered in this case to cover all vehicle classes, year of introduction, and scenario combinations severely tested the robustness of the original algorithms. One of the main issues in properly defining the necessary coefficients for the AEDT input file is that in both BADA and SAE Air1845 the coefficients used often do not have a physical meaning. They are not things like Max Thrust or Overall Pressure Ratio, but rather thrust coefficient 1 and 2, which in some way represent variation of thrust with speed and altitude and must be extracted from multiple points in the engine deck as well as consideration of multiple missions and specific data at specific altitudes. Ensuring that the points in the engine deck selected for the calculations were available for all vehicle sizes and technology packages and that the conditions needed by AEDT had been considered in the EDS execution was extremely challenging and required several iterations.

Most of the robustness issues were ironed out throughout the second year allowing the team to generate fleet level fuel burn results, however, additional issues were encountered when considering mission NOx due to the specific implementation of the Boeing Fuel Flow Method in AEDT which did not account for the potentially different behavior of modern combustors at altitude. Consideration of LTO NOx for year 2 also highlighted new robustness issues with the algorithms generating AEDT coefficients because these calculations explore a range of altitude/temperature/humidity conditions which had not been previously tested. The new algorithms developed have proven to be far more reliable in year 3 allowing for a nearly flawless link between the vehicle team and the fleet level assessments.

4.0 Technology Modeling

4.1 Technology Assessment Process

Using EDS as the modeling and simulation environment, ASDL executed the technical approach depicted in Figure 64, which has three main elements: a parametric advanced vehicle modeling, a technology modeling and assessment element, and a vehicle performance evaluation element called metrics calculations. Modeling advanced configurations (left block of Figure 64) begins with a parametric geometry model with appropriate definition to predict the aerodynamic characteristics of the vehicle. This parametric geometry model will also drive the component weight sizing and estimation. Along with vehicle aerodynamic and weight prediction, a detailed and parametric propulsion sizing and performance model is also critical to modeling advanced concepts. The propulsion model must also be able to provide a propulsion system weight based on preliminary flowpath analysis.

Once these subsystems have been synthesized based on an initial gross weight guess, the vehicle sizing is accomplished through a mission analysis, which is based on the mission definition either derived from the capability definitions or provided by the designer. The synthesis and sizing process is an iterative procedure for estimating vehicle gross weight by balancing fuel available and fuel required.

Once the vehicle is synthesized and sized with the vehicle mass converged, the three main ERA metrics are computed (middle block of Figure 64). The fuel burn metric is computed by executing a performance analysis which has been developed by ASDL to also include a set of calculations to characterize the vehicle performance in formats consistent with FAA's Aviation Environmental Design Tool (AEDT) [Roof 2007]. This feature of the system design environment allows for direct connection to fleet level modeling for estimating system-wide metrics. The emissions metric for the landing and takeoff cycle as well as for cruise is computed using an emission model developed by ASDL under a previously NASA funded NRA. The noise metric, in terms of cumulative certification noise levels, is then estimated based on information from the vehicle sizing/performance and propulsion system analyses. In order for the ERA project to make informed decisions on the technology portfolio, the system design tool set must also be able to estimate vehicle cost, ranging from technology maturation to certification costs based on the information from vehicle modeling and technologies being considered.

These computed metrics are the basis by which the potential ERA technologies are being evaluated to determine the best combinations that can achieve the ERA project goal of simultaneously meeting the fuel burn, noise, and emissions metrics. The upper-right block of Figure 64 shows a structured process to model and assess technologies, which begins with a list of candidate technologies from the ERA portfolio. First, the physical compatibility rules for this list of technologies must be established via a technology compatibility matrix (TCM). The purpose of the TCM is to define the relationships between the various technologies and configurations, whether they be compatible, incompatible, enablers or have direct interactions. Next, the impacts of each technologies modeled through the use of k-factors are organized via a technology impact matrix (TIM). The combination of the TCM and TIM produces the parametric ranges for the desired technology k-factors. Based on the number of k-factors and their established ranges, a design of experiment (DOE) is chosen. The DOE then dictate the specific input settings for each execution of advanced vehicle modeling and metrics calculation blocks of Figure 64.

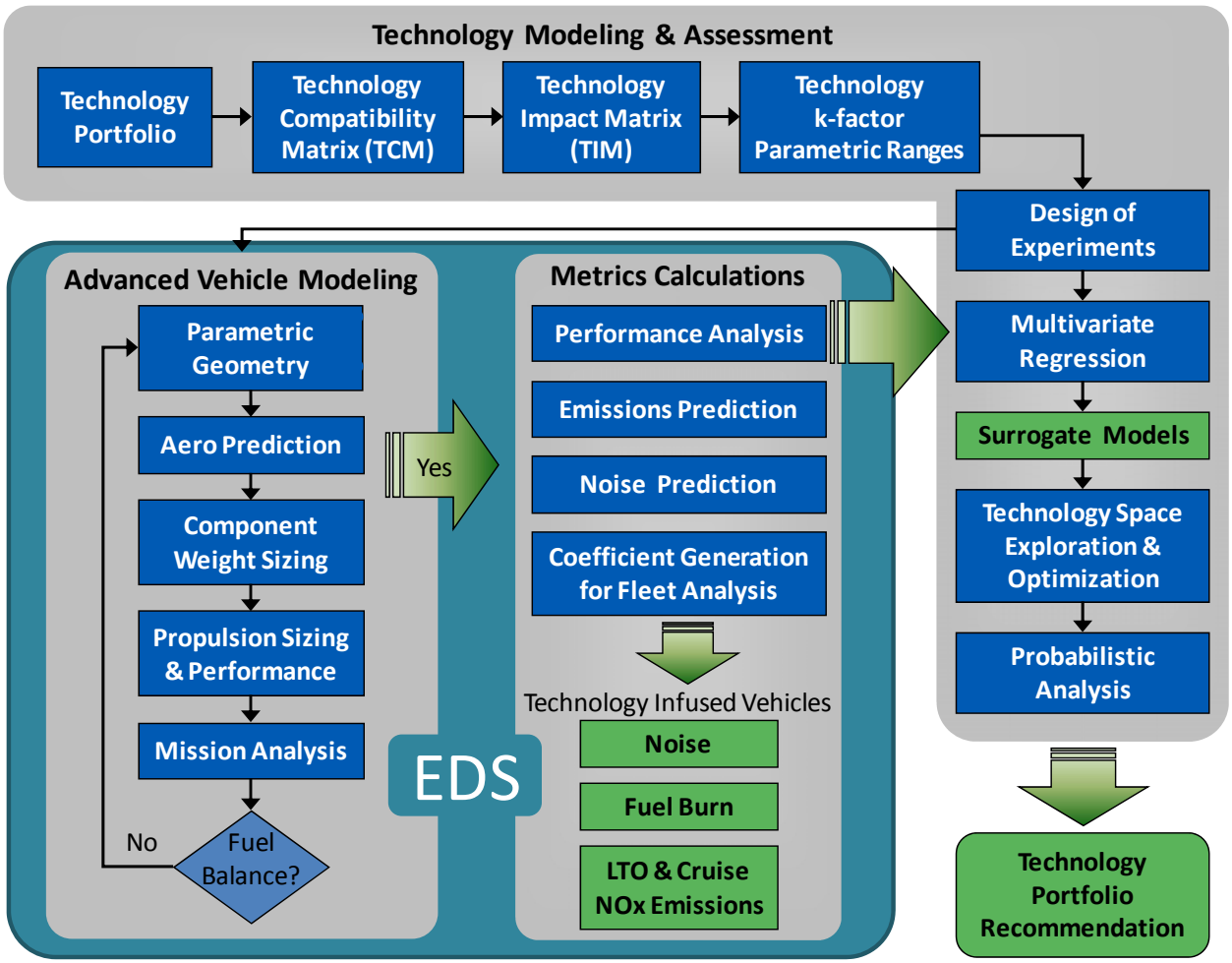

Figure 64. Technical Approach Process Chart

The computed metrics are collected for each DOE simulation and utilized in a multivariate regression to generate surrogate models. These surrogate models represent the technology space to be explored and optimized to maximize their impact. These surrogate models are also the enablers to perform probabilistic analysis to establish the uncertainty in a concept achieving the ERA goals.

4.2 Technology Compatibility Matrix (TCM)

The portfolio of technologies to be simulated onboard the fleet of ERA vehicles contains many combinations of technologies that are incompatible. The Technology Compatibility Matrix (TCM), part of which is depicted in Figure 65, is used to prevent incompatible technologies from being simultaneously applied to a single vehicle simulation. Before generating an EDS input vector representing a vehicle with a unique package of technologies applied, the TCM is used to ensure that the technology package does not contain any incompatible technology pairs.

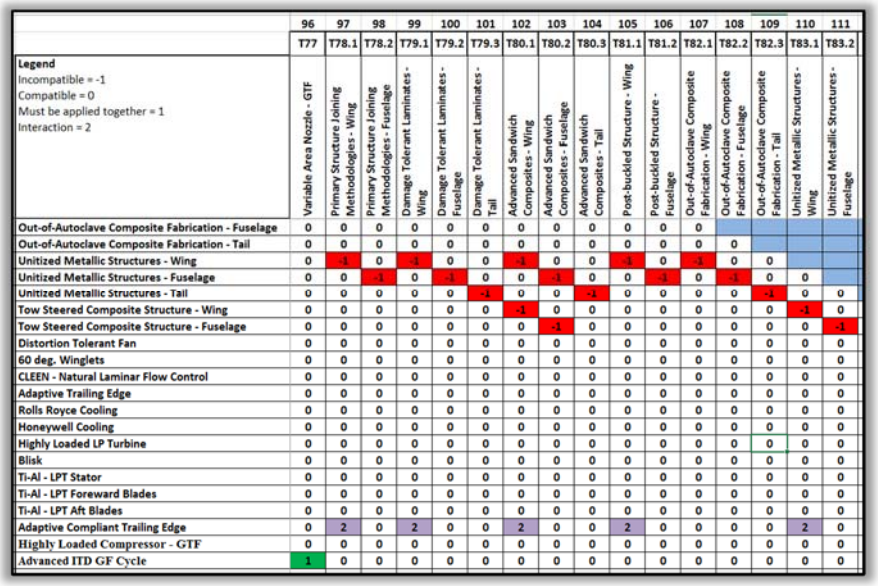

	96	97	98	99	100	101	102	103	104	105	106	107	108	109	110	111
	T77	T78.1	T78.2	T79.1	T79.2	T79.3	T80.1	T80.2	T80.3	T81.1	T81.2	T82.1	T82.2	T82.3	T83.1	T83.2
Legend Incompatible = -1 Compatible = 0 Must be applied together = 1 Interaction = 2	Variable Area Nozzle - GTF	Primary Structure Joining Methodologies - Wing	Primary Structure Joining Methodologies - Fuselage	Damage Tolerant Laminates - Wing	Damage Tolerant Laminates - Fuselage	Damage Tolerant Laminates - Tail	Advanced Sandwich Composites - Wing	Advanced Sandwich Composites - Fuselage	Advanced Sandwich Composites - Tail	Post-buckled Structure - Wing	Post-buckled Structure - Fuselage	Out-of-Autoclave Composite Fabrication - Wing	Out-of-Autoclave Composite Fabrication - Fuselage	Out-of-Autoclave Composite Fabrication - Tail	Unitized Metallic Structures - Wing	Unitized Metallic Structures - Fuselage
Out-of-Autoclave Composite Fabrication - Fuselage	0	0	0	0	0	0	0	0	0	0	0	0				
Out-of-Autoclave Composite Fabrication - Tail	0	0	0	0	0	0	0	0	0	0	0	0	0			
Unitized Metallic Structures - Wing	0	-1	0	-1	0	0	-1	0	0	-1	0	-1	0	0		
Unitized Metallic Structures - Fuselage	0	0	-1	0	-1	0	0	-1	0	0	-1	0	-1	0	0	
Unitized Metallic Structures - Tail	0	0	0	0	0	-1	0	0	-1	0	0	0	0	-1	0	0
Tow Steered Composite Structure - Wing	0	0	0	0	0	0	-1	0	0	0	0	0	0	0	-1	0
Tow Steered Composite Structure - Fuselage	0	0	0	0	0	0	0	-1	0	0	0	0	0	0	0	-1
Distortion Tolerant Fan	0	0	0	0	0	0	0	0	0	0	0	0	0	0	0	0
60 deg. Winglets	0	0	0	0	0	0	0	0	0	0	0	0	0	0	0	0
CLEEN - Natural Laminar Flow Control	0	0	0	0	0	0	0	0	0	0	0	0	0	0	0	0
Adaptive Trailing Edge	0	0	0	0	0	0	0	0	0	0	0	0	0	0	0	0
Rolls Royce Cooling	0	0	0	0	0	0	0	0	0	0	0	0	0	0	0	0
Honeywell Cooling	0	0	0	0	0	0	0	0	0	0	0	0	0	0	0	0
Highly Loaded LP Turbine	0	0	0	0	0	0	0	0	0	0	0	0	0	0	0	0
Blisk	0	0	0	0	0	0	0	0	0	0	0	0	0	0	0	0
Ti-Al - LPT Stator	0	0	0	0	0	0	0	0	0	0	0	0	0	0	0	0
Ti-Al - LPT Foreward Blades	0	0	0	0	0	0	0	0	0	0	0	0	0	0	0	0
Ti-Al - LPT Aft Blades	0	0	0	0	0	0	0	0	0	0	0	0	0	0	0	0
Adaptive Compliant Trailing Edge	0	2	0	2	0	0	2	0	0	2	0	0	0	0	2	0
Highly Loaded Compressor - GTF	0	0	0	0	0	0	0	0	0	0	0	0	0	0	0	0
Advanced ITD GF Cycle	1	0	0	0	0	0	0	0	0	0	0	0	0	0	0	0

Figure 65. Technology Compatibility Matrix (TCM) depiction showing the various relationships assumed present between ERA technology pairs.

Within the TCM, numerical values are assigned to every possible technology pair. These values have been established through internal as well as external audits completed by subject matter experts. A matrix cell value of zero is used when the pair of technologies is compatible and the two technologies are not expected to interact with each other. If a technology pair is incompatible, a value of negative one is assigned to the corresponding cell within the TCM. If a particular technology requires an accompanying technology in order to be properly applied to a vehicle, a value of one is assigned to the cell corresponding to the pair of technologies. TCM cells corresponding to pairs of technologies that are expected to interact with each other contain a value of two. The expected interactions are not necessarily modeled, but the technology pairs with likely interactions are identified nonetheless.

Whenever a discrete package of technologies is considered, the technology set is first evaluated using the TCM. If there are no incompatibilities present and no additional technologies are required according to the TCM, the EDS input vector is generated and the candidate vehicle is simulated. This process is also carried out when generating variable ranges for technology and design space explorations. For a given EDS input variable, all technologies that impact the variable are identified and a full factorial design is constructed to consider every possible subset of technologies that impact that particular variable. Each subset is then evaluated with the TCM and technology combinations are eliminated that contain any incompatibilities. The remaining (compatible) technology subsets are then used to determine the minimum and maximum possible input variable settings, properly bounding the input variable range within which technology space explorations are performed.

4.3 Technology Impact Matrix (TIM)

Any task related to the generation of EDS input vectors for candidate ERA vehicles with corresponding packages of applied technologies is performed using the Technology Impact Matrix (TIM). The various impacts of each technology contained within the ERA portfolio are

contained within the TIM database, along with the TCM which identifies the relationships between all possible pairs of ERA technologies. The TIM database contains three point estimates of every technology impact for each of the ERA vehicles. The three points correspond to the minimum possible impact, the most likely impact, and the maximum possible impact of a given technology when applied to a given ERA vehicle. When generating EDS input vectors representing unique technology packages applied to a candidate vehicle, the most likely technology impacts are typically applied to the vehicle for a single point deterministic EDS simulation. When generating input variable ranges for an explorative design of experiments whose resultant data will be used for surrogate model training, the minimum and maximum possible impacts of each technology are used. This accounts for the largest possible variability in the assumed technology impacts, determining the maximum input variable ranges required for any possible probabilistic assessment. This allows for probabilistic assessments to be performed, employing the resultant surrogate models and avoiding extrapolation of the Artificial Neural Network (ANN) mathematical representations of the EDS modeling and simulation environment. An example of the three point technology impact estimates for a given technology when applied across various ERA vehicles is shown in Figure 66, which displays the impacts of the compressor intercooler technology when applied to the engines on board the twin aisle ERA vehicles.

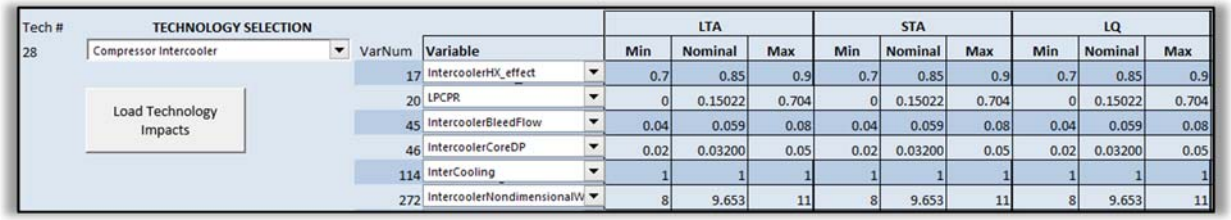

Tech #	TECHNOLOGY SELECTION			LTA			STA			LQ		
28	Compressor Intercooler	VarNum	Variable	Min	Nominal	Max	Min	Nominal	Max	Min	Nominal	Max
		17	IntercoolerHX_effect	0.7	0.85	0.9	0.7	0.85	0.9	0.7	0.85	0.9
	Load Technology Impacts	20	LPCPR	0	0.15022	0.704	0	0.15022	0.704	0	0.15022	0.704
		45	IntercoolerBleedFlow	0.04	0.059	0.08	0.04	0.059	0.08	0.04	0.059	0.08
		46	IntercoolerCoreDP	0.02	0.03200	0.05	0.02	0.03200	0.05	0.02	0.03200	0.05
		114	InterCooling	1	1	1	1	1	1	1	1	1
		272	IntercoolerNondimensionalW	8	9.653	11	8	9.653	11	8	9.653	11

Figure 66. Example of the three point estimates of technology impacts for various ERA vehicles.

4.3.1 Vehicle - Input vector generation

The primary function of the Technology Impact Matrix is to document and propagate technology impacts to desired vehicles in the form of EDS input vectors. An input vector is a combination of values for EDS variables that fully defines a vehicle. In order to establish an input vector there are multiple steps. The user first selects the package of technologies that will be applied to appropriate EDS variables. The corresponding impacts of the technology package are defined by their particular function on the aircraft, and have been quantified through literature search and by subject matter experts. Nominal, or most likely, impacts of each technology are inputted into the TIM for each vehicle class. When multiple technologies affect a single EDS input variable, technology combination rules are used to determine the resultant input variable setting for the selected technology package. These rules will be discussed in detail further in the text. With the technology impacts identified and mapped to EDS variables, an EDS input vector can be generated for a desired vehicle and selected technology package. The vector is entered into EDS and the design case is launched through its corresponding modules. However, appropriate baselines for each vehicle class must first be defined.

4.3.1.1 Baseline definition

There are two distinct baselines that are established – the "1995 baseline" and the Reference Technology Collector (RTC) – for proper use of the TIM and interpretation of vehicle design explorations. The 1995 baseline for each vehicle is representative of an aircraft of the same seat class that is in service today, and has been calibrated based on publically available data. For each ERA vehicle, the technology level is then updated to a consistent level across all vehicle classes, and the resultant RTC is used as the datum from which all performance improvements are measured.

From the baseline vehicles, Reference Technology Collectors are established as the current state-of-the-art for three engine types – the Advanced Direct Drive (ADD), the Geared Fan (GF), and Open Rotor (OR). The update from a vehicle's baseline to the RTC corresponding to a particular advanced engine architecture is performed through the TIM, applying the correct advanced cycle and vehicle RTC updates. RTC level technologies are also applied, resulting in the definition of a current starting point from which vehicle technology explorations can begin. The steps of the process by which technology packages are applied to the RTC vehicles, compatibility is verified using the TCM, and the resultant EDS input vector is generated is described in the following sections.

4.3.1.2 Tech combo rules

Each technology within the ERA portfolio contains a set of impacts that affect EDS input variables based on their expected function(s) on the engine or aircraft. As an example, some technologies are implemented to increase the efficiency of a particular ERA vehicle system, while others are used to reduce weight or influence other performance parameters. Many technologies also have accompanying negative impacts which also must be accounted. As such, the TIM employs multiple technology combination rules in order to properly apply the various types of technology impacts to the baseline definition. It is important to remember that, in the context of the technology combination rules, the baseline refers to the 1995 baseline, not the RTC's. There are a total of eight different variable categories used in the TIM – absolute, discrete, delta, scalar, noise, formula, switch, and frame.

Technologies whose impact is represented as an absolute variable are implemented as a simple replacement of baseline values. It is important to note that multiple technologies whose impacts are applied to the same variable are absolute are not applied in the same technology package; this is ensured via incompatibility in the TCM. A typical example of the use of absolute variables is how technologies such as ceramic matrix composites (CMC's) or polymer matrix composites (PMC's) affect material density. Applying advanced materials to change the density generally has one of two benefits within the engine: to reduce engine weight or to allow for higher maximum temperatures. Similar in technology combination rule to absolute impacts are discrete variable impacts.

Discrete variables are used for technologies that affect variables that are discrete in nature; logic in the TIM ensures that the value of a discrete input variable remains a whole number. If a technology impact is discrete, it too is applied as a replacement to the baseline and cannot be applied in the same technology package as another technology with a discrete impact on a given EDS variable. For example, the RTC geared turbofan cycle dictates the main fan, just before the low pressure compressor (LPC), has 18 blades; however, with the implementation of the Advanced GTF cycle, the blade count is lowered to 16, replacing the RTC values and

effectively reducing the weight of the engine. Not all technology impacts manifest as a replacement to a baseline value, delta and scalar variables act as an additive impact and a percent change respectively to the baseline value.

Technology impacts combined using the delta variable combination rule are summed and added to the baseline instead of replacing it.

$$x_{delta} = x_0 + \sum_i k_i$$

For each rule, x_0 is the baseline variable value and k_i are the individual technology impacts. This combination rule is often used for technologies that improve engine component efficiencies. As an example, in the case of the Advanced ITD GTF cycle, the high pressure turbine (HPT) efficiency is affected by two technologies, T95: Advanced ITD GTF cycle and T67: Advanced engine components. These account for a 0.25% and a 0.1% increase in HPT efficiency respectively; thus a 0.35% increase in the total HPT efficiency from the baseline value. An engine efficiency increase may allow for a decrease in total fuel burn.

The scalar technology combination rule dictates that technology impacts be represented as a percent increase or decrease from the baseline value, as calculated below.

$$x_{scalar} = x_0 \left(1 + \sum_i k_i\right)$$

Typically, the scalar rule is applied to technologies that variables like airframe drag. For example, if T3.2: Damage Arresting Stitched Composites and T86: 60 Degree Winglets were applied to the LTA, $k_{T3.2}$ is -0.1 and k_{T86} is 0.017. This would result in an 8.3% net increase in the parasitic drag of the wing. In this case, there is a possible reduction in weight due to the composite technology applied to the wing, but an increase in drag. The winglets are an example of a method by which the drag may be mitigated. A study would be required to quantify whether or not the drag reduction from the winglet is beneficial due to the added weight imposed. This could quickly be done by creating two EDS input vectors, one including the winglets and one excluding the winglets. The TIM is very effective at producing input vectors for trade studies quickly. While scalar technology combinations apply to many variables, technology impacts concerning noise variables are combined in a distinct manner.

Impacts on noise variables are calculated using a diminishing summation because sources of noise are not simply additive. Thus, the six greatest technological impacts are weighted and added to the baseline value as shown in the following equation for the same noise source,

$$x_{noise} = x_0 + (k_1 + 0.75k_2 + 0.5k_3 + 0.33k_4 + 0.16k_5 + 0.08k_6)$$

The impacts, k, are in order from largest to smallest. So, k_1 represents the largest impact on the particular EDS input variable, k_2 the second largest, and so forth. The ANOPP module within EDS predicts the noise based on several factors outputted from aircraft and engine sizing. The baseline values for noise variables in each vehicles respective TIM are zero, thus an increase or decrease in noise is simply accounted as an offset to what is predicted in ANOPP. The

remaining three variable types—formula, switch, and frame—do not have technology impact combination rules, as they serve a different purpose.

Formula variables are not calculated by the addition of technologies; rather, by some equation relating the variable to other input variables. There are only two such EDS input variables, aircraft gross weight (GW) and wing area (SW):

$$GW = TuningScalar * (\#ofEngines)\left(\frac{SLS\ Thrust}{TWR}\right)$$

$$SW = \frac{GW}{WSR}$$

where SLS Thrust is Standard Sea-Level Thrust, TWR is thrust to weight ratio, and WSR is the wing loading. The tuning scalar is present to account for airframe variation. That is, for conventional TW models, the tuning scalar is 1.05, increasing the gross weight calculation by 5% in order to provide the vehicle simulation with 5% excess weight for fuel; while, for the LTA Hybrid Wing Body (HWB) the tuning scalar is 0.92, reducing the gross weight calculation by roughly 8.3%. These are used to ensure the calculations are representative of data for similar aircraft in literature. The formula variables are used to set the initial values for the iterative vehicle sizing loop of EDS. There are multiple technologies that require more than input variable changes in order to be properly represented within EDS.

Switch variables are used to activate certain logic within EDS to simulate technologies that require more than just input variable adjustments to adequately model. For example, intercooling requires additional components and linkports that would otherwise be absent in the engine. The switch activates the architectural changes to the engine necessary to model the intercooler technology. With this switch activated, the technology T22.1: Compressor Intercooler impacts on EDS input variables are able to be propagated to the model. Finally, in addition to all of the aforementioned variable types, frame variables define all other EDS input variables required to model an aircraft.

Frame variables establish values for input variables that are not impacted by any technologies. These variables simply required to fully define the vehicle in EDS; they are not variables that are explored with technology infusion.

4.3.2 DoE Generation for Surrogate Training– Procedure

The first steps required for the design space exploration are performed using the Technology Impact Matrix tool. A comprehensive Design of Experiments (DoE) with sufficient edge points and space filling interior points is necessary to establish accurate surrogate models for desired responses. The baseline values for all vehicles must be confirmed and technology impacts need to be updated with the most current data from literature and subject matter experts. Specific vehicle design space exploration DoE's, also referred to as surrogate DoE's, are then generated. The steps are as follows: first, variable ranges must be determined to account for the variability assumed present in all compatible technology combinations that could possibly impact each variable. This is done by applying the entire portfolio of ERA technologies to obtain the absolute maxima and minima for each EDS input variable. Then, using the ranges, edge

points or upper and lower limits to each of the variables are generated. This is to ensure that the extremes of the design space are adequately represented such that if ambitious technology packages are applied, the responses can be accurately modeled via surrogate equations. Space filling points, which are randomly generated values for each variable between the ranges, are established to ensure that there is an adequate sample size within the boundaries of the design space to accurately predict responses for technology packages within the ranges. The final cases needed in the surrogate DoE's were random technology packages. These are required for their use as validation points during the surrogate equation generation. The space filling and edge points do not necessarily indicate a feasible technology package, thus it is important to test a significant portion of input vectors that were feasible technology combinations. Using the random technology packages, the validity of the surrogate equation is determined.

4.3.2.1 Variable Range Determination for an exploration

Once the minimum and maximum variable impacts of each technology are established in the tool, the absolute minimum and maximum for each variable for the exploration DoE is established, thus determining the range. For each variable, a full factorial design is constructed, considering all subsets of technologies impacting that variable. All incompatible combinations are eliminated, and the remaining compatible combinations' minimum possible impacts are applied. The minimum possible input variable value is determined by the compatible technology combination that produces it. The same procedure is conducted to determine the maximum of the range using the maximum possible impact. With the surrogate DoE ranges determined, the surrogate DoE was generated.

4.3.2.2 Generation of actual DoE for exploration

DoE generators implement the ranges for each of the design variables to determine edge points and interior points within the design space. To establish edge points or DoE vectors that are comprised of random combinations of minimum and maximum values for each input variable, the generator calculates random samples for the input variables where each variable now only has two-levels, minimum and maximum. These edge points are imperative when fitting surrogates, because if they were not part of the equation, competitive designs that push approach the limit of the design variables will not be encompassed within the surrogate equation.

In EDS, there are many variables to consider when defining a vehicle, 281 for TW models. To conduct a full factorial DoE on the edge points of the design space, approximately 2^{281} or 3.89×10^{84} points would be required; however through sensitivity studies, it has been shown that if edge points comprise 20% of the cases for the exploration DoE, the surrogate models predict well near the edges. The space filling designs are randomly sampled with uniform preference placed throughout the continuous design and technology space considered for the surrogate exploration. For a given vehicle, an exploration DoE is comprised of roughly 15,000 cases or input vectors, each representing a distinct aircraft. Further sensitivity studies were conducted during the summer of 2014 suggesting that increasing the number of cases in the surrogate DoE from 15,000 to 60,000 did not increase the accuracy of the surrogates. The edge point cases account for 20% of the input vectors and the random interior point cases account for roughly 66.6% of input vectors. The remaining 13.3% or 2,000 cases are comprised of feasible random technology packages. When training the surrogate models using the ANN's in BRAINN, 75% of the cases are used for training, 25% for validation and 0% for testing.

4.3.2.3 Random tech package generation

There is an automated functionality designed within the TIM tool that allows the user to generate random technology packages. With the use if the TIM and the previously outlined technology combination rules, the random technology packages are converted into DoE input vectors. Randomly sampled technology combinations are generated, represented by ones and zeros corresponding to ERA technologies either being, "on" or "off", and corresponding EDS input vectors are produced for each. The tool ensures that a given technology package does not have any incompatible technologies applied via consultation of the Technology Combination Matrix (TCM). If an incompatibility is present, logic in the tool discerns whether either of the two incompatible technologies is an RTC technology. If one is an RTC technology, the other is removed; however, if neither are RTC technologies, one is randomly selected and removed. After this, incompatibility audit begins again and the same actions are taken if one is found. If not, the vector is selected for use as a random technology package. The tool then converts each random technology package vector into a corresponding EDS input vector. It used a given vehicle's technology impact matrix and the technology combination rules to generate the vector of input variable settings, considering the technologies applied. 2,000 random, compatible, technology packages were generated and the resultant input vectors were appended to the end of the explorative DoE. The DoE, now containing 15,000 unique parametric vehicle design samples that lie throughout the design and technology space considered, is prepared to run in EDS in order to produce data with which surrogate models can be trained and evaluated.

4.4 Advanced Combustor Modeling

The goal of the NOx emissions prediction task is to estimate NOx emissions indices (EI) at the landing/takeoff (LTO) cycle conditions (and thereby estimate the regulated parameter Dp/F00) for all ERA candidate engine cycles. Two models have been developed; one representing current combustion technology levels (e.g. Talon II, approximately 30% below the CAEP/6 limits) herein called the "standard" or "baseline" combustors, and one representing advanced low emissions combustor technology capable of meeting the N+2 goals for the 2020 timeframe (70% below the CAEP/6 limits), herein called the "advanced" combustor.

The emissions are predicted by employing a chemical reactor network which runs using Chemkin ™. The network architecture has been developed to represent the baseline and advanced combustors assuming a rich-quench-lean (RQL) type of combustor. The network models the primary or rich combustion zone as a group of perfectly-stirred reactors (PSR) and the secondary or quench combustion zone as another group of PSRs. The lean and dilution combustion zones are each represented by single plug-flow reactors (PFR).

The operating parameters for each of the reactors in the network are determined by a "1-D flow model" which runs as part of the NPSS engine cycle. The 1-D flow model takes the combustor entrance pressure, temperature, airflow, and fuel flow (P3, T3, W3, and Wfuel, respectively) at each engine power setting and computes the reactor parameters according to a set of pre-defined rules. The model is "tuned" ahead of time to reflect either the standard or the advanced combustor. The details of the modeling process are discussed in the following sections.

The Chemkin™ reactor network model takes approximately two minutes to run the four power settings for the LTO cycle for any given engine. As a result, the model cannot be run in-line with the EDS model to predict the emissions for the several thousand ERA candidate engine cycles. Instead, the tuned models for both the standard and advanced combustors are first run

throughout the anticipated ERA design space (in terms of P3, T3, W3, and Wfuel) and a neural-net regression model is developed for each combustor. The neural-net equations are then programmed into EDS and are used for the ERA data generation.

4.4.1 Emissions Prediction Methodology

The ASDL approach to NOx emissions prediction uses analytical reactor-based models to bridge the gap between empirical and high fidelity approaches, in order to provide the capability to perform design trades at the conceptual level and to quickly predict emissions as the engine cycle and architecture are parametrically varied. The general organization and flow of the NOx emissions prediction methodology is illustrated in Figure 67 below.

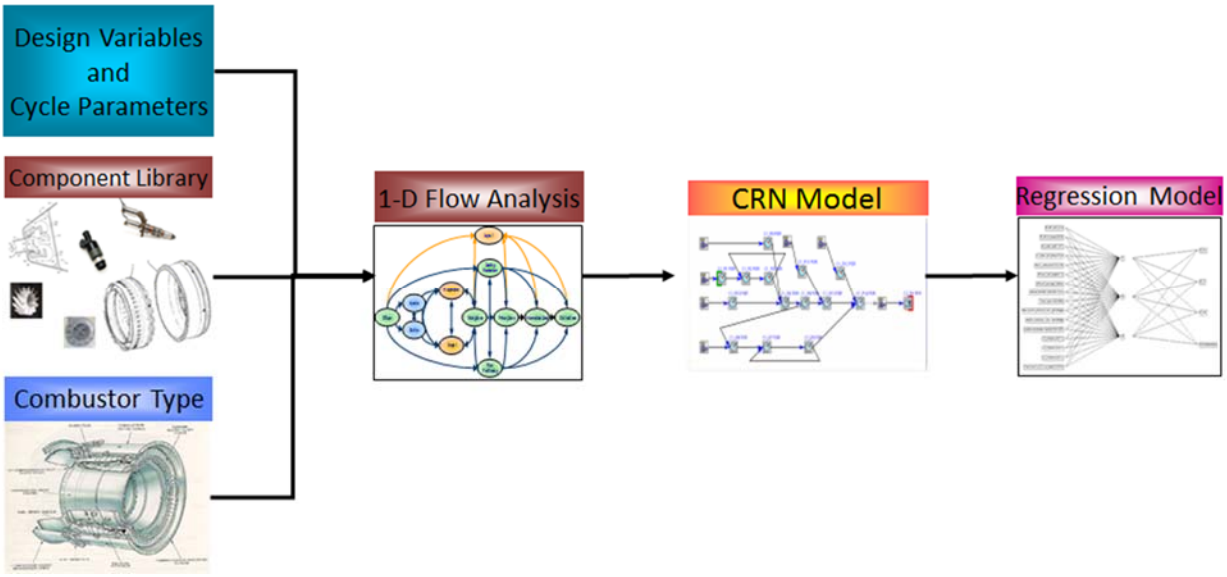

Figure 67. NOx Emissions Prediction Model

The semi-analytical model consists of three main elements: The Object-Oriented 1-D Flow Analysis Model, the Chemical Reactor Network (CRN) Model, and the Emissions Regression Model. The 1-D flow model and the CRN are wrapped and run within the ModelCenter™ environment to generate the emissions predictions for a given set of inputs. The model must first be tuned, and then the tuned model is run through a design-of-experiments (DOE) table to generate the data required for training and verifying the neural-net regression model. The general steps required for model development are summarized below:

- Model tuning
  - Establish target values of EINOx vs. Wfuel for a number of different engine cycles
  - Targets are established based upon existing engine data from the ICAO data bank
  - Calibrate the model to the target EINOx values for each engine cycle
  - Engine cycle model provides thrust and P3, T3, W3 vs. fuel flow inputs
  - Use Filtered Monte Carlo process to determine suitable values for model tuning parameters
- Regression model development

- Run a DOE on the calibrated models over a range of engine cycles, holding the tuning parameters fixed, to generate emissions data over the projected ERA engine design space
- Fit a neural net regression model to the DOE data
- Incorporate the neural net regression model into EDS
- The combustor 1-D flow model is required as an assembly in EDS to provide the necessary inputs

The ASDL method for NOx emissions prediction has its origins in the University Research Engineering Technology Institute (URETI) on Aeropropulsion & Power Technology (UAPT) during 2005-2007. This early research performed a proof-of-concept investigation of conventional single annular combustor architecture. This research was followed by NASA NRA NNX07AO08A during 2007 –2010, which extended the methodology to modern low-emissions combustor architectures.

In 2013, the methodology was applied to an RQL combustor architecture for the ERA. The main difference in this work relative to the previous work is that the quench zone model, which was originally represented by a single partially-stirred reactor (PaSR), was replaced by a group of PSRs to decrease the model execution time. The execution time was reduced from about 10 minutes per LTO cycle to about 2 minutes per LTO cycle. However, the neural-net regression model was difficult to fit, and the results were unsatisfactory. For 2014, many of the model features modified in order to improve the model performance. This report focuses on those model improvements and the final results for 2014.

4.4.2 Description of Combustor Technology Levels

For the purposes of this study, the baseline or standard combustor was taken to be the Talon II emissions level. The Talon II engines in the ICAO data base are summarized in Table 50.

Table 50. Talon II Engines in ICAO Data Base

Engine	OPR	Rated FN (kN)	Dp/F_{00}
PW4164	30.1	284.68	42.7
PW4168	31.84	302.5	46.0
PW4168A	31.84	302.5	46.0
PW4X58	28.41	258.0	39.9
PW6122A	25.7	98.31	32.8
PW6124A	28	105.87	39.4
PW4164-1D	31.3	286.9	44.9
PW4168-1D	33.1	305.1	48.5
PW4168A-1D	33.1	305.1	48.5
PW4170	33.8	311.4	49.9

The Dp/F00 values for these engines are almost linearly increasing with engine overall pressure ratio (OPR), and on average are 28.17% below the CAEP/6 limit, as shown in Figure 68.

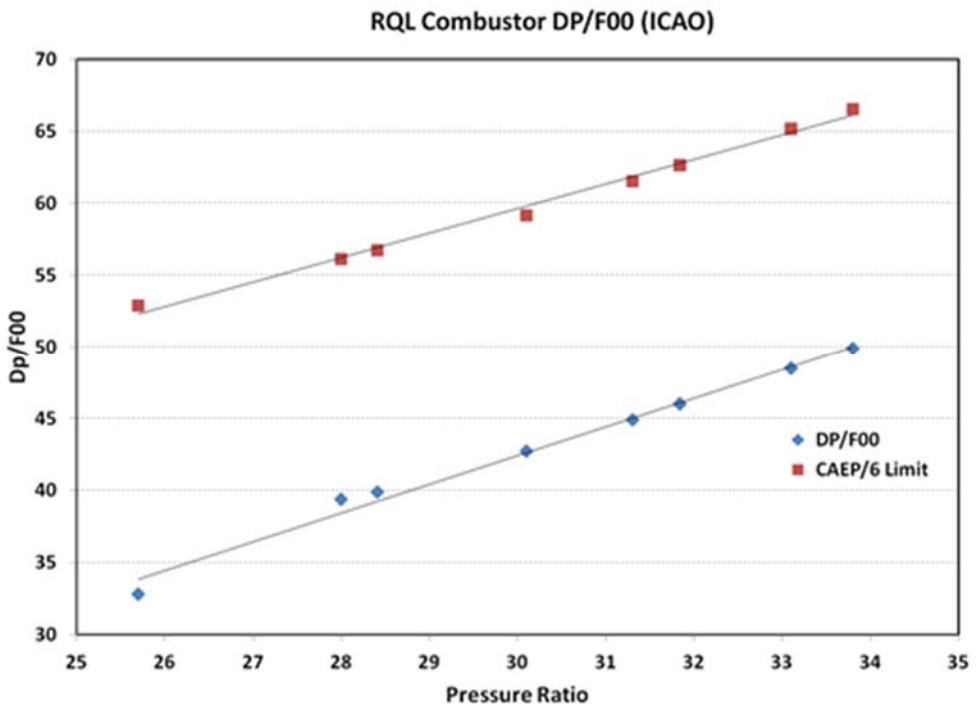

Figure 68. Talon II Emissions Relative to CAEP/6

For tuning purposes, additional engine parameters are required beyond the data available in the ICAO data base. These parameters are estimated by using calibrated EDS engine models run at the LTO conditions. Due to resource limitations, only two target engines could be calibrated in EDS. These calibrations were performed during 2013. The PW6124 and the PW4168 engines were selected, as representative of the 150-passenger and 300-passenger thrust classes, respectively. The emissions model was tuned to match the emissions levels of these two engines, which established the technology level for the standard or baseline combustor. A "sizing rule" is used to ensure that engines with about the same bypass ratio (BPR) will fall approximately along the same Dp/F_{00}-vs.-OPR line regardless of the thrust class or airflow size. Engines with higher BPR will show better emissions due to the engine cycle effects on the Dp/F_{00}-vs.-OPR characteristic.

Because the model is not a true predictive model and must be tuned to a target emissions level, the advanced combustors were assumed to meet the ERA goals (70% below CAEP/6) for the same two target engines (the PW6124 and PW4168). The emissions model, including the "sizing rule", was tuned to match these emissions levels, which established the technology level for the advanced combustor.

4.4.3 ModelCenter™ Environment

As mentioned previously, two of the model elements, the 1-D flow model, the CRN, are wrapped and run within the ModelCenter™ environment. These two model elements are described in detail in the following sections.

Chemical Reactor Network (CRN) Model

A Chemical Reactor Network (CRN) was implemented to calculate chemical compositions at each zone of the combustor. Each combustor zone was modeled using a combination of idealized simple reactors such as a Perfectly Stirred Reactor (PSR) and a Plug Flow Reactor (PRF), as shown in Figure 69.

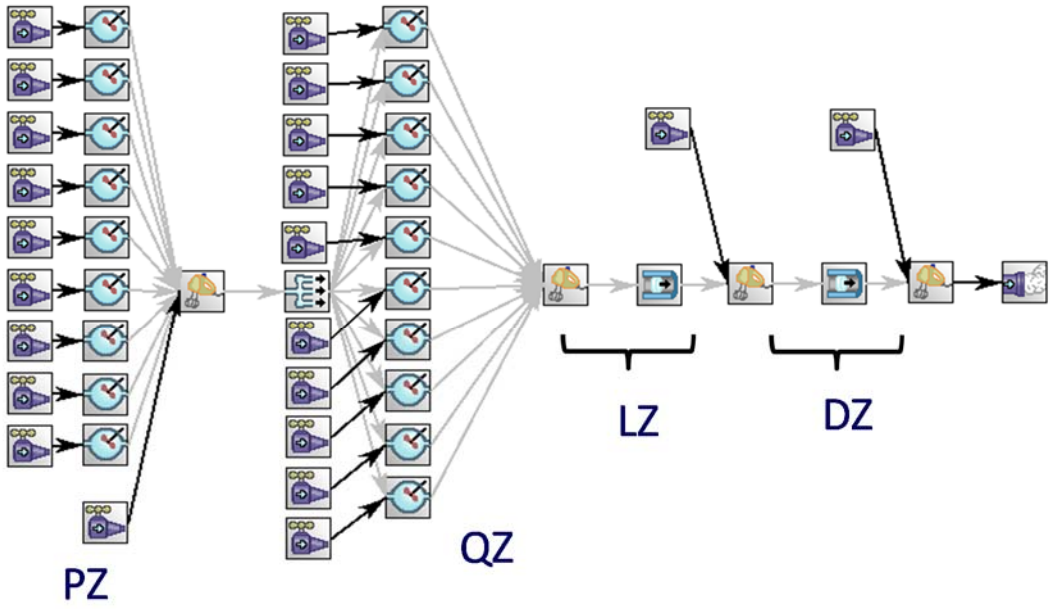

Figure 69. Chemical Reaction Network (CRN) of Rich, Quick-Quench, Lean (RQL) Combustor (Screenshot of CHEMKIN GUI)

The primary zone is modeled as a combination of pre-mixed combustion and diffusion (droplet) burning. At higher temperatures any droplets are assumed to evaporate and so the combustion is treated as completely pre-mixed. At lower temperatures, larger droplets are assumed to persist so that a portion of the combustion is treated as diffusion burning.

A group of nine PSRs are used to represent combustion in the primary zone. Even though the overall fuel-to-air ratio of the primary zone of RQL combustor is in a fuel rich condition, the non-uniform mixing of fuel and air results in local regions operating near the stoichiometric condition. These near-stoichiometric regions contribute to the NOx emissions. The nine PSRs represent the thermochemical characteristics of the overall primary zone by statistically distributing the mass flow and fuel-to-air ratio with a Gaussian distribution based on Heywood's mixing parameter $S = \frac{\sigma}{\phi}$ where σ is the standard deviation and ϕ is the mean equivalence ratio. The empirical unmixedness curve of Sturgess et al, shown in Figure 70, is used to find S as a function of the primary zone equivalence ratio.

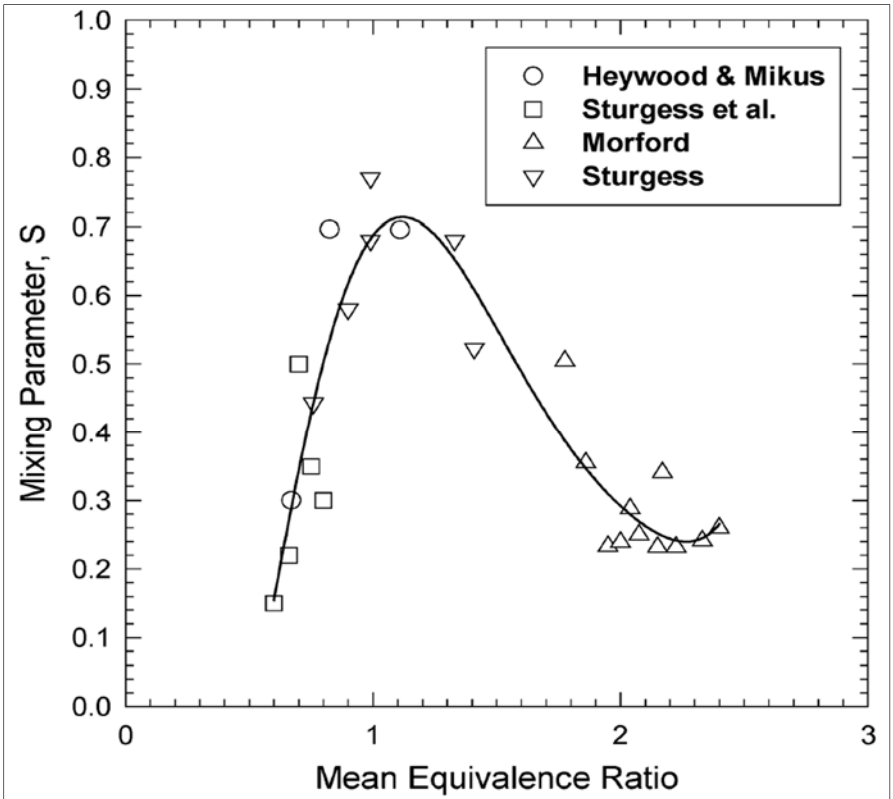

Fig. 18 Collected *S* experience for variety of practical combustors.

Figure 70. Experimental Results of Unmixedness Parameter Collected by Sturgess et al.

A uniform residence time is assigned to each PSR in the primary zone. This was an improvement from the 2013 model, in which the reactor volume was distributed in a way that resulted in different residence times in each reactor due to different temperature and density. As a result, the reacting flow spent less time in the near-stoichiometric branch and more time in the far-stoichiometric branches, diminishing the desired unmixedness effect.

In prior years, the 30-step Kollrack chemical mechanism was used to model Jet-A combustion. However the Kollrack mechanism only accounts for thermal NOx and does not account for prompt NOx and N_2O NOx pathways which are known to be important for low emissions combustors. Also the Kollrack mechanism has no pressure corrections on any reaction steps and so may not respond properly for higher OPR engine cycles. For these reasons, in 2014 the model was updated to use the GRI-MECH 3.0 mechanism. The GRI 3.0 mechanism comprises 53 species and 325 equations. It contains detailed NOx reactions, but it does not contain the Jet-A mechanism (it is intended for propane, C_3H_8). To model Jet-A, a two-stage fuel pyrolysis taken from Kollrack mechanism was added to the GRI 3.0 mechanism:

$$C_{12}H_{23} + O_2 \rightarrow 5C_2H_4 + C_2H_3 + O_2$$

$$C_{12}H_{23} + OH \rightarrow 6C_2H_4 + O$$

One of the nine PSRs is assigned to the droplet burning model, as illustrated in Figure 71. The droplet model accounts for unevaporated fuel droplets. The Sauter mean diameter (SMD) of the droplets is estimated, and the time required for the droplets to evaporate is compared to the droplet residence time.

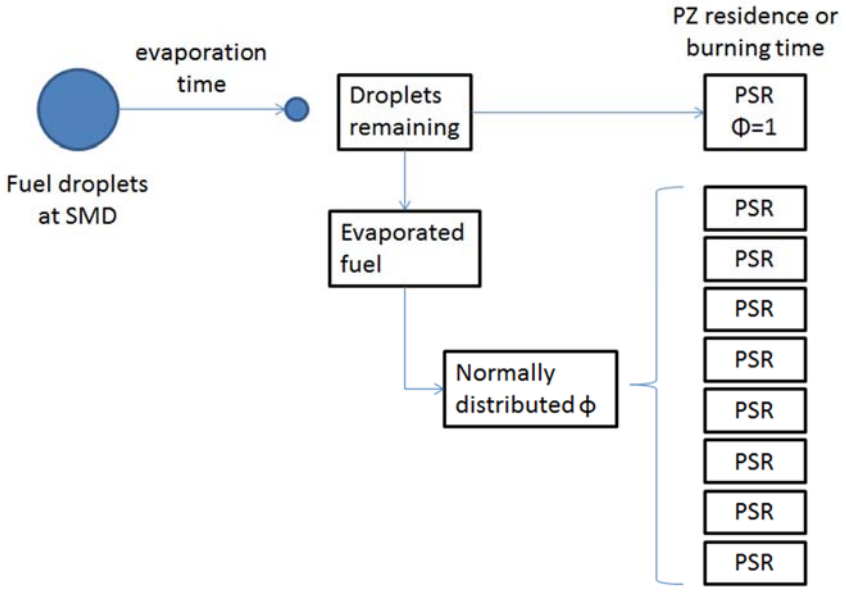

Figure 71. Droplet Model

Any unevaporated droplets are assigned to the first PSR and are burned assuming a stoichiometric equivalence ratio to simulate diffusion burning. The remaining mixture is distributed among the remaining PSRs using the Sturgess unmixedness curve.

The Quench zone, where a large volume of air flow is injected and mixed with the products of the primary zone, is represented by a group of ten PSRs. Non-uniform fuel-to-air ratio over the quench field is modeled by an asymmetric beta distribution rather than a symmetric Gaussian distribution as in the primary zone. As in the primary zone, a uniform residence time is used for the group of PSRs representing the quench zone.

The lean zone and the dilution zone are represented by PFRs because these regions are where the flow is relatively calm with lower turbulence. The final concentrations of NO and NO_2 at the combustor exit are used to compute the EINOx.

4.4.4 1-D Flow Model

The W3, P3, T3, and Wfuel entering the combustor are specified for each LTO operating condition. Take-off power is considered to be the design point. Each of the combustion zones performs the following calculations on-design:

- The equivalence ratio φ and the residence time τ are specified
- Given φ, the local air flow $\dot{m}$ and flow fraction *frac* are calculated
- The fuel-air mixture is burned at the specified φ to find the local temperature and density
- Finally the effective volume of the zone is found by $V = \frac{\dot{m}\tau}{\rho}$

Off-design, each of the combustion zones performs the following calculations:

- Given the flow fraction *frac*, calculate the local air flow $\dot{m}$ and equivalence ratio φ

- The fuel-air mixture is burned at the computed φ to find the local temperature and density
- Given the effective volume, find the residence time by $\tau = \frac{\rho V}{\dot{m}}$

After these calculations are performed, the inputs required for the Chemkin ™ model are computed. The rich zone is divided up between the nine PSRs according to the droplet model and Sturgess unmixedness curve as described above. The quench zone is divided up between the ten PSRs according to the beta distribution as described above. The output parameters are written to a file for ModelCenter ™ to pass to Chemkin™.

- The 1-D Flow Model comprises several files written in NPSS. The major files are described briefly below:
- Total_Combustor.int – the main element, which models the combustion in the rich, quench, and lean zones.
- Total_Combustor.mdl – the model file, which initializes the parameters required by Total_Combustor.int
- Chemkin_Rich.fnc – Applies the Sturgess unmixedness curve and distributes the fuel and air for the rich zone
- Droplet_Model.fnc – performs the droplet size and evaporation calculations required for the rich zone
- Volumes.fnc – computes the effective volumes of each combustion zone
- Chemkin_Inputs.view – creates the Chemkin™ input file from the 1-D flow model outputs

4.4.5 Model Tuning Process

As mentioned previously, the model is calibrated to target Dp/F_{00}-vs.-OPR lines. Previously, the targets did not account for BPR and intercooling effects on the Dp/F_{00} characteristic. While EINOx responds to (P3, T3, FAR), Dp/F00 also depends on FN and SFC. Consider the definition of Dp/F_{00}:

$$\frac{D_p}{F_{00}} = \sum_i \frac{w_{f,i} * t_i * EINOx_i}{F_{TO}} \sim \sum SFC_i * EINOx_i$$

Thus for the same EINOx-vs.-Wfuel characteristic, improving BPR improves Dp/F_{00} for a given OPR. Also, intercooling lowers the T3 out of proportion to the P3 and therefore lowers EINOx for a given OPR. To better account for these effects in 2014, the model tuning process was divided into three parts:

- Calibrate the model tuning parameters at 30 OPR
- Develop and calibrate a "sizing rule" to account for increasing OPR while holding BPR at a relatively constant value and with no intercooling
- Verify that the effects of higher BPR and intercooling look reasonable

These steps take into account the fact that the Dp/F_{00}-vs.-OPR curve is actually dependent on the additional variables BPR and intercooling. It is assumed that the N+2 goal of 70% below CAEP/6 was intended to apply to engines of similar BPR and OPR as current engines. Advanced engines with higher BPR and/or intercooling will show further improvement

due to the engine cycle, independent of the combustor technology level. The model is therefore first tuned to establish the technology level of the combustor for current OPR and BPR levels.

The first step in the tuning process sets the combustor technology level by matching the target Dp/F_{00}-vs.-OPR for the PW6124 and PW4168 engines. The second step extends these results to higher OPR engines by means of a "sizing rule" to be explained later. Since no specific targets can be set for higher BPR or intercooled engines, the third step only evaluates the results at these conditions to ensure that they appear reasonable. These steps are described in more detail in the following sections.

4.4.5.1 Calibration at 30 OPR

This step refers to the tuning of the model to match target EINOx levels using the PW6124 and PW4168 engine cycle data (at approximately 30 OPR) and thereby to establish the combustion technology levels. Two models are created, one for the current (standard or baseline) combustor technology (CAEP/6 – 30%) and one for the advanced technology (CAEP/6 – 70%).

4.4.5.2 Pareto analysis of the calibration factors

The model comprises several parameters which may be used to match the target EINOx values at each of the LTO cycle power settings. The 14 calibration parameters available are shown in Table 51.

Table 51. Combustor Technology Calibration Factors

Calibration Parameter	Definition
dPdiffP	Pressure drop
EqRatioPZ, EqRatioSZ, EqRatioDZ	Equivalence ratio of each zone. Lean zone has the same EqRatio with the secondary (quench) zone.
ResTimePZ, ResTimeSZ, ResTimeLZ, ResTimeDZ	Residence time of each zone
k_DropTime	Fraction of residence time of droplet PSR branch to ResTimePZ
k_evap	Fraction of volume allowed droplet to evaporate before burning process
EffPZ	Efficiency of primary zone
k_mixedness	Tuning parameter (multiplier) to adjust Sturgess unmixedness curve
Alpha, Beta	Shape parameter of beta distribution for the quench zone (SZ)

To reduce the number of variables required for tuning, a sensitivity study was performed by perturbing each of the calibration parameters at the PW 6124 A cycle for three cases: high power (take-off), low power (idle), and elevated pressure (2X pressure). The normalized effect of the parameters to the output NOx emission is presented in Figure 72.

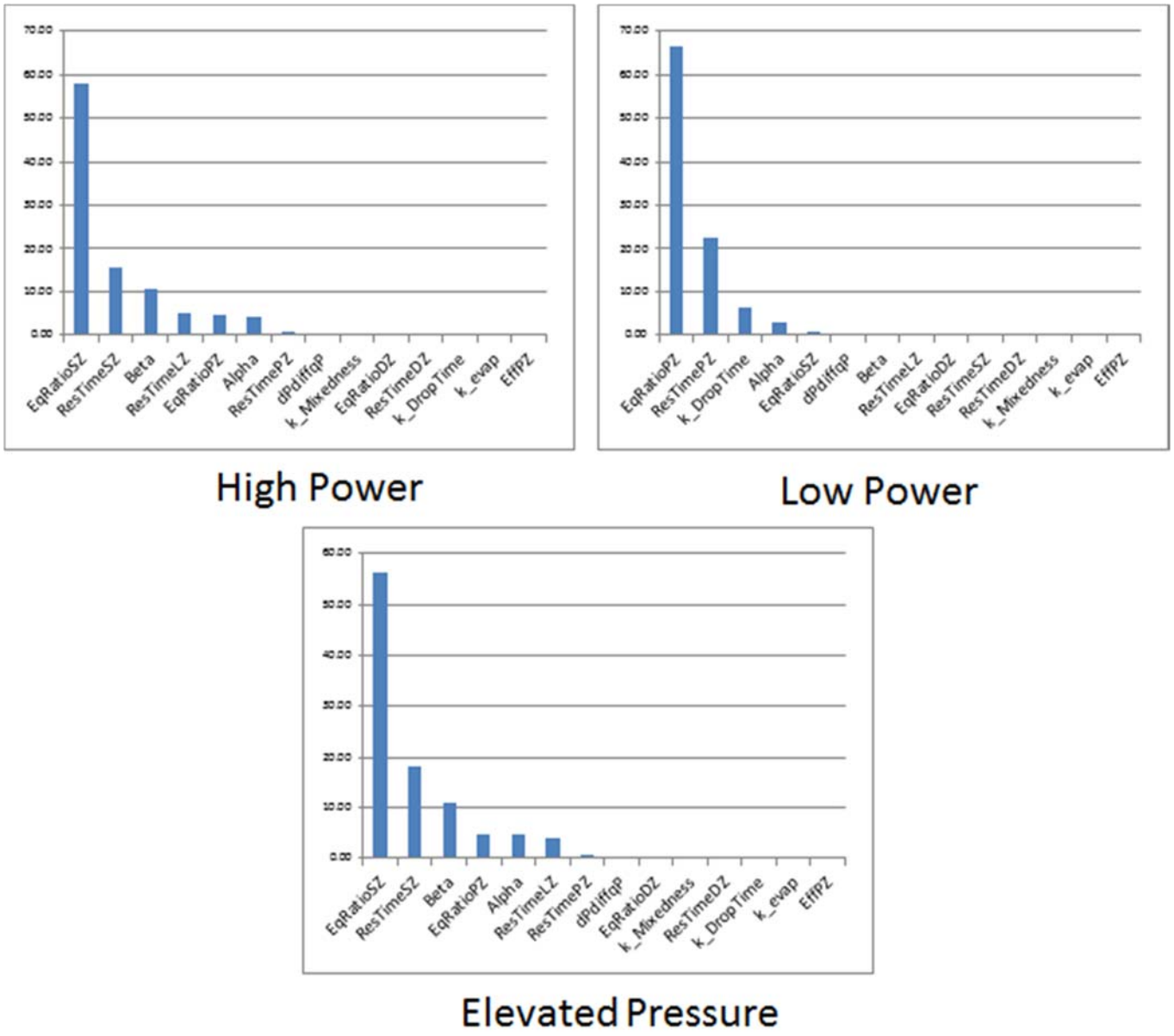

Figure 72. Sensitivity Study Results for Model Tuning Parameters

Six parameters were screened out and set to nominal values in accordance with the sensitivity analysis result. The model was calibrated with the remaining eight driving parameters, which are the design equivalence ratios and residence times in the three combustion zones, k_DropTime, and the shape parameters of the beta distribution for the quench zone. These parameters thus define the combustor technology level for the baseline and advanced combustors.

Among the eight calibration parameters, five parameters (design equivalence ratios and design residence times in combustion zones) were set to be constant since they apply only to the design or takeoff power setting, while the other three parameters (k_DropTime, Alpha, and Beta) were allowed to vary with power setting. k_DropTime determines the flow residence time of the droplet branch and Alpha and Beta determine the shape of beta distribution in Quench Zone.

The calibration processes started from generating a set of sample points of calibration parameters among the pre-determined design space for each of baseline and advanced combustors. Regression equations of EINOx as a function of the eight calibration parameters were created from a DOE and a Genetic Algorithm was used to find solutions to satisfy the target EINOx values listed in the ICAO databank. The GA was run in a "nested" fashion; first the fixed parameters were determined and then the power-varying parameters were determined.

While the above approach was successful for the baseline combustor, it failed in the case of the advanced combustor. Some of resultant sets of solutions were not realistic and the others leaded high errors. For the advanced combustor, Neural Net equations were created to generate a prediction profiler in the JMP environment. Next, a Filtered Monte Carlo process was used to investigate each parameter in the prediction profiler and the points whose gradient was too stiff or too flat were removed. The remaining points were refined through optimization using the desirability function in the JMP environment. Then the output was evaluated from the model runs with refined input values.

In both cases, the parameter k_DropTime was modeled as a function of primary zone equivalence ratio, which varies with engine power setting:

$$k\_DropTime = f(\phi_{PZ})$$

Also, for the quench zone parameters Alpha and Beta, it was found that the data correlated best when the ratio of the standard deviation to the mean of the beta distribution was modeled as a function of the equivalence ratio of Quench Zone. Then given Beta, Alpha may be calculated from the algebraic relationship.

$$\frac{\sigma}{\mu} = f(\phi_{SZ})$$

$$\alpha = f\left(\beta, \frac{\sigma}{\mu}\right)$$

The final tuning parameter values are summarized in Table 45. Keep in mind that the equivalence ratios and residences times specified in the Table apply to the Takeoff (design) condition only; off-design these values are computed as described in the 1-D Flow Model discussion.

Table 52. Results for Model Calibration at 30 OPR

	Combustor Type	
Calib. Parameter	Baseline	Advanced
dPdiffqP	0.054	0.054
EqRatioPZ	1.64635389	1.43
EqRatioSZ	0.68732829	0.64
EqRatioDZ	0.4	0.4
ResTimePZ	0.00031948	0.0002
ResTimeSZ	0.00114741	0.002
ResTimeLZ	0.00101548	0.0013
ResTimeDZ	0.0005	0.0005
k_evap	0.23	0.23
EffPZ	0.94	0.94
k_Mixedness	1	1
k_DropTime	Function of ln(EqRatioPZ)	Function of EqRatioPZ
Beta	7	7
SigMu	Function of EqRatioSZ	Function of EqRatioSZ

4.4.5.3 Calibration at Higher OPR – The "Sizing Rule"

To scale the reference (30 OPR) engine to other engines, a scaling parameter was modeled. Because the model calculates the effective volume of the reaction zone based on the input residence time, the scaling parameter is applied to the input residence time so that it is manageable during the calibration process.

One important assumption is that the scaling parameter is applicable to all reaction zones in one engine. This assumption is possible due to independent effects of the primary zone residence time and the secondary zone residence time, as shown in the calibration parameter sensitivity study. That is, the EINOx at high power is highly sensitive to the secondary zone residence time while the primary zone residence time has negligible effect. However at low power, the primary zone residence time is the dominant parameter while the secondary zone shows negligible effect. Therefore, one scaling parameter can be used for both zones for NOx prediction even though the resultant total volume may be over- or under- predicted.

The scaling parameter, which is the ratio of residence time of target engine to the residence time of reference engine, was modeled as a function of cycle parameters of target engines (pressure, temperature, flowrate and fuel-to-air ratio) at the combustor inlet. The residence time scaling relationship is defined in the equation below:

$$\frac{\tau}{\tau_{ref}} = a\left(\frac{P}{P_{ref}}\right)^{b}\left(\frac{T}{T_{ref}}\right)^{c}\left(\frac{W_3}{W_{3_{ref}}}\right)^{d}\left(\frac{\mathrm{FAR}}{\mathrm{FAR}_{ref}}\right)^{e} exp\left(f\left(\frac{1}{T}-\frac{1}{T_{ref}}\right)\right)$$

This equation results from the volume scaling following the derivation given in Mattingly. The exponents *a*, *b*, *c*, *d*, *e*, and *f* are to be found by regression analysis to match the

calibration engines to the desired Dp/F00-vs-OPR characteristic. The target engine cycles were selected from the previous year's ERA design space. To control for the effects of the engine cycle on the Dp/F00-vs-OPR line, the cycles were filtered to hold BPR about constant at a relatively low value (approx. 10-11) with no intercooling. A number of engine cycles meeting these requirements were selected randomly over the range from 30-60 OPR. Engines from both the 150-passenger and 300-passenger size classes were selected, but because of the restricted BPR range all of the calibration engines were ADD architecture.

The calibration results are shown in Figure 73. The upper line is the CAEP/6 limit, while the middle line represents the baseline target of CAEP/6 -30%.

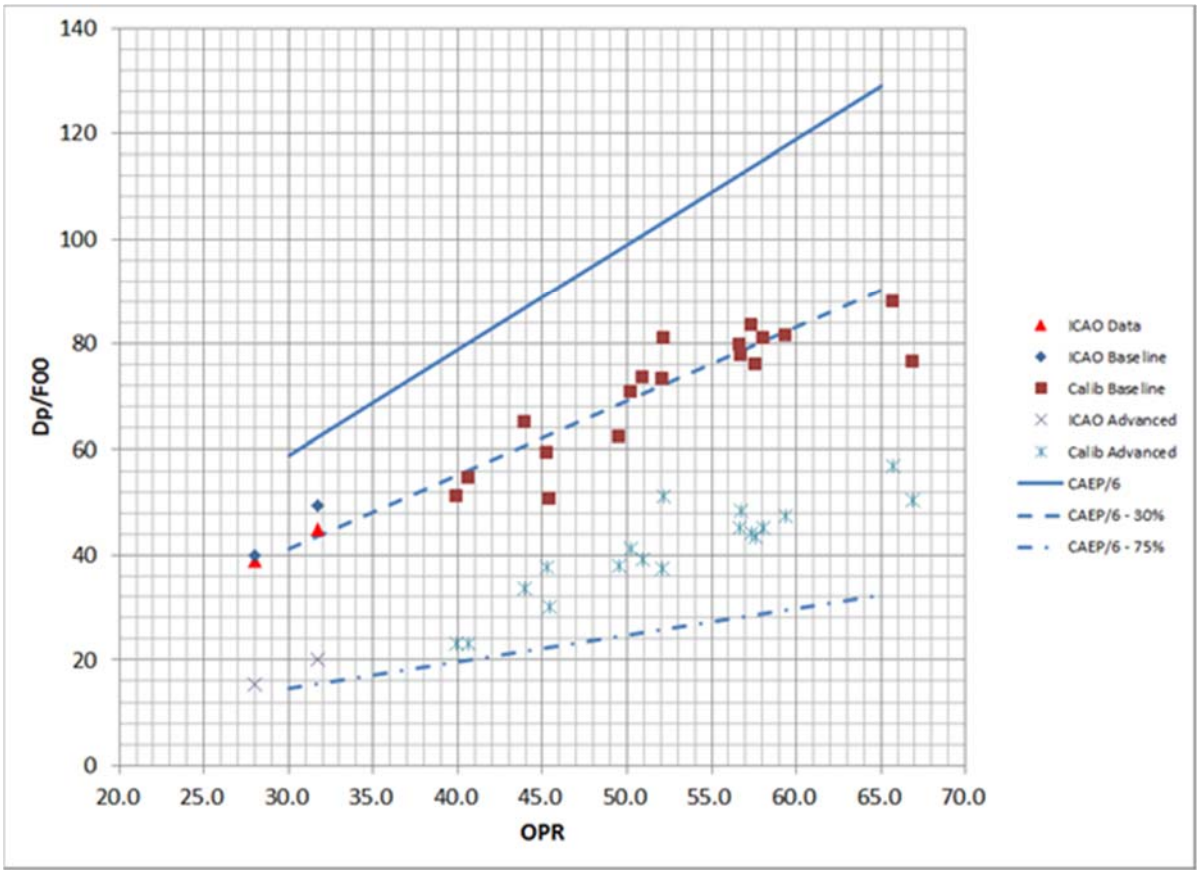

Figure 73. Calibration Result of Target Engines

It may be seen that the sizing rule achieves good agreement with the targets for the baseline combustor. The advanced combustor follows a parallel slope to the baseline combustor, because it uses the same sizing rule. The results indicate that meet the N+2 EINOx goal at 30 OPR, but advanced engine cycle technology such as higher BPR and/or intercooling may be necessary to meet the N+2 EINOx goal at higher OPR.

Because the calibration targeted Dp/F_{00} only, the model was tested to confirm that the model reflected the general trend of nitrogen oxides emissions in sub-power modes. To do that, the LTO cycle of sixty-seven engines from the previous year's ERA study were selected with similar levels of bypass ratio and low intercooler flow. Run results of those engines showed the expected physical trends, as shown in Figure 74.

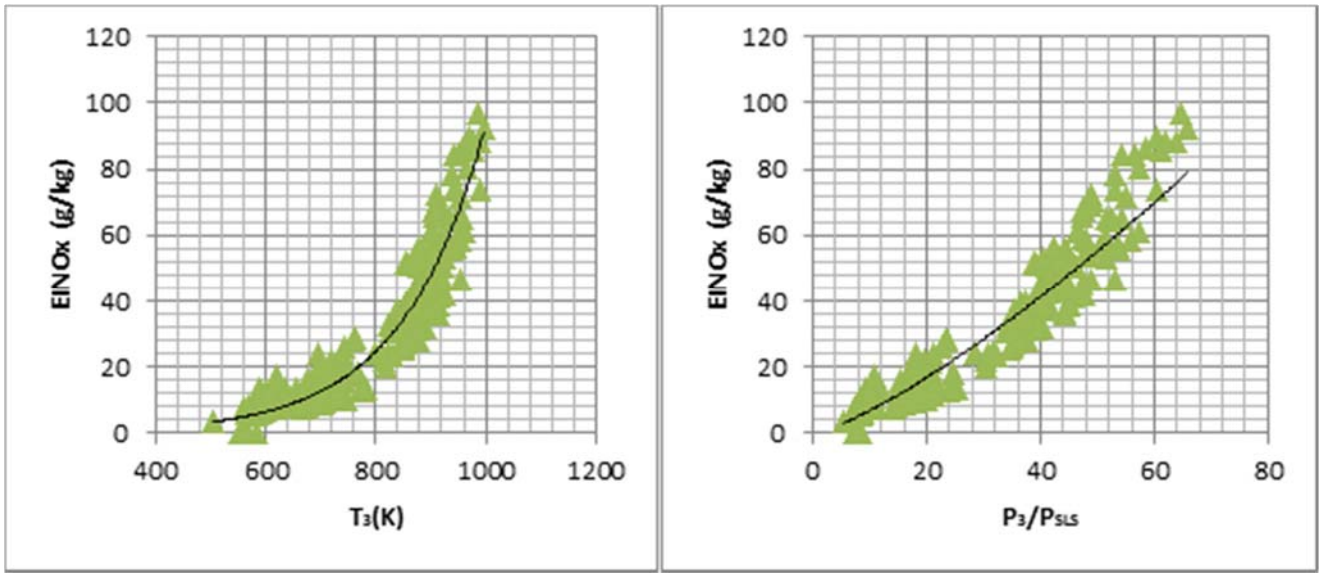

Figure 74. EINOx Predictions for Calibrated High OPR Engines

As mentioned above, the same sizing rule was applied to the advanced combustor because the same rule gave reasonable prediction of Dp/F00 for the advanced combustor engines. However, advanced technology may change the relationship between the thermodynamic cycle and the effective size (or effective residence time). Therefore, further research on the sizing principle for the advanced combustor will improve fidelity of prediction model.

4.4.5.4 Advanced Cycles – The "Intercooler Rule"

As discussed previously, many of the advanced high-OPR engine cycles require an intercooler. For these engines the emissions will be improved relative to the ERA target not because of the combustor technology but merely due to the engine operation. To account for this behavior, the combustor technology level has been separated from the cycle effects by means of the previous two calibration steps. However the intercooler results in a takeoff T3 disproportionately lower than the design P3, which causes a difficulty in applying the previously defined sizing rule. The design T3 should be determined as if there were no intercooler, and the combustor sized for that condition.

It is required to estimate a fictitious design T3 given the T3 at takeoff power to correctly size the combustor. The relationship between T3 and P3 is shown in Figure 75. A number of engine cycles generated in EDS were tested by turning on and off the intercooler flow. The "X" in the figures indicates when the intercooler is off, and the diamonds indicate when the intercooler is working. The solid black line in the figure is the regressed power series of samples without intercooler flow. The expected design T3 was calculated from the regressed relationship and applied to the sizing rule.

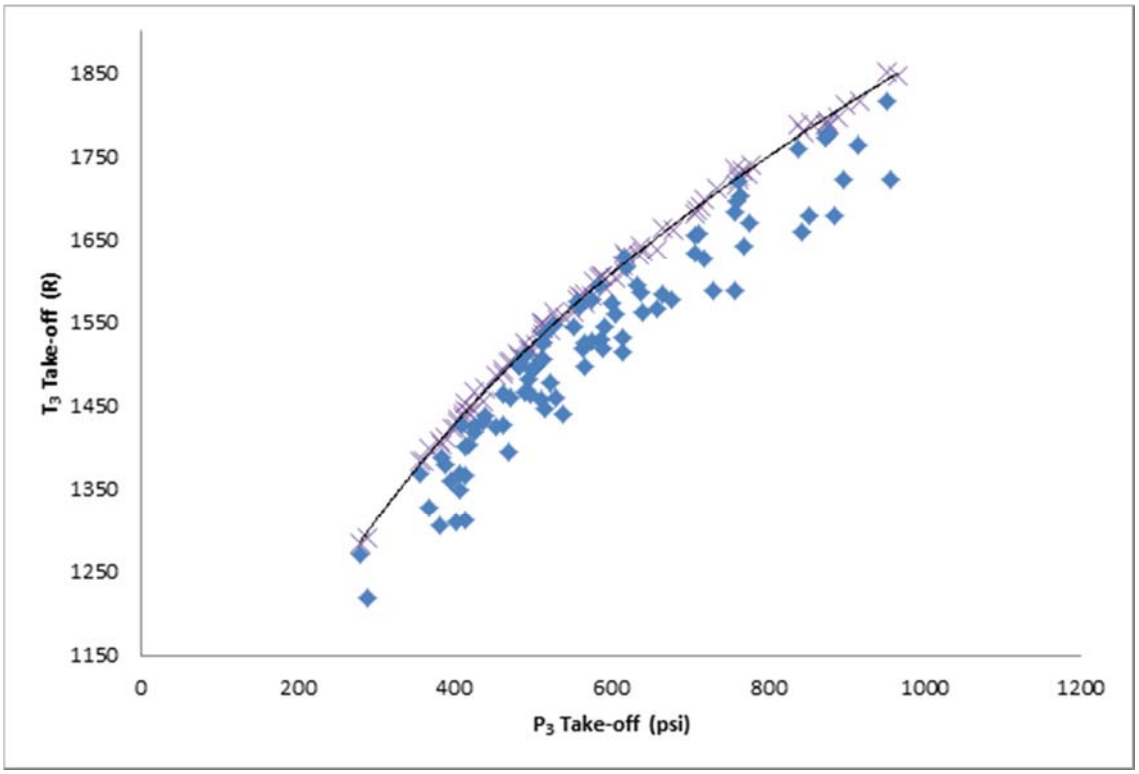

Figure 75. Relationship between T_3 and P_3 with Intercooler Effect

Figure 76 shows the results of complete model with target engines and additional validation engines after the intercooler logic was integrated to the model. Upper line is the CAEP/6 limit, middle line is CAEP/6 -30% limit, and the bottom line indicates CAEP/6 -75% for reference. The validation engines have wide range of bypass ratio and intercooler flow.

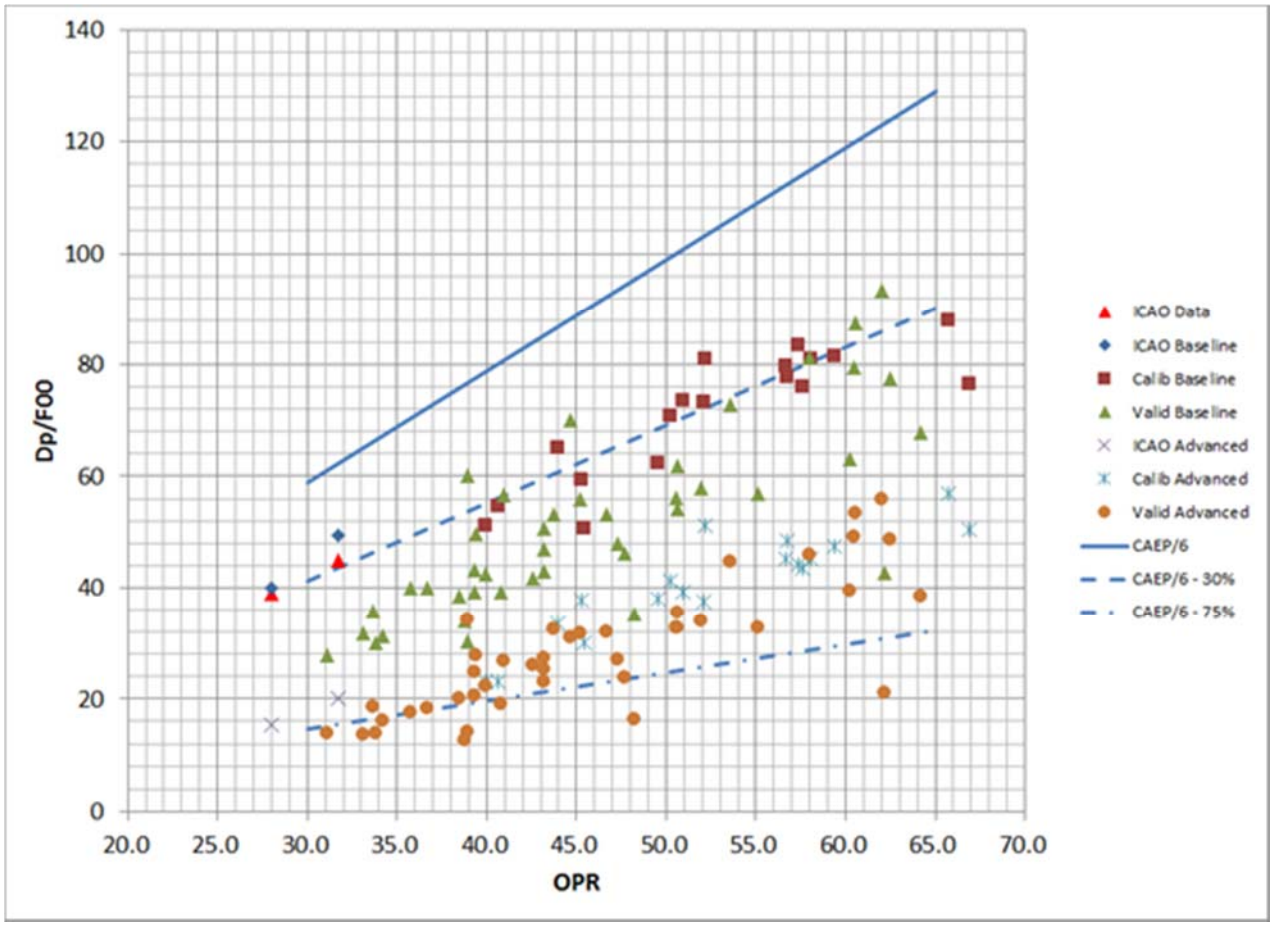

Figure 76. Results of Complete Model

It may be seen that the validation points follow the same general trends as the calibration points, but have lower emissions due to higher BPR and/or intercooling. Several of the engines do meet the N+2 EINOx goal at high OPR.

4.4.5.5 Generation of Neural Net Regression Model for EDS

A DOE table was established to generate Neural Net surrogate models for both baseline and advanced combustors. Input variables required are P3, T3, W3, and Wfuel, for each power setting (TO, CO, AP, and ID) for a number of sample engines. These input variables cannot be selected independently. Instead, alternative variables which are independent of engine flow size and vary more predictably were selected to create the DOE table. These alternative variables for the design (takeoff) condition are as follows:

$$OPR = \frac{P_3}{P_{STD}}$$

$$e_{poly} = \frac{\gamma - 1}{\gamma} \frac{ln(P_3/P_{STD})}{ln(T_3/T_{STD})}$$

$$W_c = \frac{W_3\sqrt{T_3}}{P_3}$$

$$FAR = \frac{W_{fuel}}{W_3}$$

The alternative variables for part power operation are as follows:

$$k_{P_3,i} = \frac{P_{3,i}}{P_{3,TO}}$$

$$k_{e_{poly},i} = \frac{e_{poly,i}}{e_{poly,TO}}$$

$$k_{W_c,i} = \frac{W_{c,i}}{W_{c,TO}}$$

$$k_{FAR,i} = \frac{FAR_i}{FAR_{TO}}$$

Suitable ranges for the alternative values were determined by examination of data from available EDS runs from the previous year's study. The final selected ranges are shown Table 53.

Table 53. Ranges for DOE Variables

Parameter	Minimum	Maximum
OPR	25	70
e_{poly}	0.93	1.0
Wc	2	12
FAR	0.02	0.035
$k_{P_3,CL}$	0.82	0.93
$k_{e_{poly},CL}$	0.95	1.0
$k_{W_c,CL}$	1.0	1.01
$k_{FAR,CL}$	0.9	0.95
$k_{P_3,AP}$	0.3	0.47
$k_{e_{poly},AP}$	0.85	0.99
$k_{W_c,AP}$	1.0	1.1
$k_{FAR,AP}$	0.3	0.75
$k_{P_3,ID}$	0.13	0.22
$k_{e_{poly},ID}$	0.75	0.95
$k_{W_c,ID}$	1.05	1.2
$k_{FAR,ID}$	0.3	0.6

An additional variable was provided for the intercooler delta_T3, both on- and off-design, and was allowed to vary from 50 to 250 with a bias as a function of the P3. The T3 computed using the e_{poly} from the above table was then reduced by the amount of delta_T3.

From these ranges for the design (takeoff) variables, the DOE table consists of three categories of samples: Corner points and Optimal Latin Hypercube (OLH) points for model training, and random points for model validation. For the part power variables, uniformly distributed random values were selected.

A total 1440 points were generated per each power mode for both baseline and advanced combustors. These points were run in the ModelCenter™ environment, taking approximately one week on three computers to generate the results. The results were then regressed to make the Neural Net equations. It was not possible to build one Neural Net equation suitable for all power settings; instead a separate NN equation was created for each power setting, and for each combustor type (baseline and advanced).

The NN equations were a function of the 21 variables summarized in Table 54

Table 54. EINOx Neural-Net Regression Independent Variables

Variable	Definition
P3_des	Design compressor outlet / burner inlet pressure
T3_des	Design compressor outlet / burner inlet temperature
W3_des	Design air flow rate into the burner from the compressor
Wfuel_des	Design flow rate of fuel injected into the burner from the fuel injector
P3_offdes	Calculated pressure of air leaving compressor and entering burner (from flow model)
T3_offdes	Calculated temperature of air leaving compressor and entering burner (from flow model)
W3_offdes	Calculated flow rate of air leaving compressor and entering burner (from flow model)
Wfuel_offdes	Calculated flow rate of fuel injected intot he burner from the fuel injector (from flow model)
L_Comb	Length of the combustor (as sized by the 1-D flow model)
EqRatioPZ	Equivalence ratio of the primary zone (computed from the flow model)
EqRatioSZ	Equivalence ratio of the secondary zone (computed from the flow model)
EqratioLZ	Equivalence ratio of the lean zone (computed from the flow model)
EqRatioDZ	Equivalence ratio of the dilution zone (computed from the flow model)
ResTimePZ	Residence Time of the primary zone (as determined from calibration of the model)
ResTimeSZ	Residence Time of the secondary zone (as determined from calibration of the model)
ResTimeLZ	Residence Time of the lean zone (as determined from calibration of the model)
ResTimeDZ	Residence Time of the dilutiony zone (as determined from calibration of the model)
TempPZ	Temperature of the primary zone after burning
T4	Temperature of the air (plus small amount of leftover fuel) leaving the combustor
SMD	Droplet size as computed from the droplet model within the flow model
Unmixedness	Unmixedness of the fuel within the combustor before burning occurs

The regression statistics are summarized in Table 55.

Table 55. EINOx Regression Model Statistics

Combustor	Power	Hidden Nodes	MFE, mean	MFE, stdev	MRE, mean	MRE, stdev	R^2, training	R^2, validation
Baseline	TO	21	2.7E-06	.007	.0006	.011	1	1
	CL	15	4.6E-10	.008	.0002	.023	1	1
	AP	21	7.4E-08	.132	.025	.36	.9998	.9982
	ID	15	.00016	.097	.0024	.19	.9995	.9479
Advanced	TO	25	.0008	.147	.0029	.24	.9998	.9996
	CL	18	4.2E-05	.007	.002	.04	1	1
	AP	18	.0015	.25	.023	.52	.9988	.9947
	ID	19	2.2E-05	.075	.0047	.11	.9995	.9990

The Model Fit Error (MFE) represents the distribution of the residuals of the data used to fit the model. It describes the accuracy with which the model was fit to the training data. The Model Representation Error (MRE) represents the distribution of the residuals of the validation data, additional data which was not used to fit the model. It describes the ability of the model to accurately predict the response within the ranges of the DOE variables. As a general rule, the mean errors for the MFE and MRE should be near zero, and the standard deviations should be less than one.

It may be seen that, due to the nonlinearity of the model, a relatively large number of hidden layers were required. No overfit was detected. The Approach conditions generally gave the worst fits, although all the fits were deemed to be excellent.

The NN equations were coded into the EDS model as described in the following section.

4.4.6 Incorporation of Emissions Model into EDS

All of the NPSS code for the 1-D flow model was identical to that used in the ModelCenter™ environment described above. The only difference was that the *EI.case* file in EDS was modified to create two combustor assemblies, one for the baseline combustor and one for the advanced combustor. The tuning parameter inputs for each combustor were specified when the *Total_Combustor* element was instantiated in each assembly. Then, instead of writing the 1-D flow outputs to a Chemkin™ input file, the Neural Net equations were evaluated and the EINOx values were computed for each power setting. Finally, the Dp/F_{00} parameter was computed for each combustor.

As a test of this implementation, several test cases were run with EDS. These results are shown in Figure 77.

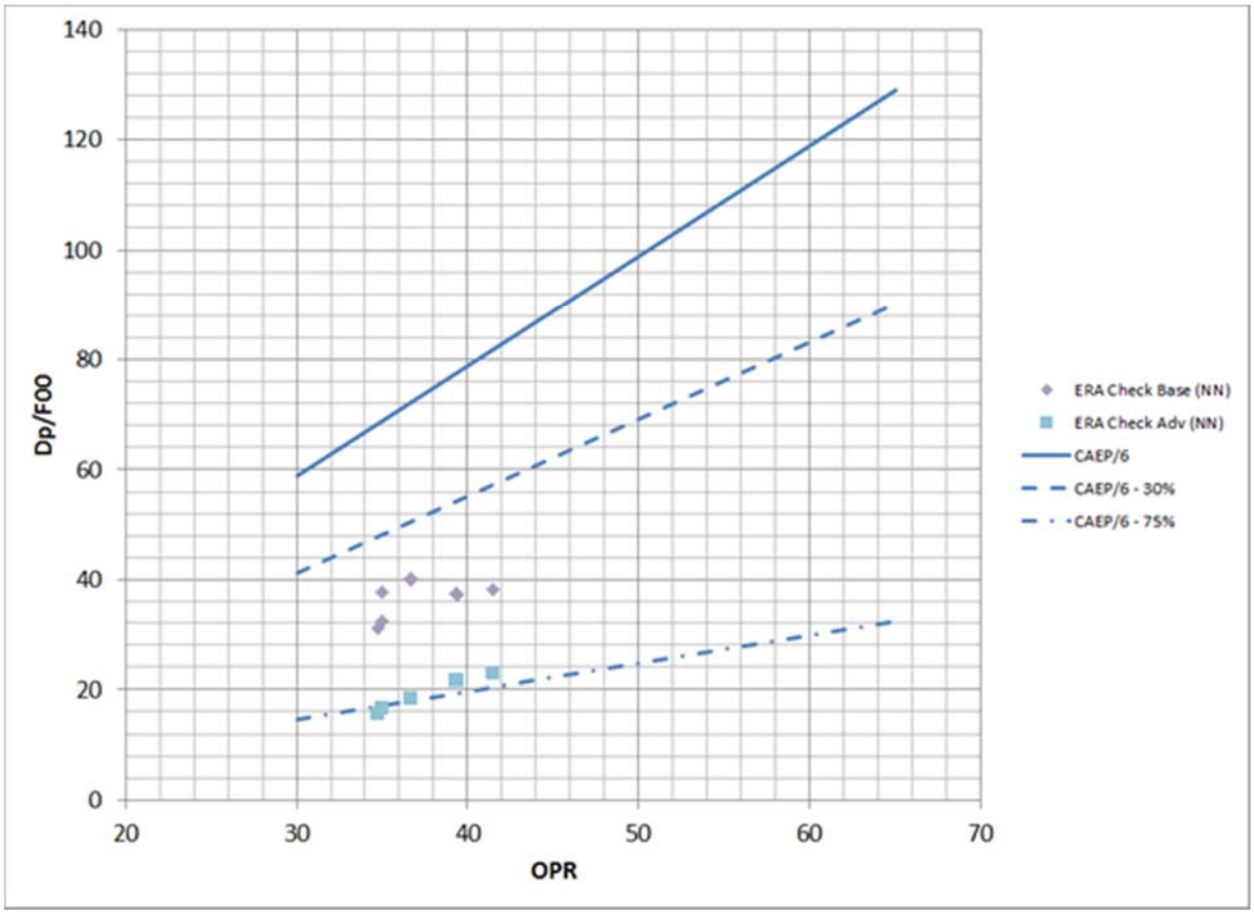

Figure 77. EDS Implementation Test Results

These test cases were run for the RTC engines, for which the BPR ranged from 13.9 to 18.8. It may be seen that the baseline combustors fall below target line due to the higher BPR than that assumed for the calibration. This is expected. Also the advanced combustors fall along the target line, again due to the higher BPR. Thus the NOx model was verified to be correctly implemented in EDS.

5.0 Surrogate Model Generation

5.1 Surrogate Modeling Methodology

Surrogate models are a mathematical representation of a complex analytical tool or group of analytical tools that are limited to a specific problem. The replacement of that analytical tool with a virtually instantaneous equation enables rapid optimization, sensitivity analysis and visualization of design tradeoffs to make better decisions. The EDS environment has over one hundred independent inputs with over 120 modeled technologies, and without speeding up the evaluation process it would be virtually impossible to evaluate them. The cost to using surrogate models is that the analytical tool must be run many times up front to generate the data from which the surrogate model is created.

The overall surrogate modeling process is shown in Figure 78. After examining the Technology Compatibility Matrix and the Technology Impact Matrix it is possible to assess the maximum and minimum limits expected for each of the variables. The set of runs that are evaluated before creating the surrogate model is coming from a set of techniques known as Design of Experiments (DOE). The DOE used for this project is a Latin hypercube that captures the variability throughout the design space. The surrogate models are then created and evaluated using a standard set of criteria that ensures the full model is adequately captured by the surrogate.

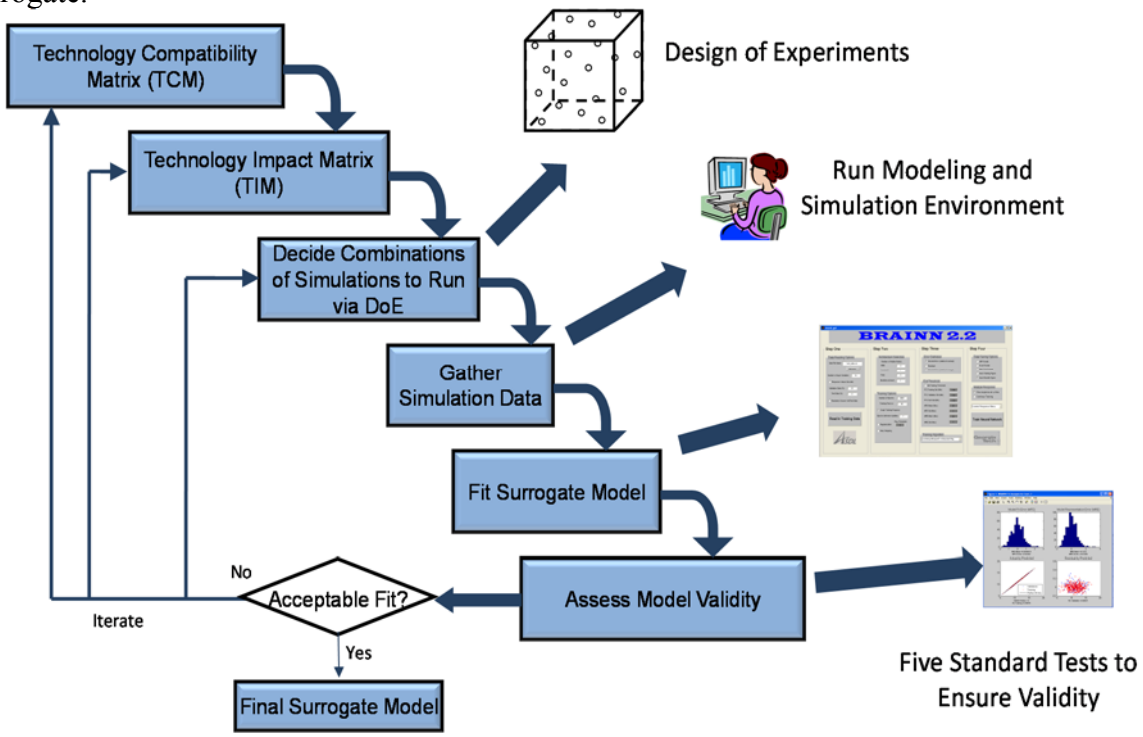

Figure 78. Surrogate Modeling Process

There are many different methods to create surrogate models and many types of surrogate models that can be created. A Multi-Layer Perceptron (MLP) feedforward Artificial Neural Network (ANN) with a single hidden layer was used in this project. The ANN is a powerful and flexible surrogate modeling method that can handle non-linear and large scale problems, and ASDL has extensive experience and knowledge in their creation and application.

Neural Nets work by mapping a set of input variables to a set of responses through a set of filters, called the hidden layer. There can be more than one hidden layer, but only one is necessary for the overwhelming majority of problems. The hidden layer consists of hidden nodes, analogous to neurons in a biological neuron. An example diagram illustrating the connections between the layers is shown in Figure 79

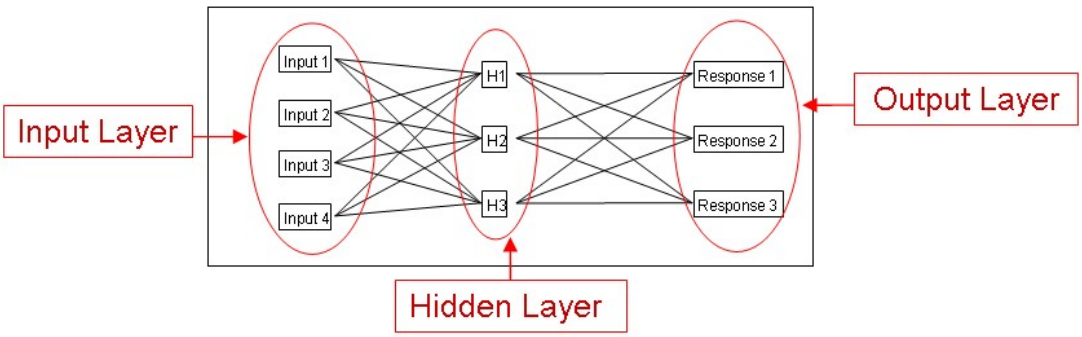

Figure 79. Neural Network Conceptual Diagram

As a conceptual example, the input layer is like a person's five senses, receiving data from the outside world. The hidden layer is like the brain, processing this data. And the output layers would be a response to stimuli, like talking or typing. As the figure shows, each of the inputs has an influence on the hidden nodes and each of the hidden nodes has an influence on the responses. The correct number of hidden nodes depends very much on the problem; the number of hidden nodes is iteratively determined for each response.

A Neural Network, like all other forms of regression, fits an equation through a given set of data. The mathematical form of the Neural Net equation is described below. The data being regressed is called the training set for a Neural Network. The training algorithm is the optimization method used to determine the coefficients for the network that minimize the training error.

The mathematics of a single hidden layer Neural Network will now be described. In a biological system the neurons are either sending or not sending a signal, based on the inputs they receive from other neurons. They therefore have a step function for their activation function- on or off. For a numerical regression the use of a step function is problematic because it is not continuous and differentiable. Most Neural Networks use something called the logistic function. The logistic sigmoid function has the effect of "squishing" the inputs to it such that it always outputs a value between 0 and 1.

$$S(z) = \frac{1}{1+e^{-z}}$$

This logistic function is used to calculate the value for each of the hidden nodes for both the function approximation and classification problems. The value of the hidden node is taken by applying the logistic function to a linear term related to the input variables.

$$H_j = S\left(a_j + \sum_{i=1}^{N}\left(b_{ij}X_i\right)\right)$$

Where: a_j is the intercept term for the j^{th} hidden node
b_{ij} is the coefficient for the i^{th} design variable
X_i is the value of the i^{th} design variable
H_j is the value of the j^{th} hidden node
and N is the number of input variables

The calculation of the final response will depend on the problem type. For function approximation, the value of the response is found through a linear term that depends on the value of the hidden nodes.

$$R_k = e_k + \sum_{j=1}^{N_H} \left(f_{jk} H_j \right)$$

Where: e_k is the intercept term for the k^{th} response
f_{jk} is the coefficient for the j^{th} hidden node and k^{th} response
H_j is the value of the j^{th} hidden node (defined above)
and N_H is the number of hidden nodes

The different steps described above can be combined to create the following unified form of the Neural Net equation for function approximation.

$$R_k = e_k + \sum_{j=1}^{N_H} \left(f_{jk} \left(\frac{1}{1 + e^{-\left(a_j + \sum_{i=1}^{N} \left(b_{ij} X_i \right) \right)}} \right) \right)$$

Where: a_j is the intercept term for the j^{th} hidden node
b_{ij} is the coefficient for the i^{th} design variable
X_i is the value of the i^{th} design variable
N is the number of input variables
e_k is the intercept term for the k^{th} response
f_{jk} is the coefficient for the j^{th} hidden node and k^{th} response
and N_H is the number of hidden nodes

The four coefficients (*a, b, e* and *f* in the above) are modified to fit the training set as well as possible, minimizing the sum square error or mean square error of the training set, depending on the training algorithm selected.

5.2 Surrogate Modeling Process Description

Using the methodology described in the previous section a set of 45 surrogates were created for 8 vehicle and engine combinations which are the LSA, LSA OWN, LTA, LTA MFN, LTA HWB, LTA BXW using the geared fan engine cycle and the LSA and LTA HWB using the open rotor engine cycle. The neural network surrogates were trained on thousands of EDS runs for each vehicle and engine combination. All surrogate models were fit as function of independent technology and cycle parameters, as well as TOGW. To improve the accuracy of some neural networks including emissions and noise surrogates, nested models were used which were fit as function of additional relevant EDS output data. The 45 response metrics created for each of the 8 vehicle and engine combinations are listed in Table 56. The names in this table appear in abbreviated form as used within EDS. A description of the full metric names and associated units is provided in Appendix A.

Due to differences in architecture the EDS models for the open rotor vehicles described several responses with different names than the geared fan vehicles. For example in the geared fan architecture the fan diameter is tracked by the response metric, diamFan; but in the open rotor architecture this response is replaced by Prop Diam. These responses are numbered 40 to 43 in Table 56

Table 56. 45 Response Metric Names for ERA Surrogates

Mission Responses	Airframe Responses	Engine Responses		
1. desBlockFuel	11. desTOGW	17. SLS_UI_OPR	27. EI_Standard_AP	37. ICAO_TO_Tt3
2. Cruise_SFC_Min	12. Fuse_Weight	18. T3max	28. EI_Standard_CO	38. ICAO_TO_Wfuel
3. Approach	13. OEW	19. ADP_BPR	29. EI_Standard_ID	39. LPC_diam
4. Cutback	14. VT_Weight	20. HPC_diam	30. EI_Standard_TO	40. Nacelle_Diam/Dnac
5. Sideline	15. Wing_Weight	21. HPCLastStageWc	31. ICAO_AP_Tt3	41. enginePodLength/Xnac
6. TOAll_TOFL	16. HT_Weight	22. HPCLastStgBladeHeight	32. ICAO_AP_Wfuel	42. engPodWt/WENG
7. TOOEO_TOFL	11. desTOGW	23. EI_NOx_AP	33. ICAO_CO_Tt3	43. diamFan/Prop Diam
8. AbortALL_TOFL	12. Fuse_Weight	24. EI_NOx_CO	34. ICAO_CO_Wfuel	44. ICAO_ID_Equiv
9. AbortOEO_TOFL		25. EI_NOx_ID	35. ICAO_ID_Tt3	45. ICAO_AP_Equiv
10. desFAR_LDGFL		26. EI_NOx_TO	36. ICAO_ID_Wfuel	

5.3 Surrogate Model Results

Over 350 surrogates were created in total for all 8 vehicle combinations. Each surrogate was evaluated by standard goodness of fit checks as described in the surrogate methodology section to ensure high fit quality and prediction accuracy. These goodness of fit checks include Model Fit Error, Model Representation Error, Actual by Predicted fit line, Residual error plot, and R-squared values. All surrogates are within a 3% error tolerance, excluding NOx and TOFL fits. NOx surrogates and TOFL fits are all within a 5% error tolerance. The fit statistics for each surrogate have been tabulated for all 8 vehicle and engine combinations in Appendix B.

Once the best goodness of fit criteria was achieved the surrogate training process was completed and the neural networks were saved in equation form. These equations were imported into the ERA Dashboard which uses the surrogate models to quickly perform technology package evaluations, design space exploration, probabilistic assessments, response tradeoffs, etc… The surrogate predictions in the dashboard were also validated against local runs in (EDS) for specific tech packages to ensure accuracy of surrogate models on feasible solutions found by the dashboard.

6.0 Probabilistic Analysis

6.1 Literature Review of Probabilistic Assessment Methods and Technology Impacts

6.1.1 Introduction and Background

Probabilistic methods take on many different meanings in a variety of disciplines from combinatorial mathematics to actuarial sciences. For our purposes in engineering analysis we refer to probabilistic methods as non-deterministic assessment techniques which allow for the inclusion of uncertainty in engineering design. There is a large body of literature for non-deterministic approaches in the context of assessing future technologies, concepts, systems, for which the impact on performance is uncertain. This review will survey various aspects of this literature and note how these areas have contributed to probabilistic methods in engineering.

Probabilistic methods have aided designers to progress beyond point designs and deterministic answers. They have facilitated uncertainty quantification and the creation of robust designs. Ryan and Townsend [Ryan 1993] discuss the benefits of probabilistic methods in aerospace applications and how they have contributed to the success of key programs. The authors describe how uncertainty in design requirements and environmental condition necessitates a level of safety in design, and while this used to be mitigated using a deterministic safety factor, probability is a better approach for measuring this uncertainty as previously demonstrated in space applications including space shuttle main engine design. They also advocate the use of probabilistic and reliability methods which model individual parameter uncertainty with probability distributions. Their work promotes probabilistic engineering approaches even if they are not highly accurate because they require engineers to know more about the problem giving them an idea about the risk involved in a design and the design parameter sensitivities; which they claim will ultimately yield a more robust design.

Probabilistic methods are employed using a number of different approaches which can be broadly categorized as analytical and numerical. Analytical approaches are further discussed in the next section. A basic numerical approach in non-deterministic assessment techniques was reported as early as 1968 [Timson 1968]. This approach is summarized in five basic steps:

1. Determine design equations relating properties at lower levels to measures of system level performance
2. Obtain subjective probabilities for subsystem properties
3. Use Monte Carlo to sample from these probabilities
4. Generate statistical measures for resulting systems performance distribution
5. Compare statistical measures across time periods for an indication of progress

This methodology bears archival value not only due to its early origin but also because this basic outline for probabilistic methods has not significantly changed in over 50 years. Much of the literature which applies probabilistic assessment techniques either knowingly, or unknowingly, employs this basic outline. There are variations on this approach but the basic structure has been used extensively.

6.1.2 Analytical Approaches

Analytical approaches for probabilistic assessment exist in the literature and were extensively used in the 1990's time frame. They are not as popular as numerical approaches but they created the framework for many of the techniques employed today. Due to their foundational nature it is relevant to mention some of these methods briefly. The underlying theory of these approaches is based upon a mathematical representation but the evaluation of the method or associated functions may be simplified by using computer simulations. This is not to be confused with numerical approaches which are also evaluated using computer simulations but are not necessarily based upon explicit mathematical theorems and are sampling based in nature.

6.1.2.1 Most Probable Point Analysis

Most Probable Point (MPP) method is a probabilistic analysis method for calculating the probability of failure given a constraint in an uncertain multi-dimensional space. The technique was applied heavily and early on by the structural reliability community [Elseifi 2001, Khalessi 1993, Lin 1993]. This method explores a joint probabilistic space by evaluating limit state functions in an effort to identify the failure region for a particular system. The MPP approach identifies the failure boundary in the joint probabilistic space while minimizing the number of limit state function evaluations as explained by [Du 2005]. This approach lost popularity due to the higher dimensionality of recent applications and the proportionally increasing cost of function evaluations with the number of random variables [Du 2005]. In the aerospace community the technique did not see extensive use for technology evaluation and implementation but it did establish how to analyze functions and constraints in a joint probabilistic space defined by multiple random variables. Typical examples of the method exist in the context of aerospace structures and systems analysis [Shi 2001, Green 2002, Lyle 2003].

6.1.2.2 Fast Probability Integration

The Fast Probability Integration technique is a probability analysis code [SwRI 1995] which is based on MPP analysis and attempts to solve the same analytical equations which represent the limit state function in a joint probabilistic space. The FPI code claims to have efficient techniques which eliminate the need for large amounts of expensive function evaluations. It also links itself directly to the analysis code removing the need for surrogate models which were at that time expensive to create and limited in the number of variables they could include [Mavris AIAA 1997-5508]. FPI has been used to assess individual technologies and their impact on system reliability [Boyce 1989, Journal of Propulsion] as well as to examine the effect of uncertain technological impacts from a holistic air traffic system perspective [Mavris AIAA 2000-5612]. The process outlined in the latter work describing how to handle uncertainty as a result of technology insertion with probability distributions is particularly relevant and still used in many applications. However advancements in computing capabilities significantly reduced the computational effort required to use more accurate techniques such as Monte Carlo simulations and surrogate models.

6.1.2.3 Other Analytical Approaches

Many other techniques exist for handling uncertainty probabilistically which are based upon mathematical formulations. These include Polynomial Chaos expansions which have been

used to address limitations in uncertainty propagation in reliability optimization [Kim 2006] and aerodynamic analyses [Yamazaki 2013]. The polynomial chaos expansions serve as efficient approximations of the model outputs to improve computational time and accuracy.

The Fourier Amplitude Sensitivity Test (FAST) is a variance based method which can probabilistically determine sensitivities to individual parameter uncertainties of a function. It models multi-dimensional systems as waves and frequencies, then applies a Fourier transform to determine the sensitivities of parameters [Cukier 1978]. Within the aerospace community it has been used in structural analysis [Adelman 1986] and the impact prediction of decaying objects in space [Ronse 2014].

These analytical methods are very popular for probabilistically handling uncertainty of various kinds but have not been extensively applied to handling uncertainty for technology modeling in the aerospace community. Numerical approaches are far more popular for this purpose and will be the focus of the next section.

6.1.3 Numerical Approaches

Numerical methods and non-deterministic approaches are the most popular ways to conduct probabilistic assessments in the literature. This is facilitated in part by advanced computing capabilities which make simulations and sampling very cheap and efficient. In addition modern software packages have simplified the use and implementation of these methods. They have also made the ensuing analysis much easier through a variety of graphical and visual interfaces. Even with these notable improvements, the basic process used in these numerical probabilistic assessments has not departed significantly from the method outlined by Timson [Timson 1968] many years ago.

The first step in the process calls for determining design equations relating properties at lower levels to measures of system level performance. Basically to form a relationship which can describe a model output by influencing one or more model inputs. These equations can be based on basic laws of science or they can be more complex metamodels. Surrogates of this nature are commonly used in probabilistic analysis and come in many forms. These include polynomial response surfaces, kriging [Rumpfkeil 2011], support vector machines [Missoum 2009], and artificial neural networks which have been described in detail earlier in Section 5.1. These surrogate models are a key enabler for numerical approaches of probabilistic assessment.

6.1.3.1 Response Surfaces

Response surfaces are powerful functions which can quickly mimic a model output which is difficult or time-consuming to obtain directly. They can be particularly useful in performing sensitivity analyses, design space exploration, sensitivity analyses, probabilistic assessments, and system optimization which can require thousands of model evaluations. They are formed by a curve fit which minimizes the error through a certain number of model evaluations which been run in advance. The response surface is typically of second order but can be formed with higher order terms to capture interaction terms and non-linearity. The predictive nature of the response surface surrogate is always verified with test points of the model to ensure high accuracy. Further reading on the fundamentals of response surfaces can be found in various texts [Myers 2002, Khuri 2006, Box 1987]. Response surfaces have been used in the probabilistic assessment of large structures [Shah 1998], space landing systems [Slade 2006], and many other technology based applications [Mercer 2006, Taylor 2002, Lin 2001]. They have also been used to assess

aircraft technology impacts [Soban 2013] and forecast uncertainty in aircraft technologies [Kirby 2000, Raczynski 2006].

6.1.3.2 Subjective Probabilty

Once a relationship has been formed between design inputs and system level outputs, the next step in Timson's approach is to obtain subjective probabilities for subsystem properties. As is the case with many phrases discussed in the literature, Subjective Probability or subjectivity in probabilistics can have different meanings. These differences can lead to misinterpretation of ideas so it is important to understand what is referred to by subjectivity. Subjectivity can describe a user input in a modeling process, or decisions made by an analyst to achieve a certain solution, or even the translation of qualitative statements into quantitative values. In all of these areas subjectivity undoubtedly plays a role, and that role has been both praised and criticized in the past. For this reason, to advantageously use subjectivity in probabilistics, analysts should be aware of its usefulness and drawbacks to best apply it to their needs. Several examples of how subjectivity has been discussed and applied in the literature are also presented.

It is important to recognize the role of bias in subjective probability which can arise from different sources including subject matter experts and also from analysts themselves. This can be a result of prior experiences, environmental factors, and the training received by the analysts as well. Bias can affect the way in which subjective probabilities are formed. Subjective probabilities are very important in probabilistic assessment because they inform the distributions of the input random variables. When these distributions are modeled accurately the results of the probabilistic assessment are credible and meaningful. However if poor assumptions are made regarding the probability distributions of random variables or the relationships between them, the results of the probabilistic assessment can be misleading or false. One such example of bias in training is the tendency in many engineering applications to assume normality of input distributions due its familiarity and ease of implementation. The normal distribution is easily understood and widely taught to practitioners such that it has become a default choice in many applications [Shah 1998, Dubos 2008, Dell'Elce 2014] even though multiple statistical tests exist to check for the appropriateness of the normal distribution including the Anderson-Darling test, D'Agostino's K-squared test, the Jarque-Bera test, etc. Conrow [Conrow 2010a] offers a detailed critique of the work published by Dubos, Saleh, and Braun [Dubos 2008] in which he states that normal distributions should not have been assumed for random variables and provides his own analysis which employs the Anderson-Darling and Kolmogorov-Smirnov [Kolmogorov 1933, Smirnov 1948] statistical tests to define distribution type.

Once the distribution types have been defined accurately, it is also important to correctly represent the relationships between random variates. Another example of bias in training and due to environmental factors is the common assumption that random variables in a probabilistic assessments are independent, even though this can be a poor assumption with consequences on probabilistic assessment results. In many applications [Prandini 1999, McCormick 2000, Zhang 2012] dependence between random variables is not modeled because it is simply ignored, a strong bias towards methodological simplicity is preferred, there is high difficulty in characterizing the underlying dependence structure, or there is an expectation of low strength in random variable dependence. However these factors are not credible as many techniques exist to measure statistical correlation including the well-known Pearson correlation coefficient, Kendall's tau parameter, Spearman's correlation parameter, etc. Techniques also exist to easily include random variable dependence in probabilistic assessments, particularly in the context of

future aircraft technology impacts. Zaidi, Jimenez, and Mavris [Zaidi 2015] suggest a copula based method for better representing the relationships between random variables in probabilistic assessments using subjective input from subject matter experts.

Conrow [Conrow 2010b] described and evaluated an earlier subjective probability scales example from 1977 in which qualitative phrases were assigned quantitative probability values from 23 respondents. For example the phrase "probably not" was assigned a probability value of the event occurring ranging from approximately 0% to 45% from the different respondents and the phrase "highly likely" was assigned values for the event occurring from approximately 50% to 95%. Conrow provides a graphic in his paper from the original authors which summarizes their work which tested 16 different qualitative phrases and how the subjects interpreted their probability values. The assessment from the original authors has been used in the past in broad applications including defense and industry in order to convert phrases into useful statistics; however Conrow cites several issues with this type of work and specifically with this example. He points to misworded probability statements, incorrect probability bounds, and distortions in the graphical grid used to summarize the results by the original authors. Conrow states that because of these deficiencies, descriptive statistics gathered from this example are not reliable. As a result he conducted a new survey using the same 16 qualitative probability statements and gathers results from 141 participant engineers and project managers. In the results of his survey he finds problems with misinterpretation from participants and also numerous outliers in the quantitative values provided by the respondents. In light of these results he states from his own text [Conrow 2003] that "estimative probability tables and scales should be viewed as more of a "last resort" than first choice and not used in a risk analysis unless they are the only available means to evaluate probability". He explains this position because definitions for probability statements are not unique to different people, there is a high degree of uncertainty associated with most statements making the range of variability too high, people are often not familiar with the systems they are subjectively analyzing or how it performs, etc. He concludes his work by stating that probability scales based on subjective probability statements leave too much room for response error and in cases where such input is required he recommends using "precisely worded probability-related scales based upon maturity, resources, etc."

Ananthasayanam and Sarkar [Ananthasayanam 2005] point out that while today's engineering activities often require preciseness and performance even under uncertain conditions, it is the subjectivity of the user which helps to propel the engineering process through its numerous design stages until a solution is found. They believe this subjectivity of the user is useful and necessary to today's engineering problems and discuss its usefulness in estimation theory and two aerospace modeling applications. Again it is important to note that these authors are referring to the subjectivity provided from a user in a modeling process rather than the subjectivity involved in quantification tasks evaluated by Conrow [Conrow 2003] earlier. They describe the estimation theory process where choice of the appropriate algorithm to analyze the data in the presence of the expected noise and uncertainty is up to the analyst. The optimization algorithm itself contains a great deal of subjectivity including initial step size, starting points of the routine, update criteria, the convergence criteria and the overall guidance of the algorithm are all subjectively decided on by the user. The authors conclude by reiterating that the subjective decisions made by the user provide simplicity, mathematical and numerical traceability, and guides the analysis to a successful conclusion.

6.1.3.3 Probabilty Distribution Encoding

After recognizing the role of subjectivity in probabilistic assessments, one is better prepared to complete Timson's second step of obtaining subjective probabilities for subsystem properties. These probabilities are often obtained by encoding distributions in a variety of ways, including surveys, interviews, and engineering judgment. It can be said that the obtaining of subjective probabilities and the encoding of distributions is the most important step in Timson's outline and of any probabilistic assessment. The validity of the subjectively encoded distributions dramatically governs the integrity of the probabilistic assessment results. For this reason, significant attention has been given to examining many different works and key examples which demonstrate this critical step. This is to underscore the importance of correctly obtaining these subjective inputs and thereby lending credibility to the outcome of the probabilistic assessment.

All probabilistic assessments require the use of probability distributions, the question is how to obtain them. Ideally probability distributions would be based on analysis of real data using statistical tests to ensure good representation by a particular type of distribution. This process and the value of sampling from valid empirical distributions is described by Conrow [Conrow 2003]. However in many applications real world data is not available, or difficult to obtain, such as with future technology impacts. Since simply assuming normal distributions is not appropriate, then numerical analyses must have some way of encoding distributions. In these situations the literature turns to subject matter experts who provide various forms of information to subjectively inform probability distributions for random variables. This process of encoding distributions and prior examples of how subject matter experts have encoded parameters for different types of distributions is the focus of this section. Subjective probabilities can also be obtained by other means such as various forms of interviews and surveys which are discussed in this section as well.

Spetzler C. S., Stael von Holstein [Spetzler 1975] wrote a seminal paper on probability encoding summarizing the practice of the Decision Analysis Group at Stanford Research Institute. They state that Probability encoding is "the process of extracting and quantifying individual judgment about uncertain quantities" and is a major part of decision analysis. They discuss three main phases of this process, the Deterministic phase, the Probabilistic phase, and the Informal phase. The Deterministic phase establishes variable definitions and the formal model, the Probabilistic phase assigns probability distributions to relevant uncertainties, and the informal phase is a judgment process where the value of the information is assessed and compared to the cost of obtaining it in order to reduce uncertainty of important variables. The authors provide classifications of variable types such as decision variables which can be controlled by the decision maker and state variables which are outside of their control. They discuss how uncertainty of a variable can be encoded directly or the underlying phenomena can be modeled and the uncertainty of associated variables can be assessed. They provide principles for encoding uncertain quantities and how to best elicit information from subjects in order to enable subject cooperation and obtain meaningful data such as employing a sensitivity analysis to determine important uncertainties and using exact definitions and meaningful scales. They review the importance of Modes of Judgment which is the intuitive process by which people assess uncertainty using cues which are not completely reliable or valid, but still produce reasonable answers while yielding systematic biases. There are three main points to understand from this section of the paper, that people are not aware of the cues they use, it is difficult to control cues used by subjects, and people can be made aware of their biases and trained to

control them. The authors continue to discuss sources of bias such as motivational and cognitive biases and other encoding phenomena such as subject adjustment and anchoring. The authors also provide a discussion on encoding methodology and define the basic types including fixed value P-method, fixed probability V-method, or the neither fixed PV method, and how to encode each type such as using a probability wheel. They also provide a description of the interview process with the subject and explain the basic steps which should be taken including motivating, structuring, conditioning, encoding, and verifying. The authors have intentionally given general guidelines for probability encoding and state that each problem will have its own application of these principles. They believe their work is unique because of several distinguishing principles; they believe the pre-encoding steps are critical and more time consuming than the encoding step, they recommend only ordinal judgments for probability assignments, find the probability wheel as an effective encoding technique for most subjects (interestingly this does not agree with later work by Abbas et al [Abbas 2008] and Brooks and O'Leary [Brooks 1983]) , recommend more than one technique be used in order to check for consistency.

Keefer and Bodily [Keefer 1983] compare the accuracy of approximations representing continuous distributions or estimating their parameters, with emphasis on those requiring just three points from the underlying CDF for use in Program Evaluation and Review Technique (PERT) and related techniques. They make comparisons based on how well the mean and variance of different methods are approximated. They note large differences in accuracy among approximation methods including a set of beta distributions. They also consider the triangular distribution in which they state that it "generally provides an imperfect representation of the actual density function, but is simple and convenient to use. Its use is often based on the premise that very little information is available about the actual distribution anyway – e.g. only subjective estimates of "high," "low," and "most likely values." They examine the accuracy of four triangular-based formulas to approximate mean and variance, providing an indication of the appropriateness of the triangular distributions over and assortment of other distributions. They use an assortment of 78 beta distributions, investigating it thoroughly because of the many shapes it can take, using alpha less than beta shape parameters, where each can take integer values ranging from 2 to 60. While they find that the beta did not perform well in general it is worth noting that Johnson [Johnson 1997] was able to obtain good results using the beta distribution when limiting the shapes that that it can assume. Triangular distribution approximations were found to perform poorly as well, particularly with respect to other candidate methods. They recommend a new three-point approximation method which is an extension of Pearson and Turkey [Pearson 1965] noting that it is generally more accurate by a wide margin and has the advantage of being median based which is useful in consistency checking but does require percentage fractiles which may be difficult to determine.

Brooks and O'Leary [Brooks 1983] performed a comparison of encoding techniques and surveyed professionals whose focus was the evaluation of uncertainty. Their study compared four encoding methods; Bisection, Fractile, Cumulative, and Probability Wheel and surveyed participants who were brokers speculating in the stock market. The authors desired this procedure because they did not want to assume or rely on understanding of statistics from the judges while trying to accurately representing their opinions. In the Bisection method the subject specifies lowest and highest possible values and the analyst suggests values for comparison beginning with the limits. The Fractile is similar to the bisection but the subject provides the values directly and begins with the median value. In the Cumulative method the subject is asked to provide a probability of falling above or below specified values. The Probability Wheel

involves participating in a lottery where the participant wins if the value exceeds a specified threshold, or with a wheel with pointer falling in a wedge. The size of the wedge is varied until the participant is indifferent to the two choices. A Friedman Test [Coyover 1908] was used by the authors because the responses were rankings. The authors report that no statistical significance was found in the difference across accuracy rankings but there was among preference ranks. The Probability Wheel was found to be the least desirable, which tends to agree with the results found by Abbas et al [Abbas 2008] in the comparison of fixed probability versus fixed value encoding techniques. The authors also generated average distributions for each subject and used the Kolmogorov-Smirnov statistical test (similar to Conrow's work [Conrow 2010a]) to determine if there were any outlier distributions among the participants. The authors also noted that subjects often asked the analyst to repeat statements multiple times, revealing the importance of the analyst as a resource in eliciting the data.

Batson and Love [Batson 1988] discuss early techniques for including risk analysis in terms of uncertainty quantification of new technologies in aircraft conceptual design studies. The authors define technology assessment as "an unbiased, systematic approach to estimating technology benefit, development cost, and schedule and to establishing the uncertainty associated with those estimates". They state that classical approaches included defining a baseline and technology improved alternatives with various technology mixes to provide a measure of technology benefit. However cost and schedule estimates were deterministic and often limited to Gantt chart with dollar amounts associated with each activity. If uncertainty was done at all, it was unsophisticated, qualitative, and an afterthought. According to the authors, risk analysis is the "identification, quantification, reduction of the uncertainty in a system. Its philosophy holds that uncertainty about new technologies is best quantified by eliciting judgment from subject matter experts and synthesizing uncertainty through mathematical models to assess system-level impact. The authors used an analytical model called Airlift Fleet Cost-Effectiveness Uncertainty estimator (AFCUE) in their work, which is a set of equations that represents the sequence of calculations in the conceptual design process. It does not replace the actual process but rather provides a very simplified representation to capture only significant factors and sensitivities. They used subjective probability encoding in order to perform uncertainty quantification, and used a four-part questionnaire for which responses are used to establish a beta distribution. They used this to generate distributions for four design input variables in the calculation of range that could be associated with technology levels. For known payload levels they generated range distributions to create range uncertainty analysis, and a 99% confidence interval by connecting min and max points across the range distributions to form a tolerance band. The different technology demonstrators were ranked according to life cycle cost including uncertainty bands. The authors feel that their approach is innovative because they have extended a cost uncertainty analysis to include performance and effectiveness. It would be easier to interpret the value of this method if it could include a correlation to TRL or another modernly known technology maturation scale.

Williams [Williams 1992] offers a discussion on how to estimate the proper distribution parameters and which distributions to select when modeling project networks under uncertainty. He acknowledges there are many forms of uncertainty to consider including temporal, financial, technical, and their interactions but focuses on temporal uncertainty and specifically those related to activity-duration which is particularly relevant to technology modeling. He indicates that five parameters must implicitly or explicitly be stated to define an activity-duration distribution; position, spread, skew, minimum, and maximum. He places the most importance on

position because it is a usually a common parameter such as mean, mode, median or target value, which experts are familiar with. He does not advise obtaining this from other sources because to do so "is to lose your best source of estimates." The author states that several criteria should be kept in mind when estimating parameters. The parameters and assumptions must be easily understood by the estimator, such as mode and 'optimistic value' where as 'certainty of minimum' is less so. Parameters must be easily estimated because even if they are easily understood, difficult estimation can compromise the quality of estimates. Easily calculated percentiles are important because it helps to show the estimator the implications of choosing a certain parameter. Applicability of lower and upper limits to the distribution should be kept in mind and other particular considerations must be considered such as a priori assumptions, availability of historical data, etc. He also recommends the triangular distribution due to its simplicity but acknowledges the usefulness of the gamma and beta distribution while noting that they are not as transparent to the project planner. He concludes with some rules and recommendations including, "the parameters and distributions used must be meaningful to the project planner; thus the problems of selecting a distribution and estimating its parameters are psychological and practical rather than mathematical". This is a key point to understand and account for regarding the encoding of probability distributions in probabilistic assessments.

Johnson [Johnson 1997] investigated a method for using a triangular distributions as a substitute for beta distributions in risk analysis. He states that while the beta distribution is suitable for uncertainty studies because it can take a wide array of shapes over a finite interval, its functional form is complex and its parameters are harder to estimate. He proposes the triangular distribution as a suitable proxy for beta because triangular is much simpler in functional form and easier to understand. He states the differences between the two are rarely significant and proposes a method to estimate triangular distribution parameters from two extreme percentiles and a median. The author admits limitations of the triangular distribution in that it cannot reasonably approximate a U-shaped, J-shaped, or uniform distribution, which can be accomplished using a beta distribution. For this reason he limits his tries to focus on investigating beta distributions which are unimodal, positively skewed, and satisfy both shape parameters greater than or equal to one. He demonstrates that his method for estimating triangular distribution parameters using a linear combination of two extreme fractiles and the median actually produces very similar distributions as a beta whose shape parameters are both greater than or equal to two (bell shaped on both sides). He also states that when comparing the error of estimating mean and variance, his procedure performs better than or comparable to previous work such as that of Keefer and Bodily [Keefer 1983] It is worth noting that when comparing probabilistic distributions Conrow [Conrow 2010a] suggests examinations such as the Anderson-Darling and Kolmogorov-Smirnov statistical tests would yield greater certainty in estimation error and a proper measure of the difference between two distributions.

Ward [Ward 1998] presents a paper on the High Speed Research Program Technology Tracking and Assessment Process used to measure technology development progress and quantify technology uncertainties and propagate them at the technology level. It has two phases, an audit phase where subjective probability distributions (beta distributions) are constructed using expert opinion from the Technology Management Team (TMT), and a metrics integration phase where uncertainties in the vehicle level metrics are quantified by processing random samples of technology level metrics through an aircraft sizing code using the subjective probability distributions developed in technology audit phase. However, Ward points out that the process requires the assessment of inherently subjective probability distributions with a high

degree of fidelity, and since a significant part of the effort of the process are allocated to this task "the process has shown itself to be more useful in a tracking and risk assessment role than as a decision tool." This indicates that development of probability distributions is difficult and for the most part resource intensive. A sensitivity analysis is employed to show the effect of a technology metrics forecasted range on the vehicle metric's values however the sensitivity analysis does not account for interactions between technologies. This is critical to any technology portfolio analysis because some may not be useable while others are may/or may not be useable to their full potential. Ward notes that the probability distributions generated are "but one possible realization of an infinite number of distributions." He points out that non-parametric methods can be used to estimate confidence bands on the empirical CDF, and notes that the size of the confidence band is inversely proportional to *N,* the number of samples. Tracking technology and vehicle distributions illustrates a changing level of uncertainty and risk. He says that one can reasonably expect uncertainty to decrease as the program progresses as measured, for example, by TRL. The author concludes by stating that the process provides management with insight into technology development and helps point to where risk mitigation strategies will be of greatest value.

Kirby and Mavris [Kirby 1999] perform work on handling technology uncertainty in preliminary aircraft design stages due to incomplete knowledge regarding the impact of future technologies. While their methodology is very involved they did show how technology impact uncertainty can be captured using Weibull distributions. The Weibull distribution is chosen because it "is a family of distributions that can assume the properties of other distributions such as an exponential, normal, or Rayleigh." They subjectively encoded Weibull distributions for technologies at given TRL levels and adjusted the Weibull distribution shape parameters to follow a range of applicable values in the probabilistic assessment. The sensitivity of the response metrics to the Weibull shape parameters and the future technology impacts, was then evaluated via a Monte Carlo simulation.

Abbas et al [Abbas 2008] present the results of an experiment comparing two methods for encoding probability distributions of continuous variables; the first gets values of a variable through comparison with a fixed probability wheel and the second through comparisons with fixed values of the variable. Their decision analysis study was conducted using human participants as judges who were asked binary questions based on different decision analysis methods described above. The results of the experiment suggested a slight superiority of fixed value over fixed probability which the authors attribute to the fact that people in general having more experience in their daily lives with making judgments similar to Fixed Value types of decisions. They mention the difficulty with fixed probability comparisons is that it requires judges to estimate the level at which an event would reach a certain probability which is not as familiar as estimating the likelihood that an event will exceed some predetermined threshold. Results from the experiments were compared by fitting the results into Beta distributions; however the authors do not claim that Beta distributions are superior to others for this analysis, only that they have been used in prior Bayesian analyses. They conclude by stating that the results were nearly indistinguishable for the two encoding methods but there were systematic differences including the fixed variable method had higher variances which is good because the authors believe subjective probabilities are often too narrow reflecting overconfidence of the judges.

Hendricks et. al. [Hendricks 2009] discuss a systems engineering approach for strategic planning of the air transportation system in which technology infusion is also considered.

Technology-based solutions are essential to the entire system and their impacts must be assessed in an uncertain future context. The uncertainty they considered stemmed from the risk of the technology in terms the improvement it attempts to make in system performance and from the estimated completion date of a technology based on its maturity. The authors suggest using the beta distribution to model these uncertainties while concurrently employing a weighting scheme based on the TRL of each technology. By varying the beta parameter they are able to model the impact and uncertainty associated with a technology based on information available about the technology program.

Jimenez et. al. [Jimenez 2011] present a comparison of four different probabilistic assessments performed on the NASA Environmentally Responsible Aviation (ERA) problem for future aircraft technology section. Each assessment is performed using a different approach to subjectively encode technology impact distributions based on the information available from subject matter experts. The four main types of input distributions evaluated are the uniform distribution, the Weibull distribution, the mode-centered Weibull distribution, and the triangular distribution. Each probabilistic assessment approach reflects varying levels of information availability and encoding effort which ultimately drives the uncertainty in the response metrics in the output of the probabilistic assessments. The level of uncertainty on the main outputs, cumulative aircraft noise and fuel burn reduction, is depicted well with data clusters for the different distribution types and other varying assumptions in each probabilistic assessment. The authors conclude by stating that while general trends can be extracted about the ERA concepts and technologies from all four probabilistic assessments, they favor the mode-centered Weibull input distribution as having the best balance of data requirements and acceptability of underlying assumptions.

6.1.3.4 Probability Distribution Sampling

After establishing subjective probabilities and accurately representing random variables, the next step in Timson's method [Timson 1968] is to use a Monte Carlo simulation to sample from the probability distributions defined in the previous step. Monte Carlo simulations are indeed powerful tools used in a multitude of disciplines to quickly generate samples from probability distributions in a pseudorandom fashion. For readers interested in the theory behind random number generators and the methods with which they are created, see Park and Miller [Park 1988]. These samples are used to evaluate objective functions to generate statistics which provide useful information about the responses of interest. There are many different variations of Monte Carlo simulations including Markov chain Monte Carlo [Metropolis 1953], Direct simulation Monte Carlo [Bird 1994, Sun 2009], and others whose evolution has been discussed by Richey [Richey 2010]. They are found in a plethora of applications in the literature [Penzo 1963, Cunningham 1979, Igarashi 1994, Moss 2005] and specifically for technology modeling purposes [Rooney 2004, Hutchings 2008, Akram 2011]. Monte Carlo simulations are particularly useful in technology modeling applications because they help analysts to quantify the impacts of many different forms of technological uncertainties which are beyond their control, yet must be accounted for.

6.1.3.5 Other Sampling Techniques

There are also other ways to sample from probability distributions such as Gibb's sampling [Geman 1984], Rubin Importance-Sampling [Rubin 1987], Sobol's sequences, and

other techniques which are surveyed in detail by [Gelfand 1990]. Sobol's sequences for uncertainty modeling are particularly useful in sampling and random number generation due to the distribution of the resulting sequences. The basic theory attempts to create an efficient and quick summation of a function to approximate the integral of the function [Sobol 1976]. It can be used to form quasi-random uniform partitions in a given interval. Quasi-random partitioning results in less randomly scattered points than traditional Monte Carlo methods such that there is more uniform dispersement of the samples. This is because quasi-random sampling generates a set of points that are "maximally self-avoiding" [Sambridge 2002]. Sambridge and Mosegaard [Sambridge 2002] also provide a helpful graphical depiction of the difference between pseudorandom and quasi-random sequences. The technique has been applied in sampling for design optimization [Mehmani 2012] and improving the development of continuous response surfaces [Paul-Dubois-Taine 2013].

6.1.3.6 Design for Robustness

The final steps in Timson's method [Timson 1968] calls for the development of statistical measures for resulting systems performance distributions and the comparison of those statistical measures across time periods for an indication of progress. These steps instruct how to handle the output data once the Monte Carlo simulation has been run and resulting probability distributions are obtained. Many different statistical measures exist which are commonly known including mean, variance, and higher order moments of distributions. These can be used to assess progress for any set of inputs that may be changing over time.

The conventional robust design methodology seeks to find settings of design variables which minimizes the response variation to noise variables which cannot be controlled [Phadke 1995]. When this philosophy is applied to probabilistic assessments, it seeks to answer a specific question of how to reduce the variability in the output subject to the uncertain input distributions. This has particular relevance to technology modeling because as technologies mature more information about their impacts becomes available. This information would naturally change the input distributions, and in principle reduce their variance and increase their mean about the expected value. Over time these changes in input distributions would have a corresponding change on the response distributions where variance decreases and mean is centered closer to target values.

Design of robustness with respect to technology modeling can also be conducted with a focus on specific responses such as direct operating cost or return on investment. Technologies can be infused in designs to make a particular concepts more insensitive to noise variables in a probabilistic assessment, such as fuel price. DeLaurentis [DeLaurentis 2000] applied a form of stochastic optimization in order to account for uncertainties in conceptual aircraft design and to identify a robust design in the face of those uncertainties. His methodology is formulated to handle uncertainties with mathematical models, operational environments, response measurement, and input requirements. It divides parameters into design variables and uncertain variables, and requires the user to assign pdf distributions to the uncertain variables based on historical data or expert opinion. Through a combined design of experiments a cdf of the response values is created by sampling the pdf distributions in each case repeatedly. The cdf is then discretized into n points, where n is the desired number of probability levels for each objective, and the discretized points of the cdf are used to generate the response surfaces which provide a functional relationship between the design variables and the cdf. He suggests not using fewer than 5 points when discretizing a cdf in order to regress it and form an appropriately

accurate representation of the cdf. This type of approach implies a relatively fast execution time is needed, at least in the preliminary run of the design of experiments which may be computationally expensive depending on the number of variables required. The methodology is applied to the design of a supersonic transport and an optimization procedure is executed where the probability of a specific economic response ($/RPM) is maximized as a function of design variables and uncertain variables, being less than a particular threshold value.

6.1.3.7 Stochastic Optimization

Stochastic optimization encompasses a general class of optimization models characterized by the generation and implementation of random variables. There are two general types of such models. One pertains to optimization algorithms where the search of preferred solutions is governed by stochastic processes. Genetic algorithms, simulated annealing, and ant colony optimization are some of the most well-known and are well documented in optimization textbooks [Vanderplaats 2001, Rao, 2009, Onwubolu 2004]. These optimization techniques are well suited for discrete objective topologies or highly nonlinear multi-modal objective functions where numerous local optima are reasonably expected. It is worth noting that, whereas these search algorithms are themselves stochastic, the objective functions upon which they are typically applied are deterministic and invariant. Optimization techniques tailored to stochastic objective functions comprise the other type of stochastic models, and are the set with which we are specifically concerned here.

Recall that Timson's method [Timson 1968] calls for the development of statistical measures for resulting systems performance distributions and the comparison of those statistical measures across time periods for an indication of progress. As this approach only provides a basic outline, it can be reasonably asked how else progress in statistical measures can be tracked besides over time periods. One such manner would be with iterative optimization problems where input distribution settings are improved with each evaluation. Stochastic optimization problems with stochastic objective functions can demonstrate improvement in statistical performance measures with each iteration.

Sues et al [Sues 1996] presented a unique stochastic optimization methodology for aeropropulsion components and demonstrated it on the design of an axial compressor. Their methodology involves three basic parts including response surface development for the objective function and each constraint, stochastic optimization using the response surfaces, and refinement of the response surface. The refinement of the response surface is about the optimum point for the objective function and about the Most Probable Point for the failure constraints. The authors state they do not discuss the FORM approach, however the handling of failure constraints using FORM and Most Probable Point method is discussed in an earlier section of this survey. They incorporate 3 types of variables in their methodology; deterministic design variables, random design variables and simple random variables whose mean values do not change during optimization. From an optimization perspective these simple random variables with fixed mean values are used to perform deterministic optimization. The methodology differentiates between single occurrence random variables (occur once during the component lifecycle) and operational random variables (vary periodically throughout the lifecycle) and use a two level Monte Carlo simulation to handle each type. The optimization scheme models single occurrence random variables in the upper level ensuring the reliability constraints are met, and models operational random variables in the lower level which maximize the expected value of the objective function during normal operating conditions. The authors claim that their methodology is different from

previous work because their objective function is performance based, that being to minimize cost of the compressor blades which is a function of the weight and efficiency of the design. It incorporates a statistical expectation for the efficiency of the design which is a function of two twist parameters in the blade design and a blade thickness variable which were assigned lognormal distributions to account for uncertainties in manufacturing. A number of other parameters including material modulus, yield strength, and rotor speeds were also incorporated as simple random variables with fixed mean values. The authors compared the results of their baseline case, the deterministic optimization, the stochastic optimization, and deterministic optimization with safety factors and concluded that the stochastic optimization yielded the best results because the stress and deflection constraints were reliability based ensuring a moderate overall cost but good performance under extreme rotor speed conditions. They admit that the safety factors in the fourth case were chosen arbitrarily resulting in a conservative solution, but are confident that the third case using stochastic optimization handles constraints well. The constraints are reliability based and formulated as very high probabilities which ensure that the actual stress does not rise above the max stress for each analysis case, yielding a design with good balance between performance and reliability.

6.1.3.8 Technology Modeling

This section reviews a number of different aerospace technology applications which borrow from various probabilistic methods discussed above. These works apply different forms of probabilistic methods to handle future technologies in a non-deterministic fashion. These applications are not presented in a particular order but are each found to be noteworthy uses of probabilistic methods in the context of future aircraft technologies.

In order to design aircraft for the future which are competitive and capable, engineers must consider the impact of developing technologies which will eventually become part of the final design. The literature contains textual references for how to conduct these technology modeling exercises including Porter et. al. [Porter 1980] and Twiss [Twiss 1992]. Since these maturing technologies are beyond the control of most conceptual designers, uncertainty and its impact on the final design must be considered. Probabilistic assessment techniques and the methods described earlier in this section provide the tools to accurately judge these uncertain technology impacts and evaluate how they can be integrated into future aircraft.

There are many considerations to make when forecasting the effect of a technology on a future aircraft including its holistic impacts, what benefits and degradations are involved with it, how it will interact with other technologies under consideration, the timeframe it is likely to mature in, its maintainability, associated costs, etc. Obviously not all of these questions can be immediately answered for complex systems like future aircraft, but the literature contains notable works which have addressed some of them.

Kirby [Kirby 2001] proposes the Technology Identification, Evaluation, and Selection methodology which contains many useful techniques for technology modeling. This methodology formalizes a normative and explorative approach to design space exploration of the vehicle and technology space. It incorporates two key techniques for evaluating a portfolio of technologies and making selections between them including the Technology Impact Matrix (TIM) and the Technology Compatibility Matrix (TCM). The TIM contains the predicted impact values of each technology if they were matured to full-scale application (TRL = 9). The TCM allows a designer to quickly remove technology combinations which are “not physically realizable” from consideration. In this methodology Weibull distributions were used to

probabilistically represent the uncertainty associated with a technological impact given its current TRL level. The TIM and TCM can be used to create many different future technology vehicles with varying levels of technological uncertainty, which can be probabilistically evaluated to determine the best suite of technologies for a particular set of requirements.

Landry and Archer [Landry 2014] present a high-level state model of the national airspace system (NAS) which can account for uncertainty within the NAS due to incorporation of various technologies and concepts. The authors perform a rigorous mapping of technologies to sources of uncertainty. They utilize multiple probability distributions including Erlang, Gamma, and Bernoulli distributions to model the source of uncertainty with each technology. They indicate the nominal distribution type and parameters for probabilistically modeling the technological uncertainty, noting the sources of uncertainty and the expected effects. They use various settings of the input distributions to reflect different assumptions and run simulations to evaluate the effects of changing these inputs. They hope to identify emergent effects and provide guidance for prioritizing the development and integration of specific technologies into the NAS.

Mavris and Bandte [Mavris 1995] point to a need for a method to identify and assess key technologies while ensuring feasibility and viability, considering all disciplines and lifecycle phases as advocated by advanced product design philosophies. Technology risk assessments are also needed to avoid optimistic or pessimistic biases. They propose a methodology that accounts for benefits and risks of technologies replacing point design solutions for ones featuring variability. The core of the proposed method is a Robust Design approach that uses RSM as an enabling technique. RSM is used to conduct analysis of variance in a screening test to pick most significant contributors to performance and economic metrics, and to conduct Monte Carlo simulations on probabilistic variables. All economic noise variables identified were given triangular distributions based on historical data which was used to determine ranges and mode, with the exception of an engine technology complexity factor that was uniformly varied. Economic target value is compared against statistics of the resulting distribution. They found that the baseline is not good enough to meet targets so technology infusion is used to achieve the required weight reduction. These technology improvements are selected by the designer and have significant impact on the feasibility of the design.

Weisbin et. al. [Weisbin 2004] propose a methodology for technology selection for new initiatives which can support selection and decision making of R&D tasks. Their methodology is demonstrated on Mars exploration rover projects. Technology options are addressed in the methodology by capturing uncertainties in the capabilities using probability distributions on performance attributes. The authors developed a technology costing procedure which includes uncertainty and an interview based peer review of the technology cost estimate. Their selection process is based on evaluations of risk, cost, and performance. Projects are selected in this trade space assuming a given total budget. Their selection process also identifies the main drivers of the result and is flexible enough to adapt many other applications.

Suh et. al. [Suh 2009] propose a methodology for estimating the impact of technology infusion in complex systems including changes to the original system, cost of technology infusion, potential market impact, and an estimation of net present value of the infused technology. Their approach focuses on the creation of Design structure Matrix (DSM) [Eppinger 1994] which is a matrix representation of the original product that includes the product components and the connections between them. Their 10 step methodology is applied to a complex printing system modeled by an 84 element DSM. A delta DSM is created describing the changes between the original and technology infused product. Value and cost of the existing

product is calculated by attribute based theories and then the value of the technology infused product is found. Uncertainty in demand and cost is incorporated using probability distributions on annual demand and machine population cost savings to determine the change in net present value of the technology infused system by Monte Carlo simulation. Their work also includes a notable literature survey and gap analysis for technology infusion problems.

Mavris et al [Mavris 1997] present a probabilistic approach that extends traditional design methods to account for disciplinary, economic, and technological uncertainty. The probabilistic approach is facilitated by Fast Probability Integration (FPI). They use FPI to determine the cumulative probability distributions of the design space, bounded by economic objectives and performance constraints. The impact of technology readiness and associated risks was also studied but not presented in this work. They placed ranges on geometric and mission design parameters to expand the original point design to a design space which is explored in two steps; first identify feasible designs and then find economically viable designs to determine the most robust solutions which exist in the design space. The authors used FLOPS and ALCCA as part of six step methodology to assess the technical feasibility and economic viability of future aircraft concepts including design space exploration and technology infusion. They also used "k" factors to perform technology infusion which actually modify technical metrics like SFC or L/D in order to simulate the discontinuity in benefits or penalties associated with a new technology. They conclude by stating the importance of including economic uncertainty in design because 80% of the design space in the conventional configuration was economically viable, which is a flawed result because uncertainty exists in economic parameters and not considering them leads to false viability.

6.2 Overview of Methodology

The approach here undertaken to conduct the probabilistic analysis follows the fundamental numerical approach for non-deterministic assessment [Timson 1968] as described above in Section 6.1.1. This approach is summarized in five basic steps:

1. Determine design equations relating properties at lower levels to measures of system level performance
2. Obtain subjective probabilities for subsystem properties
3. Use Monte Carlo to sample from these probabilities
4. Generate statistical measures for resulting systems performance distribution
5. Compare statistical measures across time periods for an indication of progress

For this application the design equations in step 1 relate technology impact factors (k-factors) to vehicle level environmental measures of performance. The underlying modeling and simulation capability is the EDS, described in Section 3.1. Significant runtime reductions are required for the implementation of the probabilistic analysis, as well as the multi-objective optimization analysis discussed later in Section 7.2. Accordingly, surrogate models were generated for a variety of intermediate vehicle environmental metrics as a function of technology impact factors and select design variables, as described in detail in Section 5.0 Surrogate Model Generation, and as reported in Appendix A: EDS Surrogates Response Names, Descriptions, and Units and Appendix B: EDS Vehicle Surrogate Fit Statistics.

The development of surrogate models requires that a training data set be first procured, in this case as a space-filling design of experiments. All experimental designs, including space-filling designs, require that the bounding minimum and maximum values of all model inputs,

namely model regression variables, be established a-priori. The identification of such value bounds is in itself predicated on the probability distributions defined for model inputs according subjective encoding in step 2 of the numerical approach method here adopted. Accordingly, the order of Step 1 and Step 2 were reversed in this effort, first conducting subjective encoding for all technology impacts across all technologies, and then leveraging on resulting distributions to determine minimum and maximum values for all technology impacts.

Subjective encoding was conducted with the elicitation of a minimum, most likely, and maximum values, found from previous experience and anecdotal evidence to be very intuitive for technologists, subject matter experts, and researchers involved in this effort. In the case of the latter, three-point estimates offered leveraged on an extensive and thorough review of published literature on each technology that is documented in the Technology Report - Jeff discussed in Section 4.5. Whenever multiple inputs were procured for a given technology impact estimate harmonization of values was attained with discussions and consensus-building activities. The minimum, most likely, and maximum impact values for each technology impact were used to define a triangular distribution on the basis of the minimum, mode, and maximum values respectively. Because it is possible for different technologies to contribute to the same technology impact factor it is necessary to consider how said impact contributions are aggregated to then establish the minimum and maximum values of the resulting aggregate. Technology combinations are governed by the Technology Compatibility Matrix (Section 4.2), and the specific aggregation rules for different technology impact factors are described in detail in Section 4.3.1.2. Aggregate minimum and maximum values for all technology impact factors are thus determined by exhaustively considering limiting technology combinations. This process is presented in detail in Section 4.3.2.

The development of surrogate models and encoding of probability distributions for the probabilistic technology impact matrix are fundamental components of the implementation of the remainder of the probabilistic analysis. The sampling of inputs pursuant of distributions, evaluation of the surrogates, and analysis of the resulting sample of environmental metrics, are all integrated in a software implementation of the method.

An initial implementation was conducted in MATLAB where native functions and capabilities are leveraged for efficient random variable sampling, array passing and array evaluation of embedded surrogate model functions, and statistical analysis and visualization of results. This implementation was developed for four fixed technology combinations, namely an ERA core technology set, and Best Fuel Burn, Best Noise, and Best NOX technology combinations identified from the ERA core technology set plus additional technologies fitting the N+2 maturation goals. This work is reported in [Jimenez 2011]. Technology assumptions and modeling, vehicle modeling, and technology combinations of interested have since been updated significantly, although the underlying methodology and implementation remain relevant for the probabilistic technology assessment domain.

6.3 Implementation of Flexible and Extensible Probabilisitic Analysis and Representative Results

While computationally efficient, a shortcoming of the above mentioned effort is that only four technology combinations were identified for analysis, and the implementation of the method did not feature extensibility to any allowable technology combination in the full combinatorial set. In response to the desire for flexibility and extensibility a second implementation was

developed in the statistical discovery and visualization software JMP. This implementation leverages on native JMP capabilities for efficient probabilistic sampling, surrogate model evaluation, and visualization and analysis of resulting samples, while facilitating the design of an interactive dashboard for analysis and results presentation. In this second implementation it is possible to select any subset of technologies as applied to any of the technology collectors, and having resolved potential technology incompatibility conflicts, readily obtain a combined sample of vehicle-level environmental metrics of interest for which descriptive statistics are automatically displayed. The probabilistic analysis interface is shown in Figure 80 where circular callouts have been placed with numbered referencing to indicate the different features of the dashboard explained next.

(1) Technology Collectors – In the leftmost area of the dashboard the different technology collectors are displayed in a vertical array, each presented with a 3-D isometric view generated in VSP. The vehicle selected by the user is highlighted whereas all other options are shown in faded greyscale.
(2) Technologies – To the right of the technology collectors is an array of rectangular objects, or buttons, each corresponding to a technology of the ERA portfolio under consideration. Technologies are color coded: reference technology collector technologies – light blue; engine fuel reduction – dark blue; engine noise – green; airframe aerodynamic – tan; airframe noise – orange; airframe weight and subsystems – red; engine emissions – grey blue. The user can select/deselect any technology by clicking on the corresponding button. The dashboard checks for possible incompatibilities between technologies, and for the applicability of technologies onto technology collectors, and displays the buttons of viable technologies accordingly.
(3) Technology Combinations Display and Controls – To the right of the array of technology buttons, on the top region, is the display of technology combinations in the ERA metric space, also referred to as the objective space in the context of multi-objective optimization analysis addressed in Section 7.2. The technology combinations displayed include the set of Pareto optimal solutions, namely those comprising the edge of the tradeoff in the objective space (see Section 7.2), and a subset of non-optimal solutions obtained by progressively removing technologies from Pareto optimal solutions. The buttons above the display control the display type, which includes options such as 2D or 3D, inclusion of only Pareto optimal solutions or additional solutions, color-coding of solutions, and scaling of the axes and display within the axes. The buttons immediately above and to the left of the display allow the user to select the ERA metrics to be used for each of the axes of the data plot. ERA goal values for the corresponding metrics are shown as green dotted lines. The user can select a technology combination by clicking on any of the solutions displayed which is immediately reflected by updating the technology selections in the array to the left. Conversely, technology combinations based on the selections to the left are shown on the technology combinations display.
(4) Vehicle 3D Geometric Wire Model – Below the technology combinations display is a 3D geometric wire model of the vehicle where the wing, engines, and tail surfaces optimally resized as a result of the inclusion of technology is shown in red and over

the original geometry. Controls to the right allow for toggling of views of the 3D model.

(5) Probabilistic Analysis Controls – The right portion of the dashboard pertains to the controls and displays for probabilistic analysis. At the top of this region of the dashboard is the button to execute the probabilistic analysis for the selected technology collector and combination of technologies. Here the user can select the sample size, i.e. the number of simulations, set by default to 500. There is also an option for the user to review and edit the probabilistic distributions for the technology impacts which are the inputs of the surrogate models that will be evaluated with the sample of inputs to yield a sample of ERA metrics outputs.

(6) Selected Technologies and Vehicle – This small portion of the display clearly indicates the technology collector and the list of technologies selected.

(7) Technology Impact Factor Statistics – This display lists all technology impact factors that will be used in the probabilistic analysis given the technologies selected. The minimum, mean, and maximum value of the probabilistic distribution of each technology impact factor is shown along with the factor units.

(8) Histograms for Technology Impact Factor Samples – When the probabilistic analysis is run samples for all technology impact factors, inputs to the surrogate models for ERA metrics, are generated. Histograms of the samples are automatically displayed along with quantiles and other statistical features.

(9) Probabilistic Sample of ERA Metrics – When evaluated with the sample inputs, the surrogate models yield a sample of ERA metric values. These are displayed in either a 2D format (where the two metrics can be selected), or in a 3D scatterplot. For the 2D display quantile density contours are generated with a kernel density estimator and displayed with color coding to easily indicate the regions of greater or lesser sample density, and thus of greater or lesser probability. Similarly cumulative probability ellipsoids can be displayed for the 3D display.

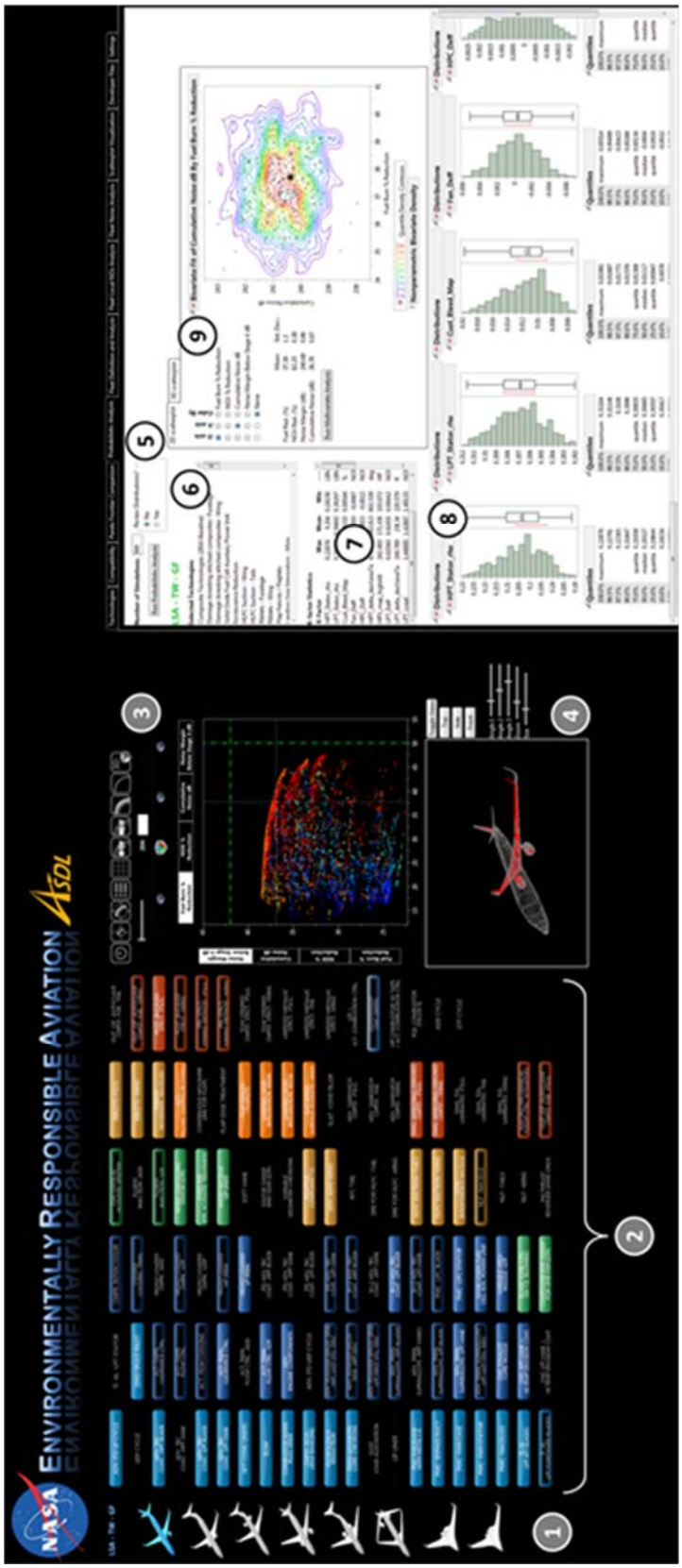

Figure 80. Probabilistic analysis interface dashboard in ERA systems analysis calculator

7.0 Results

7.1 RTC/ITD Data

Table 57. RJ Tube and Wing Geometry

Description	EDS Base	RTC – ADD	RTC - GF	ITD - GF
Fuselage Length, ft	109.90	109.90	109.90	109.90
Fuselage Diameter, ft	8.83	8.83	8.83	8.83
Wing Area, sq ft	752.5	666.4	658.4	674.9
Wing Aspect Ratio	8.29	10.00	10.00	11.00
Wing Sweep, deg	26.99	26.99	26.99	26.99
Horizontal Tail Area, sq ft	173.13	131.35	129.01	127.65
Horizontal Tail Aspect Ratio	4.59	4.59	4.59	4.59
Horizontal Tail Sweep, deg	29.49	29.49	29.49	29.49
Vertical Tail Area, sq ft	103.07	103.06	103.06	88.63
Vertical Tail Aspect Ratio	1.11	1.11	1.11	1.11
Vertical Tail Sweep, deg	43.15	43.15	43.15	43.15
Nacelle Diameter, in	61.10	65.30	68.70	61.90
Engine Nacelle Length, ft	7.33	6.99	7.27	6.54
Main Gear Length, in	47.23	47.23	47.23	47.23
Nose Gear Length, in	46.88	46.88	46.88	46.88

Table 58. RJ Tube and Wing Vehicle Characteristics

Description	EDS Base	RTC – ADD	RTC - GF	ITD – GF
TOGW, lbs	85,000	75,272	74,374	68,611
Operating Empty Weight, lbs	47,250	43,144	42,704	39,360
Fuel Weight, lbs	19,690	14,068	13,610	11,190
Design Payload, lbs	18,060	18,060	18,060	18,060
Block Fuel, lbs	15,579	11,113	10,834	8,984
Design Range, nmi	1,980	1,980	1,980	1,980
Wing Area, sq ft	752.5	666.4	658.4	674.9
Aspect Ratio	8.29	10.00	10.00	11.00
Cruise L/D	16.10	17.14	16.95	19.32
Approach Speed, kts	126.7	129.8	130.0	124.7
T/W	0.338	0.338	0.338	0.338
W/S, psf	113.0	113.0	113.0	101.7
CB/AP/SL Noise, EPNdB	85.6/93.6/98.2	75.9/88.7/86.7	72.7/86.5/83.4	70.2/82.9/81.0
Cumulative Noise, EPNdB	277.5	251.3	242.6	234.0

Table 59. RJ Tube and Wing Propulsion System Characteristics

Description	EDS Base	RTC – ADD	RTC - GF	ITD - GF
SLS Thrust, lbs	15,118	12,708	12,544	11,597
SLS Airflow, pps	452.1	486.8	577.3	586.3
Takeoff Thrust (M0.25/0K, Hot), lbs	12,923	10,863	10,723	9,913
Cruise TSFC, lb/lbf·hr	0.659	0.539	0.530	0.485
Total Engine Weight, lbs	4,207.0	3,334.4	3,190.8	2,415.8
Engine Nacelle Length, ft	7.33	6.99	7.27	6.54
Fan / Nacelle Diameter, in	50.0/61.1	51.4/65.3	54.9/68.7	54.9/61.9
FPRD / HPCPRD / OPRD (M0.80/35K)	1.63/17.0/27.5	1.55/22.0/46.7	1.45/16.0/45.6	1.35/17.5/50.3
BPRD (M0.80/35K)	5.09	10.96	13.87	18.39
OPR SLS Uninstalled	23.08	37.39	32.01	36.14
T4max (M0.25/0K) deg R	3,170	3,550	3,550	3,550
Fan Tip Mach No.	1.59	1.26	1.16	1.08
LPC / HPC / HPT / LPT Stages	0/10/2/4	4/10/2/7	3/8/2/3	3/7/2/3

Table 60. SSA Tube and Wing Geometry

Description	EDS Base	RTC – ADD	RTC - GF	RTC - OR	ITD - GF
Fuselage Length, ft	105.6	105.6	105.6	105.6	105.6
Fuselage Diameter, ft	12.75	12.75	12.75	12.75	12.75
Wing Area, sq ft	1,409	1,285	1,271	1,298	1,260
Wing Aspect Ratio	9.74	10.0	10.0	11.0	11.0
Wing Sweep, deg	25.72	25.72	25.72	25.72	25.72
Horizontal Tail Area, sq ft	359.3	309.0	303.8	298.9	285.9
Horizontal Tail Aspect Ratio	6.27	6.27	6.27	6.27	6.27
Horizontal Tail Sweep, deg	29.91	29.91	29.91	29.91	29.91
Vertical Tail Area, sq ft	277.8	245.3	241.2	277.9	214.7
Vertical Tail Aspect Ratio	1.92	1.92	1.92	1.92	1.92
Vertical Tail Sweep, deg	35.0	35.0	35.0	35.0	35.0
Nacelle Diameter, in	82.6	89.1	92.4	NA	84.6
Engine Nacelle Length, ft	9.33	9.39	9.43	7.66	8.63
Main Gear Length, in	71.4	77.9	81.2	71.4	73.4
Nose Gear Length, in	44.6	49.1	51.4	44.2	46.0

Table 61. SSA Tube and Wing Vehicle Characteristics

Description	EDS Base	RTC – ADD	RTC - GF	RTC - OR	ITD - GF
TOGW, lbs	155,000	141,395	139,816	128,474	124,722
Operating Empty Weight, lbs	83,000	77,289	76,718	76,142	70,070
Fuel Weight, lbs	45,120	37,225	36,217	25,452	27,772
Design Payload, lbs	26,880	26,880	26,880	26,880	26,880
Block Fuel, lbs	37,415	30,940	30,229	20,906	23,126
Design Range, nmi	3,330	3,330	3,330	3,330	3,330
Wing Area, sq ft	1,409	1,285	1,271	1,298	1,260
Aspect Ratio	9.74	10.0	10.0	11.0	11.0
Cruise L/D	19.57	19.13	19.04	21.92	21.81
Approach Speed, kts	130.0	132.3	132.5	130.1	128.7
T/W	0.335	0.335	0.335	0.342	0.335
W/S, psf	110.0	110.0	110.0	99.0	99.0
CB/AP/SL Noise, EPNdB	85.9/93.8/97.0	80.5/89.1/87.6	78.8/88.6/84.6	79.1/91.4/84.9	75.2/84.9/81.0
Cumulative Noise, EPNdB	276.6	257.2	252.0	255.4	241.1

Table 62. SSA Tube and Wing Propulsion System Characteristics

Description	EDS Base	RTC – ADD	RTC - GF	RTC - OR	ITD - GF
SLS Thrust, lbs	27,300	24,934	24,655	23,164	21,979
SLS Airflow, pps	795.7	916.0	1,066.3	61.38	1,096.7
Takeoff Thrust (M0.25/0K, Hot), lbs	22,783	20,809	20,576	21,529	18,343
Cruise TSFC, lb/lbf·hr	0.615	0.535	0.527	0.420	0.484
Total Engine Weight, lbs	5,897.2	5,496.1	5,316.3	1,677.5	4,033.1
Engine Nacelle Length, ft	9.33	9.40	9.43	7.66	8.63
Fan / Nacelle Diameter, in	62.6/82.6	69.1/89.1	72.4/92.4	130.7/NA	74.6/84.6
FPRD / HPCPRD / OPRD (M0.80/35K)	1.69/9.37/30.1	1.55/22.0/46.7	1.45/16.0/45.6	NA/3.35/54.4	1.35/17.5/50.3
BPRD (M0.80/35K)	5.11	10.09	12.29	NA	18.93
OPR SLS Uninstalled	28.6	40.9	36.7	53.4	36.8
T4max (M0.25/0K) deg R	3,300	3,550	3,550	3,550	3,550
Fan Tip Mach No.	1.40	1.27	1.16	NA	1.08
LPC / HPC / HPT / LPT Stages	4/9/1/4	4/10/2/7	2/8/2/3	6/5/1/1	3/7/2/3

Table 63. LSA Tube and Wing Geometry

Description	EDS Base	RTC – ADD	RTC - GF	RTC - OR	ITD - GF
Fuselage Length, ft	124.75	124.75	124.75	124.75	124.75
Fuselage Diameter, ft	12.75	12.75	12.75	12.75	12.75
Wing Area, sq ft	1,408.5	1,299.0	1,286.0	1,340.7	1,294.3
Wing Aspect Ratio	9.74	10.0	10.0	11.0	11.0
Wing Sweep, deg	25.72	25.72	25.72	25.72	25.72
Horizontal Tail Area, sq ft	359.20	314.00	309.29	313.92	297.78
Horizontal Tail Aspect Ratio	6.27	6.27	6.27	6.27	6.27
Horizontal Tail Sweep, deg	29.91	29.91	29.91	29.91	29.91
Vertical Tail Area, sq ft	277.75	249.25	245.51	277.85	223.61
Vertical Tail Aspect Ratio	1.92	1.92	1.92	1.92	1.92
Vertical Tail Sweep, deg	35.00	35.00	35.00	35.00	35.00
Nacelle Diameter, in	82.6	89.3	92.7	NA	85.3
Engine Nacelle Length, ft	9.33	9.44	9.47	7.96	8.71
Main Gear Length, in	71.38	78.08	81.48	71.38	74.08
Nose Gear Length, in	44.56	49.25	51.63	44.24	46.45

Table 64. LSA Tube and Wing Vehicle Characteristics

Description	EDS Base	RTC – ADD	RTC - GF	RTC - OR	ITD - GF
TOGW, lbs	174,857	161,265	159,649	149,757	144,579
Operating Empty Weight, lbs	91,289	85,619	85,022	85,519	78,280
Fuel Weight, lbs	46,398	38,476	37,457	27,068	29,129
Design Payload, lbs	37,170	37,170	37,170	37,170	37,170
Block Fuel, lbs	38,161	31,697	30,991	21,974	24,074
Design Range, nmi	2,960	2,960	2,960	2,960	2,960
Wing Area, sq ft	1,408.5	1,299.0	1,286.0	1,340.7	1,294.3
Aspect Ratio	9.74	10.00	10.00	11.00	11.00
Cruise L/D	19.15	19.02	18.90	21.56	21.48
Approach Speed, kts	140.3	142.4	142.7	139.3	137.9
T/W	0.312	0.312	0.312	0.342	0.312
W/S, psf	124.15	124.15	124.15	111.70	111.70
CB/AP/SL Noise, EPNdB	88.3/95.0/98.7	81.5/90.3/88.8	79.2/89.8/87.0	79.3/92.3/88.2	76.1/86.0/82.8
Cumulative Noise, EPNdB	281.98	260.59	255.99	259.9	244.86

Table 65. LSA Tube and Wing Propulsion System Characteristics

Description	EDS Base	RTC – ADD	RTC - GF	RTC - OR	ITD - GF
SLS Thrust, lbs	27,300	25,137	24,869	25,665	22,418
SLS Airflow, pps	795.7	923.1	1,075.6	67.54	1,118.7
Takeoff Thrust (M0.25/0K, Hot), lbs	22,783	20,977	20,753	23,854	18,707
Cruise TSFC, lb/lbf·hr	0.615	0.536	0.527	0.420	0.483
Total Engine Weight, lbs	5,897.1	5,568.5	5,364.2	1,881.4	4,109.0
Engine Nacelle Length, ft	9.33	9.44	9.47	7.96	8.71
Fan / Nacelle Diameter, in	62.6/82.6	69.3/89.3	72.7/92.7	137.6/NA	75.3/85.3
FPRD / HPCPRD / OPRD (M0.80/35K)	1.69/9.37/30.1	1.55/22.0/46.7	1.45/16.0/45.6	NA/3.33/54.4	1.35/17.5/50.3
BPRD (M0.80/35K)	5.11	10.03	12.32	NA	18.99
OPR SLS Uninstalled	28.61	40.94	36.66	53.30	36.74
T4max (M0.25/0K) deg R	3,300	3,550	3,550	3,550	3,550
Fan Tip Mach No.	1.40	1.26	1.16	NA	1.08
LPC / HPC / HPT / LPT Stages	4/9/1/4	4/10/2/7	2/8/2/3	6/5/1/1	3/7/2/3

Table 66. LSA Over-the-Wing Nacelle Geometry

Description	RTC – ADD	RTC – GF	ITD - GF
Fuselage Length, ft	124.75	124.75	124.75
Fuselage Diameter, ft	12.75	12.75	12.75
Wing Area, sq ft	1,311.0	1,296.7	1,286.9
Wing Aspect Ratio	10.00	10.00	11.00
Wing Sweep, deg	25.72	25.72	25.72
Horizontal Tail Area, sq ft	318.37	313.18	295.22
Horizontal Tail Aspect Ratio	6.27	6.27	6.27
Horizontal Tail Sweep, deg	29.91	29.91	29.91
Vertical Tail Area, sq ft	279.85	279.85	240.67
Vertical Tail Aspect Ratio	1.92	1.92	1.92
Vertical Tail Sweep, deg	35.0	35.0	35.0
Nacelle Diameter, in	89.7	93.0	85.1
Engine Nacelle Length, ft	9.48	9.51	8.68
Main Gear Length, in	71.38	71.38	71.38
Nose Gear Length, in	44.24	44.24	44.24

Table 67. LSA Over-the-Wing Vehicle Characteristics

Description	RTC – ADD	RTC – GF	ITD - GF
TOGW, lbs	162,758	160,984	143,749
Operating Empty Weight, lbs	85,779	85,027	78,055
Fuel Weight, lbs	39,810	38,787	28,524
Design Payload, lbs	37,170	37,170	37,170
Block Fuel, lbs	32,846	32,138	23,567
Design Range, nmi	2,960	2,960	2,960
Wing Area, sq ft	1,311.0	1,296.7	1,286.9
Aspect Ratio	10.00	10.00	11.00
Cruise L/D	18.71	18.59	21.11
Approach Speed, kts	142.0	142.2	138.2
T/W	0.312	0.312	0.312
W/S, psf	124.15	124.15	111.70
CB/AP/SL Noise, EPNdB	79.7/88.1/87.6	77.2/88.1/85.6	73.2/84.9/81.9
Cumulative Noise, EPNdB	255.37	250.93	240.00

Table 68. LSA Over-the-Wing Propulsion System Characteristics

Description	RTC – ADD	RTC – GF	ITD - GF
SLS Thrust, lbs	25,374	25,075	22,265
SLS Airflow, pps	931.8	1,084.5	1,111.1
Takeoff Thrust (M0.25/0K, Hot), lbs	21,175	20,925	18,580
Cruise TSFC, lb/lbf·hr	0.536	0.527	0.483
Total Engine Weight, lbs	5,618.8	5,405.8	4,083.7
Engine Nacelle Length, ft	9.48	9.51	8.68
Fan / Nacelle Diameter, in	69.7/89.7	73.0/93.0	75.1/85.1
FPRD / HPCPRD / OPRD (M0.80/35K)	1.55/22.0/46.7	1.45/16.0/45.6	1.35/17.5/50.3
BPRD (M0.80/35K)	10.04	12.33	18.98
OPR SLS Uninstalled	40.93	36.65	36.74
T4max (M0.25/0K) deg R	3,550	3,550	3,550
Fan Tip Mach No.	1.27	1.16	1.08
LPC / HPC / HPT / LPT Stages	4/10/2/7	2/8/2/3	3/7/2/3

Table 69. STA Tube and Wing Geometry

Description	EDS Base	RTC – ADD	RTC - GF	ITD - GF
Fuselage Length, ft	176.0	176.0	176.0	176.0
Fuselage Diameter, ft	17.08	17.08	17.08	17.08
Wing Area, sq ft	3,200	2,765	2,754	2,658
Wing Aspect Ratio	8.09	10.00	10.00	11.00
Wing Sweep, deg	30.73	30.73	30.73	30.73
Horizontal Tail Area, sq ft	843.3	609.3	605.9	547.7
Horizontal Tail Aspect Ratio	4.51	4.51	4.51	4.51
Horizontal Tail Sweep, deg	32.53	32.53	32.53	32.53
Vertical Tail Area, sq ft	433.5	387.1	384.9	329.2
Vertical Tail Aspect Ratio	1.82	1.82	1.82	1.82
Vertical Tail Sweep, deg	40.38	40.38	40.38	40.38
Nacelle Diameter, in	129.5	132.9	138.8	121.0
Engine Nacelle Length, ft	13.86	11.09	12.03	11.13
Main Gear Length, in	130.0	133.4	139.3	121.5
Nose Gear Length, in	90.75	93.13	97.26	84.80

Table 70. STA Tube and Wing Vehicle Characteristics

Description	EDS Base	RTC – ADD	RTC - GF	ITD – GF
TOGW, lbs	413,000	356,892	355,545	308,821
Operating Empty Weight, lbs	198,440	173,563	173,891	156,639
Fuel Weight, lbs	159,750	128,519	126,843	973,71.8
Design Payload, lbs	54,810	54,810	54,810	54,810
Block Fuel, lbs	141,989	114,799	113,603	86,918
Design Range, nmi	5,920	5,920	5,920	5,920
Wing Area, sq ft	3,200	2,765	2,754	2,658
Aspect Ratio	8.09	10.00	10.00	11.00
Cruise L/D	19.07	18.04	17.79	20.22
Approach Speed, kts	147.3	151.1	151.3	148.6
T/W	0.291	0.291	0.291	0.291
W/S, psf	129.1	129.1	129.1	116.2
CB/AP/SL Noise, EPNdB	93.1/96.1/99.3	86.6/93.3/90.4	83.5/92.3/87.6	80.2/89.7/85.1
Cumulative Noise, EPNdB	288.4	270.2	263.4	255.0

Table 71. STA Tube and Wing Propulsion System Characteristics

Description	EDS Base	RTC – ADD	RTC - GF	ITD - GF
SLS Thrust, lbs	61,267	51,856	51,649	44,871
SLS Airflow, pps	1,765	1,879	2,238	2,211
Takeoff Thrust (M0.25/0K, Hot), lbs	50,219	41,781	41,614	36,153
Cruise TSFC, lb/lbf·hr	0.603	0.522	0.514	0.486
Total Engine Weight, lbs	13,451	8,355	8,453	6,654
Engine Nacelle Length, ft	13.86	11.09	12.03	11.13
Fan / Nacelle Diameter, in	94.5/129.5	97.9/132.9	103.8/138.8	103.5/121.0
FPRD / HPCPRD / OPRD (M0.80/35K)	1.64/12.6/30.3	1.50/23.0/42.6	1.40/16.0/42.9	1.35/20.0/54.7
BPRD (M0.80/35K)	5.39	12.48	15.54	19.96
OPR SLS Uninstalled	31.86	42.04	39.99	43.18
T4max (M0.25/0K) deg R	3,425	3,550	3,550	3,550
Fan Tip Mach No.	1.28	1.17	1.06	1.06
LPC / HPC / HPT / LPT Stages	4/14/2/5	3/10/2/8	4/8/2/4	4/8/2/4

Table 72. STA Hybrid Wing-Body Geometry

Description	RTC – ADD	RTC – GF	ITD - GF
Fuselage Length, ft	106.9	106.9	106.9
Fuselage Diameter, ft	30.2	30.2	30.2
Wing Area, sq ft	7,064	7,070	5,875
Wing Aspect Ratio	7.95	7.95	8.48
Wing Sweep, deg	36	36	36
Horizontal Tail Area, sq ft	NA	NA	NA
Horizontal Tail Aspect Ratio	NA	NA	NA
Horizontal Tail Sweep, deg	NA	NA	NA
Vertical Tail Area, sq ft	118.8	118.8	118.8
Vertical Tail Aspect Ratio	1.95	1.95	1.95
Vertical Tail Sweep, deg	39.4	39.4	39.4
Nacelle Diameter, in	130.6	137.1	116.6
Engine Nacelle Length, ft	11.87	12.76	11.37
Main Gear Length, in	108	108	108
Nose Gear Length, in	75.35	75.35	75.35

Table 73. STA Hybrid Wing-Body Vehicle Characteristics

Description	RTC – ADD	RTC – GF	ITD - GF
TOGW, lbs	367,036	367,366	305,517
Operating Empty Weight, lbs	191,565	192,139	164,752
Fuel Weight, lbs	120,661	120,417	85,955
Design Payload, lbs	54,810	54,810	54,810
Block Fuel, lbs	107,684	107,954	76,616
Design Range, nmi	5,920	5,920	5,920
Wing Area, sq ft	7,064	7,070	5,875
Aspect Ratio	7.95	7.95	8.48
Cruise L/D	20.46	20.02	22.55
Approach Speed, kts	140.8	140.7	146.5
T/W	0.27	0.27	0.27
W/S, psf	51.96	51.96	52.01
CB/AP/SL Noise, EPNdB	82.7/82.5/92.2	77.1/82.5/88.7	74.0/82.0/86.4
Cumulative Noise, EPNdB	257.3	248.3	242.4

Table 74. STA Hybrid Wing-Body Propulsion System Characteristics

Description	RTC – ADD	RTC – GF	ITD - GF
SLS Thrust, lbs	49,641	49,596	41,211
SLS Airflow, pps	1,792	2,158	2,028
Takeoff Thrust (M0.25/0K, Hot), lbs	39,994	39,958	33,202
Cruise TSFC, lb/lbf·hr	0.527	0.516	0.486
Total Engine Weight, lbs	8,651.60	8,856.20	6,489.30
Engine Nacelle Length, ft	11.87	12.76	11.37
Fan / Nacelle Diameter, in	95.6/130.6	102.1/137.1	99.1/116.6
FPRD / HPCPRD / OPRD (M0.80/35K)	1.50/23.0/42.6	1.40/16.0/42.9	1.35/20.0/54.7
BPRD (M0.80/35K)	12.06	15.3	19.82
OPR SLS Uninstalled	42.56	39.62	43.56
T4max (M0.25/0K) deg R	3,550	3,550	3,550
Fan Tip Mach No.	1.17	1.06	1.06
LPC / HPC / HPT / LPT Stages	3/10/2/7	4/8/2/4	4/8/2/4

Table 75. LTA Tube and Wing Geometry

Description	EDS Base	RTC – ADD	RTC - GF	ITD - GF
Fuselage Length, ft	206.5	206.5	206.5	206.5
Fuselage Diameter, ft	20.50	20.50	20.50	20.50
Wing Area, sq ft	4,927	4,206	4,150	3,819
Wing Aspect Ratio	8.81	10.0	10.0	11.0
Wing Sweep, deg	30.94	30.94	30.94	30.94
Horizontal Tail Area, sq ft	1,119	828.4	812.1	683.5
Horizontal Tail Aspect Ratio	4.62	4.62	4.62	4.62
Horizontal Tail Sweep, deg	34.82	34.82	34.82	34.82
Vertical Tail Area, sq ft	528.0	443.6	434.8	346.2
Vertical Tail Aspect Ratio	1.84	1.84	1.84	1.84
Vertical Tail Sweep, deg	40.03	40.03	40.03	40.03
Nacelle Diameter, in	158.0	158.5	166.2	144.6
Engine Nacelle Length, ft	16.4	15.0	16.1	14.3
Main Gear Length, in	136.9	137.4	145.1	123.5
Nose Gear Length, in	87.3	87.6	93.0	77.9

Table 76. LTA Tube and Wing Vehicle Characteristics

Description	EDS Base	RTC – ADD	RTC - GF	ITD – GF
TOGW, lbs	657,000	560,769	553,405	458,306
Operating Empty Weight, lbs	317,000	272,714	271,414	234,489
Fuel Weight, lbs	275,950	224,006	217,941	159,767
Design Payload, lbs	64,050	64,050	64,050	64,050
Block Fuel, lbs	249,180	202,271	197,358	144,280
Design Range, nmi	7,530	7,530	7,530	7,530
Wing Area, sq ft	4,927	4,206	4,150	3,819
Aspect Ratio	8.81	10.0	10.0	11.0
Cruise L/D	18.75	19.19	19.28	21.68
Approach Speed, kts	139.0	142.1	142.6	140.8
T/W	0.296	0.296	0.296	0.296
W/S, psf	133.3	133.3	133.3	120.0
CB/AP/SL Noise, EPNdB	92.7/96.8/97.7	88.9/94.5/92.7	86.3/93.2/90.5	82.8/91.0/87.4
Cumulative Noise, EPNdB	287.2	276.1	270.0	261.3

Table 77. LTA Tube and Wing Propulsion System Characteristics

Description	EDS Base	RTC – ADD	RTC - GF	ITD - GF
SLS Thrust, lbs	97,300	83,192	82,113	67,844
SLS Airflow, pps	3,135	2,999	3,570	3,338
Takeoff Thrust (M0.25/0K, Hot), lbs	78,400	67,033	66,163	54,665
Cruise TSFC, lb/lbf·hr	0.552	0.531	0.519	0.492
Total Engine Weight, lbs	21,164	15,239	15,109	10,782
Engine Nacelle Length, ft	16.4	15.0	16.1	14.3
Fan / Nacelle Diameter, in	123.0/158.0	123.5/158.5	131.2/166.2	127.1/144.6
FPRD / HPCPRD / OPRD (M0.80/35K)	1.58/20.0/39.2	1.50/23.0/42.6	1.40/16.0/42.9	1.35/20.0/54.7
BPRD (M0.80/35K)	8.80	12.44	15.88	20.42
OPR SLS Uninstalled	40.53	42.33	39.35	43.32
T4max (M0.25/0K) deg R	3,450	3,550	3,550	3,550
Fan Tip Mach No.	1.26	1.17	1.06	1.06
LPC / HPC / HPT / LPT Stages	3/10/2/6	3/10/2/7	4/8/2/4	4/8/2/4

Table 78. LTA MFN Geometry

Description	RTC – ADD	RTC – GF	ITD - GF
Fuselage Length, ft	171.5	171.5	171.5
Fuselage Diameter, ft	21.41	21.41	21.41
Wing Area, sq ft	4,067	4,008	3,709
Wing Aspect Ratio	10.0	10.0	11.0
Wing Sweep, deg	33.0	33.0	33.0
Horizontal Tail Area, sq ft	948.5	928.1	787.7
Horizontal Tail Aspect Ratio	4.10	4.10	4.10
Horizontal Tail Sweep, deg	35.0	35.0	35.0
Vertical Tail Area, sq ft	528.0	528.0	454.1
Vertical Tail Aspect Ratio	1.42	1.42	1.42
Vertical Tail Sweep, deg	46.0	46.0	46.0
Nacelle Diameter, in	154.3	161.6	140.2
Engine Nacelle Length, ft	14.57	15.58	13.85
Main Gear Length, in	136.9	136.9	136.9
Nose Gear Length, in	87.3	87.3	87.3

Table 79. LTA MFN Vehicle Characteristics

Description	RTC – ADD	RTC – GF	ITD - GF
TOGW, lbs	553,092	545,129	453,994
Operating Empty Weight, lbs	270,904	268,910	233,203
Fuel Weight, lbs	218,138	212,169	156,741
Design Payload, lbs	64,050	64,050	64,050
Block Fuel, lbs	197,014	192,161	141,604
Design Range, nmi	7,530	7,530	7,530
Wing Area, sq ft	4,066	4,008	3,709
Aspect Ratio	10.0	10.0	11.0
Cruise L/D	19.67	19.45	21.85
Approach Speed, kts	144.1	144.6	142.6
T/W	0.280	0.280	0.280
W/S, psf	136.0	136.0	122.4
CB/AP/SL Noise, EPNdB	86.7/88.7/89.2	84.6/88.9/86.4	80.9/86.8/83.8
Cumulative Noise, EPNdB	264.6	259.9	251.6

Table 80. LTA MFN Propulsion System Characteristics

Description	RTC – ADD	RTC – GF	ITD - GF
SLS Thrust, lbs	77,597	76,459	63,313
SLS Airflow, pps	2,798	3,324	3,115
Takeoff Thrust (M0.25/0K, Hot), lbs	62,524	61,607	51,015
Cruise TSFC, lb/lbf·hr	0.533	0.520	0.493
Total Engine Weight, lbs	14,136	13,997	10,044
Engine Nacelle Length, ft	14.57	15.58	13.85
Fan / Nacelle Diameter, in	119.3/154.3	126.6/161.6	122.7/140.2
FPRD / HPCPRD / OPRD (M0.80/35K)	1.50/23.0/42.6	1.40/16.0/42.9	1.35/20.0/54.7
BPRD (M0.80/35K)	12.38	15.80	20.34
OPR SLS Uninstalled	42.36	39.39	43.35
T4max (M0.25/0K) deg R	3,550	3,550	3,550
Fan Tip Mach No.	1.17	1.06	1.06
LPC / HPC / HPT / LPT Stages	3/10/2/7	4/8/2/4	4/8/2/4

Table 81. LTA Box Wing Geometry

Description	RTC – ADD	RTC – GF	ITD - GF
Fuselage Length, ft	220.0	220.0	220.0
Fuselage Diameter, ft	20.50	20.50	20.50
Wing Area, sq ft	6,317	6,276	5,066
Wing Aspect Ratio	6.33	6.37	7.90
Wing Sweep, deg	44.0	44.0	44.0
Horizontal Tail Area, sq ft	NA	NA	NA
Horizontal Tail Aspect Ratio	NA	NA	NA
Horizontal Tail Sweep, deg	NA	NA	NA
Vertical Tail Area, sq ft	528.0	528.0	528.0
Vertical Tail Aspect Ratio	1.50	1.50	1.50
Vertical Tail Sweep, deg	47.0	47.0	47.0
Nacelle Diameter, in	166.1	174.8	152.3
Engine Nacelle Length, ft	15.89	17.06	15.05
Main Gear Length, in	136.9	136.9	136.9
Nose Gear Length, in	87.25	87.25	87.25

Table 82. LTA Box Wing Vehicle Characteristics

Description	RTC – ADD	RTC – GF	ITD - GF
TOGW, lbs	613,688	608,444	511,373
Operating Empty Weight, lbs	294,179	293,854	271,925
Fuel Weight, lbs	255,459	250,540	175,398
Design Payload, lbs	64,050	64,050	64,050
Block Fuel, lbs	230,858	227,161	158,296
Design Range, nmi	7,530	7,530	7,530
Wing Area, sq ft	6,317	6,276	5,066
Aspect Ratio	6.33	6.37	7.90
Cruise L/D	19.23	19.01	22.15
Approach Speed, kts	119.3	119.5	128.6
T/W	0.308	0.309	0.296
W/S, psf	97.1	96.9	100.9
CB/AP/SL Noise, EPNdB	88.0/92.8/94.0	85.0/91.6/91.3	83.7/90.8/88.1
Cumulative Noise, EPNdB	274.8	267.8	262.5

Table 83. LTA Box Wing Propulsion System Characteristics

Description	RTC – ADD	RTC – GF	ITD - GF
SLS Thrust, lbs	93,800	93,254	76,302
SLS Airflow, pps	3,381	4,053	3,758
Takeoff Thrust (M0.25/0K, Hot), lbs	75,581	75,141	61,481
Cruise TSFC, lb/lbf·hr	0.529	0.516	0.487
Total Engine Weight, lbs	17,419	17,354	12,147
Engine Nacelle Length, ft	15.89	17.06	15.05
Fan / Nacelle Diameter, in	131.1/166.1	139.8/174.8	134.8/152.3
FPRD / HPCPRD / OPRD (M0.80/35K)	1.50/23.0/42.6	1.40/16.0/42.9	1.35/20.0/54.7
BPRD (M0.80/35K)	12.50	15.99	20.82
OPR SLS Uninstalled	42.30	39.29	43.21
T4max (M0.25/0K) deg R	3,550	3,550	3,550
Fan Tip Mach No.	1.17	1.06	1.06
LPC / HPC / HPT / LPT Stages	3/10/2/7	4/8/2/4	4/8/2/4

Table 84. LTA Hybrid Wing-Body Geometry

Description	RTC – ADD	RTC - GF	RTC – OR*	ITD - GF
Fuselage Length, ft	120.9	120.9	120.9	120.9
Fuselage Diameter, ft	32.85	32.85	32.85	32.85
Wing Area, sq ft	10,391	10,339	8,140	8,100
Wing Aspect Ratio	6.04	6.04	6.05	6.05
Wing Sweep, deg	36.0	36.0	36.0	36.0
Horizontal Tail Area, sq ft	NA	NA	NA	NA
Horizontal Tail Aspect Ratio	NA	NA	NA	NA
Horizontal Tail Sweep, deg	NA	NA	NA	NA
Vertical Tail Area, sq ft	140.0	140.0	140.0	140.0
Vertical Tail Aspect Ratio	1.95	1.95	1.95	1.95
Vertical Tail Sweep, deg	39.4	39.4	39.4	39.4
Nacelle Diameter, in	150.4	158.4	NA	134.1
Engine Nacelle Length, ft	14.14	15.22	8.69	13.25
Main Gear Length, in	136.9	136.9	136.9	136.9
Nose Gear Length, in	87.3	87.3	87.3	87.3

*HWB OR has cruise Mach # = 0.8, all other vehicles have cruise Mach # of 0.84

Table 85. LTA Hybrid Wing-Body Vehicle Characteristics

Description	RTC – ADD	RTC - GF	RTC – OR*	ITD - GF
TOGW, lbs	540,008	537,230	423,221	421,039
Operating Empty Weight, lbs	273,774	273,149	231,460	223,613
Fuel Weight, lbs	202,183	200,030	127,711	133,377
Design Payload, lbs	64,050	64,050	64,050	64,050
Block Fuel, lbs	182,476	181,211	114,395	120,104
Design Range, nmi	7,530	7,530	7,530	7,530
Wing Area, sq ft	10,391	10,339	8,140	8,100
Aspect Ratio	6.04	6.04	6.05	6.05
Cruise L/D	21.74	21.34	26.04	23.74
Approach Speed, kts	133.8	133.8	141.8	140.6
T/W	0.270	0.270	0.270	0.270
W/S, psf	52.0	52.0	52.0	52.0
CB/AP/SL Noise, EPNdB	83.8/83.4/93.3	78.0/83.4/91.3	80.1/83.7/93.1	74.6/82.7/87.4
Cumulative Noise, EPNdB	260.5	252.7	256.9	244.8

*HWB OR has cruise Mach # = 0.8, all other vehicles have cruise Mach # of 0.84

Table 86. LTA Hybrid Wing-Body Propulsion System Characteristics

Description	RTC – ADD	RTC - GF	RTC – OR*	ITD - GF
SLS Thrust, lbs	72,600	72,600	39,240	57,116
SLS Airflow, pps	2,618	3,156	96.7	2,810
Takeoff Thrust (M0.25/0K, Hot), lbs	58,500	58,500	32,514	46,023
Cruise TSFC, lb/lbf·hr	0.534	0.522	0.418	0.495
Total Engine Weight, lbs	13,154	13,247	2,493	9,076
Engine Nacelle Length, ft	14.14	15.22	8.69	13.25
Fan / Nacelle Diameter, in	115.4/150.4	123.4/158.4	160.9/NA	116.6/134.1
FPRD / HPCPRD / OPRD (M0.80/35K)	1.50/23.0/42.6	1.40/16.0/42.9	NA/3.1/49.3	1.35/20.0/54.7
BPRD (M0.80/35K)	12.32	15.74	NA	20.21
OPR SLS Uninstalled	42.39	39.42	48.7	43.40
T4max (M0.25/0K) deg R	3,550	3,550	3,550	3,550
Fan Tip Mach No.	1.17	1.06	0.00	1.06
LPC / HPC / HPT / LPT Stages	3/10/2/7	4/8/2/4	4/4/1/1	4/8/2/4

*HWB OR has cruise Mach # = 0.8, all other vehicles have cruise Mach # of 0.84

Table 87. VLA Tube and Wing Geometry

Description	EDS Base	RTC – ADD	RTC - GF	ITD - GF
Fuselage Length, ft	225.2	225.2	225.2	225.2
Fuselage Diameter, ft	23.95	23.95	23.95	23.95
Wing Area, sq ft	6,203	5,424	5,359	5,076
Wing Aspect Ratio	7.61	10.0	10.0	11.0
Wing Sweep, deg	39.7	39.7	39.7	39.7
Horizontal Tail Area, sq ft	1,494	1,066	1,047	920
Horizontal Tail Aspect Ratio	3.60	3.60	3.60	3.60
Horizontal Tail Sweep, deg	36.6	36.6	36.6	36.6
Vertical Tail Area, sq ft	855.2	801.7	787.3	654.6
Vertical Tail Aspect Ratio	1.26	1.26	1.26	1.26
Vertical Tail Sweep, deg	44.7	44.7	44.7	44.7
Nacelle Diameter, in	129.4	136.1	141.4	122.7
Engine Nacelle Length, ft	14.78	12.63	13.59	12.45
Main Gear Length, in	115.5	122.2	127.5	108.8
Nose Gear Length, in	86.3	91.0	94.7	81.6

Table 88. VLA Tube and Wing Vehicle Characteristics

Description	EDS Base	RTC – ADD	RTC - GF	ITD – GF
TOGW, lbs	876,999	766,919	757,687	645,889
Operating Empty Weight, lbs	403,400	368,169	365,639	328,515
Fuel Weight, lbs	386,030	311,180	304,478	229,804
Design Payload, lbs	87,570	87,570	87,570	87,570
Block Fuel, lbs	347,168	280,754	275,158	207,205
Design Range, nmi	7,060	7,060	7,060	7,060
Wing Area, sq ft	6,203	5,424	5,359	5,076
Aspect Ratio	7.61	10.0	10.0	11.0
Cruise L/D	18.96	18.13	17.94	20.06
Approach Speed, kts	156.9	161.9	162.3	160.4
T/W	0.259	0.297	0.297	0.297
W/S, psf	141.4	141.4	141.4	127.2
CB/AP/SL Noise, EPNdB	99.3/104.6/100.3	87.8/95.1/93.5	85.1/94.5/90.9	82.3/91.8/88.5
Cumulative Noise, EPNdB	304.3	276.4	270.5	262.6

Table 89. VLA Tube and Wing Propulsion System Characteristics

Description	EDS Base	RTC – ADD	RTC - GF	ITD - GF
SLS Thrust, lbs	62,000	56,964	56,249	47,696
SLS Airflow, pps	1,791	2,037	2,393	2,320
Takeoff Thrust (M0.25/0K, Hot), lbs	52,038	45,897	45,321	38,430
Cruise TSFC, lb/lbf·hr	0.578	0.484	0.473	0.453
Total Engine Weight, lbs	11,965	8,515	8,170	6,331
Engine Nacelle Length, ft	14.78	12.63	13.59	12.45
Fan / Nacelle Diameter, in	94.4/129.4	101.1/136.1	106.4/141.4	105.2/122.7
FPRD / HPCPRD / OPRD (M0.80/35K)	1.76/8.81/28.1	1.50/23.0/42.6	1.40/16.0/42.9	1.35/20.0/54.7
BPRD (M0.80/35K)	4.89	12.37	14.99	19.87
OPR SLS Uninstalled	29.18	42.76	41.51	43.96
T4max (M0.25/0K) deg R	3,150	3,550	3,550	3,550
Fan Tip Mach No.	1.69	1.17	1.06	1.06
LPC / HPC / HPT / LPT Stages	4/11/2/4	3/10/2/7	4/8/2/4	4/8/2/4

Table 90. VLA Hybrid Wing-Body Geometry

Description	RTC – ADD	RTC – GF	ITD - GF
Fuselage Length, ft	143.1	143.1	143.1
Fuselage Diameter, ft	37.06	37.06	37.06
Wing Area, sq ft	15,916	15,489	12,264
Wing Aspect Ratio	7.05	7.08	7.44
Wing Sweep, deg	36.0	36.0	36.0
Horizontal Tail Area, sq ft	NA	NA	NA
Horizontal Tail Aspect Ratio	NA	NA	NA
Horizontal Tail Sweep, deg	NA	NA	NA
Vertical Tail Area, sq ft	210.0	210.0	210.0
Vertical Tail Aspect Ratio	1.95	1.95	1.95
Vertical Tail Sweep, deg	39.4	39.4	39.4
Nacelle Diameter, in	158.6	167.0	141.0
Engine Nacelle Length, ft	16.74	17.76	15.39
Main Gear Length, in	115.5	115.5	115.5
Nose Gear Length, in	86.33	86.33	86.33

Table 91. VLA Hybrid Wing-Body Vehicle Characteristics

Description	RTC – ADD	RTC – GF	ITD - GF
TOGW, lbs	827,476	805,565	637,784
Operating Empty Weight, lbs	443,190	435,616	348,546
Fuel Weight, lbs	296,716	282,380	201,668
Design Payload, lbs	87,570	87,570	87,570
Block Fuel, lbs	266,155	253,682	180,699
Design Range, nmi	7,060	7,060	7,060
Wing Area, sq ft	15,916	15,489	12,264
Aspect Ratio	7.05	7.08	7.44
Cruise L/D	22.27	22.00	23.34
Approach Speed, kts	137.3	138.2	143.6
T/W	0.310	0.310	0.310
W/S, psf	51.99	52.01	52.00
CB/AP/SL Noise, EPNdB	78.5/81.0/96.1	73.1/80.9/93.3	70.2/80.5/90.1
Cumulative Noise, EPNdB	255.6	247.3	240.8

Table 92. VLA Hybrid Wing-Body Propulsion System Characteristics

Description	RTC – ADD	RTC – GF	ITD - GF
SLS Thrust, lbs	85,440	83,189	65,884
SLS Airflow, pps	3,049	3,614	3,201
Takeoff Thrust (M0.25/0K, Hot), lbs	68,845	67,031	53,087
Cruise TSFC, lb/lbf·hr	0.486	0.473	0.456
Total Engine Weight, lbs	17,595	17,177	10,888
Engine Nacelle Length, ft	16.74	17.76	15.39
Fan / Nacelle Diameter, in	123.6/158.6	132.0/167.0	123.5/141.0
FPRD / HPCPRD / OPRD (M0.80/35K)	1.50/23.0/42.6	1.40/16.0/42.9	1.35/20.0/54.7
BPRD (M0.80/35K)	12.07	15.43	19.40
OPR SLS Uninstalled	42.55	39.30	43.87
T4max (M0.25/0K) deg R	3,550	3,550	3,550
Fan Tip Mach No.	1.17	1.06	1.06
LPC / HPC / HPT / LPT Stages	3/10/2/7	4/8/2/4	4/8/2/4

7.2 Multi-Objective Genetic Algorithm for N+2 Technology Pareto Frontier

7.2.1 Motivation for Multi-Objective Optimiztion

Resource limitations required the informed down-selection of an airframe and propulsion technology portfolio to meet environmental goals. This problem is not unique to aviation

environmental impact or to aeronautics in general and features some common traits. A research and development portfolio is typically associated with a set of aggressive performance requirements pursuant of overarching policy that frame and motivate the development of enabling technologies. Albeit methodological diversity most approaches to the composition of such a portfolio incorporate basic steps for the identification of a pool of candidate technologies, the comparative assessment of technology combinations (each embodying a unique candidate portfolio), and ultimately the down-selection of the portfolio. In this context questions that typically emerge include:

- What are the most favorable combinations of technologies relative to the goals in question?
- To what extent does the technology portfolio satisfy the goals? What is the best that can be achieved?
- What technologies (or combinations thereof) are critical in reaching prescribed goals?

There are also a number of noteworthy challenges and practical considerations. The size of the problem, and thus the magnitude of the effort, generally scales with the number of candidate technologies to be evaluated as well as with the number and nature of measures of performance with which they ought to be evaluated. The set of possible technology combinations grows very quickly with the number of candidate technologies, often resulting in a prohibitively large combinatorial set even for a modestly sized pool of candidates. This issue is further compounded by the resource expense of evaluating distinct technology combinations in terms of relevant measures of performance. Although an exhaustive examination of the combinatorial set is desired (or even ideal) it is often unrealizable in practice. A related issue pertains to the combinatorial logic required to observe technology compatibilities; it reduces the size of the total set of alternatives but typically not enough to make exhaustive exploration feasible, and instead adds to the complexity of the problem setup.

Another consideration is the plurality of goals. The comparative assessment of a pool of candidate solutions on the basis of a single measure of performance is, for the most part, trivial. However, a multiplicity of (conflicting) goals implies the need to address tradeoffs inherent across unique technology combinations. While solutions at the corners of the trade space may be readily disregarded for performing well relative to one goal and poorly in all others, solutions with a more balanced valuation profile are typically of particular interest. Adequate characterization of the technology trade space is therefore crucial in informing and supporting portfolio selection.

In lieu of the above considerations technology portfolio composition may be abstracted and generalized as a multi-objective optimization sub-problem followed by a multi-attribute decision making sub-problem. This is consistent with work by Deb (2002) who notes that the former yields the set of tradeoff optimal solutions (also referred to as non-dominated or Pareto-optimal), and the latter yields a single choice from the optimal set. We subscribe to this view and argue that a multi-objective genetic algorithm is ideally suited to address many of the traits and considerations specific to aircraft technology portfolio composition discussed above, and offer the following observations:

First, the combinatorial set associated with the pool of candidate technologies comprises a discrete solution space. The treatment of discrete solution sets is inherent in the formulation of genetic algorithms, particularly with regards to the encoding and manipulations of solutions via a genetic bit string. More specifically, by assigning each technology in the candidate pool to a single bit, the bit string efficiently encompasses the entire technology pool and defines distinct

combinations on the basis of what technologies are included (1) or not (0). The evolutionary logic of the genetic algorithm yields favorable solutions while avoiding (in most practical cases) the need to span the entire combinatorial space, thus allowing for resource savings in solution evaluation that may be significant. It may be reasonably expected that objective functions are highly sensitive to the addition or removal of a single technology from a given combination, and that a myriad of potentially steep local optima may exist. Genetic algorithms include stochastic components that allow solutions to evolve out of local optima without discarding them, unless more favorable ones are found. Ultimately, the optimization yields a set of non-dominated discrete solutions that encompass fundamental tradeoffs across the multiple objectives and that can be studied to gain insight about the technology trade space.

7.2.2 Formulation of the Technology Portfolio Problem

We formulate the technology portfolio selection problem as follows. Consider a set τ of *n* technologies T_i.

$$\tau = \{T_1, T_2 \ \dots, T_n\}$$

A technology combination is defined by the vector

$$t = [t_1, t_2, \dots, t_n\ ]$$

Where

$$t_i = \begin{cases} 1, & \text{if } T_i \text{ is included} \\ 0, & \text{if } T_i \text{ is not included} \end{cases} \quad (3)$$

To distinguish between distinct technology combinations we use superscript notation so that t_i^j refers to the inclusion of the i^{th} technology in the j^{th} combination.

The validity of concurrently including any two technologies of the set τ in a given technology combination is encoded on a pair-wise basis via the compatibility operator χ, defined as

$$\chi(T_i, T_j) = \chi_{ij} = \begin{cases} 1, & \text{if } T_i \text{ is compatible with } T_j \\ 0, & \text{if } T_i \text{ is not compatible with } T_j \end{cases} \quad (4)$$

Based on this definition a technology is always compatible with itself, so that

$$\chi_{ii} = 1$$

The technology compatibility matrix *X* with elements χ_{ij} is defined for a given technology set τ. *X* is square (n×n), symmetric, and identity diagonal.

For the simplest case where there are no technology incompatibilities and all χ_{ij}=1 there are 2^n possible technology combinations t^i. We define this 2^n set of all possible instances of the vector *t* as the domain of the alternative space and denote it as *A*. We denote the set of internally compatible technology combinations as

$$A^{\chi} \subseteq A$$

Objective functions are evaluated for technology combinations, which we express as

$$f_m(t),\ m = 1,2,\dots M$$

For the type of application considered in this paper objective functions will typically constitute some measure of system performance produced via modeling capabilities. Technologies are modeled via correction factors applied to the underlying model relations resulting in system performance changes. Accordingly, it may be necessary to create appropriate mapping functions so that the vector *t* may be used directly as an argument of the objective functions.

As a generalization we assume that the objective function f^k takes as an argument the technology attribute vector *k*. An appropriate mapping function $\vec{f}$ must be defined such that

$$\vec{f}: t \to k$$

So that the objective function *f* with argument *t* may be expressed as

$$f(t) = f^k\left(\vec{f}(t)\right)$$

We address the issue of compatibility for technology combinations by including an arbitrarily large penalty factor into the objective function for incompatible combinations. The compatibility of a given technology combination t^l may be determined by estimating the parameter

$$\phi^l = \prod\prod \chi_{ij} \quad \forall\, i,j : t_i^l = 1 \wedge t_j^l = 1$$

Because the product is inclusive of all the pairwise compatibility operators corresponding to the technologies included in the combination t^l, the result is always zero whenever there is at least one incompatibility. A penalty factor may therefore be simply defined as

$$\pi^l = \begin{cases} \Lambda \text{ if } \phi^l = 0 \\ 1 \text{ if } \phi^l = 1 \end{cases}$$

Here Λ is a constant that yields an arbitrarily large penalty to the objective function. Some caution should be exercised in selecting a value for Λ, particularly with regards to whether the optimization is a minimization or maximization of the objective function, as well as the expected range of objective function values for feasible solutions. The penalty factor may then be incorporated within the objective function as follows

$$\tilde{f}(t) = \pi^l f^k\left(\vec{f}(t)\right)$$

This approach is comparable to the creation of a pseudo-objective function for constrained problems where a penalty function is appended to the original objective function to account for the constraint (see for instance Vanderplaats, 2001, Ch. 2.5 and Ch. 5). Use of

penalty functions is much simpler and easier to visualize whenever the objective and penalty functions are continuous and well behaved. For the class of problems we address in this work the discrete nature and of the technology set and added combinatorial complexity resulting from incompatibilities are not conducive to a straightforward or visual examination of the compatibility constraint, though the principle and effect achieved via the penalty factor is ultimately the same.

Accordingly the classical optimization problem may be formulated as

$$\text{Min / Max} \qquad f(t),$$

$$\text{Subject to} \qquad \phi(\mathrm{X}, t) > 0$$

$$t \in A$$

Or, if the pseudo-objective function is to be explicitly stated in the formulation, then

$$\text{Min / Max} \qquad \tilde{f}(t),$$

$$\text{Subject to} \qquad t \in A$$

This is, of course, a generalized setup for an optimization problem; the choice of a specific algorithm or optimization approach should be adequately reflected by revising as needed the above mathematical formulation.

The literature broadly outlines two basic approaches with regards to optimization and selection which we consider here for the formulation of the technology portfolio problem. The first approach is based on the solution of the multi-objective optimization problem where all objectives are equally important. The result is a tradeoff-optimal set of feasible solutions from which a subset or a single preferred solution must be ultimately identified. Because all solutions in that set are equally optimal selection cannot be conducted solely on the basis of objectives employed in the optimization. Posterior information on the relative preference of objectives is thus collected and applied to realize the selection. In fact, Deb (2002) notes that "each trade-off solution corresponds to a specific order of importance of the objectives." The second approach solves a single objective optimization where the relative preference of multiple objectives is fully known a-priori and used to construct the objective function as a weighted objective aggregate. We find that the first approach is preferable because it produces a set of tradeoff-optimal solutions from which insight can obtained, and because it allows for the comparative assessment of choices resulting from different selection techniques and objective preference weightings.

Multi-objective optimization (first approach) is generally realized with respect the dominance of individual solutions t^j from the set A (or some relevant subset thereof). The concept of dominance is well documented in the literature, and we adopt it to this problem as follows.

For a set of performance objectives

$$\tilde{f}_m(t);\ \ m = 1,2,\dots,M$$

a technology combination t^i strongly dominates t^j if t^i is better than t^j in all M performance objectives, or

$$t^i \prec t^j \leftrightarrow \tilde{f}_m(t^i) \prec \tilde{f}_m(t^j)\ \forall\, m$$

Similarly, t^i weakly dominates t^j if t^i is no worse than t^j in all M performance objectives and t^i is better than t^j in at least one objective, or

$$t^i \preccurlyeq t^j \leftrightarrow \tilde{f}_m(t^i) \preccurlyeq \tilde{f}_m(t^j)\ \forall\, i\ \wedge \exists\, l\colon \tilde{f}_l(t^i) \prec \tilde{f}_l(t^j)$$

The set of technology combinations that are not dominated by any other technology combination comprises the non-dominated set. For any subset of solutions *B* from the total set *A* of technology combinations, there is a non-dominated set of solutions *B'* such that

$$B' \subset B \subset A$$

In this context the general purpose of an optimization routine is to identify the non-dominated set *A'* of the total set of technology combinations *A*. In practice, *A'* may not be fully identified and instead it is approximated as the non-dominated subset *B'* (Zitzler, 2003). An optimization approach evident in evolutionary algorithms is to recursively generate sets of solutions *B*, identify non-dominated solutions *B',* and retain them across iterations so as to approximate (*B'*) or explicitly identify the set of non-dominated solutions *A'*. (For simplicity we refer only to *A'* from here on.)

The preference-based selection from *A'* may be conducted according to any number of multi-attribute selection techniques. In general these techniques apply some function that combines performance objective values and corresponding objective weights into a single aggregate metric, effectively reducing the problem to a ranking of solutions according to this weighted aggregate. One of the simplest and most commonly used options is the weighted sum of scaled values, as shown below where there asterisk denotes the normalizing function value.

$$F(t^i) = \sum_{m=1}^{M} w_m \frac{f_m(t^i)}{f_m(t)^*}$$

Although the literature offers much diversity in multi-attribute decision making techniques (e.g. Sen, 1998) it also cautions to recognize and understand the inherent assumptions, limitations and shortcomings of each before committing them to use (e.g. Roman, 2004).

7.2.3 Implementation of the Multi-Objective Genetic Algorithm for the Technology Portfolio Problem

The technology portfolio problem is conducted for the 300-passenger class (Large Twin Aisle) tube-and-wing concept. We implement Deb's Non-dominated Sorting Genetic Algorithm

II (NSGA-II) (Deb, 2002) which incorporates improvements in computational efficiency, elitism, and diversity preservation over its original formulation. Non-dominated sorting featured in NSGA was originally proposed by Goldberg (1989) and is found in many variants of multi-objective genetic algorithms. This approach assigns a rank of 1 to all non-dominated solutions in a set, removes them, and recursively assigns subsequent rank values to non-dominated solutions of the remaining set.

We select the NSGA-II for several reasons. First, it has been shown to be more efficient than other competing approaches. Second, it produces more uniformly spread non-dominated sets relative to competing approaches. This is achieved by calculating the crowding distance to assess the density of solutions surrounding a particular solution. Rather than sorting solutions solely on dominance rank the NSGA-II combines rank and crowding distance into a crowded-comparison operator for sorting. The crowded comparison operator $\prec_n$ is defined as:

$$i \prec_n j \leftrightarrow (i_{rank} < j_{rank}) \vee \left((i_{rank} = j_{rank}) \wedge (i_{distance} < j_{distance})\right)$$

For continuous decision and objective spaces this feature yields some uniformity across solutions on the non-dominated set and avoids potential clustering that typically occurs otherwise with genetic algorithms. This in turn allows for a more directed management of the population size so that the Pareto hyper-surface may be more readily discerned at a more modest computational burden. A comparable effect is produced for the technology portfolio problem noting that natural clustering of solutions is more likely and reasonably expected for discrete decision and objective spaces. For a reasonably sized population all top-ranked solutions will be preserved by NSGA-II regardless of their natural clustering, as will those of subsequent ranks that offer the most uniform spreading of solutions. This feature is certainly desirable if one hopes to understand the technology trade-space by examining and characterizing the non-dominated set with respect to performance goals. Lastly, due to the popularity and broad acceptance of the NSGA-II algorithm, many commercial software products and optimization tools feature pre-packaged implementations along with several options for customization.

We implement the NSGA-II in MATLAB® via its *gamultiobj* solver. The genotype of each technology combination is encoded with a 91 bit string corresponding to each of the 91 technologies in the candidate pool. The inclusion of individual technologies is therefore handled explicitly by the corresponding binary bit. Accordingly, we set the population size at 1,500 following a heuristic factor of ~15 relative to the number of independent decision variables.

It is common practice to randomly seed the initial population to avoid the introduction of design biases. This approach, while easy to implement, may yield unfeasible solutions for the initial population. Although this rarely presents a problem for the approximation of the non-dominated set, we intentionally seed the initial population with randomly generated solutions that satisfy compatibility.

Preliminary test runs showed that, as expected, a fraction of the new solutions created with the crossover operator are incompatible. However we noticed that on average the two-point crossover option resulted in a smaller fraction of incompatible combinations. Although the issue of compatibility is addressed via a penalty function, we find that a larger fraction of feasible designs is certainly preferable. Accordingly, we adopt the two-point cross-over for which the default 0.8 crossover fraction was deemed adequate. In a similar fashion we investigated the effect of the mutation scheme and observed that it did not produce noteworthy effects except for

very high mutation rates uncharacteristic of most typical applications. A uniform mutation scheme with a 0.01 rate was thus adopted for simplicity.

The stopping criterion is the convergence of the spread of the non-dominated set. The spread is a scalar measure of the distribution of points along the Pareto front estimated as a function of the Euclidean distance between consecutive (neighboring) solutions along the Pareto front and the average value of these distances. It assumes values ranging between 0 for evenly distributed solutions and 1 for unevenly distributed (clustered) solutions. Spread convergence is achieved when the change in spread over the last N iterations is less than a tolerance value ε. Default values N=100 and $\varepsilon=10^{-4}$ were preserved.

7.2.4 Characterization of the Technology Tradespace

7.2.4.1 Visualization and Format of Results

We set the measures of performance defining N+2 environmental goals in as objective functions. It is worth noting again that these metrics are defined as improvements relative to a prescribed reference. In the case of fuel burn the reference is the mission fuel burn for the reference vehicle, whereas the limits for noise and NO_X are regulatory. The noise limit is defined as a function of takeoff gross weight whereas the goal for NO_X is defined as a function of the overall pressure ratio of the engine(s).

The resulting non-dominated set of technology combinations is visually depicted in Figure 81 as a 3-D plot with each axis corresponding to one of the N+2 measures of performance, and each data point representing a distinct technology combination. Bivariate plots are also shown. We note a number of readily identifiable features of the Pareto surface and apply differentiation with greyscale and data point markers to further facilitate their discernment.

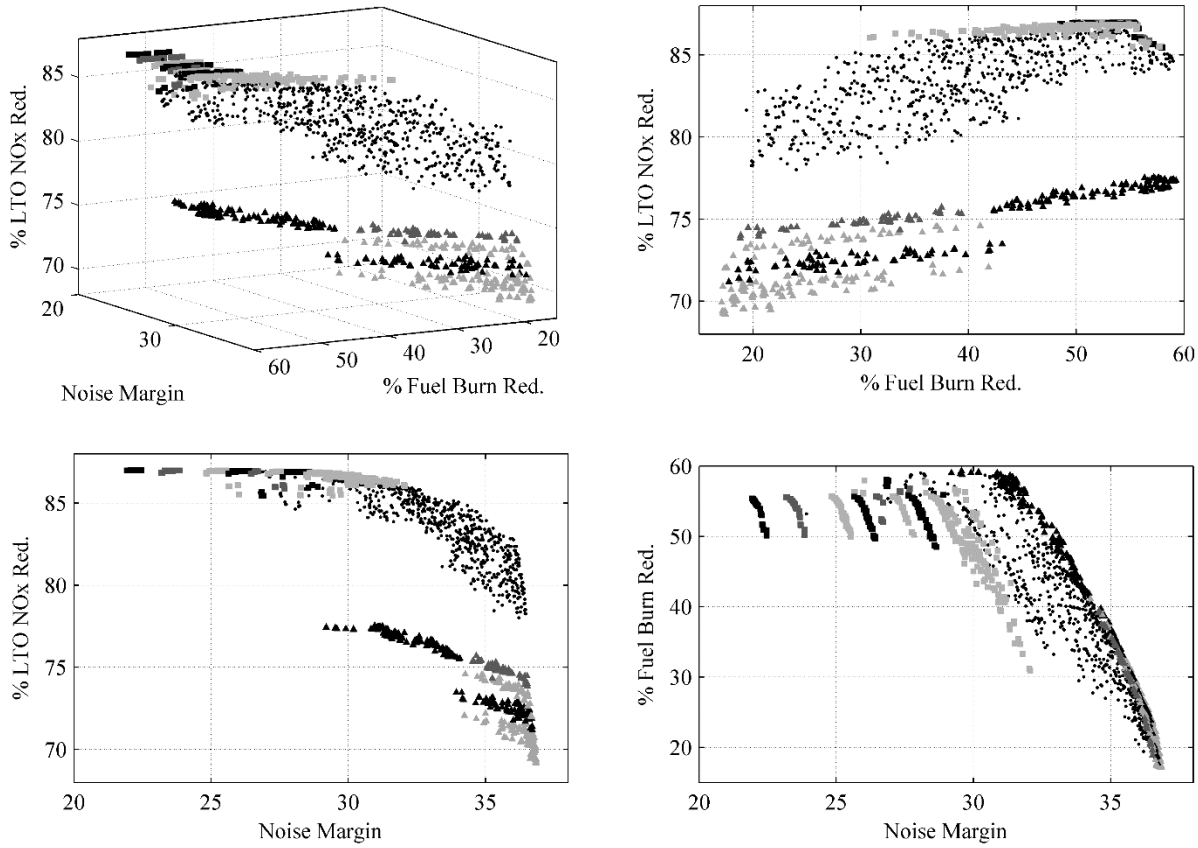

Figure 81. Pareto frontier of non-dominated technology combinations – data point greyscale and markers for feature differentiation purposes

7.2.4.2 Corners and Tradeoffs of the Technology Trade Space

The corners of the trade space are the regions of the Pareto frontier featuring solutions whose performance are among the best for one objective and among the worse for all others. They are relevant because they comprise the extremes of the Pareto frontier, and although they do not offer suitable solutions in most practical applications of multi-objective optimization, they offer a good basis upon which overarching objective tradeoffs are characterized.

Assuming that all three environmental performance objectives are in conflict, at least with respect to the technology pool under consideration, it is reasonable to expect that there are three corresponding corners. The 3-D data plot in Figure 81 indeed shows solutions populating the noise margin corner (solutions with the best noise margin, and the lowest reductions of NO_X and fuel burn). However, there is not a fuel burn or a NO_X reduction corner, but rather solutions featuring high reductions in fuel burn and NO_X concurrently, and poor noise margin. This can be attributed to the existence of solutions with high reduction of NO_X and fuel burn and their dominance over those with good performance in only one of two these objectives. Technology combinations comprising the fuel burn reduction and NO_X reduction corners indeed exist but are not preserved by the NSGA-II algorithm on account of being dominated. It is thus possible to

characterize the Pareto frontier in terms of a noise margin corner, a joint NO_X and fuel burn reduction corner, and the tradeoff between the two. In turn, understanding each of these features with regards to technologies, their effects, and the compatibility between them is most meaningful.

Technology combinations in the noise margin corner are found to contain all airframe and engine noise technologies with only a couple of exceptions. Also present are combustor technologies for NO_X, which indicates that inclusion of these two technologies is not sufficient to guarantee the highest NO_X reduction values; additional synergistic technologies impacting the engine cycle may be needed. It is worth noting that most of the airframe weight reduction technologies conducive to low fuel burn are absent, as are most engine technologies for fuel consumption reduction. These technology trends are expected, as the greatest noise margin values are obtained with quiet aircraft with a higher noise limit driven by a higher takeoff gross weight.

Solutions in the fuel burn and NO_X reduction corner feature an aggressive use of drag reduction technologies. Technologies in all solutions of this corner include higher aspect ratio wings enabled by structural technologies and spanwise load control, and adaptive wing control. Discrete roughness elements are also observed for all solutions in this corner, and are found to be exclusive to solutions featuring fuel burn reductions above ~35%. All the airframe weight reduction technologies are also featured in this corner, and advanced materials and structures are exclusive to this region of the Pareto frontier. As expected many engine technologies for specific fuel consumption are also featured in this corner, often times exclusively, including advanced engine component materials. Although both combustor technologies for NO_X are pervasive in this region we note that favorable NO_X reduction values result from their synergistic combination with engine technologies that allow for higher temperatures prior to the combustor inlet and/or that result in higher overall pressure ratio (OPR). This effect is explained in detail in following subsections. The more moderate engine noise technologies are also observed in this region and produce some clustering patterns discussed later. More aggressive engine noise technologies as well as most airframe noise technologies incur in fuel burn penalties and are not observed here.

The tradeoff between these two corners is realized by non-dominated combinations for which there is some inclusion /exclusion of compatible technologies relative to those governing each corner as described above. The degradations in noise margin allowing for greater reductions in fuel burn and NO_X can be readily appreciated in the 3-D plot of Figure 81. The plot for fuel burn reduction vs. noise margin reveals that that tradeoff between these two objectives is approximately linear across most values of NO_X reduction. The tradeoff between NO_X reduction and noise margin is somewhat richer in features. For values of noise margin between 22 and 30 dB NO_X reduction is almost invariant at 87% approx. In this region fuel burn reduction values are high, ranging between 45% and 55%. There is a smooth round tradeoff for noise margin values between 30 and 36 dB, where NO_X reduction ranges between ~87% and 83%. In this region the range of fuel burn reduction values broadens significantly and extends from 20 to 60%. For values of noise margin between 36 and 37 dB NO_X reduction drops sharply and almost linearly to approximately 69%. In this region the range of fuel burn reduction values collapses to from 20-60% to 15%.

7.2.4.3 NO_X Reduction - Compressor intercooler

One of the most obvious features of the Pareto frontier is the distinction of two major regions, one achieving significantly higher percent reduction in NO_X (round markers) over the

second one (triangular markers). Examination of the data reveals that higher NO_X reduction is attributed to the inclusion of the compressor intercooler, a technology that relaxes the compressor temperature limit and enables an increase in pressure ratio for higher fuel efficiency. This reduction in compressor airflow temperature propagates downstream and results in a lower temperature at the combustor inlet stage (T3), effectively reducing NO_X which is positively correlated with T3. In addition, the increase in compressor pressure ratio results in a higher value of OPR which in turn increases (relaxes) the CAEP/6 NO_X emissions limit value. The combination of lower NO_X amounts and a higher limiting value produces notably greater percent reductions.

7.2.4.4 NO_X Reduction through Active Control Compressor Technologies

Another noteworthy feature of the Pareto surface is the clustering of solutions into long parallel bands in the region of lower LTO NO_X reduction values. These solutions are shown in Figure 81 with triangular data points, and cluster differentiation through greyscale contrast. Data reveals that two engine technologies, namely active compressor clearance control and active compressor flow control, govern the emergence of these clusters. Both technologies increase the efficiency of the compressor which results in a reduction of combustor inlet temperature (T3) for a given pressure ratio (or alternatively allow for greater pressure increases at more modest temperature increases). Lower temperatures are ultimately manifested as lower NO_X emissions, or conversely as greater percent NO_X reductions. The four possible ways in which the two technologies can be combined yield the four corresponding clustering bands along the LTO NO_X reduction axis. Absence of both technologies leads to the lower LTO NO_X reduction values, whereas higher reduction values are achieved with the inclusion of both technologies. The latter also features two distinct regions that span the lower and upper half of fuel burn reduction values. Data results reveal that this additional segmentation and clustering stems from two mutually exclusive subsets of technologies for fuel burn reduction, one clearly less beneficial than the other with regards to that objective. Mutually exclusive subsets result from the pairwise compatibility rules defined for the complete pool of candidate technologies.

7.2.4.5 Noise Margin Improvements through Combinations of Engine Noise Technologies

A third noteworthy feature of the optimal set is the series of clusters forming a striated pattern on the high fuel burn reduction, high emissions reduction, and low noise margin corner. These clusters are most readily noted via greyscale differentiation in the top left corner of the plot for Fuel Burn Percent Reduction vs. Noise Margin in Figure 81. Inspection of these solutions reveal that discretization along the noise margin objective is produced by specific combinations of eight engine noise technologies. Six of them are passive such as noise-cancelling liners; two are active technologies featuring flow injection. From left to right clusters offer increasing noise margin as more engine noise technologies are added. The first cluster to the left does not include any of the eight engine noise technologies. Growing combinations of up to five passive technologies result in the subsequent seven solution clusters, all noted with greyscale differentiation. For the first four clusters to the left we note relatively consistent fuel burn reduction values ranging between 50% and 55% and consistent NO_X reduction at 87%. This

behavior is attributed to a fairly consistent set of fuel burn technologies in these clusters. For the next four data point clusters identified there is continuing increase in achieved noise margin along with a growing range of values fuel burn reduction, particularly for the eight cluster which spans between 30% and 60%, that can be attributed to a richer variety of fuel reduction technologies. In general each of these eight clusters encompass a two dimensional Pareto frontier with NO_X reduction approximately fixed at ~87% and a fixed subset of passive engine noise technologies where tradeoffs between noise margin and fuel burn reduction occur on the basis of what fuel burn technologies are included.

Beyond the eight identified cluster the trend of increasing noise margin and broader value ranges for fuel burn is observed to continue, albeit at the expense of small reductions in NO_X. In this central tradeoff region of the solution set the presence of numerous technologies governing performance on all objectives makes it impossible to discern distinct clusters for noise margin improvements. However we are able to broadly identify the progressive inclusion of active engine noise technologies beyond this point. Active technologies carry a fuel burn penalty that contributes, along with the inclusion and exclusion of many other technologies, to the increasing range of observed fuel burn reduction values.

7.2.4.6 Number of Technologies

It is pertinent to examine the number of technologies present in solutions of the Pareto frontier to determine any relevant correlation between the number of technologies and observed levels of performance. A 3-D plot of the Pareto frontier is shown in Figure 82 where darker shades of the greyscale denote an increasing number of technologies, ranging from 21 to 50. This number of technologies includes distinct applications of the same technology on different vehicle components such as advanced materials for different airframe elements. A consistent trend is observed with the number of technologies increasing from the noise corner of the trade space towards a region close to (but not exactly at) the fuel burn and NO_X reduction corner. This observation suggests noise margin in isolation is achievable with fewer technologies, whereas concurrent good performance of fuel burn and NO_X reduction is achievable albeit requiring a significant number of technological improvements. This trend is preserved across the two main regions of the Pareto frontier distinguished by the presence of the compressor intercooler. The technology combinations with the most technologies generally tend to favor engine fuel burn technologies, lightweight structures technologies, and airframe aerodynamic technologies that have few penalties.

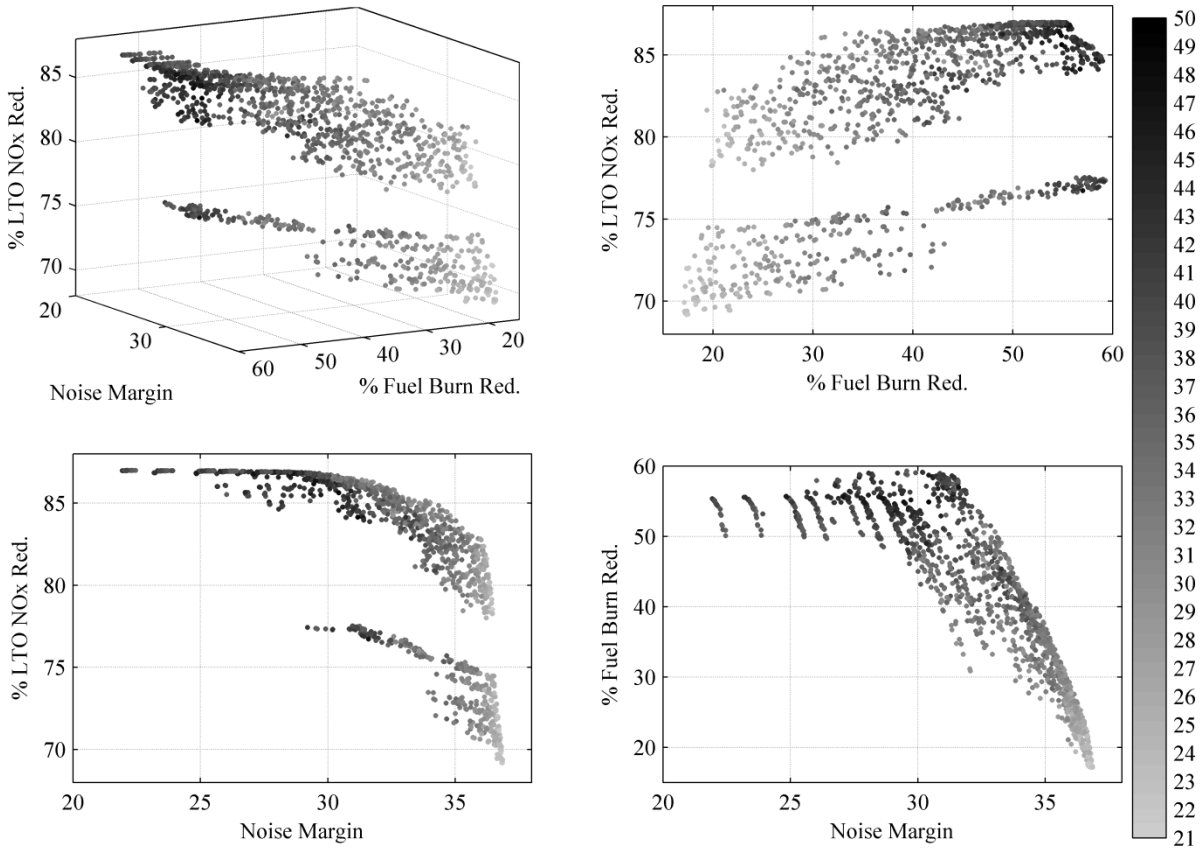

Figure 82. Pareto frontier of technology combinations indicating number of technologies present in each solution

7.2.4.7 Gap to N+2 Environmental Performance Goals

It is also pertinent to examine how solutions in the Pareto frontier approach the N+2 performance goals. The concurrent achievement of these goals is of particular relevance and defines a point in the objective space. The distance between solutions in the Pareto frontier and the N+2 goal point characterizes the remaining gap, if any, and more importantly provides a tool for the selection of a technology combination on the basis of minimizing this gap. This approach is well documented in the literature as the Euclidean distance to the ideal objective vector (see for instance Sen, 1998, p 26).

We estimate the normalized Euclidean distance to the N+2 goal point for all Pareto frontier solutions and color them accordingly in greyscale to identify the regions with the smallest gap. The 3-D plot is shown in Figure 83 Left. Closer proximity is denoted by darker greyscale, with the closest solutions in black. It is worth noting that the region of the Pareto frontier closest to the N+2 goal point is not that with the greatest number of technologies as can be noted by comparison with Figure 82, and where the compressor intercooler is not applied.

This observation can be explained in part by the fact that there are many solutions exceeding the fuel burn reduction and/or the NO_X reduction goal. The calculation of the Euclidean distance in the objective space does not assign preference or utility to the relative

location of a point of interest with respect to the reference (goal point). A larger margin above goal values contributes to a greater Euclidean distance. If selection is conducted on solely on the basis of this Euclidean distance then solutions closer to the goal are preferred over those farther away, including those that exceed a subset of goals. This approach is appropriate if indeed exceeding performance goal values presents a declining utility.

We correct this effect by defining the ideal objective vector in the classical formulation, namely as the maximum observed value along each individual objective, and then estimating the Euclidean distance to that point. The ideal objective vector is presented in Table 93 alongside N+2 goals. The 3-D plot of the Pareto frontier colored by Euclidean distance to the ideal objective vectors is shown in Figure 83 Right. As can be expected, comparison with Figure 82 indicates good correlation between proximity to the ideal objective vector and the number of technologies.

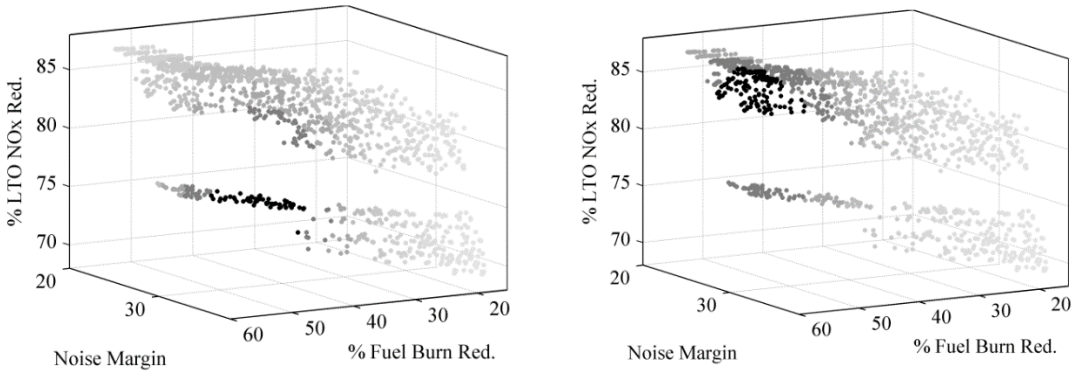

Figure 83. Pareto frontier of technology combinations with greyscale indicating Euclidean distance to N+2 goal vector (Left) and ideal objective vector (Right)

Table 93. Comparison of N+2 goals and ideal objective vector

Technology Benefits	N+2 Goals	Ideal Objective Vector
Noise (cum. Below Stage 4)	-42 dB	-37 dB
LTO NOx Emissions (below CAEP/6)	-75%	-87%
Aircraft Fuel / Energy Consumption (rel. to 2005 best in class)	-50%	-60%

7.2.4.8 Identification of Enabling Technologies

The Euclidean distance to a suitable reference vector in the objective space allows for the selection of a single technology combination. However, a more robust approach is to examine a top-ranking subset of solutions to identify the most frequently occurring technologies. Technologies identified in this manner comprise a portfolio that is common within the prescribed favorable region of the Pareto frontier and can provide some robustness against small uncertainties within this region. To do so we identify the top 30 technologies, or 2% of the population size, based on proximity to the N+2 goals and the ideal objective vector respectively,

and identify technologies present in at least 20 of the 30 combinations. Performance statistics for each set of 30 solutions are summarized in Table 94. Comparison of the two technology sets confirms that solutions near the ideal objective feature a more aggressive use of drag and weight reduction technologies that yield notably higher fuel burn and NO_X improvements, albeit at more modest noise margin. Engine technologies emerge as a common factor conducive to favorable tradeoff-optimal performance independent of the reference vector of choice.

Table 94. Performance statistics for top 30 (2%) solutions based on proximity to N+2 Goal and ideal objective

	Statistic	Fuel Burn Percent Reduction	NOX Percent Reduction	Noise Margin
N+2	Mean	48.4	76.3	33.165
	Max	51.53	76.9	33.68
	Min	45.53	75.65	32.56
Ideal Vector	Mean	56.86	84.6	30.94
	Max	58.69	85.4	31.64
	Min	55.16	83.9	30.33

7.2.5 Comparison of Vehicle Concepts' Technology Tradespace with Pareto-Optimal Sets

7.2.5.1 Formulation and Implemenation of the Comparative Assessment

The identification and analysis of the Pareto-optimal set of solutions for the 300-passenger Large Twin Aisle tube and wing concept was repeated for several other advanced vehicle concepts so as to conduct a comparative assessment. Said comparison subscribes to the view that an examination of the Pareto-optimal set reveals very insightful trends on the inherent performance tradeoffs between environmental objectives, and quantitatively bounds the capabilities of vehicle concept and the technology portfolio. By comparing entire Pareto-optimal sets rather than single design points the analysis explicitly accounts for the potentially realizable capabilities of the entire technology portfolio as applied to different vehicle concepts, offering a broader and more informed perspective. In turn the Pareto-optimal set of any vehicle concept can be examined in detail as documented in Section 7.2.4 for the Large Twin Aisle tube and wing concept.

7.2.5.2 Vehicle Concepts

Eight different vehicles are used in this study as technology collectors to contribute toward achieving the environmental performance goals. The conventional tube and wing vehicles are a basis of comparison for the other vehicles and are modeled based on what is flown today. The large twin aisle tube and wing is based off of similar parameters of the Boeing 777 and GE 90 engines. The large single aisle tube and wing is a smaller scale of this aircraft having a 150 passenger capacity. These two vehicles, the LTA and LSA, serve as a means to examine the scalability effects at the technology level and how they propagate in the generation of a Pareto optimal set. The other six vehicles are vehicles with variations in engine placement, replacement of the traditional geared turbofan engine with an open rotor engine, as well as vehicles with

exotic configurations. The conventional tube and wing vehicles including both the large twin aisle and large single aisle are configured with a different engine placement, fuselage mounted and over the wing nacelle concepts respectively. These engine placements are implemented in order to shield fan and jet noise sources. As well as changing the engine placement, an open rotor engine is a further alteration to the vehicle combinations, specifically applied to the large single aisle and the large twin aisle hybrid wing body. Exchanging the gear turbofan engine with an open rotor engine allows for an increase in propulsive efficiency thus cutting fuel consumption. One downfall of the open rotor engine is an increase of the overall noise of the aircraft, for this reason this engine is studied on the hybrid wing body in order to help mitigate the noise increase. The hybrid wing body configuration is also meant as a favorable aerodynamics and structural benefits due to good span loading. The inclusion of this configuration was inspired by the increasing studies of the hybrid wing body in recent years; although these studies gave insight to potential benefits of this aircraft, the configuration of this study was not a replica of work from these studies. Another exotic vehicle configuration used as a technology collector in this study is the box wing vehicle, this aircraft would offer low induced drag and alleged structural superiority, allowing the aircraft to achieve lower fuel consumption (Caja, 2012). Lockheed Martin as well as others have patents out for the study of this particular vehicle concept motivating the inclusion of this vehicle configuration in this study.

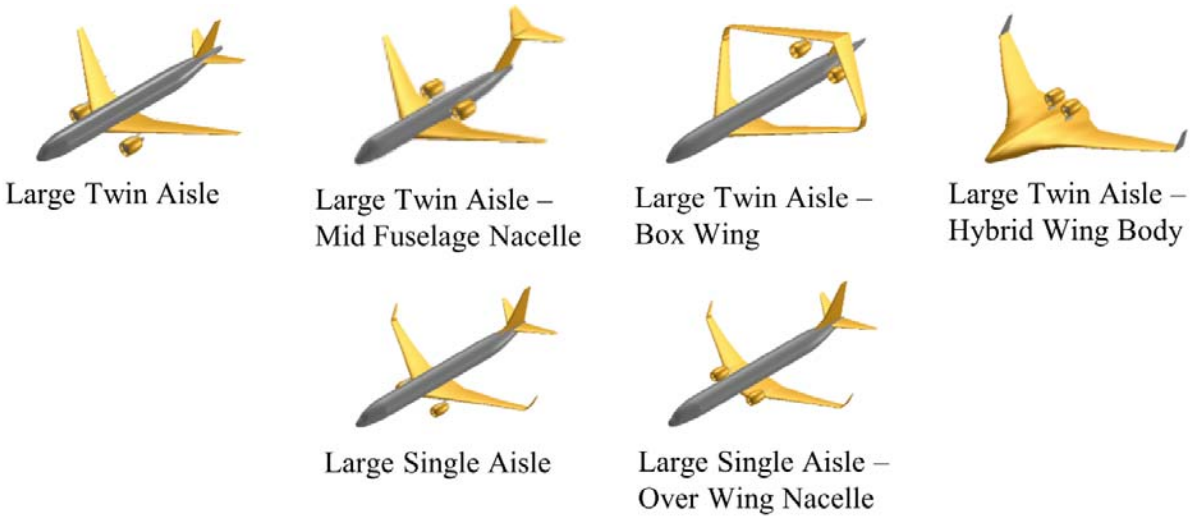

Figure 84. Vehicle concepts for Pareto-Optimal set comparison

7.2.5.3 Basis for Comparative Assessment of Pareto-Optimal Sets

A number of Pareto-optimal set characteristics are identified as the basis for the comparative assessment. The span of the Pareto set in the objective space offers a measure of the variability in performance along each environmental impact objective attributed to the technologies in the portfolio as applied to a vehicle concept. The location of the corners of the Pareto set in the objective space provide another basis for comparison in terms of extreme solutions providing the best achievable performance along any one objective. It helps compare concepts in terms of what is the best that can be achieved along each objective individually. The span of the Pareto set and location of the corners collectively inform whether solutions are able to meet or exceed individual N+2 goals.

The 'central' region of a Pareto set where optimal solutions offer a more balanced compromise relative to all objectives is typically of greater interest. In this application it is especially relevant because N+2 goals are defined to be met concurrently. These considerations are carried as a basis for comparison by means of the normalized Euclidean distance to the N+2 goal point in the objective space. This distance reflects how close any solution is to meeting all N+2 goals.

Examination of the Pareto surface also includes a characterization of clusters and features and ensuing analysis to identify underlying technology effects. In general clusters arise due to the discrete nature of the allowable combinatorial space for technologies manifested in the continuous objective space. In addition, technology incompatibilities yield larger discontinuities as mutually exclusive subsets of technologies are included or excluded from solutions as if they were a single option. The clusters are identified first by use of visual inspection and then verified by the use of hierarchical clustering with distance-based criteria such as average and centroid. By identifying technologies or technology combinations that cause the clusters or features of the Pareto frontier we know what is required to achieve the values of objectives that are represented in those features.

The numbers of technologies are evaluated for each combination within the Pareto set. The points where the greatest and least amounts of technologies are taken note of and then any visible trends are identified and examined against other features of the Pareto surface. The amount of technologies within a set can be considered less attractive than a smaller subset of technologies due to the increase in cost. Although this is not a direct correlation it is still an important gauge of which set of technologies should be investigated more to invest in.

7.2.5.4 Comparative Assessment for Vehicle Concepts

A superposition of Pareto sets for all vehicle concepts is shown in Figure 85. In general, the variability observed for any objective, or tradeoffs between objectives, within a Pareto set can be exclusively attributed to technology effects. On the other hand the difference observed between Pareto sets along any objective can be exclusively attributed to vehicle concept configuration. Pareto set span values are summarized in Table 95.

It is readily evident that, in general, variability in noise margin capabilities attributed to vehicle concept configuration are significantly greater than those attributable to technology impacts. Vehicle concepts featuring engine noise shielding, namely the HWB LTA, MFN LTA, and OWN LSA, have "flatter" Pareto frontiers along the noise margin axis and are located on higher noise margin values. This indicates that vehicle concept noise shielding features have a dominant effect on noise margin and yield the most benefits. It further suggests that noise shielding effects overwhelm, and therefore diminish, the sensitivity to technology effects which are typically of a much more moderate order of magnitude. This trend is less accentuated for the OWN LSA, suggesting that these effects and configuration benefits don't scale down favorably. This may be explained in part by the fact that noise margin is reference to takeoff gross weight, and that for LTA vehicle the greater gross weight relaxes the noise limit and allows for greater margins. Effects of a greater engine noise source for LTA vehicles may not be important given the shielding effects. For aircraft without noise shielding features Pareto frontiers are less flat and more curved along the noise margin axis, suggesting a greater sensitivity to noise technology effects relative to vehicles with noise shielding. They are also located at lower noise margin values. The most extreme case is clearly the LSA UDF where there is no shielding, and the intense noise source of the UDF engine governs the relatively poor noise performance of the

concept. The LTA HWB UDF concept presents an interesting compromise, showing noise margin values comparable to the LTA, LSA, and LTA BW.

For the fuel burn reduction and NOx reduction objectives significant variability can be attributed to the engine cycle/architecture, namely GTF or UDF. For concepts with the same engine variability is attributed to technology effects and airframe concept. These trends are most easily visualized as a superposition of the convex hull of all Pareto frontiers along the two objectives in question, as shown in Figure 86. It is readily evident that concepts with UDF feature distinctively lower values of NOx % reduction relative to concepts with the GF, although the upper bound of fuel burn reduction values are comparable for the two engine concepts. For concepts with the GF or UDF, separately, the effect of vehicle concept is most readily observed as modest differences in the range of values for these two objectives. For concepts with the GF engine tt can be noted that all vehicles have roughly the same bounds and span of values for NOx reduction and fuel burn reduction. We note however that the LTA HWB features the greatest fuel burn reduction maxima and, more notably, greatest minima, altogether suggesting the best fuel burn values on average. The LSA concepts consistently show lesser fuel burn reduction maxima.

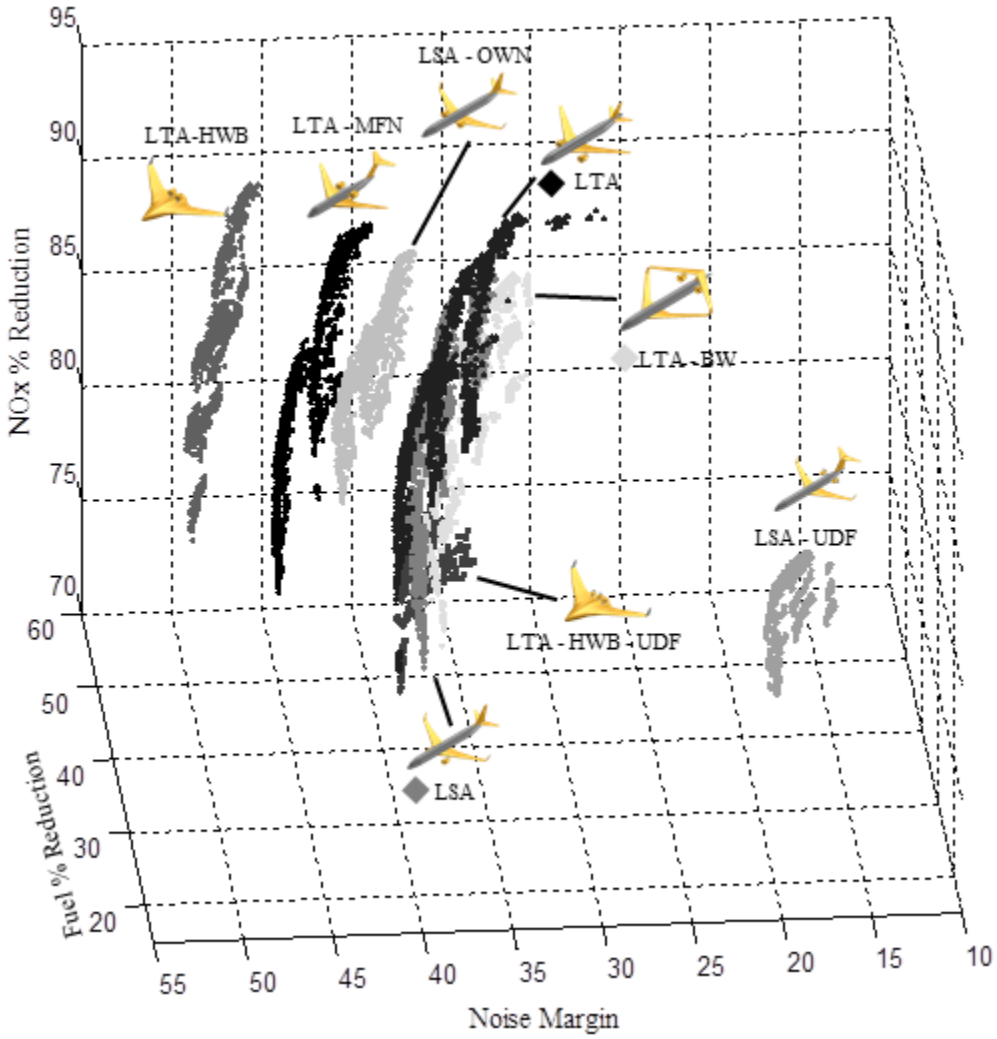

Figure 85. Superposition of Pareto sets for vehicle concepts in the objective space

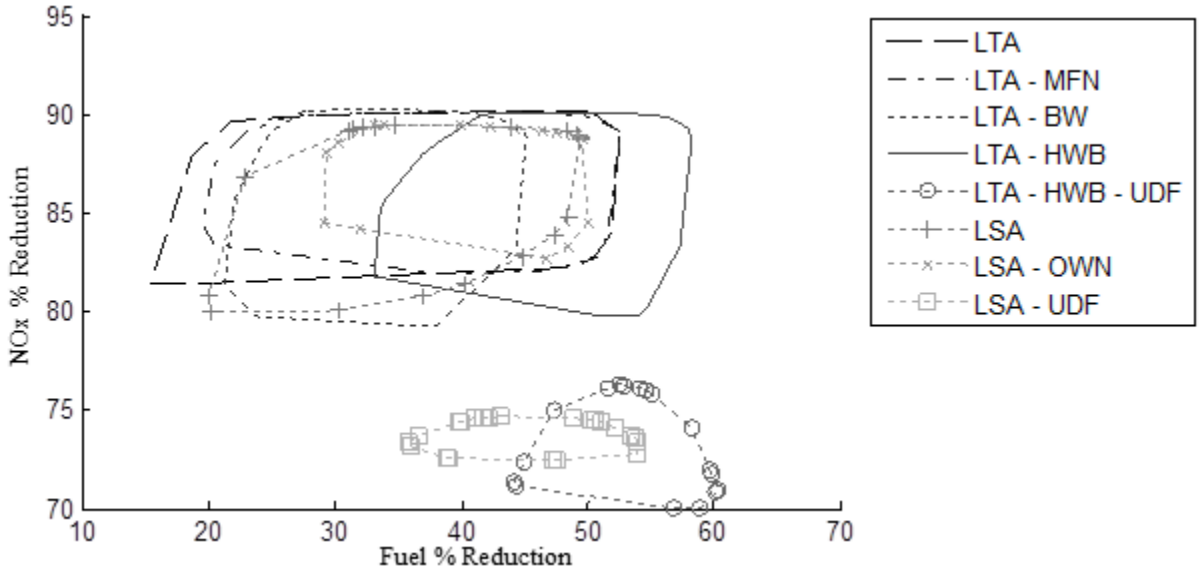

Figure 86. Superposition of vehicle concept Pareto set convex hull projections in NOX percent reduction vs fuel burn percent reduction

For all vehicles key technologies were identified as responsible for some of the most prominent clustering features observed in the Pareto frontier. Pareto set ranges and clustering technologies for all vehicle concepts are presented in Table 95. Corresponding 3D isometric scatter plots of Pareto frontiers for all vehicle concepts, with data points grey-scale coded as noted in Table 95, are shown in Figure 87 for concepts with the GF, and in Figure 88 for concepts with the UDF. It is obvious that there are similar technologies that govern the main features/clusters of each vehicle, including the compressor intercooler, blade tone control, fan vertical acoustic splitter, and the electro mechanical flight control actuators. The compressor intercooler, as stated previously, impacts the NO_X percent reduction by effectively lowering the temperature at the combustor inlet (T3). The blade tone control technology was also previously mentioned in the study of the noise corner of the large twin aisle. This technology reduces the vortices that propagated downstream which cause tonal noise as a result of pressure perturbations on stators and duct acoustic modes, thus improving the noise margin values.

Table 95. Pareto set ranges and clustering technologies for vehicle concepts

Vehicle	FB Range	NOx Range	Noise Margin Range	Cluster Technologies
LTA	15-53%	81-90%	27-41dB	Black = Compressor Intercooler OFF Blade Tone Control via Trailing Edge Blowing ON Light Gray = Compressor Intercooler ON Blade Tone Control via Trailing Edge Blowing ON Med. Gray = Compressor Intercooler ON Blade Tone Control via Trailing Edge Blowing OFF
LTA-MFN	19-53%	82-90%	39-48dB	Black = Compressor Intercooler ON

				Light Gray = Compressor Intercooler OFF
LTA-BW	21-45%	79-90%	32-38dB	Black = Compressor Intercooler OFF Blade Tone Control via Trailing Edge Blowing OFF Fan Vertical Acoustic Splitter ON Light Gray = Compressor Intercooler OFF Blade Tone Control via Trailing Edge Blowing ON Fan Vertical Acoustic Splitter OFF Mid gray = Compressor Intercooler ON Blade Tone Control via Trailing Edge Blowing ON Fan Vertical Acoustic Splitter OFF Dark Gray = Compressor Intercooler ON Blade Tone Control via Trailing Edge Blowing OFF Fan Vertical Acoustic Splitter OFF
LTA-HWB	33-58%	80-90%	45-51dB	Black = Compressor Intercooler ON Light Gray = Compressor Intercooler OFF
LSA	20-49%	80-89%	33-39dB	Black = Compressor Intercooler OFF Blade Tone Control via Trailing Edge Blowing OFF Fan Vertical Acoustic Splitter ON Light Gray = Compressor Intercooler OFF Blade Tone Control via Trailing Edge Blowing ON Fan Vertical Acoustic Splitter OFF Mid gray = Compressor Intercooler ON Blade Tone Control via Trailing Edge Blowing ON Fan Vertical Acoustic Splitter OFF Dark Gray = Compressor Intercooler ON Blade Tone Control via Trailing Edge Blowing OFF Fan Vertical Acoustic Splitter OFF
LSA-OWN	29-50%	83-89%	37-43dB	Black = Compressor Intercooler OFF Blade Tone Control via Trailing Edge Blowing ON Fan Vertical Acoustic Splitter OFF Light Gray = Compressor Intercooler OFF Blade Tone Control via Trailing Edge Blowing OFF Fan Vertical Acoustic Splitter OFF Mid Gray = Compressor Intercooler ON Blade Tone Control via Trailing Edge Blowing ON Fan Vertical Acoustic Splitter OFF Dark Gray = Compressor Intercooler ON Blade Tone Control via Trailing Edge Blowing OFF Fan Vertical Acoustic Splitter OFF
LSA-UDF	36-54%	72-75%	14-19dB	Black = Electro Mechanical OFF Light Gray = Electro Mechanical ON

LTA-HWB-UDF	44-60%	70-76%	33-39dB	Black = DRE for HLFC – Wing OFF Mid Gray = DRE for HLFC ON HLFC Suction – Wing OFF Light Gray = All other points

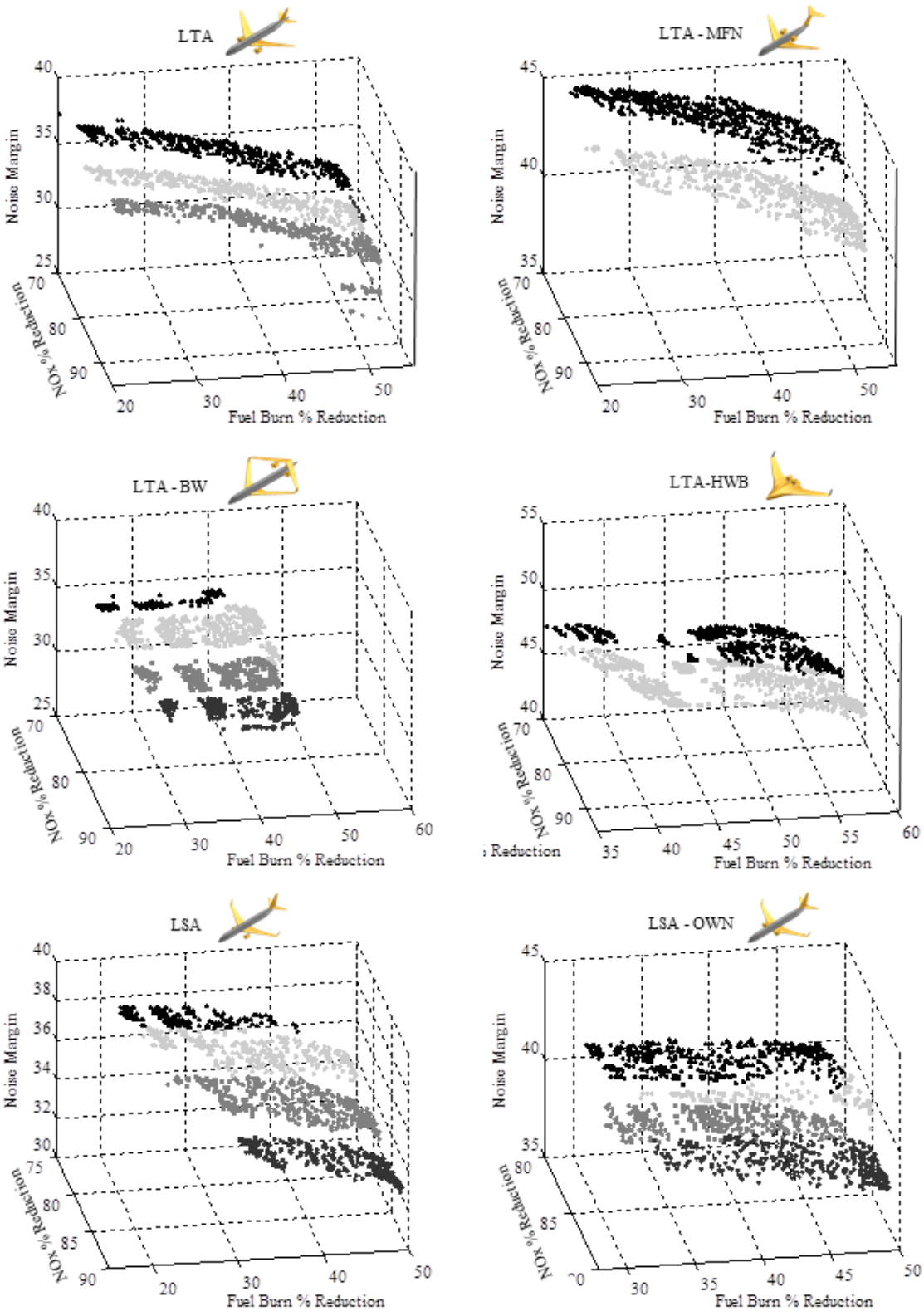

Figure 87. Pareto set clustering associated with identified influencing technologies - GF

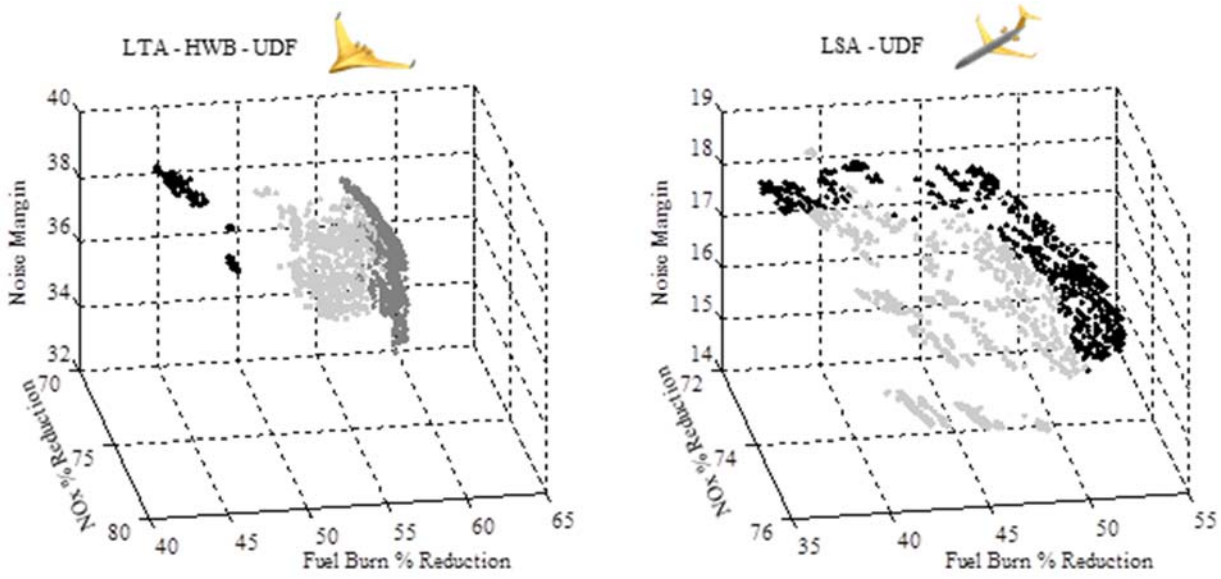

Figure 88. Pareto set clustering associated with identified influencing technologies - UDF

The number of technologies present in each of the points of the Pareto front is also examined. Corresponding 3D isometric scatter plots of Pareto frontiers for all vehicle concepts, with data points grey-scale coded to indicate a smaller (darker data points) or larger (lighter data points) number of technologies are shown in Figure 89 for concepts with the GF, and in Figure 90 for concepts with the UDF. Comparative assessment of all Pareto fronts indicate the same general trend for all vehicles where there is an increase in number of technologies with proximity to fuel burn and NOx corner.

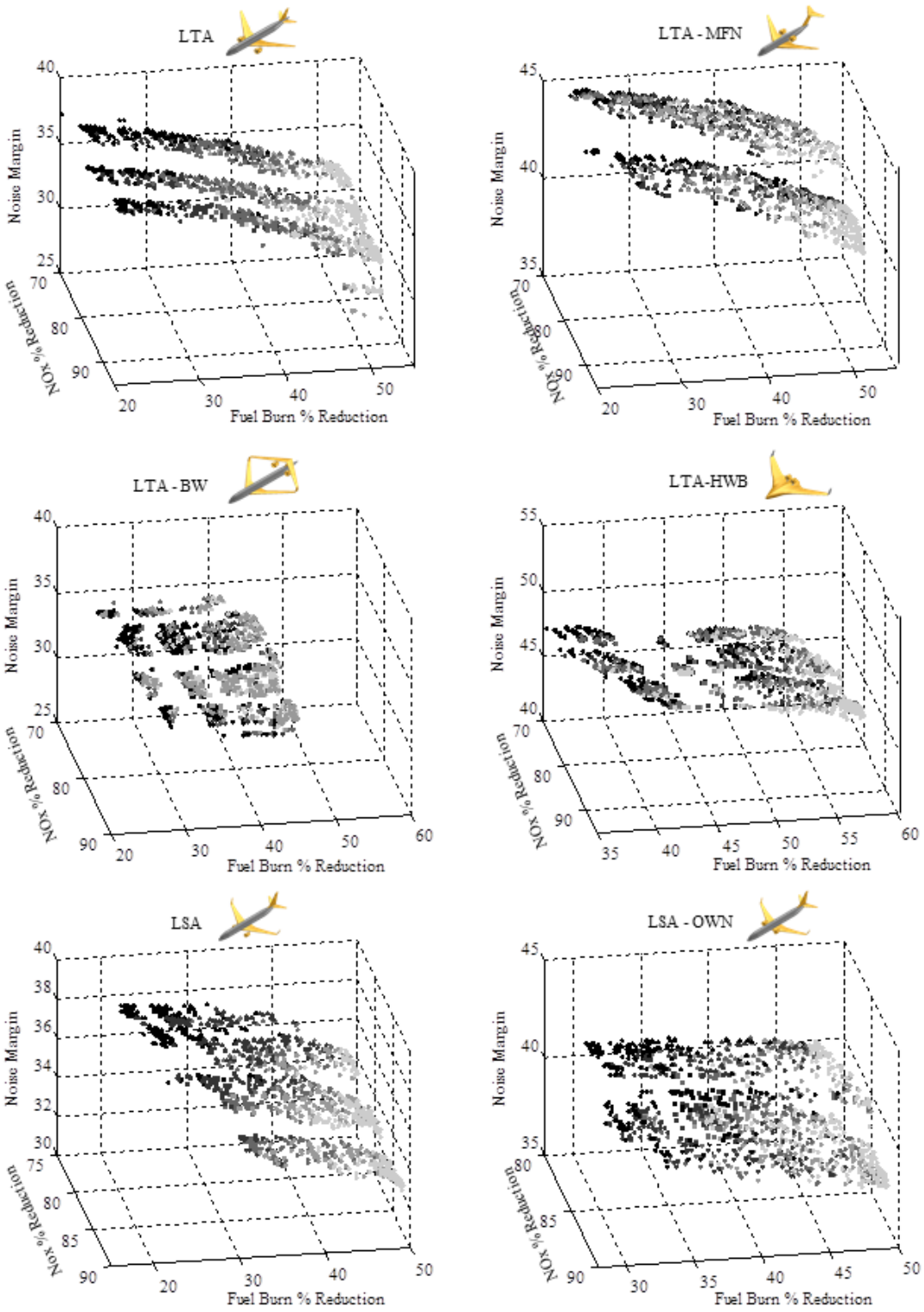

Figure 89. Trends in the number of technologies per solution in Pareto optimal sets - GF

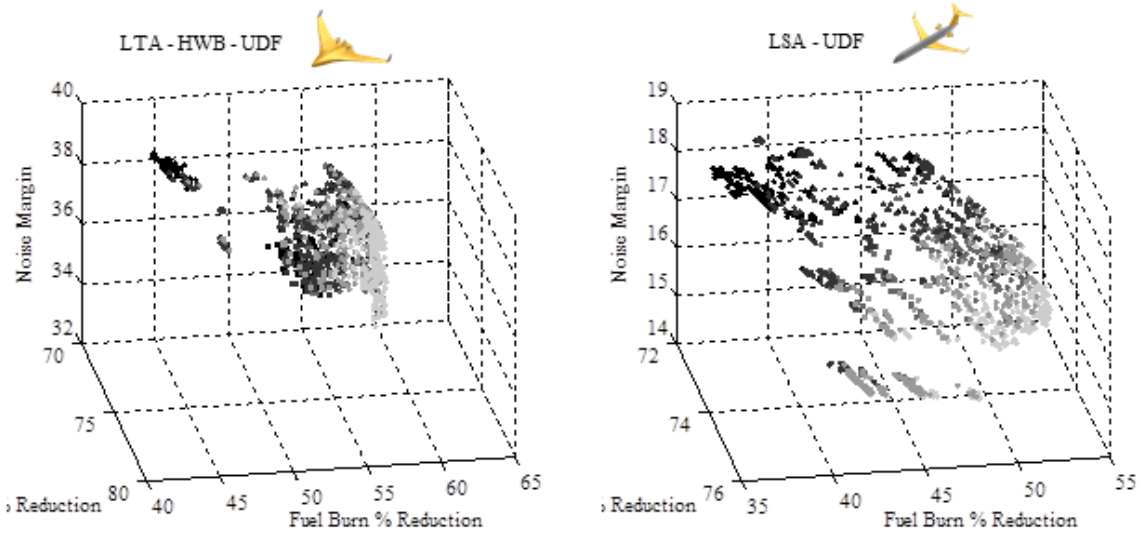

Figure 90. Trends in the number of technologies per solution in Pareto optimal sets - UDF

Broad impact critical technologies are identified as those that appear in all solutions of the Pareto set for all vehicle concepts. There is a total of sixteen technologies meeting this criterion. They are presented in Table 96, where they are organized by technology impact area. Results suggest the importance of engine fuel burn and noise technologies areas.

Table 96. Broad impact critical technologies appearing in all Pareto-optimal solutions for all vehicle concepts

Vehicle Set	Impact Area	Amt. of Techs	Representative Technologies
All 8 Vehicles	Engine Fuel Burn	5	Advanced TBC Coatings - HPT Blade
			Advanced TBC Coatings - LPT Blade
			Polymer Matrix Composites (PMC) - Nacelles
			PMC Fan Blade with Metal Leading Edge
			Highly Loaded LP Turbine
	Engine Noise	2	Combustor Noise Plug Liner
			Active Pylons Shaping/Blowing
	Engine Emission Tech	1	RQL Combustor
	2010 Baseline Techs	2	Zero Splice Inlet
			Excrescence Reduction
	Other	2	Blisk
			Ti-Al - LPT Aft Blades
GTF Only	Engine Fuel Burn	3	Polymer Matrix Composites (PMC) - Fan Case
			Polymer Matrix Composites (PMC) - Fan Stator
			Polymer Matrix Composites (PMC) - Bypass Duct
	Engine Noise	3	Aft Cowl Liners
			Compound Rotor Sweep for UHB Fan (GTF)
			Variable Area Nozzle - GTF
	2010 Baseline Techs	1	Fixed Geometry Core Chevrons
UDF Only	Engine Fuel Burn	2	Active Turbine Clearance Control
			Active Compressor Clearance Control
	Engine Noise	1	Lip Liner

7.3 Technology Portfolio Performance Comparison to ERA Goals

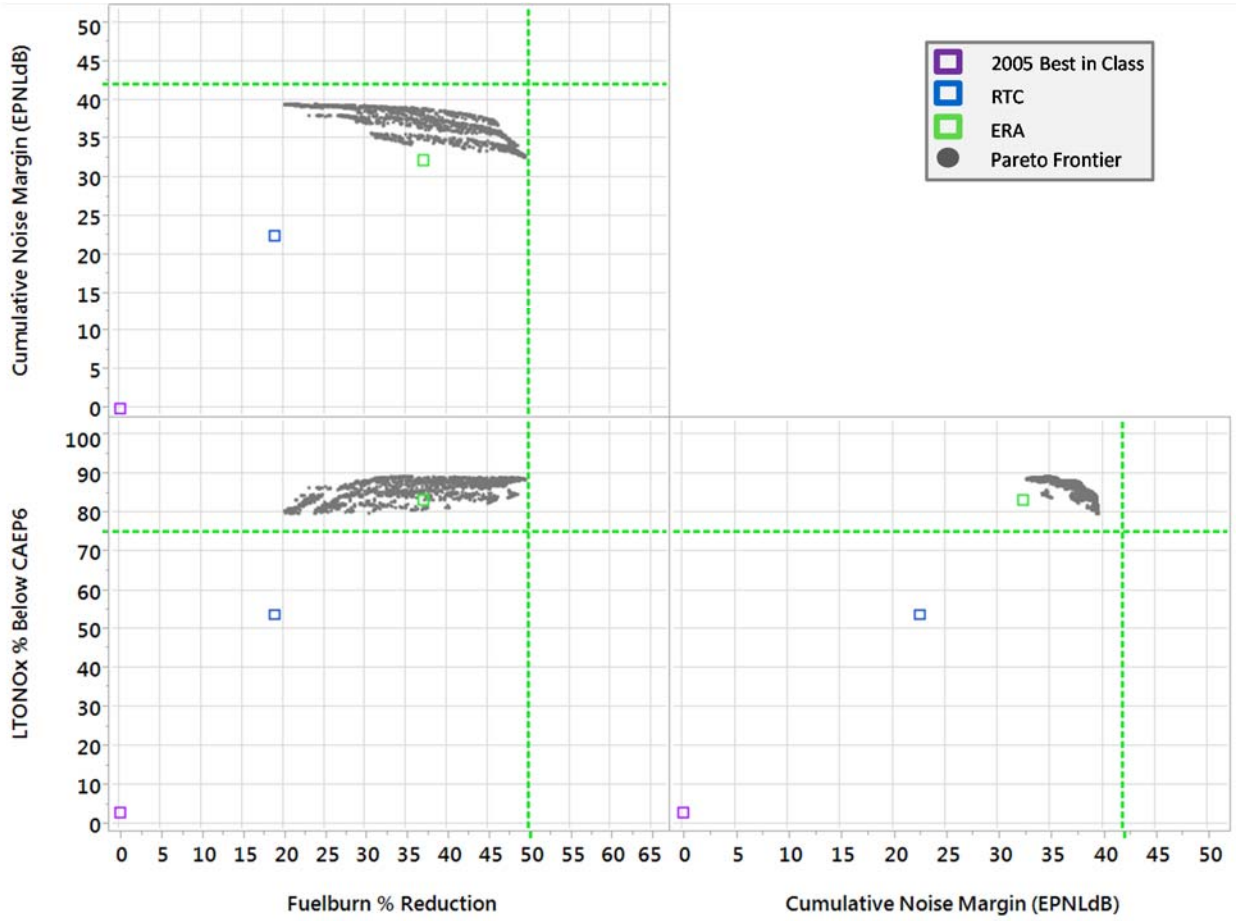

Figure 91. LSA T&W Technology Portfolio Performance

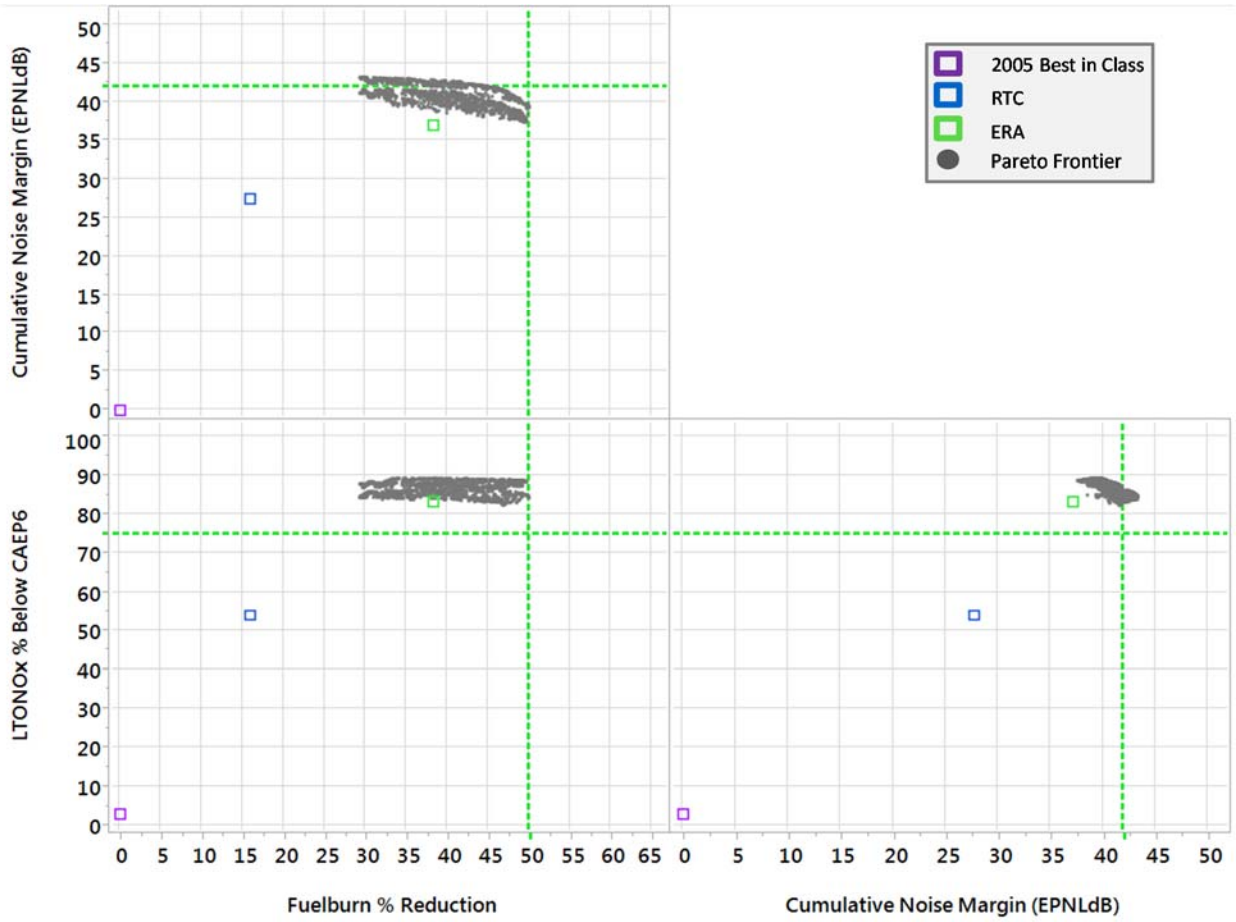

Figure 92. LSA OWN Technology Portfolio Performance

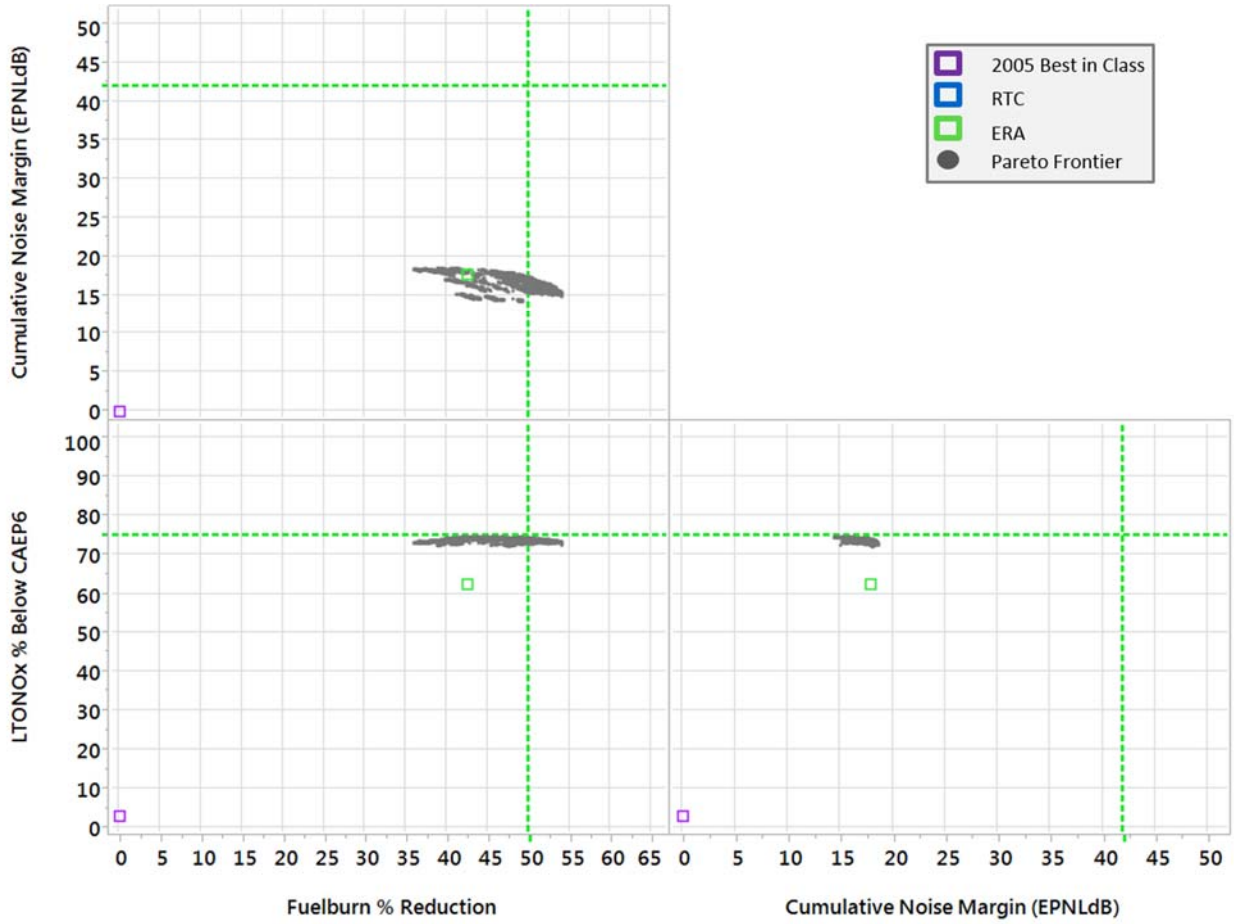

Figure 93. LSA OR Technology Portfolio Performance

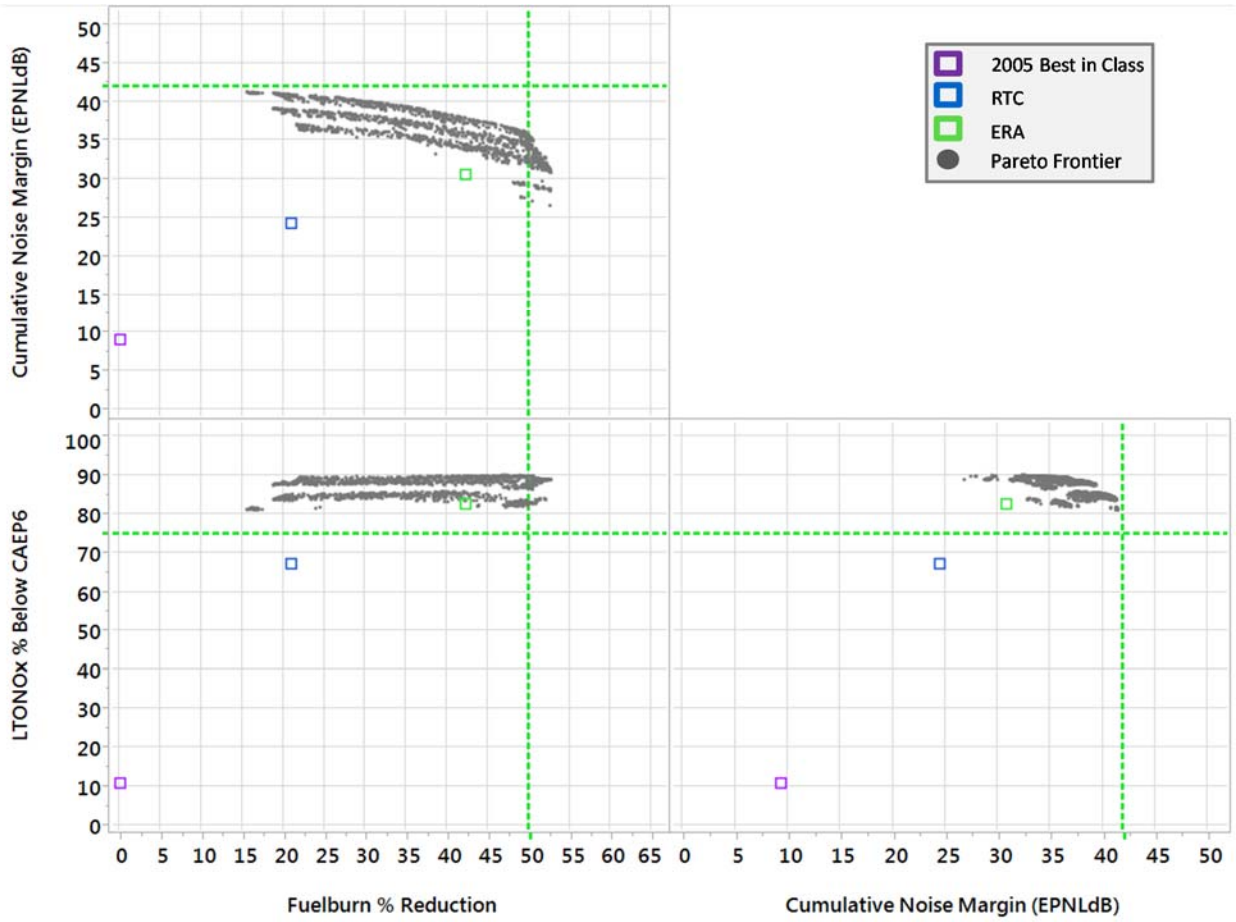

Figure 94. LTA T&W Technology Portfolio Performance

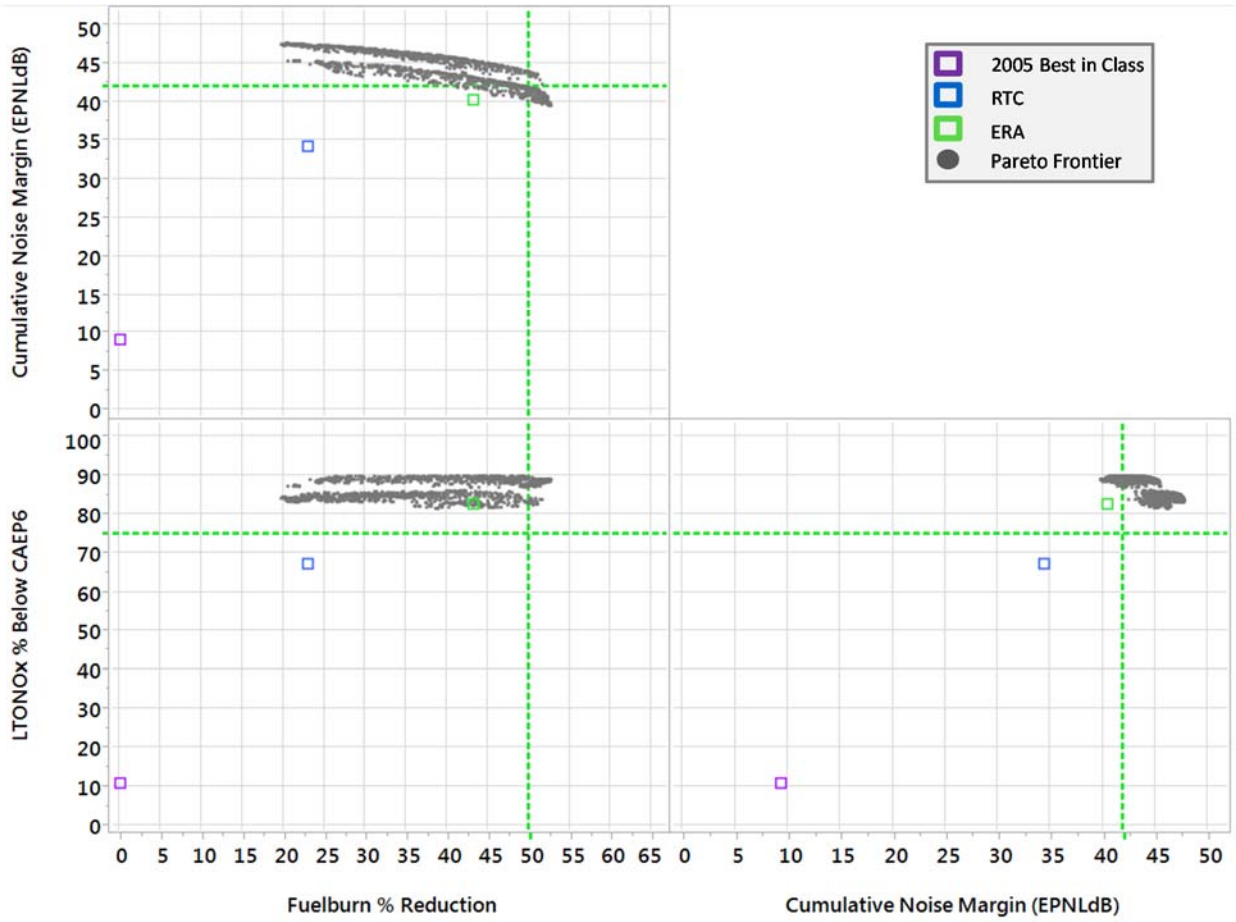

Figure 95. LTA MFN Technology Portfolio Performance

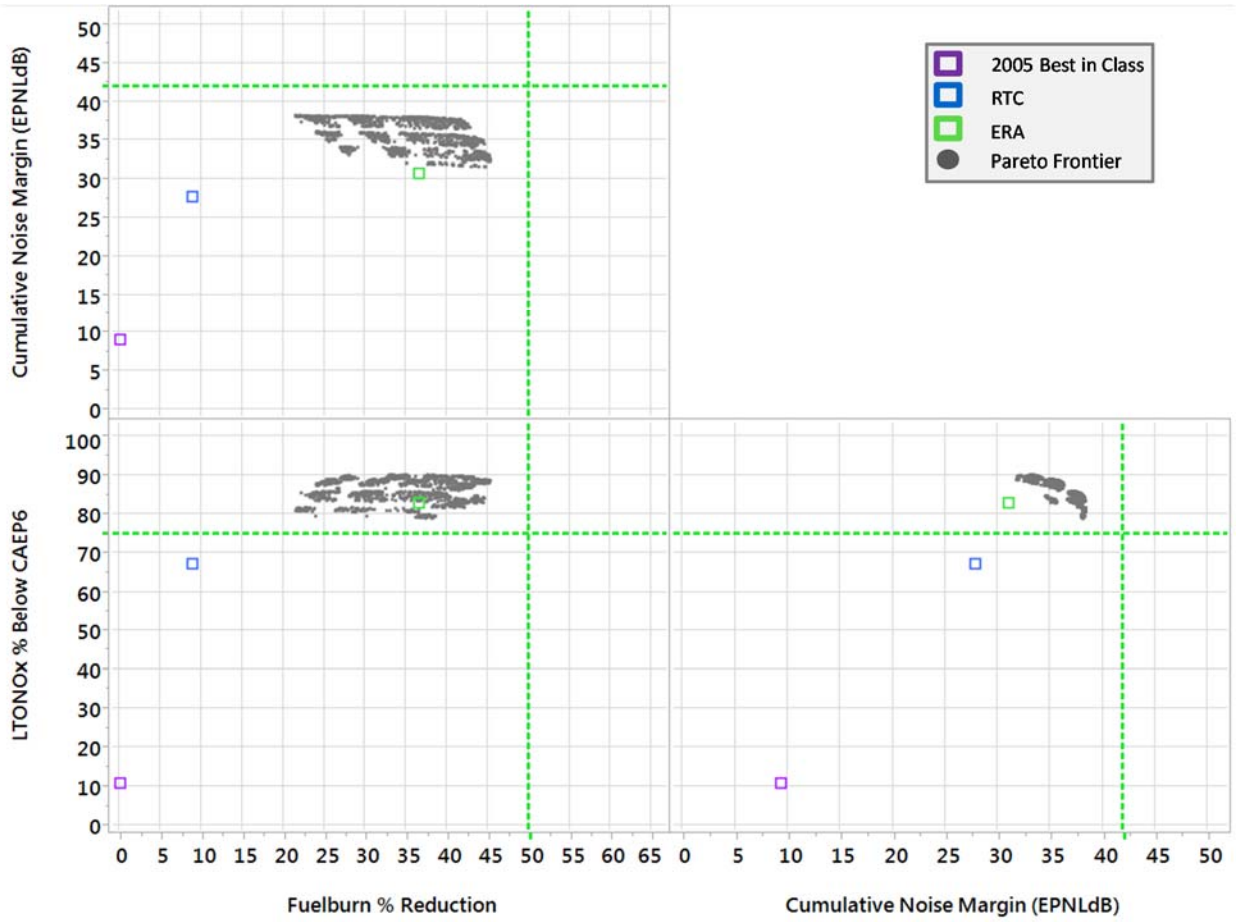

Figure 96. LTA BW Technology Portfolio Performance

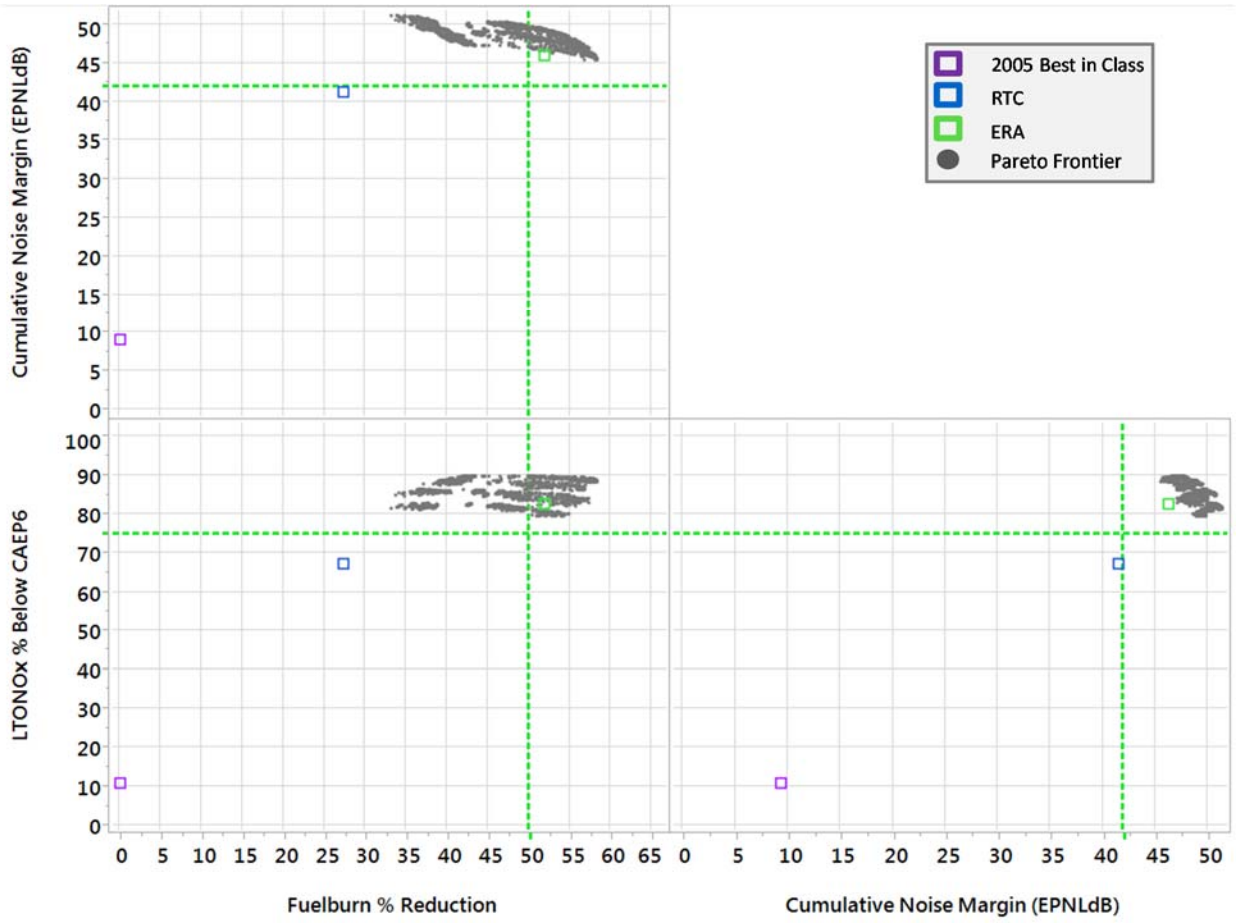

Figure 97. LTA HWB Technology Portfolio Performance

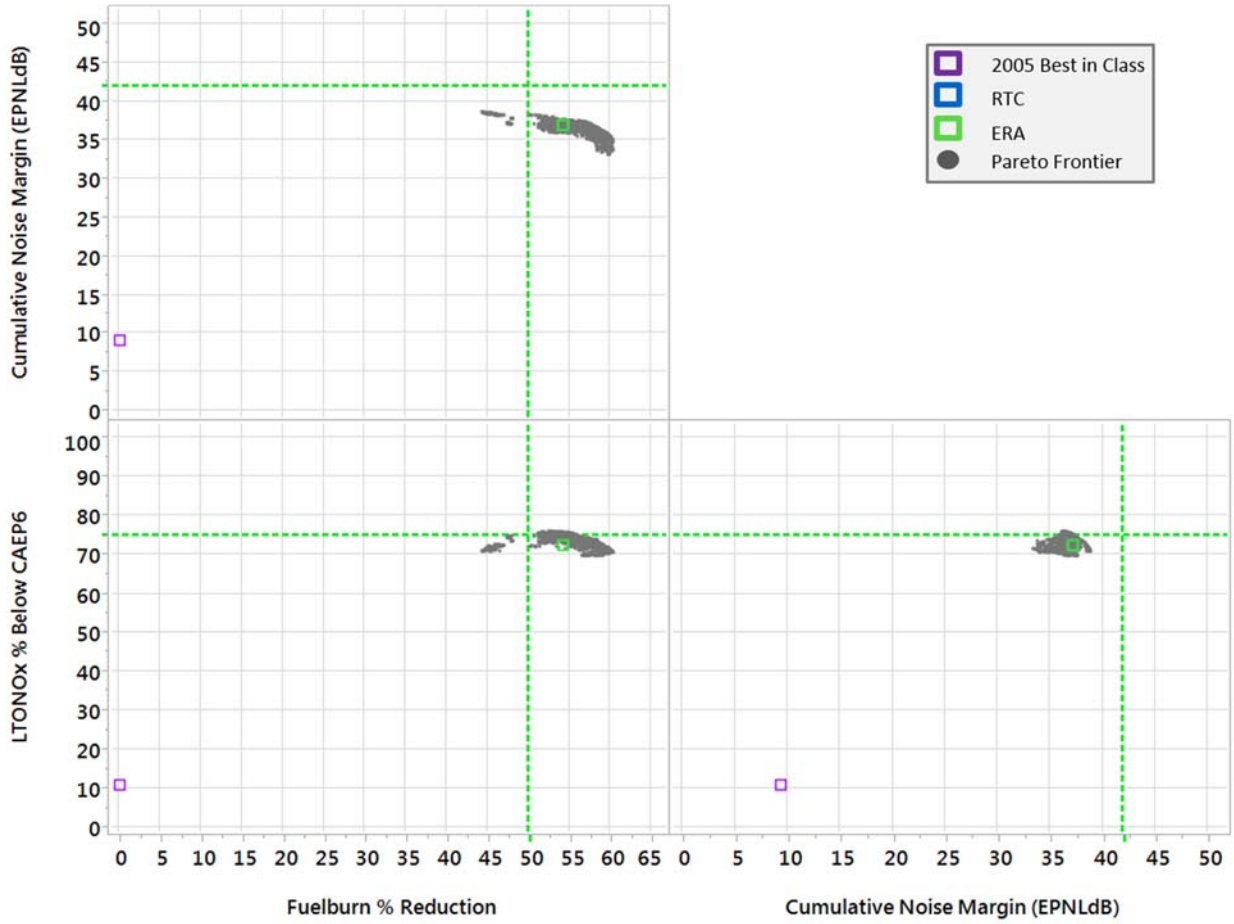

Figure 98. LTA HWB OR Technology Portfolio Performance

7.4 Comparison of ERA Technologies to Goal

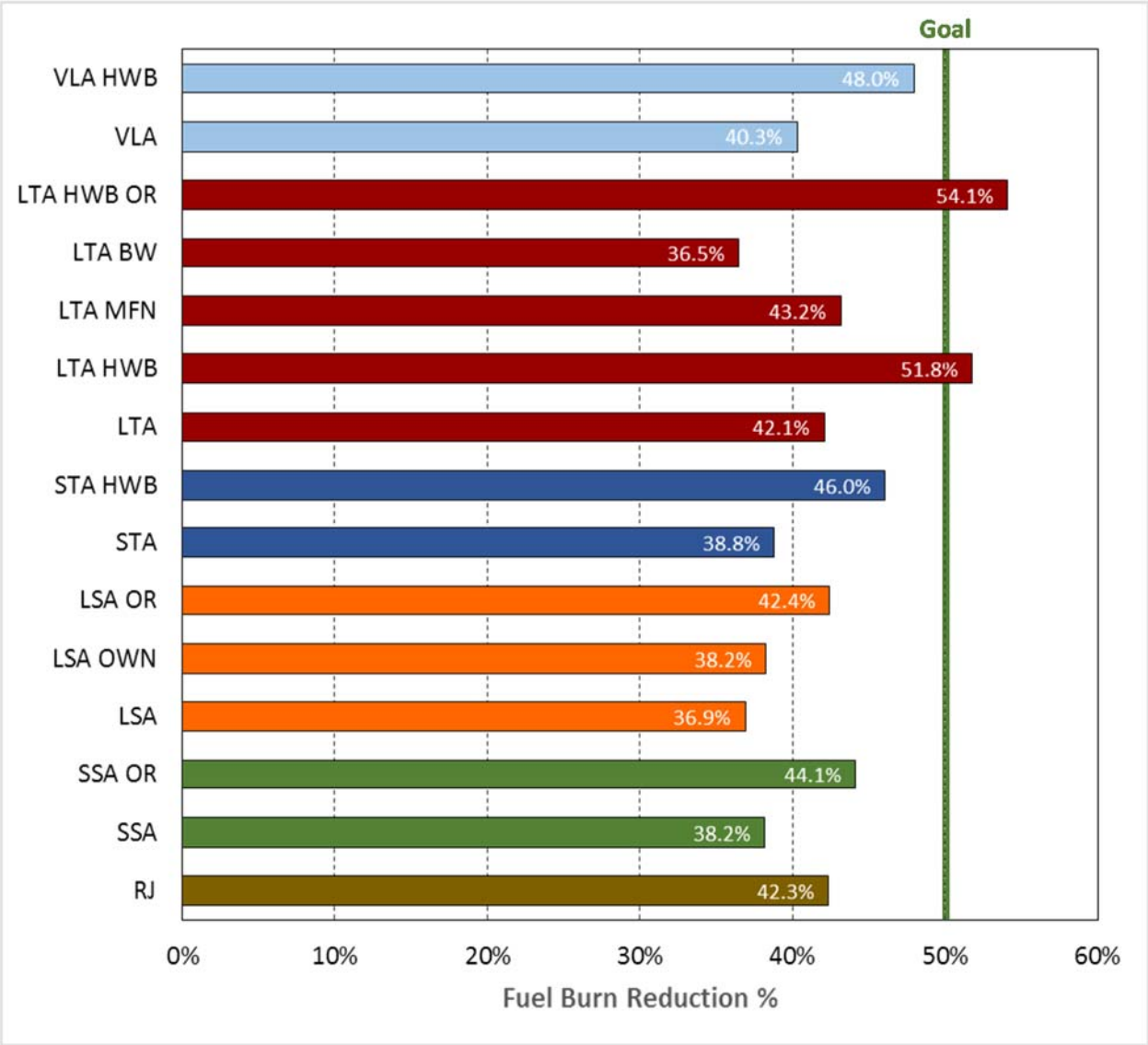

Figure 99. ERA Comparison to Fuel Burn Goal

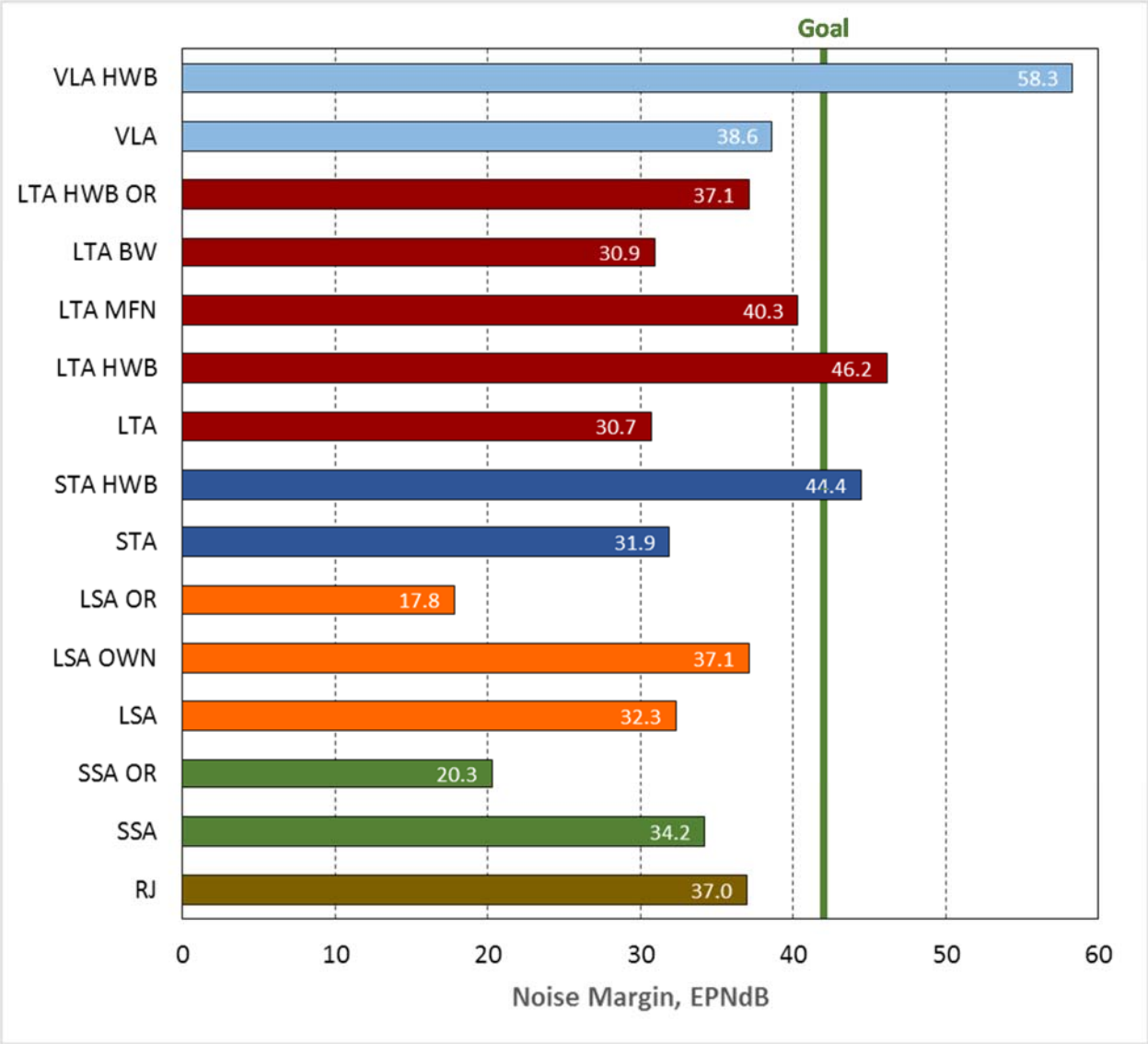

Figure 100. ERA Comparison to Noise Margin Goal

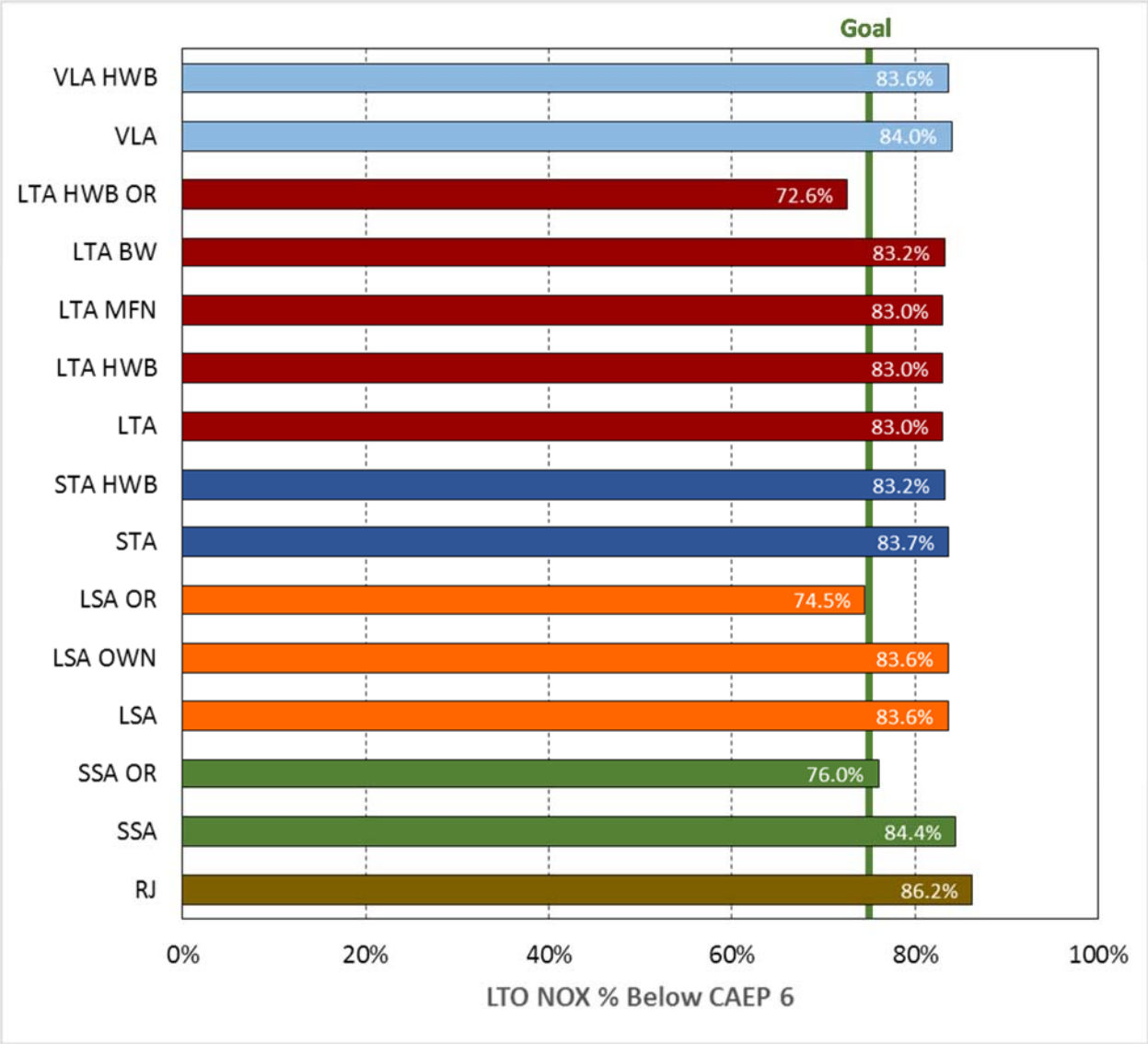

Figure 101. ERA Comparison to Emissions Goal

8.0 References

[Abbas 2008] Ali E. Abbas, David V. Budescu, Hsiu-Ting Yu, Ryan Haggerty, "A Comparison of Two Probability Encoding Methods: Fixed Probability vs. Fixed Variable Values"; Decision Analysis Vol. 5, No. 4, December 2008, pp. 190–202

[Adelman 1986] Howard M. Adelman, Raphael T. Haftka, "Sensitivity Analysis of Discrete Structural Systems" AIAA Journal, May 1986, Vol.24: 823-832

[Akram 2011] Farooq Akram, Matthew Prior, Dimitri Mavris, "An Improved Methodology for Gas Turbine Technology Portfolio Planning, Including Technology Synergy Matrices and Real Options Analysis" 49th AIAA Aerospace Sciences Meeting including the New Horizons Forum and Aerospace Exposition, Jan 2011, AIAA 2011-578

[Ananthasayanam 2005] Ananthasayanam,A., Sarkar,A., "The Necessary and Useful Feature of Subjectivity in Estimation Theory" Jan 2005, AIAA 2005-1076

[AVID 2014] AVID APEX, AVID LLC, http://www.avidaerospace.com/software/avid-apex, cited on October 10, 2014

[Batson 1988] Batson R. G., Love R. M., "Risk Analysis Approach to Transport Aircraft Technology Assessment," Journal of Aircraft, American Institute of Aeronautics and Astronautics, Vol. 25, No. 2, February, 1988, pp. 99-105

[Bellocq 2010] Bellocq, et al., "Advanced Open Rotor Performance Modeling For Multidisciplinary Optimization Assessments," ASME GT2010-22963.

[Berton 2010] Berton, J., and Guynn, M., 2010, "Multi-Objective Optimization of Turbofan Design Parameters for an Advanced, Single-Aisle Transport". 10th AIAA Aviation Technology, Integration, and Operations (ATIO) Conference, September.

[Berton 2011] Berton, J., "Empennage Noise Shielding Benefits for an Open Rotor Transport," 17th AIAA/CEAS Aeroacoustics Conference, June 2011, AIAA 2011-2764.

[Biermann 1942] Biermann, D., Gray, W.H., Maynard, J., D., "Wind-Tunnel Tests of Single and Dual-Rotating Tractor Propellers of Large Blade Width," NACA Wartime Report, September 1942

[Bird 1994] G. A. Bird, Molecular Gas Dynamics and the Direct Simulation of Gas Flows, Volume 1, Clarendon Press, 1994

[Bradley 2004] Bradley, K. R.: "A Sizing Methodology for the Conceptual Design of Blended-Wing-Body Transports," NASA/CR-2004-213016, September 2004.

[Brooks 1983] Brooks D. G., O'Leary T. J., "A Comparison of Encoding Techniques," OMEGA The International Journal of Management Science, Vol. 11, No. 1 pp 49-55, 1983

[Bonet 2011] John T. Bonet, Harvey G. Schellenger, Blaine K. Rawdon, Kevin R. Elmer, Sean R. Wakayama,Derrell L. Brown, Yueping Guo, 2011, NASA/CR-2011-XXXXXX, Environmentally Responsible Aviation (ERA) Project – N+2 Advanced Vehicle Concepts Study and Conceptual Design of Subscale Test Vehicle (STV), Boeing Research & Technology, Huntington Beach, CA

[Box 1987] George E. P. Box, Norman Richard Draper "Empirical model-building and response surfaces" Wiley, 1987

[Buttazzo 2009] Guido Buttazzo, Aldo Frediani, Best Wing System: An Exact Solution of the Prandtl's Problem, Variational Analysis and Aerospace Engineering, Springer Optimization and Its Applications, Vol. 33, 2009, DOI 10.1007/978-0-387-95857-6_11

[Caja 2012] Caja, R. and Scholz, D., "Box Wing Flight Dynamics in the Stage of Conceptual Aircraft Design," Deutsche Gesellschaft fur Luft-und Raumfahrt-Lilienthal-Oberth eV , 2012.

[Converse 1984] Converse, G., and Giffin, R., 1984. Extended Parametric Representation of Compressors Fans and Turbines. Vol. I -CMGEN User's Manual. Tech. Rep. NASA CR-174645, March.

[Conrow 2003] Conrow, E., Effective Risk Management: Some Keys to Success, Second Edition, American Institute of Aeronautics and Astronautics, 2003

[Conrow 2010a] Conrow, E., Management and Technology Associates, Redondo Beach, California; "Space Program Schedule Change Probability Distributions", Sept 2010, AIAA 2010-8834

[Conrow 2010b] Conrow,E., Management and Technology Associates, Redondo Beach, California; "Evaluation of Subjective Probability Statements", Sept 2010, AIAA 2010-8739

[Croft 2012] Croft, John, "Open rotor noise not a barrier to entry: GE", 5 July 2012. http://www.flightglobal.com/news/articles/open-rotor-noise-not-a-barrier-to-entry-ge-373817/

[Coyover 1908] Coyover W.J., Practical Nonparametric Statistics, John Wiley, New York 1980

[Cunningham 1979] E.P. Cunningham, "Probability of Crashing from Monte Carlo Simulation" Journal of Spacecraft and Rockets, 1979, Vol.16: 348-350

[Cukier 1978] Cukier, R. I., Levine, H. B., and Shuler, K. E., "Nonlinear Sensitivity Analysis of Multiparameter Model Systems, "Journal of Computational Physics, Vol.26, No.1, 1978, pp.1-42

[Deb, 2002] Deb, K., Multi-Objective Optimization Using Evolutionary Algorithms, John Wiley & Sons, Ltd., West Sussex, England, 2002, Ch. 1

[DeLaurentis 2000] Daniel DeLaurentis, Dimitri Mavris, "Uncertainty modeling and management in multidisciplinary analysis and synthesis" 38th Aerospace Sciences Meeting and Exhibit, Jan 2000, AIAA 2000-422

[Dell'Elce 2014] Dell'Elce, L. and Kerschen, G., "Probabilistic Assessment of Lifetime of Low-Earth-Orbit Spacecraft: Uncertainty Propagation and Sensitivity Analysis", Journal of Guidance, Control, And Dynamics, 2014, pp. 1-14

[de Luis 2008] de Luis, Jorge, "A Process for the Quantification of Aircraft Noise and Emissions Interdependencies," Ph.D. Thesis, School of Aerospace Engineering, Georgia Institute of Technology, April 2008.

[Du 2005] Du, X., Probabilistic Engineering Design, Chapter 7, University of Missouri-Rolla, September 2005

[Dubos 2008] Dubos, G. F., Saleh, J. H., and Braun, R., "Technology Readiness Level, Schedule Risk, and Slippage in Spacecraft Design," Journal of Spacecraft and Rockets, Vol. 45, No. 4, 2008

[Elseifi 2001] M. Elseifi, M. Khalessi, H.-Z. Lin, "A convex set based optimization algorithm for structural reliability analysis" 19th AIAA Applied Aerodynamics Conference, 2001, 2001-1520

[Eppinger 1994] S. Eppinger, D. Whitney, R. Smith, and D. Gebala, "A Model-Based Method For Organizing Tasks In Product Development," Research in Engineering Design, Vol 6, 1994, pg. 1–13

[Fischer 1989] Fischer, B., Klug, H., "Configuration Studies for a Regional Airliner Using Open-Rotor Ultra-High-Bypass Ratio Engines," AIAA/ASME/SAE/ASEE 25th Joint Propulsion Conference, July 1989, AIAA 89-2580.

[GE Aircraft Engines 1987] GE Aircraft Engines, "Full Scale Technology Demonstration of a Modern Counterrotating Unducted Fan Engine Concept: Component Test." NASA-CR-180868. Dec, 1987.

[Gelfand 1990] Alan E. Gelfand; Adrian F. M. Smith, Sampling-Based Approaches to Calculating Marginal Densities, Journal of the American Statistical Association, Vol. 85, No. 410, Jun 1990, pp. 398-409

[Geman 1984] S. Geman and D. Geman, Stochastic relaxation, Gibbs distributions, and the Bayesian restoration of images, IEEE Transactions on Pattern Analysis and Machine Intelligence PAMI-6, 721–741, 1984

[General Electric Company 1977] General Electric Company, "Study of Unconventional Aircraft Engines Designed for Low Energy Consumption Vol II," NASA-CR-187630, February 1977.

[General Electric Company 1987] General Electric Company, "Full Scale Technology Demonstration of a Modern Counterrotating Unducted Fan Engine Concept - Design Report," NASA-CR-180867, NASA Glenn Research Center, Contract NAS3-24210, December 1987. [ ]

[Gern 2013] Gern, F.H., "Conceptual Design and Structural Analysis of an Open Rotor Hybrid Wing Body Aircraft," AIAA-2013-1688, 54thAIAA/ASME/ASCE/AHS/ASC Structures, Structural Dynamics and Materials Conference, April 8-11, 2013, Boston, Massachusetts.

[Ghenaiet 2010] Ghenaiet, A., 2010. "Optimization of Turbofan Propulsion System Using a Genetic Algorithm". In Proceedings of ASME Turbo Expo 2010: Power for Land, Sea and Air. GT2010-22420.

[Glassman 1995] Glassman, A., 1995. Design Geometry and Design/Off-Design Performance Computer Codes for Compressors and Turbines. Tech. Rep. NASA CR 198433.

[Goldberg 1989] Goldberg, D. E., Genetic Algorithms in Search, optimization and Machine Learning, Addison Wesley, 1989

[Goldsmith 1982] Goldsmith, I. M. "Advanced turboprop testbed systems study," 1982.

[Green 2002] Lawrence Green, Hong-Zong Lin, M. Khalessi, "Probabilistic Methods for Uncertainty Propagation Applied to Aircraft Design" 20th AIAA Applied Aerodynamics Conference, 2002, 2002-3140

[Gronstedt 2009] Gronstedt, T., and Kyprianidis, K., 2009, "Optimizing the Operation of the Intercooled Turbofan Engine". In Proceedings of ASME Turbo Expo 2009: Power for Land, Sea and Air. GT2009-22519.

[Guha 2001] Guha, A., "Optimum Fan Pressure Ratio for Bypass Engines with Separate or Mixed Exhaust Streams," *Journal of Propulsion and Power*, Vol. 17, No 5., 2001.

[Guynn 2009] Guynn, M., Berton, J., Fisher, K., Tong, M., and Thurman, R., 2009. Engine Concept Study for an Advanced Single-Aisle Transport. Tech. Rep. NASA/TM- 2009-215784.

[Guynn 2011] Guynn, M., et al., “Initial Assessment of Open Rotor Propulsion Applied to an Advanced Single-Aisle Aircraft,” 11th AIAA Aviation Technology, Integration, and Operations Conference, September 2011, AIAA 2011-7058.
[Guynn 2011] Mark D. Guynn, Jeffrey J. Berton, Kenneth L. Fisher, William J. Haller, and Michael T. Tong, Douglas R. Thurman. "Refined Exploration of Turbofan Design Options for an Advanced Single-Aisle Transport." NASA/TM–2011-216883
[Hahn 2010] Hahn, A. “Ultra-High Bypass Ratio Engine Quick-Look Integration Study”. Environmentally Responsible Aviation Project, February 2010
[Hall 2007] Hall, C., and Crichton, D., 2007. “Engine Design Studies for a Silent Aircraft”. *Journal of Turbomachinery*, 129, July, pp. 479–487.
[Hendricks 2009] Eric Hendricks, Hernando Jimenez, Dimitri Mavris, "A Systems Engineering Enabled Capability for Commercial Aviation Strategic Planning" 47th AIAA Aerospace Sciences Meeting including The New Horizons Forum and Aerospace Exposition, Jan 2009, AIAA 2009-1199
[Hendricks 2011] Hendricks, E., “Development of an Open Rotor Cycle Model in NPSS Using a Multi-Design Point Approach,” ASME GT2011-46694.
[Henne 1989] Henne, P., “MD-90 Transport Aircraft Design,” AIAA/AHS/ASEE Aircraft Design, Systems and Operations Conference, Seattle 1989, AIAA 89-2023.
[Hoff 1990] Hoff, G.E., et al. “Experimental Performance and Acoustic Investigation of Modern, Counterrotating Blade Concepts," NASA CR-185158, January 1990.
[Howe 1996] D. Howe, The Prediction of Aircraft Wing Mass, Journal of Aerospace Engineering, April 1996, 210, (G2), pp 135-145
[Hughes 2008] Hughes, Chris and Theresa Zeug. "NASA/GE Aviation Collaborative Partnership Research in Ultra High Bypass Cycle Propulsion Concepts." Fundamental Aeronautics Program 2nd Annual Meeting, October 7-9 2008, Atlanta, Georgia
[Hutchings 2008] Christopher Hutchings, Evin Stump, "Adaptive Cost Models for Rapidly Evolving Technologies" AIAA SPACE 2008 Conference & Exposition, Sep 2008, AIAA 2008-7702
[ICAO 2010] ICAO Engine Emissions Databank, http://www.caa.co.uk/default.aspx?catid=702, last update, December 2010.
[Igarashi 1994] S. Igarashi, "Analysis of Gas Film Lubrication Using the Monte Carlo Direct Simulation Method" Rarefied Gas Dynamics: Theory and Simulations, 1994: 303-310
[Jemitola 2013] P. O. Jemitola, G. Monterzino, and J. Fielding, Wing Mass Estimation Algorithm for Medium Range Box Wing Aircraft, Vol. 117, No. 1189, The Aeronautical Journal, March 2013
[Jimenez 2011] Hernando Jimenez, Graham Burdette, Jeff Schutte, Dimitri Mavris, "Probabilistic Technology Assessment for NASA Environmentally Responsible Aviation (ERA) Vehicle Concepts" 11th AIAA Aviation Technology, Integration, and Operations (ATIO) Conference, Sep 2011, AIAA 2011-6967
[Johnson 1997] Johnson, D., “The Triangular Distribution as a proxy for the Beta Distribution in Risk Analysis,” The Statistician, Vol. 46, No. 2, 1997, pp. 387-398
[Keefer 1983] Keefer, D. K., Bodily, S. E., “Three-Point Approximations for Continuous Random Variables,” Management Science, Vol 29. No. 5, May 1983, pp. 595-609
[Khalessi 1993] M. Khalessi, H. Lin, “Most-Probable-Point-Locus Structural Reliability Method” 34th Structures, Structural Dynamics and Materials Conference, 1993, AIAA 1993-1439
[Keefer 1983] Keefer, D. K., Bodily, S. E., “Three-Point Approximations for Continuous Random Variables,” Management Science, Vol 29. No. 5, May 1983, pp. 595-609
[Kestner 2011] Kestner, B., Schutte, J., Gladin, J., and Mavris, D., 2011. “Ultra High Bypass Ratio Engine Sizing and Cycle Selection Study for a Subsonic Commercial Aircraft in the N+2 Timeframe”, Proceedings of ASME Turbo Expo 2011. GT2011-45370.
[Kestner 2012] Kestner, B., et al., Surrogate Modeling for Simultaneous Engine Cycle and Technology Optimization for Next Generation Subsonic Aircraft. In Proceedings of ASME Turbo Expo 2012. GT2012-68724.
[Khuri 2006] André I. Khuri, “Response Surface Methodology and Related Topics” World Scientific, 2006
[Kim 2006] Nam H. Kim, Haoyu Wang, Nestor V. Queipo, “Efficient Shape Optimization Under Uncertainty Using Polynomial Chaos Expansions and Local Sensitivities” AIAA Journal, May 2006, Vol.44: 1112-1116
[Kirby 1999] Michelle R. Kirby and Dimitri N. Mavris, "Forecasting Technology Uncertainty in Preliminary Aircraft Design" Georgia Institute of Technology, 1999 World Aviation Conference, October 1999, San Francisco, CA, SAE Paper 1999-01-5631
[Kirby 2000] Michelle Kirby, Dimitri Mavris, "A Method for Technology Selection Based On Benefit, Available Schedule and Budget Resources", 2000 World Aviation Conference, Oct 2000, AIAA 2000-5563.

[Kirby 2001] Michelle Rene Kirby, "A Methodology for Technology Identification, Evaluation, and Selection in Conceptual and Preliminary Aircraft Design" PhD Thesis, Georgia Institute of Technology, March 2001

[Kirby 2008]Kirby, M., and Mavris, D., 2008. "The Environmental Design Space," 26th International Congress of the Aeronautical Sciences. ICAS-2008-4.7.3.

[Kolmogorov 1933] Kolmogorov, A., "Sulla determinazione empirica di una legge di distribuzione (On the empirical determination of a distribution law)," Giorn. Ist. Ital. Attuar., Vol. 4, 1933, pp. 83-91

[Kurzke 1999] Kurzke, J., 1999, "Gas Turbine Cycle Design Methodology: A Comparison of Parameter Variation With Numerical Optimization". *Journal of Engineering for Gas Turbines and Power*, 121, January, pp. 6-11.

[Kurzke 2009] Kurzke, J., 2009. "Fundamental Differences Between Conventional And Geared Turbofans". In Proceedings of ASME Turbo Expo 2009: Power for Land, Sea and Air. GT2009-59745.

[Landry 2014] Steven J. Landry, Julian Archer, "Modeling the Effect of Uncertainty and NextGen Concepts and Technologies on the National Airspace System" 14th AIAA Aviation Technology, Integration, and Operations Conference, June 2014, AIAA 2014-2422

[Lange 1974] R. H. Lange, J. F. Cahill, E. S. Bradley, R. R. Eudaily, C. M. Jenness and D. G. MacWilkinson, Feasibility Study of the Transonic Biplane Concept for Transport Aircraft Application, NASA CR-132462, 1974

[Lin 1993] H. Lin, "Calculation Of Failure Probability By Using X-Space Most-Probable-Point" 34th Structures, Structural Dynamics and Materials Conference, 1993, AIAA 1993-1624

[Lin 2001] Hong-Zong Lin, M. Khalessi, Mark Lin, Eric Fox, M. Elseifi, "Development of UNIPASS - A unified probabilistic assessment software system", 19th AIAA Applied Aerodynamics Conference, AIAA 2001-1644

[Lyle 2003] Karen Lyle, Sharon Padula, Alan Stockwell, "Application of Probabilistic Analysis to Aircraft Impact Dynamics" 44th AIAA/ASME/ASCE/AHS/ASC Structures, Structural Dynamics, and Materials Conference, April 2003, 2003-1482

[Lytle, 1999] Lytle, J., 1999. The Numerical Propulsion System Simulation: A Multidisciplinary Design for Aerospace Vehicles. Tech. Rep. NASA TM-1999-209194, September

[Lytle 2000] Lytle, J., 2000. The Numerical Propulsion System Simulation: An Overview. Tech. Rep. NASA TM-2000-209915, June..

[McKay 2009] McKay, Bruce G. "Next Generation Propulsion & Air Vehicle Considerations." AIAA 2009-4803. 45th AIAA/ASME/SAE/ASEE Joint Propulsion Conference & Exhibit, August 2-5 2009, Denver, Colorado, AIAA 2009-4803

[Manglesdorf 2012] Mark Manglesdorf, Kenneth C. Martin, Bruce G. McKay, 2012, NASA/CR—2012–000000, Environmentally Responsible Aviation - Lockheed Martin ERA Team, Langley Research Center, Hampton, Virginia (first author), Lockheed Martin Aeronautics Company, Marietta, Georgia (the other authors)

[Mavris 1995] Mavris D. N., Bandte O., Brewer J. T., "A Method for the Identification and Assessment of Critical Technologies Needed for an Economically Viable HSCT," Proceedings of the 1st AIAA Aircraft Engineering, Technology, and Operations Congress, Los Angeles, CA, September 19-21, 1995

[Mavris 1997] Dr. Dimitri N. Mavris, George C. Mantis, and Michelle R. Kirby, "Demonstration of a Probabilistic Technique for the Determination of Aircraft Economic Viability", Georgia Institute of Technology AIAA-1997-5585-706

[McCormick 2000] McCormick, D. J. and Olds, J. R., "Approximation of Probabilistic Distributions Using Selected Discrete Simulations" 8th AIAA/USAF/NASA/ISSMO Symposium on Multidisciplinary Analysis and Optimization, AIAA 2000-4863, September 2000

[McCullers 2009] McCullers, L.A., FLOPS User's Guide Ver. 8.11, NASA Langley Research Center, Hampton, VA, September 2009

[Mehmani 2012] Ali Mehmani, Jie Zhang, Souma Chowdhury, Achille Messac, "Surrogate-Based Design Optimization with Adaptive Sequential Sampling" 53rd AIAA/ASME/ASCE/AHS/ASC Structures, Structural Dynamics and Materials Conference, Apr 2012, AIAA 2012-1527

[Mercer 2006] Carolyn Mercer, William Haller, Michael Tong, "Adaptive Engine Technologies for Aviation CO2 Emissions Reduction", 42nd AIAA/ASME/SAE/ASEE Joint Propulsion Conference & Exhibit, July 2006, AIAA 2006-5105

[Metropolis 1953] N. Metropolis, A. W. Rosenbluth, M. N. Rosenbluth, A. H. Teller, and E. Teller, Equation of state calculations by fast computing machines, Journal of Chemical Physics, 21, 1953

[Missoum 2009] Samy Missoum, Christoph Dribusch, Phil Beran, "A Multifidelity Approach for the Construction of Explicit Decision Boundaries: Application to Aeroelasticity", 50th AIAA/ASME/ASCE/AHS/ASC Structures, Structural Dynamics, and Materials Conference, May 2009, AIAA 2009-2193

[Moss 2005] James N. Moss, Graeme A. Bird, "Direct Simulation Monte Carlo Simulations of Hypersonic Flows With Shock Interactions" AIAA Journal, Dec 2005, Vol.43: Pg. 2565-2573
[Myers 2002] Raymond H. Myers, Douglas C. Montgomery "Response Surface Methodology" J. Wiley & Sons, 2002, 2nd edition
[NASA 2006] Numerical Propulsion System Simulation (NPSS) User's Guide, version 1.6.4 rev V, NASA Glenn Research Center, November 2006.
[Nickol 2009] Nickol, C.L. and McCullers, L.A., "Hybrid Wing Body Configuration System Studies," AIAA-2009-0931, 47th AIAA Aerospace Sciences Meeting and Exhibit, January 5-8, 2009, Orlando, Florida.
[Niskode 2010] Niskode, P., Stickes, R., Allmon, B., DeJong, R., "FAA CLEEN Consortium Open Session," October 27, 2010, Presentation given at plenary session.
[Onat 1979] Onat, E., and Klees, G., 1979. A Method to Estimate Weight and Dimensions of Large and Small Gas Turbine Engines. Tech. Rep. NASA-CR-159481, January.
[Onwubolu 2004] Godfrey C. Onwubolu, B. V. Babu, New Optimization Techniques in Engineering, 2004
[Park 1988] Park, S. K., and K. W. Miller, Random number generators: Good ones are hard to find, Communications of the ACM, 31 , 1192 – 1201, 1988
[Paul-Dubois-Taine 2013] Arthur Paul-Dubois-Taine, Siva Nadarajah, "Sensitivity-Based Sequential Sampling of Cokriging Response Surfaces for Aerodynamic Data" 31st AIAA Applied Aerodynamics Conference, Jun 2013, AIAA 2013-2652
[Pearson 1965] Pearson and Turkey, "Approximate Means and standard Deviations based on Distances between Percentage Points of Frequency Curves", Biometrika, Vol 52, No 3-4, 1965
[Phadke 1995] Madhan S. Phadke, "Quality Engineering Using Robust Design" 1st edition, Prentice Hall, 1995
[Pitera 2011] David M. Pitera, Mark DeHaan, Derrell Brown, Ronald T. Kawai, Steve Hollowell, Peter Camacho, David Bruns, and Blaine K. Rawden, "Blended Wing Body Concept Development with Open Rotor Engine Integration", November 2011, NASA/CR–2011-217303.
[Penzo 1963] P. A. Penzo, L. J. Skidmore, "Monte Carlo Simulation of the Midcourse Guidance for Lunar Flights" AIAA Journal, Apr 1963, Vol.1: 820-831
[Porter 1980] Alan L. Porter, Frederick A. Rossini, Stanley R. Carpenter, "A Guidebook for Technology Assessment and Impact Analysis" (North Holland Series in System Science and Engineering), Feb 1980
[Prandini 1999] Prandini, M., Lygeros, J., Nilim, A., and Sastry, S., "A Probabilistic Framework for Aircraft Conflict Detection," Guidance, Navigation, and Control Conference and Exhibit, AIAA 1999-4144, 1999
[Prandtl 1924] Ludwig Prandtl, Induced Drag of Multiplanes, NACA TN 182, 1924
[Raczynski 2006] Christopher Raczynski, Michelle Kirby, Dimitri Mavris, "A Dynamic Process for Strategic Roadmapping and Technology Portfolio Management", 6th AIAA Aviation Technology, Integration and Operations Conference (ATIO), 2006, AIAA 2006-7789
[Rallabhandi 2008]] Rallabhandi, S., and Mavris, D., 2008, "Simultaneous Airframe and Propulsion Cycle Optimization for Supersonic Aircraft Design". *Journal of Aircraft*, 45, January-February.
[Rao, 2009] Singiresu S. Rao, Engineering Optimization: Theory and Practice, 2009
[Re 2005] Richard J. Re, "Longitudinal Aerodynamic Characteristics and Wing Pressure Distributions of a Blended-Wing-Body Configuration at Low and High Reynolds Numbers", August 2005, NASA/TM-2005-213754.
[Richey 2010] Matthew Richey, "The Evolution of Markov Chain Monte Carlo Methods", The American Mathematical Monthly, Vol. 117, No. 5 (May 2010), pp. 383-413
[Roman 2004] Roman, F., et al. "Selection Without Reflection is a Risky Business..." Proceedings of the 10th AIAA/ISSMO Multidisciplinary Analysis and Optimization Conference, Albany, NY, August 30-September 1, 2004
[Ronse 2014] A. L. A. B. Ronse, E. Mooij, "Statistical Impact Prediction of Decaying Objects" Journal of Spacecraft and Rockets, November 2014, Vol.51: 1797-1810
[Roof 2007] Roof, C., et. al., "Aviation Environmental Design Tool (AEDT) System Architecture," Doc #AEDT-AD-01, January 29, 2007.
[Rooney 2004] Brendan Rooney, Alicia Hartong, "A Discrete-Event Simulation of Turnaround Time and Manpower of Military RLVs" Space 2004 Conference and Exhibit, Sep 2004, AIAA 2004-6111
[Rubin 1987] Rubin, D. B., Comment on "The Calculation of Posterior Distributions by Data Augmentation," by M. A. Tanner and W. H. Wong, Journal of the American Statistical Association, 82, 543-546
[Rumpfkeil 2011] Markus Rumpfkeil, Wataru Yamazaki, Mavris Dimitri, "A Dynamic Sampling Method for Kriging and Cokriging Surrogate Models", 49th AIAA Aerospace Sciences Meeting including the New Horizons Forum and Aerospace Exposition, Jan 2011, AIAA 2011-883

[Ryan 1993] Robert Ryan, John Townsend, "Application of Probabilistic Analysis/Design Methods In Space Programs - The Approaches, The Status, And The Needs" 34th Structures, Structural Dynamics and Materials Conference, April 1993, AIAA 1993-1381

[Salam 2012] I. R. Salam and C. Bil, Preliminary Aerodynamic and Structural Design Tradeoff for a Box-Wing Airliner, AIAA 2012-0251, 2012

[Sambridge 2002] Malcolm Sambridge, Klaus Mosegaard, "Monte Carlo Methods in Geophysical Inverse Problems" Reviews of Geophysics, 40, 3, September 2002

[Schutte 2009] Schutte, J., "Simultaneous Multi-Design Point Approach to Gas Turbine On-Design Cycle Analysis for Aircraft Engines," Ph.D. Thesis, School of Aerospace Engineering, Georgia Institute of Technology, May 2009.

[Schutte 2012a] Schutte, J., Tai, J., Mavris, D., "Multi-Design Point Cycle Design Incorporation into the Environmental Design Space," 48th AIAA/ASME/SAE/ASEE Joint Propulsion Conference & Exhibit, July 2012, AIAA 2012-3812.

[Schutte 2012b] Schutte, J., Tai, J., Sands, J., and Mavris, D., "Cycle Design Exploration Using Multi-Design Approach," ASME GT2012-69334, 2012 Turbo Expo, Copenhagen, Denmark, July 2012.

[Sen 1998] Sen, P., Yang, J-B., Multiple Criteria Decision Support in Engineering Design, Springer-Verlag, Gateshead, Great Britan, 1998, Ch. 3

[Shah 1998] A. Shah, C. Chamis, "Probabilistic Assessment of Large Structures Under Pressure", 39th AIAA/ASME/ASCE/AHS/ASC Structures, Structural Dynamics, and Materials Conference and Exhibit, 1998, AIAA 1998-1824

[Shi 2001] Pan Shi, Sankaran Mahadevan, "Aircraft Structures Reliability Under Corrosion Fatigue" 19th AIAA Applied Aerodynamics Conference, 2001, 2001-1377

[Slade 2006] Richard Slade, Paul Sharp, Royston Jones, Vassili Toropov, "Analysis, Optimization and Probabilistic Assessment of an Airbag Landing System for the ExoMars Space Mission", 11th AIAA/ISSMO Multidisciplinary Analysis and Optimization Conference, Sep 2006, AIAA 2006-7001

[Smirnov 1948] Smirnov, N. V., "Table for Estimating the Goodness of Fit of Empirical Distributions," The Annals of Mathematical Statistics 19, Vol. 2, 1948, pp. 279-281

[Soban 2013] Danielle S. Soban, Dimitri N. Mavris, "Assessing the Impact of Technology on Aircraft Systems Using Technology Impact Forecasting", Journal of Aircraft, 2013, Vol.50: 1380-1393

[Sobol 1976] Sobol, I., "Uniformly Distributed Sequences with an Additional Uniform Property," USSR Computational Mathematics and Mathematical Physics , Vol. 16, No. 5, 1976, pp. 236–242].

[Spetzler 1975] Spetzler C. S., Stael von Holstein C-A. S., "Probability Encoding in Decision Analysis," Management Science, Vol. 22, No. 3, November 1975

[Sues 1996] Robert Sues, David Oakley, Graham Rhodes, Dale Hopkins, "Reliability-based optimization for design of aeropropulsion components" 37th Structure, Structural Dynamics and Materials Conference, Apr 1996, AIAA 1996-1609

[Suh 2009] Eun Suk Suh, Michael R. Furst, Kenneth J. Mihalyov, and Olivier de Weck, "Technology Infusion for Complex Systems: A Framework and Case Study", Wiley InterScience, Systems Engineering Vol. 13, No. 2, 2010

[Sun 2009] Quanhua Sun, Jing Fan, Iain D. Boyd, "Improved Sampling Techniques for the Direct Simulation Monte Carlo Method" Computers & Fluids, Feb 2009; 38 (2), Pg. 475–479

[SwRI 1995] Southwest Research Institute, FPI User's and Theoretical Manual. San Antonio, TX, 1995

[Taylor 2002] James Taylor, Francis Curran, "Integrated Technology Assessment Center (ITAC) Update", 38th AIAA/ASME/SAE/ASEE Joint Propulsion Conference & Exhibit, July 2002, AIAA 2002-3550

[Timson 1968] Timson, F. S., "Measurement of Technical Performance in Weapon System Development Programs: A Subjective Probability Approach," Memorandum RM-5207-ARPA, The RAND Corporation, December 1968

[Tong 2002] Tong, M., Halliwell, I., and Ghosn, L., 2002. "A Computer Code for Gas Turbine Engine Weight and Disk Life Estimation". In 2002 ASME Turbo Expo. GT-2002-30500.

[Tong 2009] Tong, Michael T. and Naylor, Bret A., "An Object-Oriented Computer Code for Aircraft Engine Weight Estimation," NASA/TM-2009-215656, NASA Glenn Research Center, December 2009.

[Twiss 1992] Brian C. c, "Forecasting for Technologists and Engineers: A Practical Guide for Better Decisions", IEE Management of Technology Series, Jul 1992, Peter Peregrinus Ltd, London, United Kingdom

[Vanderplaats 2001] Vanderplaats, G., N., *Numerical Optimization Techniques for Engineering Design*, 3rd Ed., Vanderplaats Research and Development, Colorado Springs CO, 2001, p.73

[Van Zante 2011] Van Zante, D., “Open Rotor Research at NASA Glenn," Tech. rep., National Aeronautics and Space Administration, 2011.
[Van Zante 2013] Van Zante, D. E., “The NASA Environmentally Responsible Aviation Project/General Electric Open Rotor test campaign," Grapevine, TX, United states, 2013.
[Van Zante 2014] Van Zante, Dale E., et al. "Progress in open rotor propulsors: The FAA/GE/NASA open rotor test campaign." Aeronautical Journal 118.1208 (2014): 1181-1213.
[Ward 1998] Technology Tracking for the High-Speed Research Program; Clay A. Ward, The Boeing Company; AIAA and SAE, 1998 World Aviation Conference, Anaheim, CA, Sept 1998; AIA-1998-5549
[Weisbin 2004] Charles R. Weisbin,* Guillermo Rodriguez, Alberto Elfes, and Jeffrey H. Smith, “Toward a Systematic Approach for Selection ofNASA Technology Portfolios,” Wiley Periodicals, Inc, Systems Engineering, Vol. 7, No. 4, 2004

[Weisbrich 1982] Weisbrich, A. L., J. Godston, and E. Bradley. "Technology and benefits of aircraft counter rotation propellers.," 1982.
[Williams 1992] Williams, T. M. “Practical Use of Distribution in Network Analysis,” Journal of the Operational Research Society, Vol. 43, No. 3 (Mar. 1992), pp. 265-270
[Whitfield 1990] Whitfield, C.E., Mani, R., Gliebe, P.R., "High Speed Turboprop Aeroacoustic Study," NASA-CR-185242, 1990.
[Wolkovitch 1986] Julian Wolkovitch, The Joined Wing: An Overview, Journal of Aircraft, Vol. 23, No. 3, 1986, pp. 161-178, doi: 10.2514/3.45285
[Yamazaki 2013] Wataru Yamazaki, “Stochastic Drag Analysis via Polynomial Chaos Uncertainty Quantification” 51st AIAA Aerospace Sciences Meeting including the New Horizons Forum and Aerospace Exposition, January 2013, AIAA 2013-962
[Young 2002] Young, J.B., and Wilcock, R.C., 2002. “Modeling the Air-Cooled Gas Turbine: Part 2 – Coolant Flows and Losses”. *Journal of Turbomachinery*, 124, January, pp. 214–221.
[Zaidi 2015] Turab Zaidi, Hernando Jimenez, Dimitri N. Mavris, "Copulas Theory for Probabilistic Assessment - an Overview with Application to Airplane Performance Analysis", AIAA Journal of Aircraft, accepted for publication Jan 2015. Presented at 14th AIAA Aviation Technology, Integration, and Operations Conference, June 2014, AIAA 2014-2171
[Zhang 2012] Zhang, J., Messac, A., Zhang, J., and Chowdhury, S., "Improving the Accuracy of Surrogate Models Using Inverse Transform Sampling," 53rd AIAA/ASME/ASCE/AHS/ASC Structures, Structural Dynamics and Materials Conference, AIAA 2012-1429, 2012
[Zitzler 2003] Zitzler, E., et al. “Performance Assessment of Multi-Objective Optimizers: An Analysis and Review,” IEEE Transactions on Evolutionary Computation, Vol 7, No. 2, April 2003, pp. 117-132
[Zorumski 1982] Zorumski, William E., "Aircraft Noise Prediction Program Theoretical Manual," NASA TM-83199, 1982.

9.0 Appendices

9.1 Appendix A: EDS Surrogates Response Names, Descriptions, and Units

1. desBlockFuel – Mission Block Fuel (lbs)
2. Cruise_SFC_Min – Specific Fuel Consumption at Cruise (lbm/(hr-lbf))
3. Approach – Noise Level (dB)
4. Cutback – Noise Level (dB)
5. Sideline – Noise Level (dB)
6. TOAll_TOFL – All Engines Operating Takeoff Field Length (feet)
7. TOOEO_TOFL – One Engine Operating Takeoff Field Length (feet)
8. AbortALL_TOFL – Abort All Engines Operating Takeoff Field Length (feet)
9. AbortOEO_TOFL – Abort One Engine Operating Takeoff Field Length (feet)
10. desFAR_LDGFL – Design Landing Field Length (feet)
11. desTOGW – TakeOff Gross Weight (lbs)
12. Fuse_Weight – Fuselage Weight (lbs)
13. OEW – Operating Empty Weight (lbs)
14. VT_Weight – Vertical Tail Weight (lbs)
15. Wing_Weight – Wing Weight (lbs)
16. HT_Weight – Horizontal Tail Weight (lbs)
17. SLS_UI_OPR – Overall Pressure Ratio at Sea Level Static
18. T3max – Maximum Compressor Exit Temperature (R)
19. ADP_BPR – Fan Bypass Ratio at Aerodynamic Design Point
20. HPC_diam – High Pressure Compressor Diameter (in)
21. HPCLastStageWc – Compressor Exit Corrected Airflow (lbm/sec)
22. HPCLastStgBladeHeight – Compressor Last Stage Blade Height (in)
23. EI_NOx_AP – Approach Advanced Combustor Emissions (grams of NOx/kN of Thrust)
24. EI_NOx_CO – Cutout Advanced Combustor Emissions (grams of NOx/kN of Thrust)
25. EI_NOx_ID – Idle Advanced Combustor Emissions (grams of NOx/kN of Thrust)
26. EI_NOx_TO – Takeoff Advanced Combustor Emissions (grams of NOx/kN of Thrust)
27. EI_Standard_AP – Approach Standard Combustor Emissions (grams of NOx/kN of Thrust)
28. EI_Standard_CO – Cutout Standard Combustor Emissions (grams of NOx/kN of Thrust)
29. EI_Standard_ID– Idle Standard Combustor Emissions (grams of NOx/kN of Thrust)
30. EI_Standard_TO – Takeoff Standard Combustor Emissions (grams of NOx/kN of Thrust)
31. ICAO_AP_Tt3 – Approach Total Temperature Compressor Exit (R)
32. ICAO_AP_Wfuel – Approach Fuel Flow (lbs)
33. ICAO_CO_Tt3 – Cutout Total Temperature Compressor Exit (R)
34. ICAO_CO_Wfuel – Cutout Fuel Flow (lbs)
35. ICAO_ID_Tt3 – IdleTotal Temperature Compressor Exit (R)
36. ICAO_ID_Wfuel – Idle Fuel Flow (lbs)
37. ICAO_TO_Tt3 – Takeoff Total Temperature Compressor Exit (R)
38. ICAO_TO_Wfuel – Takeoff Fuel Flow (lbs)
39. LPC_diam – Low Pressure Compressor Diameter (in)
40. Nacelle_Diam/Dnac – Nacelle Diameter (in)

41. enginePodLength/Xnac – Nacelle Length (in)
42. engPodWt/WENG – Engine Weight (lbs)
43. diamFan/Prop Diam – Engine Fan Diameter (in)
44. ICAO_ID_Equiv – Combustor Equivalence Ratio at Idle Power Setting
45. ICAO_AP_Equiv – Combustor Equivalence Ratio at Approach Power Setting

9.2 Appendix B: EDS Vehicle Surrogate Fit Statistics

9.2.1 LSA Vehicle Fit Statistics

Surrogate Name	MFE Mean Absolute Value	MFE Standard Deviation	MRE Mean Absolute Value	MRE Standard Deviation
AbortALL_TOFL	0.0039	0.5021	0.0050	0.4803
AbortOEO_TOFL	0.0035	0.6063	0.0662	0.5798
ADP_BPR	0.0125	0.9964	0.5573	1.1981
Approach	0.0007	0.1200	0.0345	0.1179
Cruise_SFC_Min	0.0005	0.3158	0.1872	0.3550
Cutback	0.0004	0.2259	0.0976	0.2143
desBlockFuel	0.0017	0.4146	0.1600	0.3930
desFAR_LDGFL	0.0001	0.0690	0.0142	0.0756
desTOGW	0.0017	0.2788	0.0989	0.2955
diamFan	0.0005	0.1805	0.0675	0.1661
EI_NOx_AP	0.0000	0.0361	0.0045	0.0640
EI_NOx_CO	0.0009	0.1011	0.0053	0.1337
EI_NOx_ID_Lower	0.0000	0.0132	0.0021	0.0169
EI_NOx_TO	0.0021	0.1042	0.0154	0.1581
EI_Standard_AP	0.0003	0.2696	0.0113	0.3338
EI_Standard_CO	0.0012	0.3689	0.0455	0.3470
EI_Standard_ID_Lower	0.0002	0.0283	0.0018	0.0618
EI_Standard_TO	0.0053	0.4426	0.0481	0.5815
enginePodLength	0.0015	0.8031	0.1933	0.9658
engPodWt	0.0066	0.7299	0.2351	0.7348
Fuse_Weight	0.0000	0.0024	0.0000	0.0024
HPC_diam	0.0039	0.5659	0.1289	0.5850
HPCLastStageWc	0.0062	0.8302	0.1027	0.8413
HPCLastStgBladeHeight	0.0062	0.7743	0.0916	0.7945
HT_Weight	0.0003	0.0732	0.0065	0.0751
ICAO_AP_Equiv	0.0001	0.3430	0.0329	0.3470
ICAO_AP_Tt3	0.0001	0.1714	0.0572	0.1621
ICAO_AP_Wfuel	0.0096	0.8275	0.0670	0.8427
ICAO_CO_Tt3	0.0032	0.2244	0.0081	0.2034
ICAO_CO_Wfuel	0.0034	0.7566	0.3267	0.7832

ICAO_ID_Equiv	0.0044	0.5205	0.1784	0.6224
ICAO_ID_Tt3	0.0146	0.2142	0.0290	0.2028
ICAO_ID_Wfuel	0.0000	0.0014	0.0002	0.0013
ICAO_TO_Tt3	0.0002	0.2581	0.0375	0.2483
ICAO_TO_Wfuel	0.0174	0.8641	0.2587	0.8288
LPC_diam	0.0070	0.4697	0.2229	0.5383
Nacelle_Diam	0.0008	0.1698	0.0498	0.1587
OEW	0.0003	0.1465	0.0454	0.1296
Sideline	0.0072	0.2270	0.0891	0.2203
SLS_UI_OPR	0.0033	0.2425	0.1456	0.2749
T3max	0.0005	0.2962	0.0459	0.3201
TOAll_TOFL	0.0033	0.5291	0.0550	0.5432
TOOEO_TOFL	0.0061	0.7702	0.2924	0.9496
VT_Weight	0.0040	0.0544	0.0138	0.0561
Wing_Weight	0.0002	0.2065	0.0904	0.1575

9.2.2 LSA OWN Vehicle Fit Statistics

Surrogate Name	MFE Mean Absolute Value	MFE Standard Deviation	MRE Mean Absolute Value	MRE Standard Deviation
AbortALL_TOFL	0.0008	0.2422	-0.1723	0.4205
AbortOEO_TOFL	0.0010	0.2518	-0.0066	0.3515
ADP_BPR	0.0086	1.0002	-0.3500	0.9809
Approach	0.0001	0.0897	0.0013	0.0820
Cruise_SFC_Min	0.0000	0.0018	0.0004	0.0017
Cutback	0.0004	0.1961	-0.0280	0.1555
desBlockFuel	0.0010	0.3189	0.1762	0.3406
desFAR_LDGFL	0.0001	0.0701	-0.0382	0.0724
desTOGW	0.0008	0.2820	0.0681	0.2836
diamFan	0.0003	0.1834	-0.0436	0.1583
EI_NOx_AP	0.0011	0.0375	0.0029	0.0638
EI_NOx_CO	0.0000	0.1429	0.0089	0.1218
EI_NOx_ID_Lower	-0.0010	0.0103	-0.0030	0.0176
EI_NOx_TO	-0.0002	0.1369	0.0222	0.1431
EI_Standard_AP	-0.0018	0.2075	0.0107	0.3005
EI_Standard_CO	0.0194	0.3954	-0.0113	0.4307
EI_Standard_ID_Lower	0.0000	0.0245	0.0068	0.0404
EI_Standard_TO	0.0140	0.3272	0.0276	0.2933
enginePodLength	0.0032	0.5512	0.1845	0.5707
engPodWt	0.0039	0.6894	-0.1859	0.7734
Fuse_Weight	0.0000	0.0023	0.0007	0.0024
HPC_diam	0.0025	0.5356	0.2401	0.5525
HPCLastStageWc	0.0205	0.9236	0.2423	0.9183
HPCLastStgBladeHeight	0.0056	0.7580	0.2518	0.7909
HT_Weight	0.0011	0.0290	0.0049	0.0280
ICAO_AP_Equiv	0.0018	0.3647	0.0112	0.3670
ICAO_AP_Tt3	0.0000	0.1166	0.0427	0.1301
ICAO_AP_Wfuel	0.0020	0.7215	0.1551	0.6939
ICAO_CO_Tt3	0.0004	0.1956	0.0148	0.1612
ICAO_CO_Wfuel	0.0026	0.5853	0.1392	0.6243
ICAO_ID_Equiv	-0.0029	0.5087	0.0154	0.5361
ICAO_ID_Tt3	0.0003	0.2067	-0.0281	0.1948
ICAO_ID_Wfuel	0.0000	0.0014	0.0000	0.0013
ICAO_TO_Tt3	0.0035	0.2369	0.0323	0.2253
ICAO_TO_Wfuel	0.0032	0.6077	0.1291	0.6630
LPC_diam	0.0032	0.5722	0.1170	0.5408
Nacelle_Diam	0.0003	0.1512	-0.0715	0.1368
OEW	-0.0001	0.1357	-0.0730	0.1479
Sideline	0.0005	0.2103	-0.0173	0.1675

SLS_UI_OPR	0.0004	0.2078	0.1550	0.2405
T3max	0.0007	0.2735	0.0335	0.2825
TOAll_TOFL	0.0001	0.2148	0.0805	0.2223
TOOEO_TOFL	0.0018	0.4961	-0.0325	0.6508
VT_Weight	0.0001	0.0332	-0.0016	0.0336
Wing_Weight	-0.0002	0.0434	0.0246	0.0421

9.2.4 LTA Vehicle Fit Statistics

Surrogate Name	MFE Mean Absolute Value	MFE Standard Deviation	MRE Mean Absolute Value	MRE Standard Deviation
AbortALL_TOFL	0.0018	0.4733	-0.0017	0.7474
AbortOEO_TOFL	-0.0020	0.6664	-0.0855	0.4888
ADP_BPR	0.0072	0.6449	-0.2170	0.6574
Approach	-0.0003	0.1941	-0.0245	0.2334
Cruise_SFC_Min	-0.0043	0.2728	-0.0060	0.3443
Cutback	0.0000	0.1680	-0.0506	0.1510
desBlockFuel	0.0017	0.2271	0.0091	0.2768
desFAR_LDGFL	0.0003	0.0709	-0.0010	0.0861
desTOGW	0.0016	0.3400	-0.0113	0.5202
diamFan	0.0003	0.1827	0.0005	0.2039
EI_NOx_AP	-0.0105	0.0847	-0.0178	0.1460
EI_NOx_CO	-0.0001	0.1145	-0.0318	0.1332
EI_NOx_ID_Lower	0.0000	0.0081	-0.0012	0.0239
EI_NOx_TO	0.0000	0.1968	-0.0053	0.3086
EI_Standard_AP	0.0000	0.2820	-0.0214	0.3691
EI_Standard_CO	-0.0002	0.2028	0.0115	0.3753
EI_Standard_ID_Lower	0.0004	0.0280	-0.0012	0.0841
EI_Standard_TO	0.0021	0.7861	0.0246	1.4084
enginePodLength	0.0028	0.5179	-0.0164	0.5985
engPodWt	0.0083	0.7006	0.0283	0.6921
Fuse_Weight	0.0000	0.0032	0.0001	0.0035
HPC_diam	0.0197	0.4070	-0.0137	0.5386
HPCLastStageWc	0.0051	0.7806	0.3272	0.8166
HPCLastStgBladeHeight	0.0011	0.4340	-0.0005	0.5857
HT_Weight	0.0004	0.0180	0.0001	0.0174
ICAO_AP_Equiv	0.0000	0.0034	-0.0003	0.0030
ICAO_AP_Tt3	0.0005	0.1454	0.0424	0.1491
ICAO_AP_Wfuel	0.0013	0.5416	-0.0112	0.7381
ICAO_CO_Tt3	0.0082	0.1942	-0.0557	0.2115
ICAO_CO_Wfuel	0.0015	0.4544	-0.0112	0.5955
ICAO_ID_Equiv	0.0000	0.0023	0.0004	0.0025
ICAO_ID_Tt3	0.0003	0.1554	-0.0026	0.1632
ICAO_ID_Wfuel	0.0000	0.0029	0.0001	0.0041
ICAO_TO_Tt3	0.0008	0.2176	-0.0078	0.3486
ICAO_TO_Wfuel	0.0105	0.4570	0.0123	0.6304
LPC_diam	-0.0002	0.3550	0.0135	0.4704
Nacelle_Diam	0.0003	0.1574	-0.0018	0.1750
OEW	0.0004	0.1299	0.0003	0.1566
Sideline	0.0003	0.1785	-0.0667	0.2003

SLS_UI_OPR	0.0003	0.2177	0.0001	0.2556
T3max	0.0008	0.2867	0.0112	0.3380
TOAll_TOFL	0.0032	0.5623	-0.0187	0.5562
TOOEO_TOFL	0.0141	1.1926	-0.2561	1.0912
VT_Weight	0.0000	0.0450	-0.0005	0.0552
Wing_Weight	0.0037	0.0800	0.0042	0.1010

9.2.6 LTA MFN Vehicle Fit Statistics

Surrogate Name	MFE Mean Absolute Value	MFE Standard Deviation	MRE Mean Absolute Value	MRE Standard Deviation
AbortALL_TOFL	0.0002	0.2245	-0.0509	0.2180
AbortOEO_TOFL	0.0002	0.2245	0.0509	0.2180
ADP_BPR	0.0016	0.1254	0.0385	0.1266
Approach	0.0004	0.0741	0.0096	0.0752
Cruise_SFC_Min	0.0005	0.2311	0.1913	0.2782
Cutback	0.0008	0.2095	0.0955	0.1948
desBlockFuel	0.0001	0.1614	0.0338	0.1735
desFAR_LDGFL	0.0000	0.0930	0.0674	0.1247
desTOGW	0.0008	0.3118	0.1861	0.3795
diamFan	0.0000	0.2422	0.0983	0.1947
EI_NOx_AP	0.0000	0.1155	0.0102	0.1303
EI_NOx_CO	0.0002	0.1274	0.0237	0.1249
EI_NOx_ID_Lower	0.0000	0.0137	0.0007	0.0130
EI_NOx_TO	0.0002	0.1993	0.0457	0.2119
EI_Standard_AP	0.0008	0.3022	0.0068	0.3976
EI_Standard_CO	0.0058	0.5305	0.1699	0.5065
EI_Standard_ID_Lower	0.0004	0.0360	0.0018	0.0440
EI_Standard_TO	0.0654	0.9952	0.0511	1.0463
enginePodLength	0.0055	0.5356	0.0633	0.5325
engPodWt	0.0083	0.7482	0.0047	0.7489
Fuse_Weight	0.0000	0.0055	0.0000	0.0006
HPC_diam	0.0045	0.5780	0.1185	0.5568
HPCLastStageWc	0.0353	0.8323	0.3571	0.8585
HPCLastStgBladeHeight	0.0000	0.0033	0.0013	0.0035
HT_Weight	0.0009	0.0382	0.0139	0.0380
ICAO_AP_Equiv	0.0000	0.3657	0.1721	0.3679
ICAO_AP_Tt3	0.0011	0.1426	0.0143	0.1416
ICAO_AP_Wfuel	0.0038	0.5110	0.3720	0.6275
ICAO_CO_Tt3	0.0001	0.2852	0.1149	0.3164
ICAO_CO_Wfuel	0.0015	0.3863	0.0926	0.3796
ICAO_ID_Equiv	0.0004	0.5292	0.1385	0.5101
ICAO_ID_Tt3	0.0002	0.1809	0.0095	0.1545
ICAO_ID_Wfuel	0.0000	0.0030	0.0015	0.0033
ICAO_TO_Tt3	0.0013	0.2894	0.0621	0.2817
ICAO_TO_Wfuel	0.0000	0.0173	0.0049	0.0165
LPC_diam	0.0022	0.4978	0.2985	0.4885
Nacelle_Diam	0.0003	0.1742	0.0524	0.1241
OEW	0.0002	0.1465	0.0553	0.1462
Sideline	0.0007	0.1601	0.0135	0.1373

SLS_UI_OPR	0.0002	0.2048	0.1074	0.1976
T3max	0.0007	0.2446	0.0470	0.2212
TOAll_TOFL	0.0009	0.2955	0.0143	0.2664
TOOEO_TOFL	0.0008	0.2765	0.0069	0.2883
VT_Weight	0.0000	0.0075	0.0004	0.0070
Wing_Weight	0.0008	0.0537	0.0076	0.0386

9.2.8 LTA Box Wing Vehicle Fit Statistics

Surrogate Name	MFE Mean Absolute Value	MFE Standard Deviation	MRE Mean Absolute Value	MRE Standard Deviation
AbortALL_TOFL	0.0012	0.1404	0.0237	0.1757
AbortOEO_TOFL	0.0004	0.1430	0.0276	0.1824
ADP_BPR	0.0054	0.7662	0.1977	0.6837
Approach	0.0009	0.0919	0.0055	0.0826
Cruise_SFC_Min	0.0005	0.2020	0.1482	0.2261
Cutback	0.0006	0.1733	0.0334	0.1550
desBlockFuel	0.0008	0.1317	0.0106	0.1363
desFAR_LDGFL	0.0019	0.0625	0.0187	0.0659
desTOGW	0.0015	0.2545	0.0323	0.2576
diamFan	0.0002	0.2148	0.0373	0.2143
EI_NOx_AP	0.0000	0.0237	0.0002	0.0211
EI_NOx_CO	0.0001	0.0965	0.0276	0.1137
EI_NOx_ID_Lower	0.0000	0.0099	0.0011	0.0103
EI_NOx_TO	0.0004	0.1752	0.0355	0.2454
EI_Standard_AP	0.0006	0.2625	0.0533	0.4021
EI_Standard_CO	0.0052	0.4016	0.1440	0.4960
EI_Standard_ID_Lower	0.0000	0.0401	0.0069	0.0454
EI_Standard_TO	0.0018	0.4818	0.0411	0.6993
enginePodLength	0.0080	0.8844	0.1105	0.9318
engPodWt	0.0057	0.8479	0.1361	0.8661
Fuse_Weight	0.0000	0.0005	0.0001	0.0005
HPC_diam	0.0022	0.4462	0.1857	0.4641
HPCLastStageWc	0.0066	0.8362	0.3448	0.8733
HPCLastStgBladeHeight	0.0001	0.5002	0.2480	0.5292
HT_Weight	N/A	N/A	N/A	N/A
ICAO_AP_Equiv	0.0000	0.0037	0.0012	0.0035
ICAO_AP_Tt3	0.0003	0.1616	0.0070	0.1312
ICAO_AP_Wfuel	0.0168	0.6157	0.2911	0.6744
ICAO_CO_Tt3	0.0005	0.2364	0.0941	0.2445
ICAO_CO_Wfuel	0.0018	0.5221	0.0525	0.5452
ICAO_ID_Equiv	0.0000	0.0029	0.0007	0.0028
ICAO_ID_Tt3	0.0007	0.1906	0.0544	0.1700
ICAO_ID_Wfuel	0.0001	0.0036	0.0013	0.0037
ICAO_TO_Tt3	0.0009	0.2973	0.0475	0.2672
ICAO_TO_Wfuel	0.0005	0.5245	0.2049	0.5673
LPC_diam	0.0033	0.3937	0.1062	0.3766
Nacelle_Diam	0.0013	0.1946	0.0018	0.1852
OEW	0.0012	0.1272	0.0365	0.1092
Sideline	0.0004	0.1970	0.0241	0.1799

SLS_UI_OPR	0.0072	0.2385	0.1653	0.2568
T3max	0.0020	0.3187	0.0665	0.2835
TOAll_TOFL	0.0003	0.1611	0.0047	0.2105
TOOEO_TOFL	0.0004	0.1875	0.0192	0.2310
VT_Weight	0.0000	0.0068	0.0003	0.0062
Wing_Weight	0.0000	0.0136	0.0012	0.0109

9.2.10 LTA HWB Vehicle Fit Statistics

Surrogate Name	MFE Mean Absolute Value	MFE Standard Deviation	MRE Mean Absolute Value	MRE Standard Deviation
AbortALL_TOFL	0.0023	0.4251	0.1429	0.6336
AbortOEO_TOFL	0.0024	0.4813	0.1633	0.6370
ADP_BPR	0.0047	0.6824	0.3029	0.6797
Approach-FixedValue(82.9dB)	0.5700	0.1793	N/A	N/A
Cruise_SFC_Min	0.0005	0.2162	0.2138	0.2611
Cutback	0.0016	0.1355	0.0384	0.1417
desBlockFuel	0.0007	0.1377	0.0898	0.1640
desFAR_LDGFL	0.0000	0.0747	0.0033	0.0768
desTOGW	0.0011	0.3317	0.1747	0.4662
diamFan	0.0007	0.2578	0.0806	0.1979
EI_NOx_AP	0.0011	0.0428	0.0077	0.1648
EI_NOx_CO	0.0006	0.1327	0.0699	0.1253
EI_NOx_ID_Lower	0.0002	0.0115	0.0019	0.0109
EI_NOx_TO	0.0025	0.2244	0.0084	0.2461
EI_Standard_AP	0.0047	0.2969	0.0442	0.4482
EI_Standard_CO	0.0006	0.4200	0.2273	0.3948
EI_Standard_ID_Lower	0.0000	0.0330	0.0118	0.0397
EI_Standard_TO	0.0028	0.7138	0.0042	0.7677
enginePodLength	0.0001	0.5556	0.1103	0.5753
engPodWt	0.0012	0.9696	0.1535	0.8765
Fuse_Weight	0.0000	0.0028	0.0000	0.0018
HPC_diam	0.0025	0.5903	0.1175	0.6442
HPCLastStageWc	0.0057	0.8626	0.4918	0.9862
HPCLastStgBladeHeight	0.0030	0.4817	0.0808	0.4675
HT_Weight	N/A	N/A	N/A	N/A
ICAO_AP_Equiv	0.0002	0.3707	0.0702	0.3743
ICAO_AP_Tt3	0.0000	0.1302	0.0059	0.1067
ICAO_AP_Wfuel	0.0073	0.5170	0.1771	0.5478
ICAO_CO_Tt3	0.0104	0.2597	0.1545	0.2643
ICAO_CO_Wfuel	0.0009	0.3891	0.0278	0.3733
ICAO_ID_Equiv	0.0002	0.4681	0.0846	0.4810
ICAO_ID_Tt3	0.0006	0.1859	0.0304	0.1539
ICAO_ID_Wfuel	0.0000	0.0025	0.0013	0.0027
ICAO_TO_Tt3	0.0025	0.2758	0.0636	0.2756
ICAO_TO_Wfuel	0.0015	0.3698	0.1435	0.3761
LPC_diam	0.0027	0.5281	0.2807	0.5061
Nacelle_Diam	0.0095	0.1690	0.0219	0.1195
OEW	0.0000	0.1060	0.0324	0.1053
Sideline	0.0015	0.1899	0.1012	0.2005

SLS_UI_OPR	0.0004	0.2422	0.2086	0.2816
T3max	0.0006	0.2329	0.0255	0.2215
TOAll_TOFL	0.0020	0.4520	0.0897	0.5403
TOOEO_TOFL	0.0110	0.4097	0.0832	0.5141
VT_Weight	N/A	N/A	N/A	N/A
Wing_Weight	0.0000	0.0251	0.0030	0.0249

9.2.11 LSA UDF (Open Rotor) Vehicle Fit Statistics

Surrogate Name	MFE Mean Absolute Value	MFE Standard Deviation	MRE Mean Absolute Value	MRE Standard Deviation
AbortALL_TOFL	0.0033	0.1387	-0.0586	0.2474
AbortOEO_TOFL	-0.0003	0.1456	-0.0629	0.2701
Approach	-0.0007	0.2489	-0.0867	0.2535
Cruise_SFC_Min	0.0034	0.1251	-0.0115	0.1342
Cutback	-0.0003	0.1424	0.0395	0.1566
desBlockFuel	0.0015	0.3436	0.0620	0.3425
desFAR_LDGFL	0.0001	0.0723	-0.0747	0.1501
desTOGW	-0.0002	0.2061	0.0278	0.2630
EI_NOx_AP_lower	-0.0001	0.0115	-0.0013	0.0142
EI_NOx_CO	0.0000	0.1047	0.0263	0.1659
EI_NOx_ID	0.0000	0.0087	-0.0002	0.0079
EI_NOx_TO	0.0008	0.0768	0.0567	0.1773
EI_Standard_AP_lower	0.0000	0.0105	-0.0002	0.0132
EI_Standard_CO	-0.0009	0.1158	-0.0817	0.1668
EI_Standard_ID	-0.0001	0.0083	-0.0096	0.0142
EI_Standard_TO	-0.0002	0.0852	0.1008	0.1993
Fuse_Weight	0.0000	0.0018	-0.0162	0.0183
HPC_diam	0.0013	0.3604	0.1240	0.4116
HPCLastStageWc	0.0041	0.4799	0.2590	0.5359
HPCLastStgBladeHeight	0.0097	0.5979	0.0521	0.7588
HT_Weight	-0.0003	0.0879	-0.0151	0.1539
ICAO_AP_Equiv	0.0089	0.3471	0.2448	0.5310
ICAO_AP_Tt3	0.0001	0.0713	0.0925	0.1301
ICAO_AP_Wfuel	-0.0088	0.4992	-0.0013	0.6078
ICAO_CO_Tt3	0.0004	0.0529	0.0470	0.0828
ICAO_CO_Wfuel	-0.0161	0.3535	-0.0340	0.3358
ICAO_ID_Equiv	-0.0008	0.3934	0.1784	0.5017
ICAO_ID_Tt3	-0.0012	0.1143	0.0749	0.1254
ICAO_ID_Wfuel	0.0053	0.6466	-0.0036	0.6909
ICAO_TO_Tt3	-0.0011	0.0583	0.0012	0.0810
ICAO_TO_Wfuel	0.0010	0.3800	0.0215	0.3816
LPC_diam	0.0010	0.3102	-0.0379	0.3481
OEW	0.0002	0.1230	-0.2116	0.2643
Sideline	-0.0004	0.1325	-0.0033	0.1270
SLS_UI_OPR	0.0002	0.1122	0.0635	0.1720
T3max	0.0000	0.0663	0.0111	0.0583
TOAll_TOFL	0.0006	0.1611	-0.0152	0.2702
TOOEO_TOFL	0.0003	0.1459	-0.0123	0.2563
VT_Weight	-0.0005	0.0307	-0.0036	0.0321

Wing_Weight	-0.0002	0.0586	-0.0286	0.0818
WENG	0.0088	0.6824	0.0352	0.7752
UDF_Prop_Diam	0.0001	0.1044	0.0307	0.1047
Xnac	0.0170	0.6333	0.1130	0.6990
Dnac	0.0001	0.1192	0.0025	0.1176

9.2.12 LTA

9.2.13 HWB UDF (Open Rotor) Vehicle Fit Statistics

Surrogate Name	MFE Mean Absolute Value	MFE Standard Deviation	MRE Mean Absolute Value	MRE Standard Deviation
AbortALL_TOFL	0.0002	0.1520	0.0138	0.2150
AbortOEO_TOFL	0.0021	0.1691	0.0134	0.2215
Approach-FixedValue(84.8dB)	1.2250	0.5224	N/A	N/A
Cruise_SFC_Min	0.0001	0.1094	0.0034	0.1117
Cutback	0.0004	0.1802	0.0076	0.2146
desBlockFuel	0.0007	0.1354	0.0114	0.1341
desFAR_LDGFL	0.0001	0.0720	0.0041	0.0747
desTOGW	0.0007	0.2306	0.0619	0.2797
EI_NOx_AP_lower	0.0000	0.0608	0.0000	0.0680
EI_NOx_CO	0.0040	0.5174	0.0280	0.6106
EI_NOx_ID	0.0008	0.1381	0.0324	0.1675
EI_NOx_TO	0.0007	0.2263	0.0445	0.2348
EI_Standard_AP_lower	0.0000	0.0684	0.0065	0.0790
EI_Standard_CO	0.0048	0.5030	0.0379	0.5729
EI_Standard_ID	0.0005	0.1235	0.0219	0.1392
EI_Standard_TO	0.0002	0.1901	0.0581	0.2410
Fuse_Weight	0.0000	0.0011	0.0000	0.0009
HPC_diam	0.0100	0.3977	0.1040	0.4482
HPCLastStageWc	0.0066	0.7028	0.1248	0.7483
HPCLastStgBladeHeight	0.0015	0.3437	0.0266	0.3541
HT_Weight	N/A	N/A	N/A	N/A
ICAO_AP_Equiv	0.0003	0.1184	0.0145	0.1789
ICAO_AP_Tt3	0.0002	0.0484	0.0113	0.0855
ICAO_AP_Wfuel	0.0000	0.0051	0.0016	0.0094
ICAO_CO_Tt3	0.0000	0.0509	0.0073	0.0689
ICAO_CO_Wfuel	0.0003	0.0130	0.0034	0.0191
ICAO_ID_Equiv	0.0008	0.1963	0.0543	0.2408
ICAO_ID_Tt3	0.0001	0.0647	0.0154	0.0770
ICAO_ID_Wfuel	0.0000	0.0019	0.0004	0.0028
ICAO_TO_Tt3	0.0000	0.0713	0.0038	0.0853
ICAO_TO_Wfuel	0.0000	0.0121	0.0021	0.0170
LPC_diam	0.0051	0.3298	0.0351	0.3422
OEW	0.0003	0.1147	0.0110	0.0987
Sideline	0.0014	0.1424	0.0049	0.1971
SLS_UI_OPR	0.0001	0.3270	0.0146	0.4663
T3max	0.0010	0.1520	0.0065	0.1877
TOAll_TOFL	0.0002	0.1965	0.0252	0.2452
TOOEO_TOFL	0.0002	0.1849	0.0216	0.2309
VT_Weight	N/A	N/A	N/A	N/A

Wing_Weight	0.0000	0.0308	0.0031	0.0291
WENG	0.0043	0.6629	0.0309	0.7074
UDF_Prop_Diam	0.0021	0.2607	0.0151	0.2728
Xnac	0.0110	0.8683	0.1427	1.0590
Dnac	0.0009	0.2602	0.0066	0.2767

REPORT DOCUMENTATION PAGE

Form Approved
OMB No. 0704-0188

1. REPORT DATE *(DD-MM-YYYY)*	2. REPORT TYPE	3. DATES COVERED *(From - To)*
01-05-2016	Contractor Report	

4. TITLE AND SUBTITLE

Application of Deterministic and Probabilistic System Design Methods and Enhancements of Conceptual Design Tools for ERA Project

5a. CONTRACT NUMBER
NNL12AA12C

5b. GRANT NUMBER

5c. PROGRAM ELEMENT NUMBER

6. AUTHOR(S)

Mavris, Dimitri N.; Schutte, Jeff S.

5d. PROJECT NUMBER

5e. TASK NUMBER

5f. WORK UNIT NUMBER
338881.02.07.07.08.66

7. PERFORMING ORGANIZATION NAME(S) AND ADDRESS(ES)
NASA Langley Research Center
Hampton, Virginia 23681

8. PERFORMING ORGANIZATION REPORT NUMBER

9. SPONSORING/MONITORING AGENCY NAME(S) AND ADDRESS(ES)
National Aeronautics and Space Administration
Washington, DC 20546-0001

10. SPONSOR/MONITOR'S ACRONYM(S)
NASA

11. SPONSOR/MONITOR'S REPORT NUMBER(S)
NASA/CR-2016-219201

12. DISTRIBUTION/AVAILABILITY STATEMENT
Unclassified - (Unlimited)
Subject Category 01
Availability: NASA STI Program (757) 864-9658

13. SUPPLEMENTARY NOTES
Final Report

Langley Technical Monitor: Frank H. Gern

14. ABSTRACT

This report documents work done by the Aerospace Systems Design Lab (ASDL) at the Georgia Institute of Technology, Daniel Guggenheim School of Aerospace Engineering for the National Aeronautics and Space Administration, Aeronautics Research Mission Directorate, Integrated System Research Program, Environmentally Responsible Aviation (ERA) Project. This report was prepared under contract NNL12AA12C, "Application of Deterministic and Probabilistic System Design Methods and Enhancement of Conceptual Design Tools for ERA Project".

15. SUBJECT TERMS

Application; Conceptual design; Probabilistic system; System deisgn; Tools

16. SECURITY CLASSIFICATION OF:			17. LIMITATION OF ABSTRACT	18. NUMBER OF PAGES	19a. NAME OF RESPONSIBLE PERSON
a. REPORT	b. ABSTRACT	c. THIS PAGE			STI Help Desk (email: help@sti.nasa.gov)
					19b. TELEPHONE NUMBER *(Include area code)*
U	U	U	UU	240	(757) 864-9658